# The Role of Acyl-CoA Oxidase in Peroxisome Division and Longevity in Yeast

Christopher Gregg

A Thesis

in

The Department

of

Biology

Presented in Partial Fulfillment of the Requirements

For the Degree of Doctor of Philosophy at

Concordia University

Montreal, Quebec, Canada

February 2009

*Your file Votre référence*
*ISBN:* 978-0-494-63448-6
*Our file Notre référence*
*ISBN:* 978-0-494-63448-6

## ABSTRACT

The Role of Acyl-CoA Oxidase in Peroxisome Division and Longevity in Yeast

Christopher Gregg, Ph.D.

Concordia University 2009

Acyl-CoA oxidase (Aox) is an enzyme that carries out the first step of β-oxidation of free fatty acids in peroxisomes. Here I describe a novel role for Aox in peroxisome biogenesis. I found that the peroxisome becomes competent for division only after it acquires the complete set of matrix proteins involved in lipid metabolism. Overloading the peroxisome with matrix proteins promotes the relocation of Aox from the matrix to the membrane. The binding of Aox to Pex16p, a membrane-associated peroxin required for peroxisome biogenesis, initiates the biosynthesis of phosphatidic acid and diacylglycerol (DAG) in the membrane. The formation of these two lipids and the subsequent transbilayer movement of DAG initiate the assembly of a complex between the peroxins Pex10p and Pex19p, the dynamin-like GTPase Vps1p, and several actin cytoskeletal proteins on the peroxisomal surface. This protein team promotes membrane fission, thereby executing the terminal step of peroxisome division.

One of my objectives was to understand what role (if any) Aox and other peroxisomal enzymes of fatty acid oxidation may play in regulating yeast longevity. I found that Aox is an essential component of the protein network controlling the chronological lifespan of yeast placed on a low-calorie diet called calorie restriction (CR). My findings lead to the conlusion that fatty acid oxidation in peroxisomes controls

longevity by modulating the rate of ATP synthesis in mitochondria, but not by generating the ROS hydrogen peroxide.

Recent studies in Dr. Titorenko's laboratory identified novel small molecules that greatly increase the chronological lifespan of yeast. My experiments with one of these novel anti-aging drugs, a commercially available compound further referred to as "LA", revealed that it extends yeast longevity under CR conditions. My studies aimed at elucidating the molecular mechanisms by which LA increases yeast lifespan revealed that lack of Aox or any other enzyme of peroxisomal fatty acid oxidation does not impair the anti-aging effect of LA. My findings demonstrated that LA extends yeast longevity by: (1) reducing the damaging effect of ROS on cellular macromolecules; and (2) amplifying the so-called "hormetic" effect of ROS through the activation of stress-protecting and other anti-aging proteins.

**Acknowledgements**

I am grateful to my supervisor, Dr. Vladimir Titorenko, for his guidance and support during the years I spent in his laboratory. I would like to thank the members of my committee, Dr. Patrick Gulick and Dr. Reginald Storms, for their valuable suggestions during the course of my graduate research and studies.

Many thanks to all of my current and former lab-mates Tatiana Boukh-Viner, Simon Bourque, Subrata Chowdhury, Alex Goldberg, Tong Guo, Pavlo Kyryakov, Oleh Petriv, Bahador Abadi, Alex Alexandrian, Mohammad Sharif Askari, Zeinab Aziz, Farhana Banu, Gabriella Bazdikian, Adam Beach, Guillaume Beaudoin, Adrian Buensuceso, Michelle Tali Burstein, Aman Brar, Andre Cerracchio, Andrew Chang, David Cyr, Ozlem Doygun, Colin Goldfinch, Alexandra Greco, Sandra Haile, Karen Hung Yeung San, Ahmed Hossain, Mara Inniss, Mulanda Kayembe, Sukhdeep Kenth, Hyun Young Kim, Karine Lalonde, Jeffrey MacKenzie Lee, Sabrina Lo, Michael A. London, Lawrence Ma, Gayane Machkalyan, Patrick Marcoux, Haider Mashhedi, Svetlana Milijevic, Janine Morcos, Ramandeep Mudhar, Andrew Naimi, Parisa Namitabar, Florentina Negoita, Mehdi Noei, Reza Noei, Jordan O'Byrne, Aloysius Oluoha, Peter Quashie, Nishant Ramlal, Sonia Rampersad, Vincent Richard, Mohammad Hassan Salah, Elyse Schmidt, Arash B. Shokouhi, Rhoda Sollazzo, Jonathan Solomon, Victor Uscatescu, Lisiana Vigliotti, Laura Whelton and Vivianne Wong for their friendship and support.

I am grateful to my parents for their invaluable support.

## Table of Contents

## List of Figures

**List of Abbreviations**

ACO, aconitase; Aox, acyl-CoA oxidase; EE, ergosteryl esters; ER, the endoplasmic reticulum; Erg, ergosterol; FFA, free fatty acids; CCO, cytochrome c oxidase; CR, calorie restriction; CFU, colony forming units; CW, Calcofluor White M2R; D, diauxic growth phase; DAG, diacylglycerols; DHR, dihydrorhodamine 123; DMSO, dimethylsulfoxide; ETC, electron transport chain in mitochondria; GTP-bp, GTP-binding and hydrolyzing proteins; L, logarithmic growth phase; LB, lipid bodies; LPA, lysophosphatidic acid; LPAAT, LPA acyltransferase; OG, n-octyl-β-D-glucopyranoside; P1 to P5, immature peroxisomal vesicles P1 to P5; P6, mature peroxisomes P6; PA, phosphatidic acid; PAP,

PA phosphatase; PBDs, peroxisome biogenesis disorders; PC, phosphatidylcholine; PD, post-diauxic growth phase; PMPs, peroxisomal membrane proteins; PNS, postnuclear supernatant; PPT, pre-peroxisomal template; PPT, pre-peroxisomal template; PPV1, pre-peroxisomal vesicles 1; PPV2, pre-peroxisomal vesicles 2; PS, phosphatidylserine; PTS1, peroxisomal targeting signal type 1; PTS2, peroxisomal targeting signal type 2; ROS, reactive oxygen species; SDH, succinate dehydrogenase; SOD, superoxide dismutase; ST, stationary growth phase; SV, secretory vesicles; TAG, triacylglycerols; TCA, tricarboxylic acid (cycle); TLC, thin-layer chromatography; 20KgP, 20,000 x *g* pellet; 20KgS, 20,000 x *g* supernatant; 200KgP, 200,000 x *g* pellet; 200KgS, 200,000 x *g* supernatant.

# Introduction

## 1.1 Peroxisome function and pathology

Most eukaryotic cells possess organelles called peroxisomes [1-3]. Delimited by a single lipid bilayer, peroxisomes contain a fine granular matrix and occasionally a paracrystalline core [3]. These organelles contain at least one hydrogen peroxide-producing oxidase and a catalase that decomposes the hydrogen peroxide produced during oxidation of fatty acids, purines and amino acids [1]. Peroxisomes do not have their own DNA and lack independent transcription and protein synthesis machineries [1-3]. Therefore all peroxisomal proteins are encoded by nuclear genes [1-3]. The majority of these proteins are synthesized on free polysomes in the cytosol [1-3], though two peroxisomal membrane proteins (PMPs) are produced on ribosomes found on the rough endoplasmic reticulum (ER) [4, 5].

Peroxisomes are typically responsible for the degradation and biosynthesis of lipids [6-8]. The degradation of prostaglandin and polyamines can also occur within the peroxisomes, while purines and amino acids are often catabolized by α- and β-oxidation [9, 10]. Biosynthetic metabolic pathways that result in the formation of ether phospholipids (plasmalogens), cholesterol, bile acids and polyunsaturated fatty acids are also housed in the peroxisome [10, 11].

The so-called peroxisomal disorders are often lethal, as they result in global developmental delay and cause progressive neurological deficits [12-21]. The failure of peroxisomes to assemble into functionally intact organelles results in peroxisome biogenesis disorders that affect many peroxisomal metabolic pathways [12-16]. The

failure of peroxisomes to assemble correctly is caused by autosomal recessive mutations in any of twelve *PEX* genes encoding proteins called peroxins [17, 18]. Interest in peroxisome biogenesis disorders greatly stimulated studies aimed at understanding of the molecular mechanisms that govern peroxisome assembly, maintenance and inheritance [6, 7, 15, 23].

Peroxisomes also serve as an intracellular signaling compartment and organizing platform that orchestrate developmental decisions from inside of the cell [23-38]. A greater understanding of how peroxisomes fit into the process of development, differentiation and morphogenesis has been gained in recent years [38]. Such research provides insight into the mechanisms underlying the severe neurological dysfunction and developmental delay characteristic of peroxisome biogenesis disorders [30, 38].

## 1.2 A revision of the peroxisome biogenesis paradigm: The peroxisomal endomembrane system

Because peroxisomes function outside of the secretory and endocytic pathways of dynamic vesicular flow [39] it was believed that they were autonomous, static and homogenous organellar compartments [40]. This view on peroxisome biogenesis did not include intercompartmental vesicular trafficking or membrane fusion [41]. Until recently, the "growth and division" model for peroxisome biogenesis was a generally accepted paradigm of the assembly and maintenance of this organelle. In this model, all peroxisomes have the same function and structure and their progressive growth is due solely to the posttranslational import of peroxisomal membrane and matrix proteins

(Figure 1.1). The "growth and division" model for peroxisome biogenesis envisioned that new peroxisomes are formed only due to division of the pre-existing peroxisomes and that the endoplasmic reticulum (ER) serves only as a source of lipids for the growing peroxisomes.

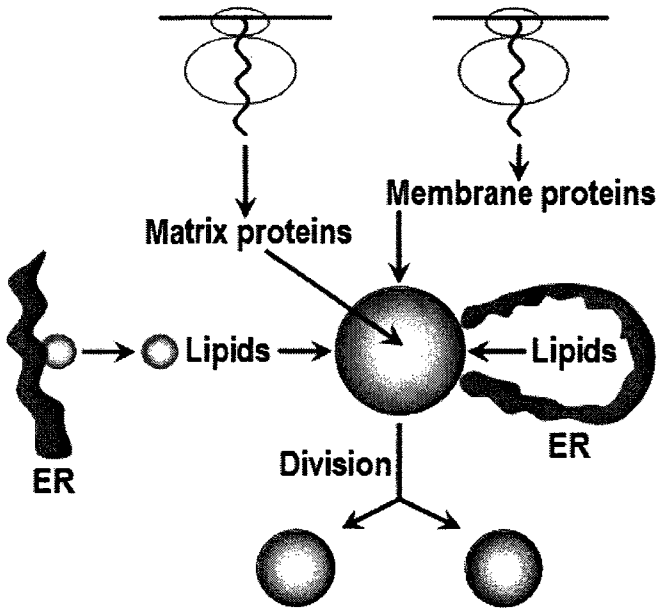


**Figure 1.1.** The "growth and division" model for peroxisome biogenesis postulated that all peroxisomal matrix and membrane proteins are posttranslationally imported into identical peroxisomes. According to this model, peroxisomes then undergo division to form new ones. This model considered ER only as a source of lipids for the growing peroxisomes.

In the current model for peroxisome biogenesis, the ER is used as an endomembrane template for the formation of vesicles that contain a distinct set of proteins. In the yeast *Yarrowia lipolytica*, the formation of peroxisomes begins with the movement of group I peroxisomal membrane proteins (PMPs) such as Pex2p and Pex16p to the ER (Figure 1.2) [23, 42, 43]. This process is followed by the *N*-linked

glycosylation of the PMPs and their subsequent movement to a distinct subdomain of the ER, which becomes the pre-peroxisomal template (PPT) [7, 30]. The PPT then buds from the ER to form two different kinds of vesicles, PPV1 and PPV2, each containing Pex2p and Pex16p (Figure 1.2) [7, 30, 43]. These vesicles are distinct from secretory vesicles (SV) derived from other specialized domains of the ER. These SV bud from the ER to initiate the export of their cargo proteins via the Golgi apparatus to the external medium of a cell, to the cell's plasma membrane and to the cell wall [23, 43, 44].

PPV1 and PPV2 undergo post-translation sorting of two partially overlapping sets of group II PMPs. This process results in the formation of peroxisomal precursors called P1 and P2, the most immature peroxisomal vesicles (Figure 1.2) [7, 30, 45]. These vesicles contain a limited amount of matrix proteins but almost a complete set of PMPs [7, 30, 45]. They undergo fusion to form P3 which has a greater density than its precursors [7, 30, 45, 46]. The maturation of P3 is a stepwise process, involving the selective import of lipids and matrix proteins. This leads to the formation of P4, P5 and finally the mature P6 peroxisome, the largest and most dense peroxisomal subform, which contains a complete set of matrix and membrane proteins (Figure 1.2) [7, 30, 45, 46].

Selective import of matrix proteins is dependent on how intermediates in the peroxisomal assembly pathway differ in their competency to import specific matrix proteins. Only P1 and P2 are competent for the import of matrix enzyme malate synthase (MLS), but they lose this competency as they mature such that P3 to P6 cannot import the enzyme. P3 peroxisomes are the only subform able to import a 62-kD protein reactive

to the type 1 peroxisomal targeting signal (62-kD SKL). P4 peroxisomes selectively import isocitrate lyase (ICL), another matrix protein. This could imply that peroxisomal import machinery is assembled in a temporally ordered manner in distinct intermediates as peroxisomes mature [7, 30, 43, 46-50].

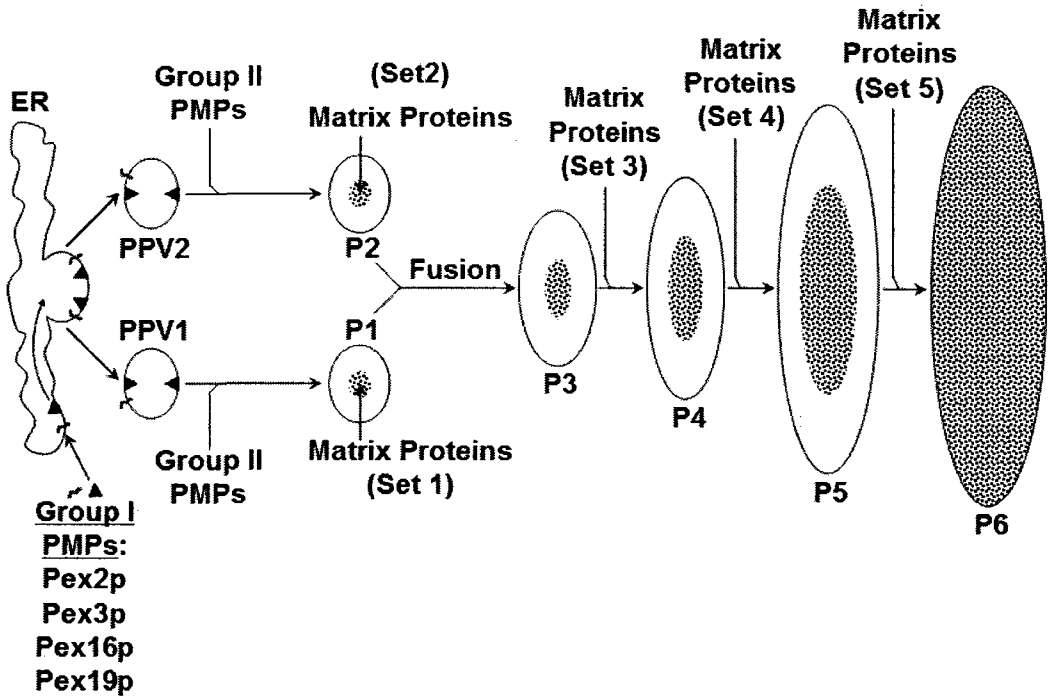


**Figure 1.2.** A model for the multistep peroxisome assembly pathway acting in the yeast *Y. lipolytica*.

In *Y. lipolytica*, peroxisomes do not grow and divide at the same time [45, 51]. The maturation process - which involves the import of matrix proteins and lipids - leads to the maturation of peroxisomes, and only fully mature peroxisomes, P6, are able to divide (Figure 1.3). In immature peroxisomes membrane scission is inhibited by Pex16p, a membrane associated peroxin. The negative action of this protein is abolished in response to its binding to the matrix protein Aox [45, 51]. As peroxisomes mature,

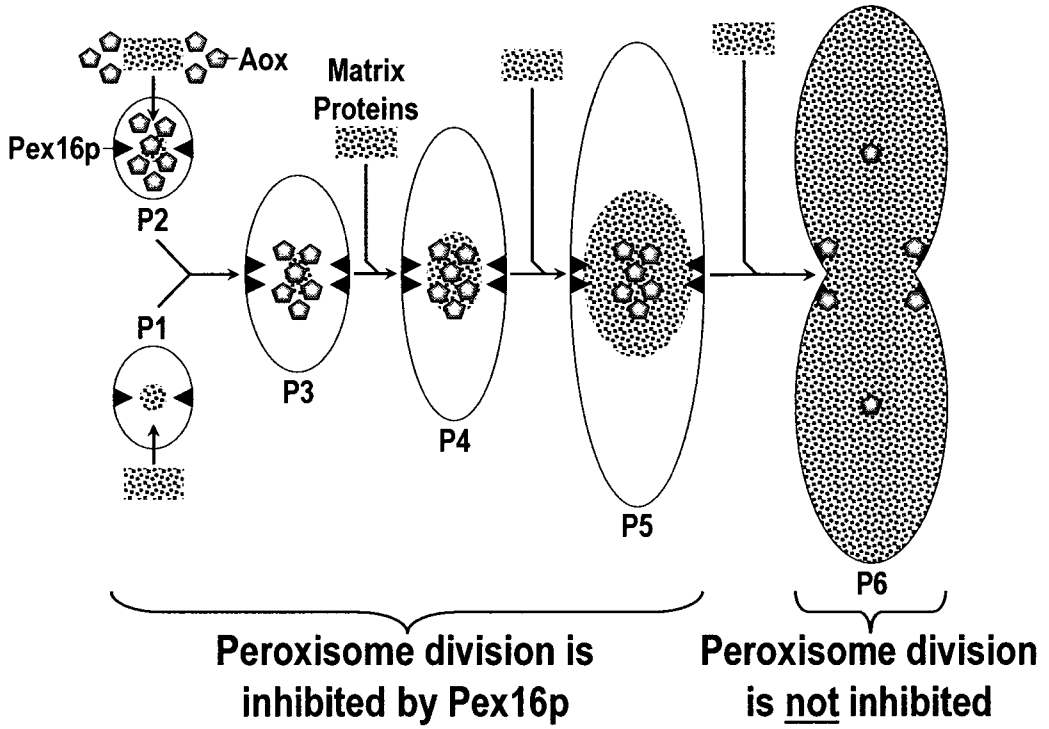


**Figure 1.3.** Pex16p/Aox-dependent mechanism of peroxisome division.

the import of matrix proteins leads to an increase in the density of proteins inside of the peroxisome. In P6 peroxisomes the matrix protein Aox is no longer only located in the matrix of the peroxisomes but is evenly distributed between the matrix and the membrane (Figure 1.3) [45, 51]. The membrane-bound Aox interacts with Pex16, thereby terminating its negative effect on membrane scission and allowing the division of the mature peroxisome (Figure 1.3) [45, 51]. The temporal and spatial regulation of Aox and Pex16p interaction separates the processes of peroxisome maturation and division, ensuring that only mature, metabolically active peroxisomes undergo division. The multistep pathway of peroxisome assembly described in *Y. lipolytica* has also been observed in human fibroblasts and the yeast *Pichia pastoris* [15, 120, 124].

## 1.3 Coordination of compartment assembly and division in the peroxisomal endomembrane system

Division and assembly of the peroxisomal endomembrane system are governed by a distinct set of proteins. Two proteins, ADP-ribosylation factor 1 (ARF1) and the coat protein complex type I (COPI), both known for their role in the peroxisome-to-ER retrograde protein transport in virus-infected cells, have also been shown to induce the proliferation of the peroxisomal endomembrane system [52-56]. These proteins have been demonstrated to promote the membrane scission event required for peroxisome division in evolutionarily diverse organisms. Yeast and mammalian cells deficient in ARF1 and COP1 accumulate elongated tubular peroxisomes, suggesting that both proteins drive peroxisome division [52, 53]. Furthermore, the incubation of highly purified rat liver peroxisomes with cytosol resulted in the recruitment of ARF1 and COPI to the peroxisomal membrane [57]. This observation supports the notion that ARF1 and COPI must bind to peroxisomes for the proliferation of the peroxisomal endomembrane system to be initiated. Moreover, the type 3 of yeast ARF1 has been found to negatively control peroxisome division *in vivo* [53]. Taken together, these findings imply that the peroxisomal endomembrane system uses the same set of core proteins as the classical secretory system of vesicular flow in order to communicate with the ER for purposes of proliferation. Some peroxisome-specific proteins are also implicated in this process, including a distinct set of PMPs as well as dynamin-related protein DLP1/DRP3A/Vps1p, which is recruited from the cytosol to the peroxisome surface using the Fis1p receptor

[58, 59]. How these proteins interact under different metabolic conditions in a given cell or tissue type has yet to be established.

Two pathways seemed to be involved in the assembly and division of peroxisomes in the peroxisomal endomembrane system. One pathway involves the ER-dependent formation of individual compartments within the peroxisomal endomembrane system and is coordinated with the second pathway, which controls the division of peroxisomal compartments [45, 51]. One strategy for the coordination of compartment assembly and division is that a few peroxisomal vesicles derived from the ER undergo stepwise maturation and then divide [45, 51]. A second strategy involves the rapid formation of many vesicles from the ER or the proliferation of a few pre-existing ER-derived carriers [45, 51] followed by their maturation into fully functional peroxisomes by the import of membrane and matrix proteins.

Regardless of the strategy(s) that evolutionarily distant organisms employ for coordinating the assembly and division of individual compartments of the peroxisomal endomembrane system, the tubulation, constriction and scission of these compartments is regulated, depending on cellular and/or environmental conditions of a particular cell type, either by signals emanating from within these compartments [45] or by extraperoxisomal signals that are generated inside the cell in response to certain extracellular stimuli [59]. A distinct group of transcriptional factors induce the transcription of genes encoding proteins of the Pex11p family [58]. Pex11p-type proteins play a role in peroxisome division either directly, by activating peroxisome division, or indirectly, by recruiting dynamin-related proteins from the cytosol [59]. Before peroxisome division occurs, it is

necessary for each peroxisome's membrane to undergo expansion of their membranes by acquiring lipids. The most likely source of these lipids is the ER, which is a principle site for the biosynthesis of phospholipids [61]. It has been suggested that oil bodies are a source of lipids for the peroxisomes in oilseeds [62] and in *Y. lipolytica* [63]. The transfer of phospholipids in *Y. lipolytica* has been observed to take place between a subcompartment of the ER and acceptor membranes of the P3 and P4 peroxisomal intermediates [64]. Although several working models have been proposed for ER-associated lipid-transfer proteins [65], the mechanism underlying the transfer of lipids from the ER to the peroxisomal membrane is yet to be established.

## 1.4 Yeast as a valuable model system for unveiling the molecular and cellular mechanisms of aging

Biological aging can be defined as the progressive decline in the ability of an organism to resist stress, damage and disease [66]. It is characterized by the appearance of degenerative and neoplastic disorders [67-69]. At the demographic level, aging manifests itself as an exponential increase in the mortality rate with the age of the cohort [66].

The yeast *Saccharomyces cerevisiae* has proven to be a valuable model in aging research [70] and the mechanics of aging seem to be conserved from yeast to humans [71]. In the lab one can monitor the chronological aging of yeast cells or the replicative aging of yeast cells. Replicative aging is defined as the number of times a mother cell is able to bud (Figure 1.4) [71]. Replicative aging has proven to be a good model for studying how "mitotic" cells in higher eukaryotes age and divide [72].

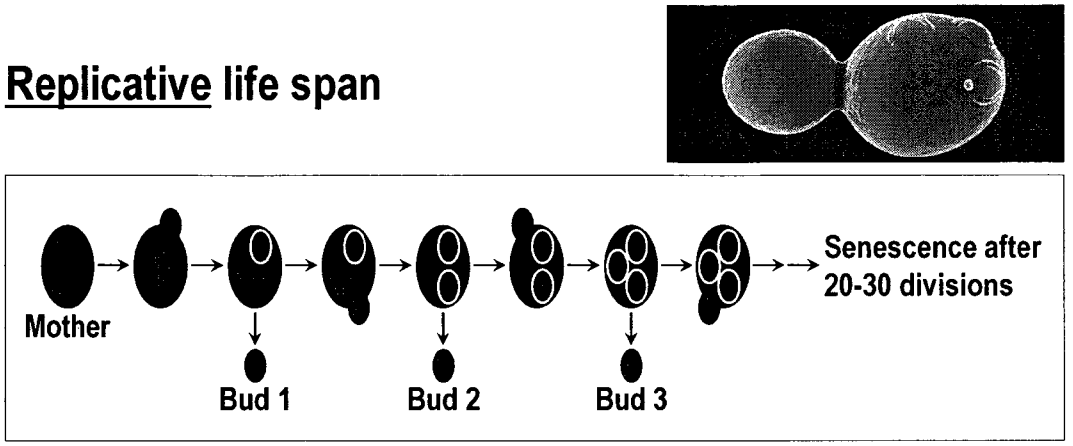


**Figure 1.4.** The replicative lifespan of yeast is defined as the maximum number of buds (*i.e.*, daughter cells) that a mother cell can produce before senescence. It mimics aging of dividing or "mitotic" human cells.

Chronological aging is the amount of time a population of yeast cells remain viable in a non-dividing state (Figure 1.5) [71, 72]. A simple assay can be done to measure the amount of viable cells versus the amount of total cells in a yeast culture in stationary phase for a range of time-points. The curves obtained from such an analysis represent the chorological lifespan of a yeast cells and is a good model for the majority of cells in higher eukaryotes (*i.e.*, "post-mitotic" cells which are no longer dividing) [71, 72].

## 1.5 Effect of genetic manipulations and dietary regimens on lifespan

The lifespan of yeast can be extended by certain genetic manipulations. Sir2p, an $NAD^+$ histone deacetylase, was the first protein extensively studied in the regulation of replicative aging of *S. cerevisiae* [71, 73, 74]. Mutations in the gene encoding Sir2p result in the silencing of extrachromosomal rDNA circles, which shortens the replicative

lifespan of yeast cells. Conversely, overproduction of Sir2p protein leads to an extension of lifespan that is dependant on stress response transcription factors and effectors such as Msn2p/Msn4p and superoxide dismutase [71 - 73]. Sirt1 is the mammalian homologue of Sir2p and has been shown to extend lifespan in mice by the deacetylation and regulation of various proteins such as the tumor suppressor p53 [75 - 77]. Various components of

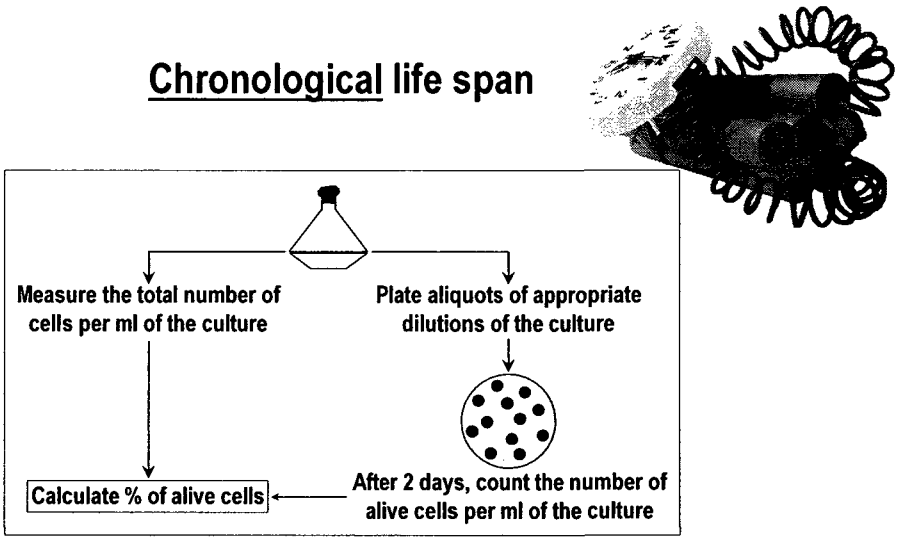


**Figure 1.5.** The chorological lifespan is defined as the length of time a yeast cell remains viable in a nondividing state. It mimics aging of nondividing or "post-mitotic" human cells.

the insulin/IGF-1 glucose signalling pathway have also been implicated in the regulation of both replicative and chronological aging in *S. cerevisiae* [71, 73, 74]. Mutations in the genes *RAS2*, *CYR1*, *PKA1* and *SCH9* lengthen both types of lifespan while mutations in the genes encoding either Msn2p or Msn4p stress-resistance transcriptional factors nullify this lifespan extension (Figure 1.6) [75, 77, 78]. Similar phenotypes have been found in three other model organisms (*i.e.* mice, the nematode worm *C. elegans*, and the fruit fly *D. melanogaster*). In fact, knocking out components of

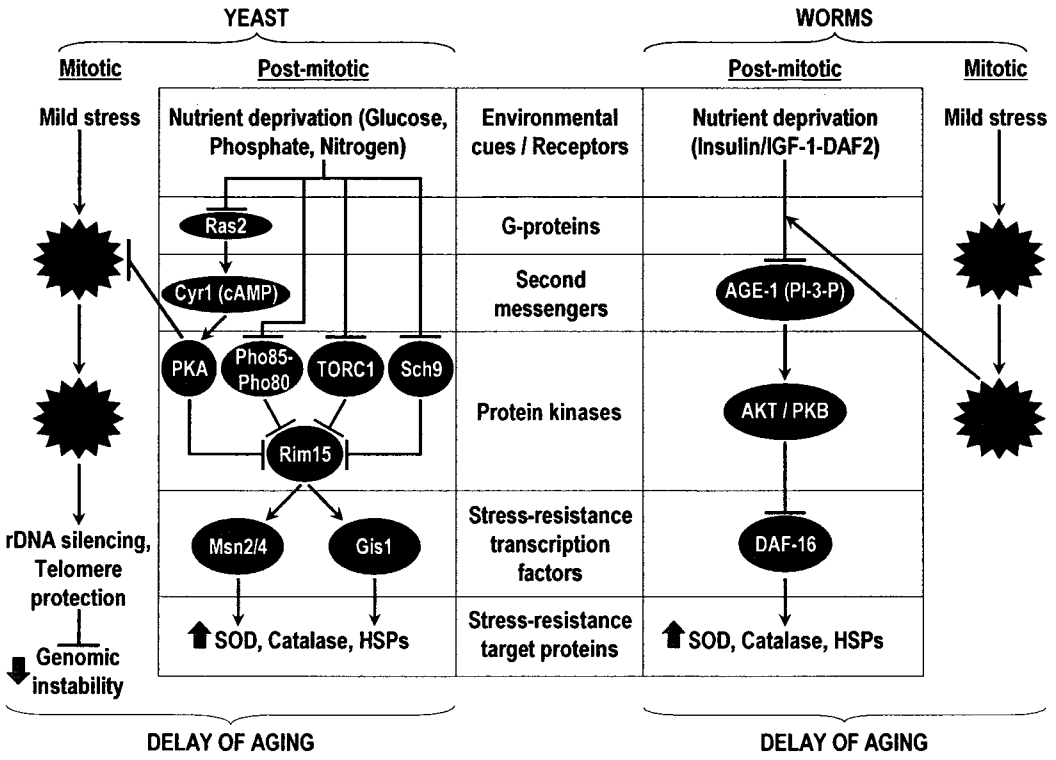


**Figure 1.6.** Longevity pathways are conserved across phyla and governed by an evolutionarily conserved nutrient-sensing signal transduction network.

the insulin/IGF-1 pathway enhances lifespan of these higher eukaryotic organisms in a stress response-dependent fashion [75, 77, 78]. Taken together, these findings strongly suggest that longevity pathways are conserved across phyla and governed by an evolutionarily conserved nutrient-sensing signal transduction network (Figure 1.6) [75, 77, 78].

Many mutations that extend lifespan have major side effects, including irreversible developmental or reproductive defects [79, 80]. One intervention that extends lifespan without such costs is the imposition of a calorie restriction (CR) diet. CR diet is defined as a dietary regimen that is low in calories but does not undernourish the organism [79, 80]. CR has been shown to extend lifespan in a wide range of

evolutionarily distant organisms including yeast, rotifers, spiders, worms, fish, mice, rats and nonhuman primates [79 - 82]. Lifespan extension is observed when animals are fed 25%-60% of the carbohydrates, fats or proteins that are given to control animals fed ad libitum [79, 80]. CR has also been found to delay the onset of age related diseases such as cancer, atherosclerosis, type II diabetes and neurodegeneration [83]. In fact, CR reduces age-associated neuronal loss in most mouse models of neurodegenerative disorders such as Parkinson's disease [64] or Alzheimer's disease [85]. The CR dietary regimen also prevents age-associated declines in psychomotor and spatial memory tasks [86], loss of dendritic spines necessary for learning [87] and improves the brain's plasticity and ability for self-repair [88].

In yeast, CR is imposed by reducing the glucose concentration in the complete YEPD medium from 2% to 0.5% [89] or to 0.2% (this study). This rich medium allows cells to continue to feed on yeast extract and peptone which provide an abundance of amino acids, nucleotides and vitamins, even as glucose levels are rapidly depleted. This reduction in the level of glucose from 2% to 0.5% or to 0.2% could impose a state of partial energy (ATP) limitation. Other dietary restriction protocols, which limit amino acids and other nutrients [90, 91], drastically slow the growth rate and make it more difficult to impose energy limitation.

## 1.6 Reactive oxygen species (ROS) and aging

It has been known for many years that CR extends lifespan but only recently have the mechanisms governing its anti-aging effect emerged. The answer to how CR extends

lifespan has proven to be quite complex as there are many observed consequences to such a diet, including specific changes in metabolism, neuroendocrine signaling and apoptotic cell death machinery. These effects often have striking differences depending on the tissue type that they are observed in [73, 77]. The "free radical theory" of aging, a generally accepted theory of aging, is that cumulative oxidative damage of various cellular constituents inflicted by the progressive generation of reactive oxygen species (ROS) causes organisms to function less effectively over time and results in age-associated degenerative disorders [92]. The age-related irreversible oxidative damage can be observed in DNA, RNA, protein and lipids. Importantly, the extent of such oxidative damage correlates with the age of an organism [93 - 96]. Thus, it seems very likely that oxidative damage does limit lifespan. In fact, the enzyme superoxide dismutase (SOD), which is responsible for reducing ROS in cells, has been found to extend lifespan when over-expressed in *Drosophila* [97] and in stationary phase yeast cells [98].

Though ROS are generated in multiple compartments in the cell and by multiple enzymes within the cell, most ROS produced in a cell (up to 90%) are made in the mitochondrion (Figure 1.7) [99 - 102]. ROS are also generated by a family of NADP/H oxidases and by so-called phagocytic oxidases in the plasma membrane [99 - 102], in reactions catalyzed by cytosolic amino acid oxidases, cyclooxygenases, lipid oxigenases and xanthine oxidase [99 - 102], and during lipid metabolism in peroxisomes [7, 30]. The steady-state level of ROS within a cell is the result of a balance between the rate of its formation and decomposition due to anti-oxidant scavenger reactions that take place in various cellular locations (Figure 1.8). The most important anti-oxidant enzymes are

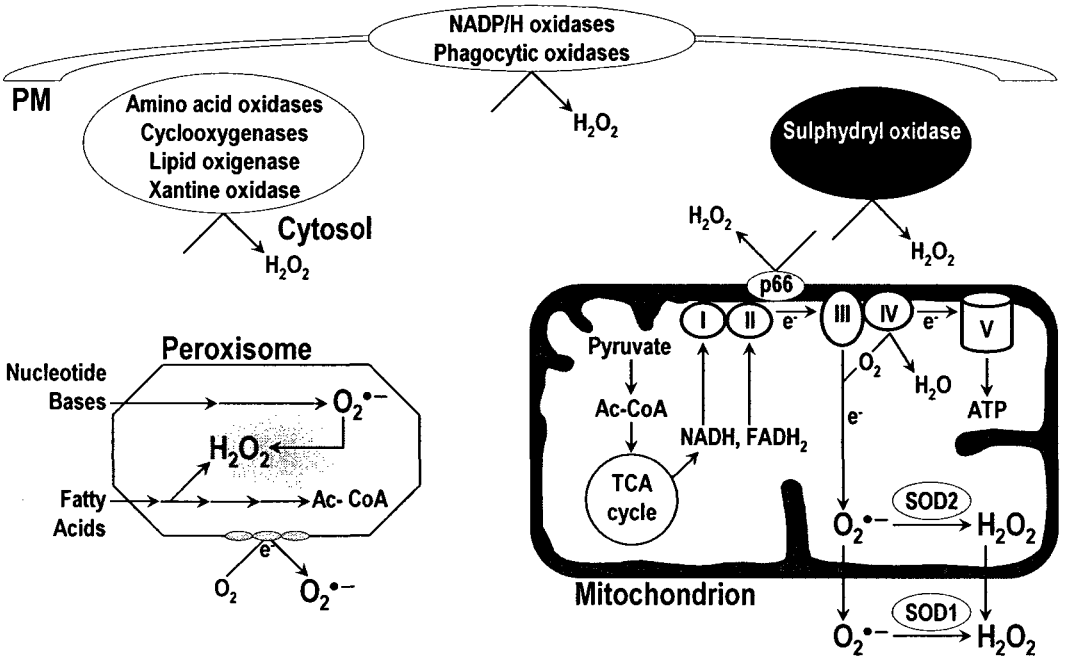


**Figure 1.7.** ROS are generated by numerous enzymes in multiple compartments within the cell, mostly (~ 90%) within mitochondria.

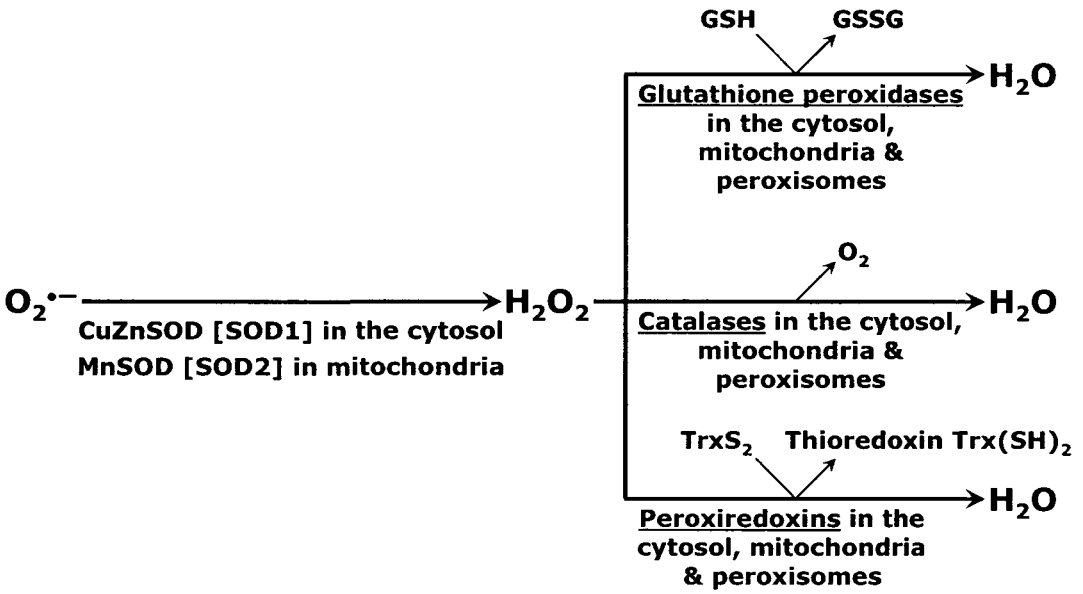


**Figure 1.8.** Detoxification of ROS occurs in antioxidant scavenger reactions.

CuZnSOD (SOD1) subform of superoxide dismutase in the cytosol and the MnSOD (SOD2) subform of the same enzyme found in mitochondria (Figure 1.8). Both these enzymes are responsible for converting superoxide radicals to a less toxic and more stable ROS, hydrogen peroxide [99 - 102]. Hydrogen peroxide is then further detoxified by: 1) glutathione peroxidases in the cytosol, mitochondria and peroxisomes; 2) catalases in the cytosol, mitochondria and peroxisomes; and 3) peroxiredoxins in the cytosol, mitochondria and peroxisomes (Figure 1.8) [99 - 102].

Most of the known targets for the oxidative damage caused by ROS are mitochondrial proteins, DNA and lipids, including: 1) aconitase, a [4Fe-4S] cluster enzyme of the TCA cycle; 2) Lys4p, a [4Fe-4S] cluster enzyme of lysine biosynthesis that takes place in the mitochondrion; 3) succinate dehydrogenase (SDH), a [3Fe-3S] cluster- and heme-containing enzyme of the TCA that also functions as complex II of the electron transfer chain (ETC) in the mitochondrial membrane; 4) cytochrome c, a heme-containing mobile component of the mitochondrial ETC; 5) cytochrome c oxidase, a

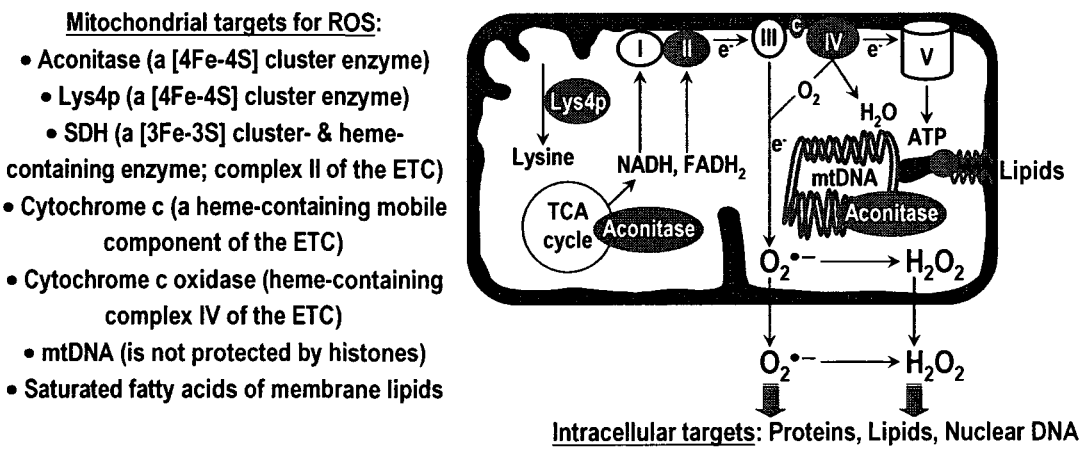


**Figure 1.9.** Major targets of oxidative damage by ROS in mitochondria.

heme-containing complex IV of the mitochondrial ETC; 6) the mitochondrial DNA (mtDNA) nucleoid that, in contrast to chromatin in the nucleus, lacks histones; and 7) saturated fatty acids of membrane lipids (Figure 1.9) [99 - 102].

Although high intracellular and intraorganellar levels of ROS can cause oxidative damage to various cellular constituents, low concentrations of intracellular ROS can activate cellular processes that protect cellular macromolecules from oxidative damage (Figure 1.10) [99 - 102]. Furthermore, such low concentrations of ROS activate a protein team that protects the cell from apoptosis [99 - 102], one of the forms of programmed cell death [39]. Extension of lifespan by the induction of a mild-stress response is called hormesis. These protective functions of the cell are initiated by ROS sensors present in the mitochondrion (*i.e.*, protein kinases PKD1, PKCδ, Src, Abl, PI3 kinase and Akt), plasma membrane (*i.e.*, the Ras protein), and cytosol (*i.e.*, the PNC1 protein) (Figure 1.10) [99 - 102]. Some of these sensors interact with cytosol-to-nucleus and mitochondria-to-nucleus shuttling proteins (*i.e.*, p32 and Hsp27p, respectively), thereby promoting their relocation to the nucleus. In the nucleus, these two shuttling proteins activate a distinct group of transcriptional factors and cofactors (*i.e.*, SIRT1, FOXO3, p53, NF-κB, DET1 and COP1), all of which function as global transcriptional activators of genes encoding oxidative stress-response and anti-apoptotic proteins [99 - 102]. Moreover, some of the ROS sensors in the cytosol and mitochondrion phosphorylate and inactivate the pro-apoptotic factors Bad and JNK, thereby delaying the intrinsic, mitochondria-dependent apoptotic pathway of programmed cell death (Figure 1.10) [99 - 102]. The intrinsic pathway of apoptosis also depends on the delicate balance between

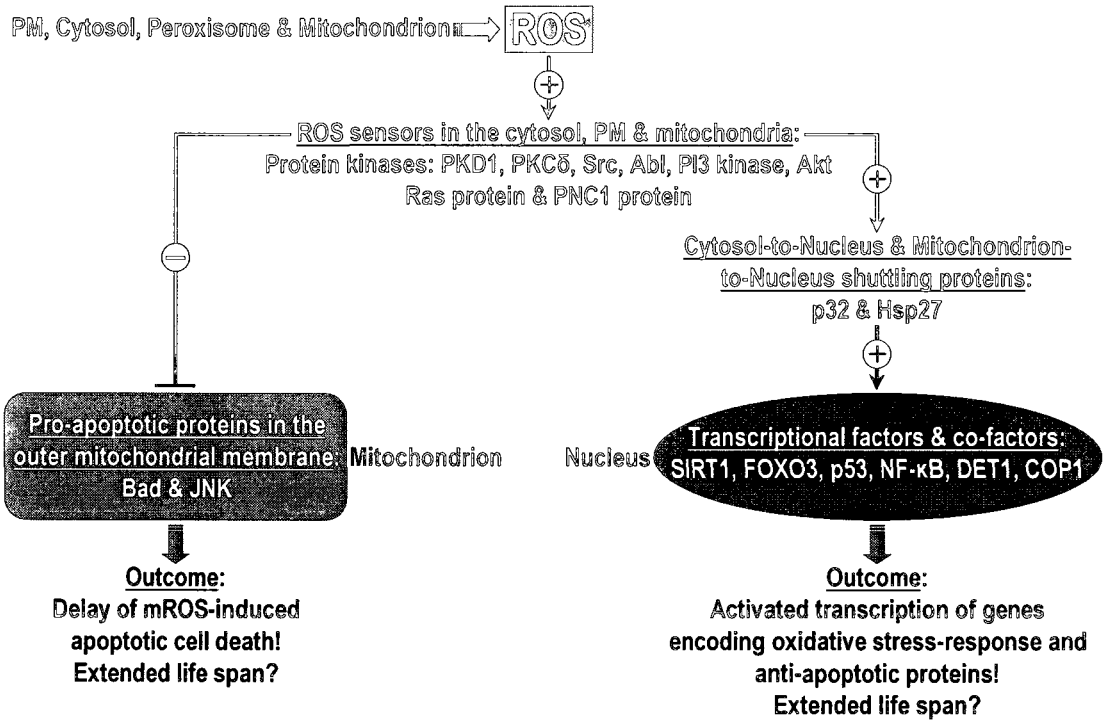


**Figure 1.10.** Low concentrations of intracellular ROS activate cellular processes that protect cellular macromolecules from oxidative damage.

**Mitochondrial fusion maintains a tubular mitochondrial network, thereby:**

- Facilitating transfer of the mitochondrial membrane potential (*i.e.*, energy) from $O_2$-rich to $O_2$-poor cellular regions
- Complementing mtDNA mutations that accumulate with aging
- Hampering the intrinsic pathway of apoptosis

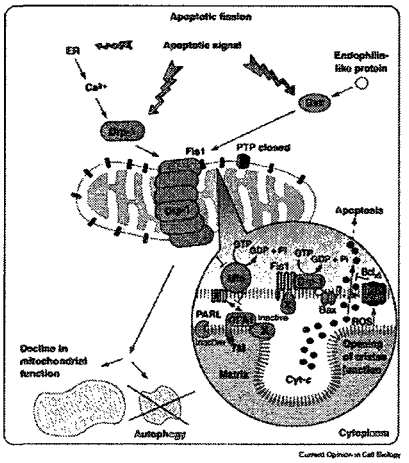


**Mitochondrial fission breaks down the mitochondrial network, thereby:**

- Ensuring inheritance of mitochondria by newly formed daughter cells
- Causing respiratory defects
- Leading to loss or mutation of mtDNA that remains uncomplemented
- Promoting the intrinsic pathway of apoptosis

**Figure 1.11.** A delicate balance between mitochondrial fission and fusion controls the intrinsic pathway of apoptosis and, perhaps, aging.

mitochondrial fission and fusion [101, 104 - 106]. Mitochondrial fusion maintains a tubular mitochondrial network, thereby: 1) facilitating transfer of the mitochondrial membrane potential (*i.e.*, energy) from $O_2$-rich to $O_2$-poor cellular regions; 2) complementing mtDNA mutations that accumulate with aging; and 3) hampering the intrinsic pathway of apoptosis (Figure 1.11) [101, 104 - 106]. On the other hand, mitochondrial fission breaks down the mitochondrial network, thereby: 1) ensuring inheritance of mitochondria by newly formed daughter cells; 2) causing respiratory defects; 3) leading to loss or mutation of mtDNA that remains uncomplemented; and 4) promoting the intrinsic pathway of apoptosis (Figure 1.11) [101, 104 - 106].

Apoptosis is known to be an essential part of human development and physiology [39]. Recent evidence suggests that mitochondria-dependent apoptosis, a pathway of programmed cell death, may play a role in the aging of evolutionarily distant organisms including many unicellular organisms [107]. Characteristic markers of apoptosis such as DNA cleavage, chromatin condensation, externalization of phosphatidylserine to the outer leaflet of the plasma membrane, and cytochrome c release from the mitochondria has recently been observed in yeast (Figure 1.12; data from Dr. Titorenko's laboratory) [108]. The apoptotic phenotype was observed in yeast cells with a mutation in the *CDC48* gene [109]. ROS have been implicated as central regulators of yeast apoptosis, which leads to even more similarity towards apoptosis in metazoan organisms [110]. The identification of several yeast orthologues of mammalian apoptotic regulators has provided the final proof that yeast and metazoan apoptosis are two versions of the same cellular program. These key apoptotic regulators in yeast cells include: 1) the yeast

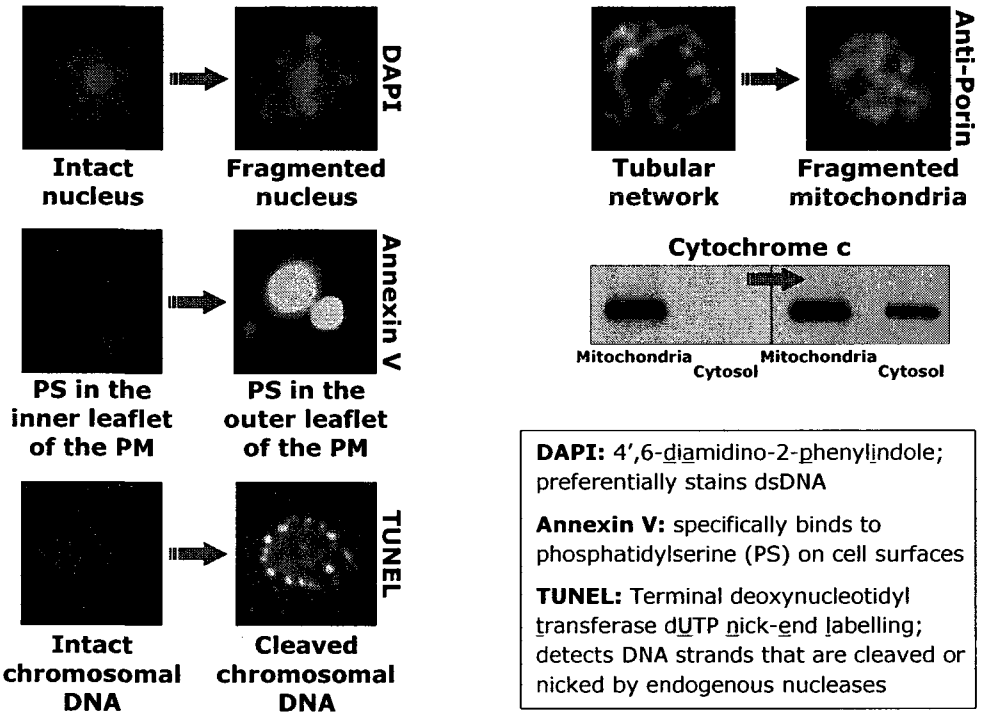


**Figure 1.12.** Hallmark events of apoptotic cell death in yeast. Data from Dr. Titorenko's laboratory.

metacaspase Yca1p [109]; 2) an HtrA2/Omi-like protein, the yeast apoptotic serine protease Nma111p [111]; 3) the yeast apoptosis inducing factor Aif1p [112]; 4) the yeast histone chaperone Asf1p [113]; and 5) the yeast mitochondrial fission protein Drp1p [114] (Figure 1.13). The hallmark events of apoptosis have been observed in aging yeast cells [115], suggesting that apoptosis plays a role in regulating yeast longevity. Recent unpublished findings from Dr. Titorenko's laboratory provided evidence that the oxidation of free fatty acids in peroxisomes initiates a cascade of events that leads to an intrinsic, mitochondria-dependent apoptotic pathway of age-related programmed cell death.

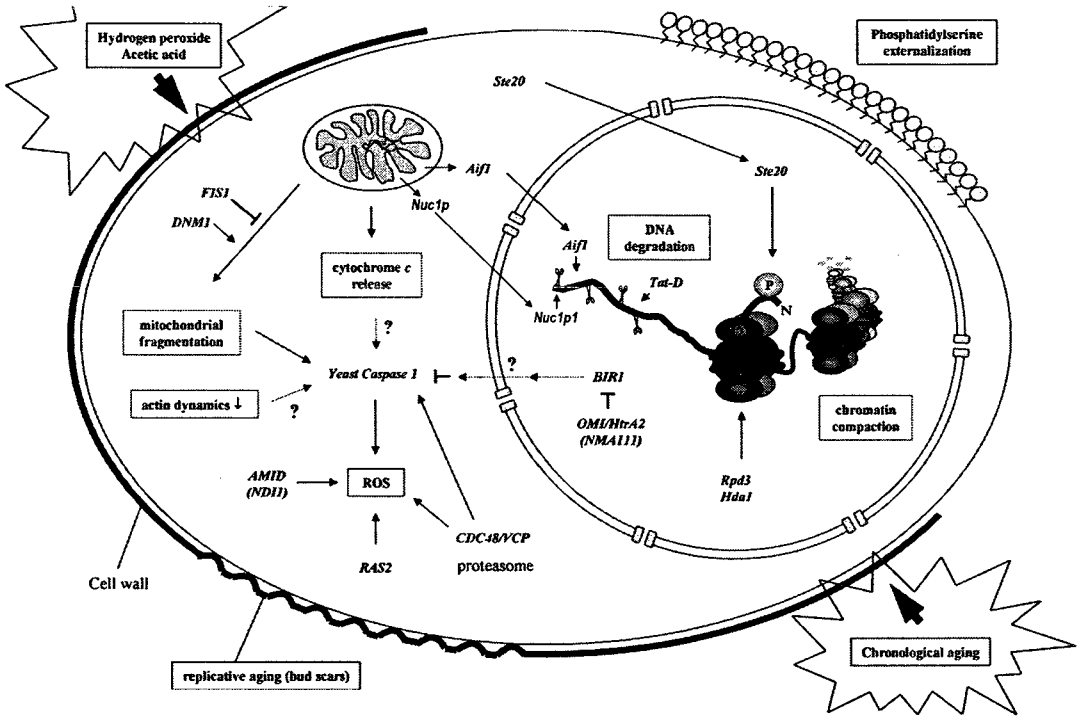


**Figure 1.13.** The basic machinery of yeast apoptosis.

In this thesis I will also look at the role of a novel anti-aging small molecule that was identified in Dr. Titorenko's laboratory. This molecule is called LA. I found that LA greatly increases the lifespan of yeast grown under CR conditions. My findings provide evidence that LA extends longevity in part by modulating ROS production in mitochondria. It seems that such LA-dependent specific modulation of ROS increases yeast lifespan not only by reducing the damaging effect of ROS on cellular macromolecules but also by amplifying the "hormetic" effect of ROS through the activation of stress-protecting and other anti-aging proteins.

## 1.7 Thesis outline and contributions of colleagues

Chapter 2 describes findings providing evidence for a novel role for Aox in

peroxisome biogenesis. I found that the peroxisome becomes competent for division only after it acquires the complete set of matrix proteins involved in lipid metabolism. Overloading the peroxisome with matrix proteins promotes the relocation of Aox from the matrix to the membrane. The binding of Aox to Pex16p, a membrane-associated peroxin required for peroxisome biogenesis, initiates the biosynthesis of phosphatidic acid and diacylglycerol (DAG) in the membrane. The formation of these two lipids and the subsequent transbilayer movement of DAG initiate the assembly of a complex between the peroxins Pex10p and Pex19p, the dynamin-like GTPase Vps1p, and several actin cytoskeletal proteins on the peroxisomal surface. This protein team promotes membrane fission, thereby executing the terminal step of peroxisome division. Chapter 3 outlines evidence that Aox is an essential component of the protein network controlling the chronological lifespan of yeast placed on a CR diet. My analysis of the mechanism by which Aox and other peroxisomal enzymes of fatty acid oxidation regulate yeast longevity led to the conclusion that fatty acid oxidation in peroxisomes controls longevity by modulating the rate of ATP synthesis in mitochondria, but not by generating the ROS hydrogen peroxide. In particular, my findings provide evidence that the efficiency of acetyl-CoA formation via peroxisomal fatty acid oxidation modulates the efficiency of electron flow through the mitochondrial electron transport chain, activities of several well-known target enzymes for the oxidative damage by ROS, the mitochondrial membrane potential, and the maintenance of a mitochondrial tubular network. The mechanism by which a novel anti-aging small molecule called LA greatly extends yeast longevity under CR conditions is described in Chapter 4. My findings demonstrate that,

although fatty acid oxidation in peroxisomes is essential for delaying aging, it is not required for the ability of LA to extend yeast longevity. This chapter also describes a body of evidence that LA extends yeast longevity not only by reducing the damaging effect of ROS on cellular macromolecules but also by amplifying the so-called "hormetic" effect of ROS through the activation of stress-protecting and other anti-aging proteins.

The findings presented in Chapter 2 have been published in *The Journal of Cell Biology* [Guo, T., Gregg, C., Boukh-Viner, T., Kyryakov, P., Goldberg, A., Bourque, S., Banu, F., Haile, S., Milijevic, S., Hung Yeung San, K., Solomon, J., Wong, V. and Titorenko, V.I. A signal from inside the peroxisome initiates its division by promoting the remodeling of the peroxisomal membrane. *J. Cell Biol.* (2007) 177:289-303]. This article was an Editors' Choice article in *Science* (2007) 316:801. I carried out and supervised more than 40% of all of the work described in this publication and prepared the first draft of sections relevant to my work. I am an equally contributed (together with Dr. Guo Tong) co-author on this publication. Dr. V. Titorenko provided intellectual leadership of this project and edited the manuscript.

The data described in Chapter 3 are presented in the manuscript of a paper that is currently in preparation for submission to *Cell Metabolism*. I carried out and supervised more than 40% of all of the work described in this manuscript and prepared the first draft of sections relevant to my work. Dr. V. Titorenko provided intellectual leadership of this project and is editing the manuscript.

The data described in Chapter 4 are presented in the manuscript of a paper that is

currently in preparation for submission to *Nature Chemical Biology*. I carried out and supervised more than 30% of all of the work described in this manuscript and prepared the first draft of sections relevant to my work. Dr. V. Titorenko provided intellectual leadership of this project and is editing the manuscript.

All abbreviations, citations, and the numbering of figures and tables that have been used in the published paper and in the manuscripts in preparation have been changed to the format of this thesis.

# 2 Acyl-CoA oxidase functions as a molecular switch that controls peroxisome division

## 2.1 Abstract

In the yeast *Y. lipolytica*, peroxisomes begin as two vesicles called P1 and P2 that gradually mature into metabolically active peroxisomes, P6. Only P6 peroxisomes are able to divide. The step-wise maturation of peroxisomes involves the import of matrix proteins and membrane lipids over time. The division of the mature peroxisome P6 requires a change in the composition of its membrane lipids, which is preceded by the relocation of a protein called Aox from the matrix to the membrane of P6. My findings show that the movement of Aox from the matrix to the membrane of peroxisomes does not require interaction of Aox with a specific protein but rather occurs whenever the protein concentration within the peroxisomal matrix reaches a critical mass. The interaction of Aox with Pex16p initiates a cascade of events that ultimately alters the lipid composition in the membrane to assume a shape that is more energetically favourable for peroxisome division. Such re-shaping of the membrane of mature peroxisomes P6 promotes the recruitment to the peroxisomal surface of a protein machinery that drives peroxisome division by promoting the fission of the peroxisomal membrane.

## 2.2 Introduction

In the "growth and division" model of peroxisome biogenesis, peroxisomal membrane and matrix proteins are synthesized on cytosolic polyribosomes and then specifically targeted to the peroxisome. Daughter peroxisomes are formed by the division

of these peroxisomes [116]. Daughter peroxisomes then undergo the same process of growth and division [61]. Though some findings support this model, certain details of this process had not been elucidated including the means by which the growth and division of peroxisomes is coordinated. It was possible that only peroxisomes that had undergone growth and maturation were competent for division. It was also possible that immature peroxisomal vesicles first proliferated by dividing and only then grew and matured by importing matrix and membrane proteins. This latter pattern, whereby it is the immature peroxisomes that divide, was observed in the yeast *Candida boidinii* [60]. Finally, there was a possibility that both mature and immature peroxisomes divided in a process that was independent to that of their growth and maturation.

Data on purification, protein profiling and electron microscopic analysis of mammalian and yeast peroxisomes have provided important information regarding the process of peroxisomal development. It was established that the population of peroxisomes in a cell consists of several peroxisomal subforms that differ in their size, morphology, buoyant density and protein composition [64, 117 - 120]. By monitoring of the *in vivo* dynamics of peroxisomal protein localization, it was demonstrated that there are several peroxisomal subforms, each differing in their competency to import various proteins [64, 117 - 120]. In yeast [120] and in mammals [121], most peroxisomal proteins are imported into small peroxisomal vesicles of intermediate buoyant density. By acquiring various proteins, these peroxisomal vesicles gradually mature to peroxisomes of high buoyant density. Recent findings in human and yeast cells have suggested that

several peroxisomal subforms are organized into a multistep peroxisome assembly pathway [15, 45, 50, 122 - 124]. The pathway operates by the conversion of subforms in a temporally ordered manner, involves the stepwise import of distinct subsets of matrix and membrane proteins into different intermediates along the pathway, and leads to the assembly of mature peroxisomes (Figure 1.2) [7, 15, 30, 123, 125].

It has been demonstrated that the mass of immature peroxisomal vesicles P1 to P5 is not more than 1-2% of that of mature peroxisomes [42, 45]. The peroxin Pex16p, which is attached to the matrix surface of the membrane [126], negatively regulates the division of immature peroxisomal vesicles, preventing their excessive proliferation [45, 50, 127]. The negative control of membrane scission by Pex16p is necessary for the growth of yeast grown on medium containing oleic acid. Indeed, the lack of Pex16p resulted in the excessive proliferation of immature peroxisomal precursors [45, 126] and impaired the utilization of oleic acid as a carbon source [126].

As peroxisomes mature from P1 to P5 subforms, the import of distinct subsets of matrix proteins results in increasing fractions of matrix proteins that are present in mature peroxisomes [45, 125]. When the increase of the total mass of matrix proteins reaches a critical level, the redistribution of the heteropentameric Aox complex from the matrix of the peroxisome to its membrane is observed. Aox is present in the early P2 intermediate [45] of the peroxisome assembly pathway and its relocation to the peroxisomal membrane occurs only in the mature peroxisome P6, in which the mass of matrix proteins is greatest [45]. Overloading peroxisomes with any matrix proteins other than Aox was suggested be a major factor in the relocation of Aox complex to the membrane of

peroxisomes [45].

Inside mature peroxisomes, the membrane-bound pool of Aox complex interacts with Pex16p. The interaction between Pex16p and Aox requires that the Aox heteropentamer has its Aox4p and Aox5p subunits [45]. The formation of the Pex16p/Aox supramolecular complex, which contains 2 molecules of Aox and two molecules of Pex16p [45], terminates the negative action of Pex16p on scission of the peroxisomal membrane. Thus, mature peroxisomes become division-competent. It is this interaction between Aox and Pex16p that regulates the temporal and spatial separation of the processes of peroxisome assembly and division in *Y. lipolytica*. Such separation may provide an important advantage for the efficient, stepwise assembly of mature, metabolically active peroxisomes.

In the above described model for peroxisome growth and division in *Y. lipolytica* (Figure 1.3), the interaction between Aox and Pex16p terminates the negative action of Pex16p on scission of the peroxisomal membrane, thereby allowing mature peroxisomes to divide [45]. Membrane scission involves strong membrane bending and a transient reorganization of the equilibrium bilayer configuration of the membrane into highly curved non-bilayer intermediates (Figure 2.1) [128 - 135]. These energetically unfavourable processes require a specialized team of proteins [136 - 155] and a distinct set of membrane lipids, including phosphoinositides [134, 140, 146, 156 - 160], phosphatidic acid (PA) [134-136, 139, 142, 157-160] and diacylglycerol (DAG) [134, 135, 141, 142, 157 - 160].

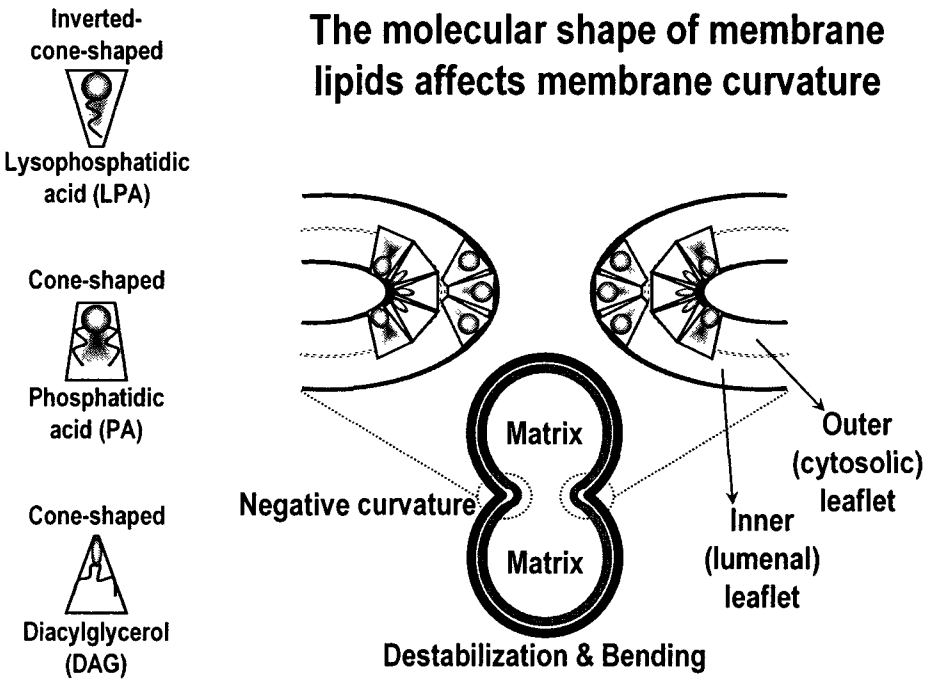


**Figure 2.1.** Membrane scission involves strong membrane bending and a transient reorganization of the equilibrium bilayer configuration of the membrane into highly curved non-bilayer intermediates. The molecular shape of lipids influences membrane curving.

Cone-shaped PA induces negative monolayer curvature in the outer (cytosolic) leaflet of a membrane bilayer in the constricted neck (Figure 2.2) [134, 135, 157 - 160] DAG, which has even more conical shape [133, 157 - 161] and is capable of very rapid transbilayer movement and lateral partitioning [135, 161 - 163], is a particularly potent inducer of negative monolayer curvature and membrane bending (Figure 2.2) (Figure 2.2) [133 – 135, 157 - 163].

The key challenge for me was to determine whether or not the interaction between Pex16p and Aox promotes specific changes in the lipid composition of the peroxisomal membrane that could trigger membrane destabilization, bending, scission and fission

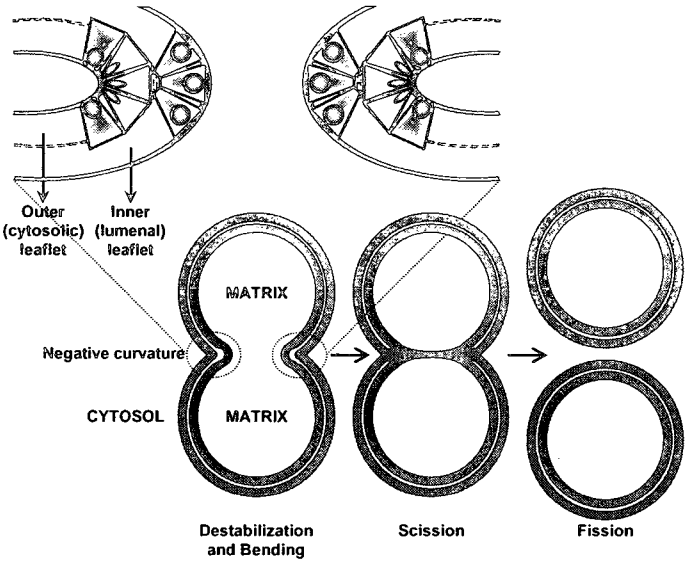


**Figure 2.2.** By influencing membrane curvature, the molecular shape of lipids could regulate the rate and efficiency of the membrane destabilization, bending, scission and fission events required for the division of mature peroxisomes.

events required for the division of mature peroxisomes. It should be stressed that aforementioned model for the Pex16p/Aox-dependent mechanism of peroxisome division (Figure 1.3) does not specify what it is that causes Aox to be relocated from the matrix to the membrane in mature peroxisomes P6. Using an *in vitro* assay to reconstruct the processes that occur within the peroxisome, I tested three possible molecular mechanisms underlying such relocation of Aox within P6. First, it is plausible that the relocation of Aox is due only to an increase in the total mass of matrix proteins above a critical level. In this mechanism, this movement of Aox is not caused by its interaction with any specific protein in the matrix (Figure 2.3). Second, it is possible that: 1) a specific matrix protein rather than protein mass in the peroxisomal matrix initiates the relocation of Aox

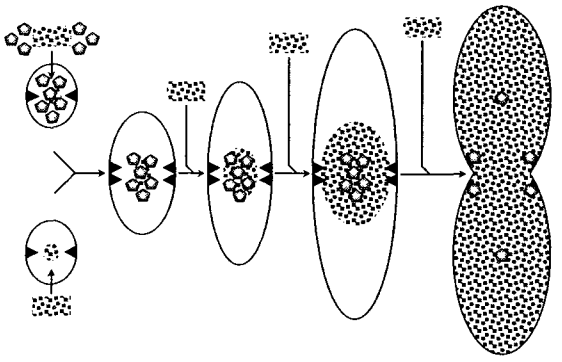

**Figure 2.3.** First possible molecular mechanism underlying the relocation of Aox from the matrix to the membrane within mature peroxisomes P6. The relocation of Aox is due only to an increase in the total mass of matrix proteins above a critical level. In this mechanism, this movement of Aox is not caused by its interaction with any specific protein in the matrix.

from the matrix to the membrane; and 2) this specific matrix protein is present already in the early peroxisomal precursors P1 and P2 and is activated only when the total mass of matrix proteins exceeds a critical level (Figure 2.4). Third, it is conceivable that: 1) a

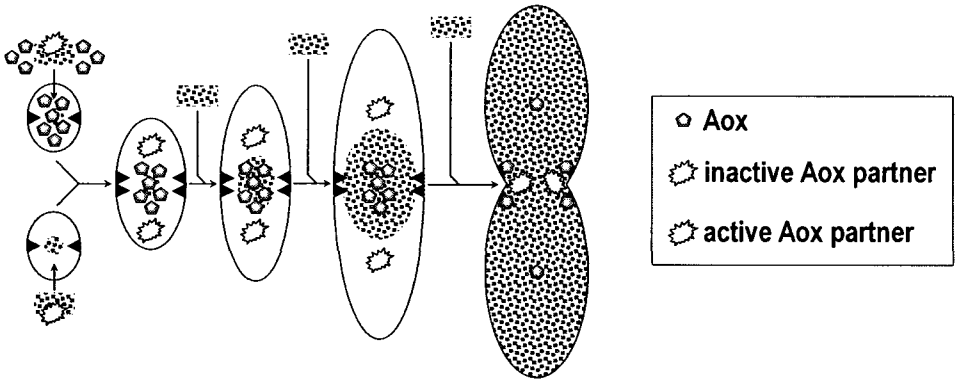


**Figure 2.4.** Second possible molecular mechanism underlying the relocation of Aox from the matrix to the membrane within mature peroxisomes P6. A specific matrix protein rather than protein mass in the peroxisomal matrix initiates the relocation of Aox from the matrix to the membrane. This specific matrix protein is present already in the early peroxisomal precursors P1 and P2 and is activated only when the total mass of matrix proteins exceeds a critical level.

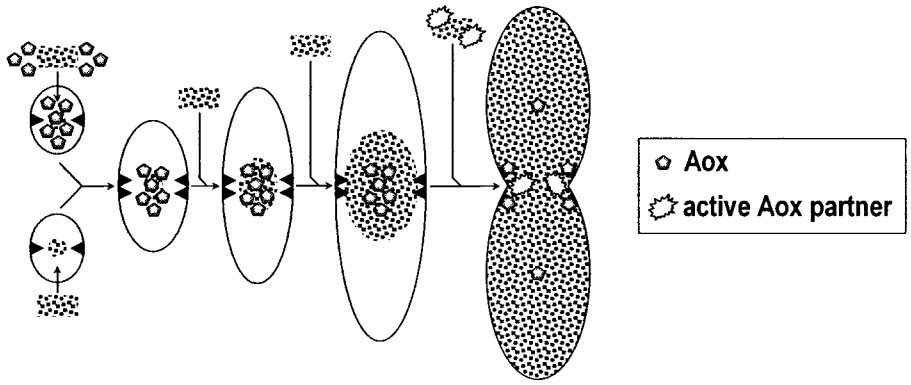


**Figure 2.5.** Third possible molecular mechanism underlying the relocation of Aox from the matrix to the membrane within mature peroxisomes P6. A specific matrix protein rather than protein mass in the peroxisomal matrix initiates the relocation of Aox from the matrix to the membrane. This specific matrix protein is imported to the peroxisome only during the last step of peroxisome maturation, during the conversion of P5 to P6.

specific matrix protein rather than protein mass in the peroxisomal matrix initiates the relocation of Aox; and 2) this specific matrix protein is imported to the peroxisome only during the last step of peroxisome maturation, during the conversion of P5 to P6 (Figure 2.5). The data presented in this chapter provide comprehensive evidence that the relocation of Aox from the matrix to the membrane of P6 is due to an increase in the total mass of matrix proteins above a critical level and that it is not promoted by the interaction of Aox with any specific matrix protein. Moreover, the findings that I describe in this chapter clearly demonstrate that the interaction between Pex16p and Aox results in an intraperoxisomal signalling cascade that activates the biosynthesis and transbilayer movement of a distinct set of membrane lipids. The change in the lipid content of the peroxisomal membrane is followed by the assembly of a multicomponent protein complex on the surface of the mature peroxisome, P6. The protein complex that forms

carries out membrane fission and completes the process of peroxisome division.

## 2.3 Materials and Methods

### Strains, media and reagents

The *Y. lipolytica* wild-type strain *P01d* [164], the mutant strains *pex2Δ* [64], *pex19Δ* [165], *pex16Δ* and *PEX16-TH* [126], the single *AOX* gene knock-out strains [164], and the media, growth conditions and genetic techniques for *Y. lipolytica* [48] have been previously described. Targeted integrative disruption of the *ABP1*, *DPP1*, *PEX10*, *SLA1*, *SLC1* and *VPS1* genes was performed with the *URA3* gene of *Y. lipolytica*, using a previously described modification of the sticky-end polymerase chain reaction procedure [164]. Antibodies to Pex2p [64], Pex16p [48], Pex19p [165] and thiolase [50] have been previously described. Monospecific antibodies to Dpp1p, Pex10p, Slc1p and Vps1p were raised in rabbit against their peptides GAPRPDMLARCRPMSWMRP, CRQGVREQNLLPIR, GRIFPQYCSVTAKKALKWYP and MDKELISTVNKLQDALA, respectively. Purification of the DAG-binding C1b domain of protein kinase C [166] and its labeling with the fluorophore Alexa Fluor 488 [167] were performed as described previously. SDS-PAGE and immunoblotting [48] were performed as described. Cholic acid (sodium salt), ergosterol, hydroxylapatite, n-octyl-ß-D-glucopyranoside, palmitoyl-CoA agarose, and Triton X-100 were purchased from Sigma-Aldrich Canada Ltd. PIP-Strips were from Echelon Biosciences. Alexa Fluor 488 signal-amplification kit for fluorescein-conjugated probes was purchased from Molecular Probes. Monoclonal anti-phosphatidylserine antibody was purchased from Upstate USA.

Fluorescein-conjugated goat anti-rabbit IgG antibodies and fluorescein-conjugated goat anti-mouse IgM antibodies were from Jackson ImmunoResearch Laboratories. N-palmitoyl-D-*erythro*-sphingosine (ceramide), 1,2-dioleoyl-*sn*-glycerol (diacylglycerol), 1,2-dioleoyl-*sn*-glycero-3-phosphate (phosphatidic acid), 1,2-dioleoyl-*sn*-glycero-3-phosphocholine (phosphatidylcholine), 1-oleoyl-2-hydroxy-*sn*-glycero-3-phosphate (lysophosphosphatidic acid), 1,2-dioleoyl-*sn*-glycero-3-phosphoethanolamine (phosphatidylethanolamine), L-$\alpha$-phosphatidylinositol (phosphatidylinositol), and 1,2-dioleoyl-*sn*-glycero-3-[phospho-L-serine] (phosphatidylserine) were from Avanti Polar Lipids. [$C^{14}$]-labeled lipids, HiTrap Blue HP, Resource Q, Resource S, and Superose 12 were from GE Healthcare.

**Subcellular fractionation and isolation of organelles**

The initial step in the subcellular fractionation of oleic acid-grown cells included the differential centrifugation of lysed and homogenized spheroplasts at 1,000 × g for 10 min at 4°C in a JS13.1 rotor (Beckman) to yield a postnuclear supernatant (PNS) fraction. The PNS fraction was further subjected to differential centrifugation at 20,000 × g for 30 min at 4°C in a JS13.1 rotor (Beckman) to yield pellet (20KgP) and supernatant (20KgS) fractions. The 20KgS fraction was further subfractionated by differential centrifugation at 200,000 × g for 1 h at 4°C in a TLA110 rotor (Beckman) to yield pellet (200KgP) and supernatant (200KgS) fractions. To purify immature peroxisomal vesicles P1 to P5, the

200KgP subcellular fraction was subjected to centrifugation on a discontinuous sucrose (18, 25, 30, 35, 40, and 53%, wt/wt) gradient at 120,000 × g for 18 h at 4°C in a SW28 rotor (Beckman). 36 fractions of 1 ml each were collected. Different subforms of immature peroxisomal vesicles peaked at densities of 1.18 g/cm$^3$ (fraction 5, P5), 1.14 g/cm$^3$ (fraction 15, P3 + P4), 1.11 g/cm$^3$ (fraction 23, P1), and 1.09 g/cm$^3$ (fraction 30, P2) were recovered [46]. The peak fractions containing immature peroxisomal vesicles P1, P2, P3 + P4 and P5 were recovered, and 4 vol of 0.5 M sucrose in buffer H (5 mM MES, pH 5.5, 1 mM KCl, 0.5 mM EDTA, 0.1% ethanol, 1 × protease inhibitor cocktail [PIC] [46] were added to each of them. Peroxisomes were pelleted onto a 150-µl cushion of 2 M sucrose in buffer H by centrifugation at 200,000 × g for 20 min at 4°C in a TLA110 rotor (Beckman). Individual pellets of different subforms of immature peroxisomal vesicles were resuspended in 3 ml of 50% (wt/wt) sucrose in buffer H.

For purification of immature peroxisomal vesicles P1 and P2, pellets of P1 and P2 resuspended in 50% (wt/wt) sucrose in buffer H were overlaid with 30, 28, 26, 24, 22, and 10% sucrose (all wt/wt in buffer H). After centrifugation at 120,000 × g for 18 h at 4°C in a SW28 rotor (Beckman), 18 fractions of 2 ml each were collected. P1 and P2 were pelleted, resuspended and subjected to a second flotation on the same multistep sucrose gradient. Gradients were fractionated into 2-ml fractions as above, and P1 and P2 were recovered [46] and used for biochemical analyses.

For purification of immature peroxisomal vesicles P3 and P4, pellets of P3 and P4 resuspended in 50% (wt/wt) sucrose in buffer H were overlaid with 38%, 35%, 33% and

20% sucrose (all wt/wt in buffer H). After centrifugation at 120,000 × g for 18 h at 4°C in a SW28 rotor (Beckman), 18 fractions of 2 ml each were collected. P3 and P4 were pelleted, resuspended in 3 ml of 50% (wt/wt) sucrose in buffer HE (20 mM MES, pH 5.5, 20 mM EDTA, 0.1% ethanol), overlaid with 39, 37, 35, 33, and 20% sucrose (all wt/wt in buffer HE), and subjected to centrifugation as above. Gradients were fractionated into 2-ml fractions, and P3 and P4 were recovered and pelleted. After resuspension in 3 ml of 50% (wt/wt) sucrose in buffer H, P3 and P4 were again subjected to flotation on the second multistep sucrose gradient described above. Gradients were fractionated into 2-ml fractions, and P3 and P4 were recovered [46] and used for biochemical analyses.

Highly purified mature peroxisomes P6 were isolated from the 20 KgP subcellular fraction by isopycnic centrifugation on a discontinuous sucrose gradient as described previously [64]. 4 vol of 0.5 M sucrose in buffer H were added to the peak peroxisomal fraction 4 recovered after isopycnic centrifugation on a discontinuous sucrose gradient. Peroxisomes were sedimented through a 150-µl cushion of 2 M sucrose in buffer H by centrifugation at 200,000 × g for 20 min at 4°C in a TLA110 rotor (Beckman). The resultant pellet of mature peroxisomes P6 was resuspended in buffer H containing 1 M sorbitol and was subjected to further centrifugation on a linear 20-60% (wt/wt) sucrose gradient (in buffer H) at 197,000 × g for 18 h at 4°C in a SW41Ti rotor (Beckman). Peak peroxisomal fraction 5 equilibrating at a density of 1.21 g/cm$^3$ was recovered, and peroxisomes were sedimented through a 150-µl cushion of 2 M sucrose in buffer H by centrifugation at 200,000 × g for 20 min at 4°C in a TLA110 rotor (Beckman). Pellet of

mature peroxisomes P6 was resuspended in 55% (wt/wt) sucrose in buffer H, overlaid with 50, 45, 40, 30, and 20% sucrose (all wt/wt in buffer H), and subjected to centrifugation at 120,000 × g for 18 h at 4°C in a SW28 rotor (Beckman). 18 gradient fractions of 2 ml each were collected. Peak peroxisomal fraction 11 equilibrating at a density of 1.21 g/cm$^3$ was recovered [64] and used for biochemical analyses.

The free form of the ER [64] and the P3- and P4-associated subcompartment of the ER [46] were purified from *Y. lipolytica* cells as described previously. Subcellular fractionation of *S. cerevisiae* cells grown in glucose-containing YEPD medium and isolation of functional ER membranes were performed according to established procedures [168].

**Peroxisome subfractionation and extraction**

Highly purified peroxisomes were lysed by addition of 10 vol of ice-cold LB buffer (20 mM HEPES-KOH, pH 8.0, 50 mM NaCl, and 1 × protease inhibitor cocktail [PIC] [48], followed by incubation on ice for 30 min with occasional agitation. The suspension was centrifuged at 200,000 × g for 20 min at 4°C in a TLA110 rotor (Beckman). The pellet of membranes recovered after centrifugation of osmotically lysed peroxisomes was resuspended in ice-cold EB buffer (10 mM HEPES-KOH, pH 8.0, 5 mM EDTA, and 1 × protease inhibitor cocktail [PIC] [48] to a final concentration of 1.0 mg/ml. Equal aliquots of the suspension of membranes were then exposed to 1 M NaCl, 0.1 M $Na_2CO_3$,

pH 11.0, or 0.5% (vol/vol) Triton X-100 [48]. After incubation on ice for 30 min with occasional agitation, the samples were subjected to centrifugation at 100,000 × g for 30 min at 4°C in a TLA110 rotor (Beckman). Equal portions of the pellet and supernatant fractions were analyzed by SDS-PAGE, followed by immunoblotting.

**Protease protection analysis**

The pellet of highly purified mature peroxisomes was gently resuspended in ice-cold PPB buffer (5 mM MES, pH 5.5, 1 M sorbitol, 1 mM KCl, and 0.5 mM EDTA). Equal aliquots (10 or 20 μg of total protein) of these peroxisomes were incubated with 0, 5, 10 or 50 μg of trypsin for 30 min on ice, either in the presence or absence of Triton X-100 at 0.5% (vol/vol) final concentration. The reaction was terminated by addition of trichloroacetic acid to 10% final concentration. The protein precipitates were washed with ice-cold 80% (vol/vol) acetone, and equivalent fractions of each reaction were subjected to SDS-PAGE and immunoblotting.

**Lipid analyses**

Highly purified peroxisomes were lysed by addition of 10 vol of ice-cold LB buffer (20 mM HEPES-KOH, pH 8.0, 50 mM NaCl, and 1 × protease inhibitor cocktail [PIC] [48], followed by incubation on ice for 30 min with occasional agitation. The suspension was centrifuged at 200,000 × g for 20 min at 4°C in a TLA110 rotor (Beckman). For extraction of membrane lipids, the pellet of membranes recovered after centrifugation of osmotically lysed peroxisomes and contained 1 mg of membrane protein was

resuspended in 1.0 ml of chloroform/methanol (1:1, v/v). After incubation on ice for 15 min with occasional agitation, samples were subjected to centrifugation at 20,000 × g for 15 min at 4°C. The chloroform phase was separated and dried under nitrogen. The lipid film was dissolved in 100 µl of chloroform (for the analysis of diacylglycerol, ergosterol and ceramide) or 100 µl of chloroform/methanol (1:1, v/v) (for the analysis of phosphatidylethanolamine, phosphatidic acid, phosphatidylcholine, phosphatidylinositol, phosphatidylserine, and lysophosphosphatidic acid). 25 µl of each sample were spotted on 60Å silica gel plates for thin-layer chromatography (TLC) (Whatman). The lipids were developed in the following solvent systems: chloroform/acetone (4.6:0.4, v/v) (for the analysis of diacylglycerol, ergosterol and ceramide) and chloroform/methanol/water (65:25:4, v/v) (for the analysis of phosphatidylethanolamine, phosphatidic acid, phosphatidylcholine, phosphatidylinositol, phosphatidylserine, and lysophosphatidic acid). All lipids were detected using 5% phosphomolybdic acid in ethanol and visualized by heating for 30 min at 110°C. Lipids were quantitated by densitometric analysis of TLC plates as described previously [169], using lipid standards in the 0.1-0.5 µg range for calibration.

For monitoring enzymatic activities of LPAAT and PAP, highly purified peroxisomes were lysed by addition of 10 vol of ice-cold LB buffer (20 mM HEPES-KOH, pH 8.0, 50 mM NaCl, and 1 × protease inhibitor cocktail [PIC] [48], followed by incubation on ice for 30 min with occasional agitation. The suspension was centrifuged at 200,000 × g for 20 min at 4°C in a TLA110 rotor (Beckman). The pellet of membranes recovered after centrifugation of osmotically lysed peroxisomes was resuspended in ice-

cold buffer R (20 mM MES-KOH, pH 6.0, 150 mM NaCl, 5 mM DTT, 10% glycerol) containing 1% (w/v) n-octyl-β-D-glucopyranoside (OG). After incubation on ice for 20 min with occasional agitation, the sample of detergent-solubilized peroxisomal membrane proteins (PMPs) was subjected to centrifugation at 100,000 × g for 20 min at 4°C in a TLA110 rotor. The resulting supernatant of solubilized PMPs was depleted of Pex16p by immunoaffinity chromatography under native conditions using anti-Pex16p antibodies covalently linked to protein A-Sepharose [170]. For the reconstitution of peroxisomal liposomes carrying Pex16p, detergent-solubilized PMPs immunodepleted of Pex16p were supplemented with Pex16p, which was purified from membranes of osmotically lysed immature peroxisomal vesicles P1 by immunoaffinity chromatography under native conditions using anti-Pex16p antibodies covalently linked to protein A-Sepharose [170]. After elution with buffer E (20 mM HEPES-KOH, pH 7.5, 250 mM $MgCl_2$, 5 mM DTT, 10% glycerol) containing 1% (w/v) OG, purified Pex16p was dialyzed against buffer R supplemented with 1% (w/v) OG. For the reconstitution of peroxisomal liposomes lacking Pex16p, detergent-solubilized PMPs immunodepleted of Pex16p were supplemented only with buffer R containing 1% (w/v) OG. Detergent-solubilized PMPs immunodepleted of Pex16p and either supplemented or not supplemented with purified Pex16p in buffer R containing 1% (w/v) OG were then added to the films of unlabeled lipids, which were initially extracted from the membranes of highly purified peroxisomes using chloroform/methanol (1:1, v/v) and then dried down by a gentle stream of nitrogen. The lipid films were dissolved by gentle agitation for 20 min at room temperature. For monitoring LPAAT activity, the unlabeled lipids, which

were extracted from the membranes of highly purified peroxisomes using chloroform/methanol (1:1, v/v), were supplemented with [$^{14}$C]-labeled lysophosphatidic acid and unlabeled oleoyl-CoA (a co-substrate of LPAAT) dissolved in chloroform/methanol (1:1, v/v). The mix of unlabeled membrane lipids and [$^{14}$C]-labeled lysophosphatidic acid was then dried down by a gentle stream of nitrogen. For monitoring PAP activity, the unlabeled lipids, which were extracted from the membranes of highly purified peroxisomes using chloroform/methanol (1:1, v/v), were supplemented with [$^{14}$C]-labeled phosphatidic acid dissolved in chloroform/methanol (1:1, v/v). The mix of unlabeled membrane lipids and [$^{14}$C]-labeled phosphatidic acid was then dried down by a gentle stream of nitrogen. For evaluating the positive effect of phosphatidylcholine on LPAAT and PAP, equal aliquots of unlabeled lipids extracted from the membranes of highly purified peroxisomes using chloroform/methanol (1:1, v/v) were first mixed with an appropriate [$^{14}$C]-labeled lipid substrate of LPAAT or PAP in chloroform/methanol (1:1, v/v) and were then supplemented with various quantities of phosphatidylcholine dissolved in chloroform/methanol (1:1, v/v). The mix of unlabeled membrane lipids, a [$^{14}$C]-labeled lipid substrate, and unlabeled phosphatidylcholine was then dried down by a gentle stream of nitrogen. The lipid films were finally dissolved by gentle agitation for 20 min at room temperature in buffer R containing detergent-solubilized PMPs, immunodepleted or not immunodepleted of Pex16p, in 1% (w/v) OG. To dilute the detergent OG below its critical micellar concentration, thereby promoting the formation of peroxisomal liposomes, 3 volumes of buffer D (20 mM MES-KOH, pH 6.0, 150 mM NaCl) were added to the mixture of detergent-solubilized PMPs and

membrane lipids dissolved in buffer R containing 1% (w/v) OG. To remove the detergent, the samples were dialyzed in a Tube-O-Dialyzer (7.5-kD cutoff) (Chemicon) against buffer D containing 0.1% Biobeads SM2 (Bio-Rad). After overnight dialysis at 4°C, samples were transferred to the bottom of ultraclear centrifuge tubes (Beckman) and supplemented with 4 volumes of 65% (w/w) sucrose in buffer D in order to adjust the sucrose concentration of the samples to 52% (w/w). Samples were overlaid with 40% and then with 20% sucrose (both w/w in buffer D) and lastly with buffer D alone. After centrifugation at 200,000 × g for 18 h at 4°C in a SW50.1 rotor (Beckman), 18 fractions of 275 µl each were collected. Peroxisomal liposomes were recovered at the 40%/20% sucrose interface. The recovered peroxisomal liposomes were transferred from ice to 26°C. Samples were taken at the indicated times after the transfer. Lipids were extracted from the membrane and analyzed by TLC. To calculate the initial rates of the LPAAT and PAP reactions, the [$^{14}$C]-labeled lysophosphatidic acid, phosphatidic acid and diacylglycerol were separated by TLC and quantified by autoradiography.

To evaluate the transbilayer distribution of DAG and PS in the membrane bilayers of different peroxisomal subforms, the suspension of highly purified peroxisomes in ice-cold H250S buffer (5 mM MES-KOH, pH 5.5, 250 mM sorbitol, 1 mM KCl, 0.5 mM EDTA, 1 × protease inhibitor cocktail [PIC] [48] at 1 mg protein/ml was divided into two equal aliquots. One aliquot remained untreated, whereas peroxisomal vesicles in the other aliquot were lysed by addition of 10 vol of ice-cold LB buffer (20 mM HEPES-KOH, pH 8.0, 50 mM NaCl, and 1 × protease inhibitor cocktail [PIC] [48], followed by incubation on ice for 30 min with occasional agitation. The suspension of lysed

peroxisomes was divided into two equal aliquots. One aliquot was dialyzed in a Tube-O-Dialyzer (7.5-kD cutoff) (Chemicon) against buffer MR (10 mM MES/KOH, pH 5.5, 1 mM KCl, and 0.5 mM EDTA) containing 250 mM sorbitol. The suspension of lysed peroxisomes in the other aliquot was dialyzed in a Tube-O-Dialyzer (7.5-kD cutoff) (Chemicon) against buffer HR (10 mM HEPES/KOH, pH 7.5, 1 mM KCl, and 0.5 mM EDTA) containing 250 mM sorbitol. After overnight dialysis at 4°C, resealed peroxisomes RPA that were formed in the aliquot dialyzed against buffer MR containing 250 mM sorbitol and resealed peroxisomes RPB that were formed in the aliquot dialyzed against buffer HR containing 250 mM sorbitol were pelleted onto a 150-µl cushion of 2 M sucrose in buffer MR or HR, respectively, by centrifugation at 100,000 × g for 20 min at 4°C in a TLA110 rotor (Beckman). Individual pellets of RPA and RPB were resuspended in 500 µl of 50% (wt/wt) sucrose in buffer MR or HR, respectively. The sample containing RPA was overlaid with 1.5 ml of 45% sucrose, 1 ml of 40% sucrose, 1 ml of 25% sucrose, and 1 ml of 10% sucrose (all wt/wt in buffer MR). The sample containing RPB was overlaid with 1.5 ml of 45% sucrose, 1 ml of 40% sucrose, 1 ml of 25% sucrose, and 1 ml of 10% sucrose (all wt/wt in buffer HR). Both samples were subjected to centrifugation at 200,000 × g for 18 h at 4°C in a SW50.1 rotor (Beckman). 9 fractions of 555 µl each were collected. Resealed peroxisomes RPA and RPB floated to low density during centrifugation in the sucrose density gradient. Proteins from equal volumes of gradient fractions were analyzed by immunoblotting with antibodies to Pex16p and Pex19p. Equal volumes of gradient fractions were also subjected to lipid extraction, which was followed by TLC and visualization of lipids.

Resealed peroxisomes RPA and RPB, which were recovered in the peak fractions of the flotation gradients, and a highly purified subform of the intact peroxisomes from which these two types of resealed peroxisomes were formed, were used to evaluate the orientation in which the membranes delimiting RPA and RPB were resealed. RPA and RPB were pelleted onto a 150-µl cushion of 2 M sucrose in buffer MR or HR, respectively, by centrifugation at 100,000 × g for 20 min at 4°C in a TLA110 rotor (Beckman). Intact peroxisomes were pelleted onto a 150-µl cushion of 2 M sucrose in buffer H (5 mM MES, pH 5.5, 1 mM KCl, 0.5 mM EDTA, 0.1% ethanol, 1 × protease inhibitor cocktail [PIC] [48] by centrifugation at 100,000 × g for 20 min at 4°C in a TLA110 rotor (Beckman). Individual pellets of RPA, RPB and intact peroxisomes were resuspended in ice-cold buffer H at 1 mg protein/ml. Serial dilutions of RPA, RPB and intact peroxisomes in the range of 10-50 µg protein/ml were made in ice-cold buffer H. Anti-Pex16p rabbit IgG or anti-Pex19p rabbit IgG were added to concentrations 4 and 5 µg/ml, respectively. After incubation for 30 min on ice, samples were subjected to centrifugation at 100,000 × g for 10 min at 4°C in a TLA110 rotor (Beckman). The pellets were resuspended in 200 µl of ice-cold buffer H and supplemented with fluorescein-conjugated goat anti-rabbit IgG. After incubation for 30 min on ice, samples were subjected to centrifugation at 100,000 × g for 10 min at 4°C in a TLA110 rotor (Beckman). The pellets were resuspended in 200 µl of ice-cold buffer H and supplemented with Alexa Fluor 488 goat anti-fluorescein/Oregon Green IgG at 15 µg/ml. Following incubation for 30 min on ice, samples were subjected to centrifugation at 100,000 × g for 10 min at 4°C in a TLA110 rotor (Beckman). The pellets were

resuspended in 200 µl of ice-cold buffer H and supplemented with Alexa Fluor 488 chicken anti-goat IgG at 20 µg/ml. After incubation for 30 min on ice, samples were subjected to centrifugation at 100,000 × g for 10 min at 4°C in a TLA110 rotor (Beckman). The pellets were resuspended in 200 µl of ice-cold buffer H and placed into the wells of a 96-well microplate. The fluorescence of samples was measured using the Wallac Victor 2 Multi-label microplate fluorescence reader with filters set at 485 (+/- 7.5) nm (excitation) and 510 (+/- 5) nm (emission). Controls were made for each dilution of RPA, RPB and intact peroxisomes. The controls included normal rabbit IgG at 4 or 5 µg/ml added instead of anti-Pex16p rabbit IgG or anti-Pex19p rabbit IgG, respectively. Background fluorescence, which was due to the nonspecific binding of rabbit IgG and/or fluorescein- or Alexa Fluor 488-labeled antibodies to the peroxisomal membrane, was subtracted.

In intact peroxisomes, Pex19p is a peripheral membrane protein that resides on the outer (cytosolic) face of the peroxisome [51]. Because this protein is attached to the surface of intact peroxisomes, it is accessible to anti-Pex19p IgG exogenously added to these peroxisomes [51]. Importantly, the membranes of intact peroxisomes RPA and RPB are not permeable to the exogenously added IgG molecules. In fact, none of Pex16p, a peripheral membrane protein residing on the inner (lumenal) face of the peroxisome, in intact peroxisomes and only a minor portion of this protein in RPA was accessible to anti-Pex16p IgG [51]. The observed accessibility of the RPB-associated form of Pex16p to anti-Pex16p IgG was due to the inside-out orientation of the membrane delimiting most of the RPB species formed during peroxisome resealing. In addition, although the

levels of Pex19p, a peripheral membrane protein residing on the peroxisomal surface, in intact peroxisomes, RPA and RPB were very similar to each other [51], only a minor portion of Pex19p in the mostly inside out-oriented RPB species was accessible to anti-Pex19p IgG [51]. Altogether, these findings imply that, if the ratio "fluorescence for RPA ($F_{RPA}$)/fluorescence for intact peroxisomes ($F_{IP}$)" or "fluorescence for RPB ($F_{RPB}$)/fluorescence for intact peroxisomes ($F_{IP}$)" is calculated for Pex19p, it is equal to the fraction of the total pool of Pex19p that resides on the outer (cytosolic) face of those RPA or RPB species whose delimiting membranes acquired the outside-out orientation during their resealing. At the same time, the ratio "($F_{IP}$ - $F_{RPA}$)/$F_{IP}$" or "($F_{IP}$ - $F_{RPB}$)/$F_{IP}$", if calculated for Pex19p, equals the fraction of Pex19p that resides on the inner (lumenal) face of those RPA or RPB species whose delimiting membranes acquired the inside-out orientation during their resealing. Hence, the ratio "$F_{RPA}/F_{IP}$" or "$F_{RPB}/F_{IP}$" for Pex19p is equal to the fraction of those RPA or RPB species that are present in the outside-out orientation ($n^{oo}_{RPA}$ and $n^{oo}_{RPB}$, respectively). Moreover, the ratio "($F_{IP}$ - $F_{RPA}$)/$F_{IP}$" or "($F_{IP}$ - $F_{RPB}$)/$F_{IP}$" for Pex19p equals the fraction of those RPA or RPB species that were resealed in the inside-out orientation ($n^{io}_{RPA}$ and $n^{io}_{RPB}$, respectively).

Resealed peroxisomes RPA and RPB, which were recovered in the peak fractions of the flotation gradients, and a highly purified subform of the intact peroxisomes from which these two types of resealed peroxisomes were formed, were used to calculate the percentage of DAG and PS residing in the cytosolic and lumenal leaflets of the membrane bilayers in different peroxisomal subforms. RPA and RPB were pelleted onto a 150-µl cushion of 2 M sucrose in buffer MR or HR, respectively, by centrifugation at

100,000 × g for 20 min at 4°C in a TLA110 rotor (Beckman). Intact peroxisomes were pelleted onto a 150-µl cushion of 2 M sucrose in buffer H (5 mM MES, pH 5.5, 1 mM KCl, 0.5 mM EDTA, 0.1% ethanol, 1 × protease inhibitor cocktail [PIC] [48] by centrifugation at 100,000 × g for 20 min at 4°C in a TLA110 rotor (Beckman). Individual pellets of RPA, RPB and intact peroxisomes were resuspended in ice-cold buffer H at 1 mg protein/ml. Serial dilutions of RPA, RPB and intact peroxisomes in the range of 10-50 µg protein/ml were made in ice-cold buffer H. The DAG-binding C1b domain of protein kinase C labeled with the fluorophore Alexa Fluor 488 or anti-PS mouse IgM were added to concentrations 5 and 1 µg/ml, respectively. After incubation for 30 min on ice, samples were subjected to centrifugation at 100,000 × g for 10 min at 4°C in a TLA110 rotor (Beckman). For samples that were exposed to Alexa Fluor 488-tagged C1b domain, the pellets were resuspended in 200 µl of ice-cold buffer H and placed into the wells of a 96-well microplate. The fluorescence of these samples was measured using the Wallac Victor 2 Multi-label microplate fluorescence reader with filters set at 485 (+/- 7.5) nm (excitation) and 510 (+/- 5) nm (emission). Controls for monitoring DAG were made for each dilution of intact peroxisomes P5 and P6 and of the P5- and P6-based RPA and RPB, all of which contained DAG [51]. The controls included the corresponding dilutions of intact peroxisomes P4 and of the P4-based RPA and RPB, all of which did not contain DAG [51]. Background fluorescence, which was due to the nonspecific binding of Alexa Fluor 488-tagged C1b domain to the peroxisomal membrane, was subtracted. For samples that were exposed to anti-PS mouse IgM, the pellets were resuspended in 200 µl of ice-cold buffer H and supplemented with fluorescein-conjugated

goat anti-mouse IgM antibodies at 5 μg/ml. After incubation for 30 min on ice, samples were subjected to centrifugation at 100,000 × g for 10 min at 4°C in a TLA110 rotor (Beckman). The pellets were resuspended in 200 μl of ice-cold buffer H and supplemented with Alexa Fluor 488 rabbit anti-fluorescein/Oregon Green IgG at 15 μg/ml. Following incubation for 30 min on ice, samples were subjected to centrifugation at 100,000 × g for 10 min at 4°C in a TLA110 rotor (Beckman). The pellets were resuspended in 200 μl of ice-cold buffer H and supplemented with Alexa Fluor 488 goat anti-rabbit IgG at 20 μg/ml. After incubation for 30 min on ice, samples were subjected to centrifugation at 100,000 × g for 10 min at 4°C in a TLA110 rotor (Beckman). The pellets were resuspended in 200 μl of ice-cold buffer H and placed into the wells of a 96-well microplate. The fluorescence of samples was measured using the Wallac Victor 2 Multi-label microplate fluorescence reader with filters set at 485 (+/- 7.5) nm (excitation) and 510 (+/- 5) nm (emission). Controls were made for each dilution of RPA, RPB and intact peroxisomes. The controls included normal mouse IgM at 1 μg/ml added instead of anti-PS mouse IgM. Background fluorescence, which was due to the non-specific binding of mouse IgM and/or fluorescein- or Alexa Fluor 488-labeled antibodies to the peroxisomal membrane, was subtracted.

The fraction of a monitored lipid, either DAG or PS, residing in the cytosolic leaflet of the membrane bilayer of the intact peroxisome can be calculated as:

$$F_{IP}/(F_{IP} + F_{IL}), \quad (1)$$

where $F_{IP}$ is the fluorescence of a lipid-specific fluorescent probe specifically bound to

intact peroxisomes or to the species of RPA and RPB that are present in the outside-out orientation. In equation 1, $F_{IP}$ equals the fluorescence of this probe specifically bound to the outer (cytosolic) leaflet of the peroxisomal membrane bilayer delimiting intact peroxisomes or those species of RPA and RPB that were resealed in the outside-out orientation. Furthermore, $F_{IL}$ in equation 1 is the fluorescence of a lipid-specific fluorescent reporter molecule that would, if it could, bind specifically to the inner (lumenal) leaflet of the peroxisomal membrane bilayer delimiting intact peroxisomes. $F_{IL}$ can be monitored by measuring the fluorescence of this reporter molecule bound to the surface of those species of RPA and RPB that were resealed in the inside-out orientation.

The value of $F_{RPA}$, the fluorescence of a lipid-specific fluorescent reporter molecule specifically bound to the surface of RPA, can be calculated as:

$$F_{RPA} = (n^{oo}_{RPA} \times F_{IP}) + (n^{io}_{RPA} \times F_{IL}), (2)$$

where $n^{oo}_{RPA}$ is the fraction of the RPA species that are present in the outside-out orientation. The value of $n^{oo}_{RPA}$ for each of the outside out-oriented species of RPA formed during resealing of osmotically lysed peroxisomal subforms P1 to P6 was calculated for a Pex19p-specific fluorescent reporter molecule as described above. In equation 2, the value of $n^{io}_{RPA}$ for each of the inside out-oriented species of RPA formed during resealing of osmotically lysed peroxisomal subforms P1 to P6 was calculated for a Pex19p-specific fluorescent reporter molecule as described above. Based on equation 2, $F_{IL}$ can be calculated as:

$$F_{IL} = \frac{F_{RPA} - (n^{oo}_{RPA} \times F_{IP})}{n^{io}_{RPA}} \quad (3)$$

The value of $F_{RPB}$, the fluorescence of a lipid-specific fluorescent reporter molecule specifically bound to the surface of RPB, can be calculated as:

$$F_{RPB} = (n^{oo}_{RPB} \times F_{IP}) + (n^{io}_{RPB} \times F_{IL}), \quad (4)$$

where $n^{oo}_{RPB}$ is the fraction of the RPB species that are present in the outside-out orientation. The value of $n^{oo}_{RPB}$ for each of the outside out-oriented species of RPB formed during resealing of osmotically lysed peroxisomal subforms P1 to P6 was calculated for a Pex19p-specific fluorescent reporter molecule as described above. In equation 4, the value of $n^{io}_{RPB}$ for each of the inside out-oriented species of RPB formed during resealing of osmotically lysed peroxisomal subforms P1 to P6 was calculated for a Pex19p-specific fluorescent reporter molecule as described above. Based on equation 4, $F_{IL}$ can be calculated as:

$$F_{IL} = \frac{F_{RPB} - (n^{oo}_{RPB} \times F_{IP})}{n^{io}_{RPB}} \quad (5)$$

Based on equation 3, equation 1 for calculating the fraction of a monitored lipid, either DAG or PS, residing in the cytosolic leaflet of the membrane bilayer of the intact peroxisome can be rewritten as:

$$\frac{F_{IP}}{F_{RPA} - (n^{oo}_{RPA} \times F_{IP})} \quad (6).$$
$$F_{IP} + \frac{}{n^{io}_{RPA}}$$

Furthermore, based on equation 5, equation 1 for calculating the fraction of a monitored lipid, either DAG or PS, residing in the cytosolic leaflet of the membrane bilayer of the intact peroxisome can be also rewritten as:

$$\frac{F_{IP}}{F_{RPB} - (n^{oo}_{RPB} \times F_{IP})} \quad (7).$$
$$F_{IP} + \frac{}{n^{io}_{RPB}}$$

For each of the intact peroxisomal subforms P1 to P6, equations 6 and 7 were used for calculating the fraction of a monitored lipid, either DAG or PS, residing in the cytosolic leaflet of the membrane bilayer.

**Protein-lipid overlay assay**

To evaluate the lipid-binding specificity of Pex16p, the pellet of membranes recovered after centrifugation of osmotically lysed peroxisomes was resuspended in buffer TBSO (10 mM Tris-HCl, pH 8.0, 150 mM NaCl, 0.5% n-OG) and incubated for 30 min on ice. Samples were subjected to centrifugation at 100,000 × g for 30 min at 4°C in TLA110 rotor (Beckman). Under these conditions, n-OG completely solubilized the vast majority of all membrane proteins [171]. The supernatants of n-OG-solubilized proteins were then incubated at 5 μg/ml with the PIP-Strips (Echelon Biosciences) at 4°C overnight. After washing the PIP-Strip five times for 5 min each with TBSO, Pex16p was detected by immunoblotting with anti-Pex16p antibodies.

## Chemical cross-linking and immunoprecipitation under denaturing conditions

Highly purified mature peroxisomes of wild-type and mutant strains were osmotically lysed by addition of 10 vol of ice-cold LCC buffer (20 mM sodium phosphate buffer, pH 7.5, and 150 mM NaCl), followed by incubation on ice for 30 min with occasional agitation. The suspension was centrifuged at 200,000 × g for 20 min at 4°C in a TLA110 rotor (Beckman). The pellet of membranes recovered after centrifugation of osmotically lysed peroxisomes was resuspended in ice-cold LCC buffer to a final concentration of 0.5 mg/ml. Cross-linking with the thiol-cleavable cross-linker dithiobis (succinimidylpropionate) (DSP) (Pierce Chemical Co.) was initiated by the addition of cross-linker (50 mM stock in DMSO) and continued for 1 h at 4°C. Cross-linking was quenched by addition of 0.1 vol of 1 M Tris-HCl, pH 7.5, and incubation for 30 min at

4°C. SDS was added to 1.25%, and samples were warmed at 65°C for 20 min and then cooled to room temperature. 4 vol of 60 mM Tris-HCl, pH 7.4, 1.25% (vol/vol) Triton X-100, 190 mM NaCl, and 6 mM EDTA were added to the cooled samples, which were then cleared of any nonspecifically binding proteins by incubation for 20 min at 4°C with protein A-Sepharose washed five times with 10 mM Tris-HCl, pH 7.5. The cleared samples were then subjected to immunoprecipitation with anti-Vps1p, anti-Pex10p or anti-Pex19p antibodies under denaturing, nonreducing conditions. These antibodies were covalently linked to protein A-Sepharose as described previously [172]. Bound proteins were washed five times with 50 mM Tris-HCl, pH 7.5, 150 mM NaCl, 1% (v/v) Triton X-100, and eluted with 2% SDS at 95°C for 5 min. Eluted proteins were analyzed by SDS-PAGE under reducing conditions, *i.e.*, with DTT in the sample buffer, followed by silver staining.

For identifying proteins that interact with Vps1p or Pex19p in the cytosol, wild-type and mutant cells were subjected to subcellular fractionation (see above) to yield the 200S (cytosolic) fraction in buffer H (5 mM MES, pH 5.5, 1 mM KCl, 0.5 mM EDTA, 0.1% ethanol, 1 × protease inhibitor cocktail [PIC] [48] containing 1 M sorbitol. 9 vol of ice-cold LCC buffer (20 mM sodium phosphate buffer, pH 7.5, and 150 mM NaCl) were added to the recovered cytosolic fraction. Cross-linking with DSP was initiated by the addition of cross-linker (50 mM stock in DMSO) and continued for 1 h at 4°C. Cross-linking was quenched by addition of 0.1 vol of 1 M Tris-HCl, pH 7.5, and incubation for 30 min at 4°C. SDS was added to 1.25%, and samples were warmed at 65°C for 20 min and then cooled to room temperature. 4 vol of 60 mM Tris-HCl, pH 7.4, 1.25% (vol/vol)

Triton X-100, 190 mM NaCl, and 6 mM EDTA were added to the cooled samples, which were then cleared of any nonspecifically binding proteins by incubation for 20 min at 4°C with protein A-Sepharose washed five times with 10 mM Tris-HCl, pH 7.5. The cleared samples were then subjected to immunoprecipitation with anti-Vps1p or anti-Pex19p antibodies under denaturing, nonreducing conditions. These antibodies were covalently linked to protein A-Sepharose as described previously [172]. Bound proteins were washed five times with 50 mM Tris-HCl, pH 7.5, 150 mM NaCl, 1% (v/v) Triton X-100, and eluted with 2% SDS at 95°C for 5 min. Eluted proteins were analyzed by SDS-PAGE under reducing conditions, *i.e.*, with DTT in the sample buffer, followed by silver staining.

**Electron microscopy and morphometric analysis**

Whole cells were fixed in 1.5% $KMnO_4$ for 20 min at room temperature, dehydrated by successive incubations in increasing concentrations of ethanol, and embedded in Poly/Bed 812 epoxy resin (Polysciences). Ultrathin sections were cut using an Ultra-Cut E Microtome (Reichert-Jung). Silver/gold thin sections from the embedded blocks were examined in a JEOL JEM-2000FX transmission electron microscope. For morphometric analysis of random electron microscopic sections of cells, 12 × 14-cm prints and 8 × 10-cm negatives of 35-40 cell sections of each strain at 24,000-29,000 magnification were scanned and converted to digitized images with an HP ScanJet 4400c (Hewlett-Packard Co.) and Adobe Photoshop 6.0 software (Adobe Systems Inc.). Quantitation of digitized images was performed using the Discovery Series Quantity One 1-D Analysis Software

(Bio-Rad Laboratories). Relative area of peroxisome section (%) was calculated as "area of peroxisome section/area of cell section × 100". Peroxisomes were counted in electron micrographs, and data are expressed as the number of peroxisomes per $\mu m^3$ of cell section volume.

Resealed peroxisomes RPA and RPB floated to low density during centrifugation in a multistep sucrose density gradient. A 200-µl aliquot of the peak fraction of purified RPA in MR buffer (10 mM MES/KOH, pH 5.5, 1 mM KCl, and 0.5 mM EDTA) or a 200-µl aliquot of the peak fraction of purified RPB in HR buffer (10 mM HEPES/KOH, pH 7.5, 1 mM KCl, and 0.5 mM EDTA) was mixed with 400 µl of ice-cold 150 mM sodium cacodylate buffer, pH 7.2, containing 3% glutaraldehyde. Immediately after mixing the sample and glutaraldehyde solution, 600 µl of 2% $OsO_4$ in ice-cold CD buffer (100 mM sodium cacodylate, pH 7.2) was added. After a 2-h incubation on ice, the resealed peroxisomes RPA and RPB were sedimented at 100,000 × g for 20 min at 4°C in a Beckman TLS55 rotor (Beckman) onto a bed (25–50 µl) of hardened, low-melting 2.5% NuSieve GTG agarose (FMC). The pellet was postfixed in a solution of 1% $OsO_4$ plus 2.5% $K_2Cr_2O_7$ in ice-cold CD buffer for 2 h on ice. The pellet was then rinsed twice with ice-cold CD buffer and exposed to 0.05% tannic acid in the same buffer. After a 30-min incubation on ice, the pellet was washed once with ice-cold CD buffer and three times with water. The pellet was incubated overnight with 2% uranyl acetate in water at 4°C and then washed three times with water. After dehydration in a graded ethanol series, the fixed and stained sample was embedded in Poly/Bed 812 epoxy resin (Polysciences). Silver/gold thin sections from the embedded blocks were examined in a JEOL JEM-

2000FX transmission electron microscope.

**Immunoaffinity chromatography under native conditions**

Covalent coupling of affinity-purified antibodies to protein A-Sepharose for immunoaffinity chromatography was performed as described previously [47]. For immunoaffinity chromatography under native conditions, peroxisomal matrix proteins recovered in the supernatant fraction after centrifugation of osmotically lysed peroxisomes and peroxisomal liposomes were diluted with an equal volume of 50 mM Tris-HCl, pH 7.5, buffer containing 300 mM NaCl, 1% (v/v) Triton X-100 and protease inhibitor cocktail. The pellets of PMPs recovered after centrifugation of osmotically lysed peroxisomes and peroxisomal liposomes were resuspended in 25 mM Tris-HCl, pH 7.5, buffer containing 150 mM NaCl, 0.5% (v/v) Triton X-100 and protease inhibitor cocktail. Samples were cleared of any non-specifically binding proteins by incubation for 20 min at 4°C with protein A-Sepharose washed five times with 10 mM Tris-HCl, pH 7.5. The cleared samples were then subjected to immunoaffinity chromatography. Bound proteins were washed five times with 25 mM Tris-HCl, pH 7.5, 150 mM NaCl, 0.5% (v/v) Triton X-100, and eluted with 100 mM glycine, pH 2.8. Proteins were precipitated by addition of trichloroacetic acid to 10%, washed in ice-cold 80% (v/v) acetone, and then subjected to SDS-PAGE followed by immunoblotting.

**Reconstructing *in vitro* the relocation of Aox from the matrix to the membrane and its interaction with membrane-bound Pex16p using peroxisomal and non-peroxisomal proteins**

For preparing peroxisomal liposomes, the immature peroxisomal vesicles P1 to P5 and mature peroxisomes P6 were purified as described above. Peroxisomes were osmotically lysed by incubation on ice for 20 min in 20 mM HEPES-KOH buffer, pH 8.0, containing 50 mM NaCl and protease inhibitor cocktail. The lysate was subjected to centrifugation at 100,000 × *g* for 20 min at 4°C in a TLA110 rotor (Beckman) to yield a supernatant containing peroxisomal matrix proteins (including Aox) and a pellet of peroxisomal membrane proteins (PMPs). Matrix proteins were dialyzed against buffer R (20 mM MES-KOH, pH 6.0, 150 mM NaCl, 5 mM DTT, 10% glycerol) containing 1% (w/v) n-octyl-ß-D-glucopyranoside (OG). Immunoaffinity chromatography under native conditions (see the protocol described above) using anti-Aox1p antibodies covalently linked to protein A-Sepharose was used to deplete these peroxisomal matrix proteins of Aox. Aox complex for the reconstitution of peroxisomal liposomes was purified from the matrix of peroxisomes by immunoaffinity chromatography using anti-Aox3p antibodies covalently linked to protein A-Sepharose, as described above. After elution with buffer E (20 mM HEPES-KOH, pH 7.5, 250 mM $MgCl_2$, 5 mM DTT, 10% glycerol), purified Aox complex was dialyzed against buffer R containing 1% (w/v) OG. The pellet of PMPs recovered after centrifugation of osmotically lysed peroxisomes was resuspended in ice-cold buffer R containing 1% (w/v) OG. After incubation on ice for 20 min with occasional agitation, the sample of detergent-solubilized PMPs was subjected to

centrifugation at 100,000 × *g* for 20 min at 4°C in a TLA110 rotor. The resulting supernatant of solubilized PMPs was depleted of the Aox-Pex16p complex by immunoaffinity chromatography under native conditions (see the protocol described above) using anti-Aox1p antibodies covalently linked to protein A-Sepharose. Pex16p for the reconstitution of peroxisomal liposomes was purified, by immunoaffinity chromatography using anti-Pex16p antibodies covalently linked to protein A-Sepharose (as described above), from the pellet of PMPs recovered after centrifugation of osmotically lysed peroxisomes resuspended in ice-cold buffer R containing 1% (w/v) OG. After elution with buffer ER (20 mM HEPES-KOH, pH 7.5, 250 mM $MgCl_2$, 5 mM DTT, 10% glycerol, 1% (w/v) OG), purified Aox complex was dialyzed against buffer R containing 1% (w/v) OG.

Detergent-solubilized PMPs immunodepleted of the Aox-Pex16p complex and either supplemented or not supplemented with purified Pex16p were mixed with either dialyzed matrix proteins immunodepleted of Aox or dialyzed soluble non-peroxisomal proteins, as well as and with purified Aox complex. After incubation on ice for 20 min with occasional agitation, the mixture of peroxisomal matrix proteins (or of soluble non-peroxisomal proteins) and PMPs (all in buffer R containing 1% (w/v) OG) was added to the lipids extracted from the membrane of the corresponding peroxisomal subform and dried down by a gentle stream of nitrogen. The lipid film was dissolved by gentle agitation for 20 min at room temperature. To dilute the detergent OG below its critical micellar concentration, thereby promoting the formation of peroxisomal liposomes, 3 volumes of buffer D (20 mM MES-KOH, pH 6.0, 150 mM NaCl) were added to the

mixture of peroxisomal matrix proteins (or soluble non-peroxisomal proteins), detergent-solubilized PMPs and membrane lipids dissolved in buffer R containing 1% (w/v) OG. To remove the detergent, the samples were dialyzed in a Tube-O-Dialyzer (7.5-kD cutoff) (Chemicon) against buffer D containing 0.1% Biobeads SM2 (Bio-Rad). After overnight dialysis at 4°C, samples were transferred to the bottom of ultraclear centrifuge tubes (Beckman) and supplemented with 4 volumes of 65% (w/w) sucrose in buffer D in order to adjust the sucrose concentration of the samples to 52% (w/w). Samples were then overlaid with 40% and then with 20% sucrose (both w/w in buffer D) and lastly with buffer D alone. After centrifugation at 200,000 × *g* for 18 h at 4°C in a SW50.1 rotor (Beckman), 18 fractions of 275 µl each were collected. Peroxisomal liposomes were recovered at the 52%/40% sucrose interface.

**Mass spectrometry**

Proteins were resolved by SDS-PAGE and visualized by silver staining (Shevchenko et al., 1996). Protein bands were excised from the gel, reduced, alkylated and in-gel-digested with trypsin (Shevchenko et al., 1996). The proteins were identified by matrix-assisted laser desorption/ionization mass spectrometric peptide mapping (Jiménez et al., 1998), using a Micromass M@LDI time-of-flight mass spectrometer (Waters). Database searching using peptide masses was performed with the Mascot web-based search engine.

## 2.4 Results

### 2.4.1 Lipid composition of the peroxisomal membrane is changed during the last step of the assembly of the division-competent mature peroxisome

Thin layer chromatography revealed that, in wild-type cells, the levels of phosphatidic acid (PA) and diacylglycerol (DAG) increased in peroxisomal vesicles that were being converted from P5 to P6 (Figure 2.6). PA and DAG are cone-shaped lipids that can induce membrane fission during organelle division (Figure 2.1). As the levels of PA and DAG increased, the levels of lysophosphatidic acid (LPA) decreased during the conversion of P5 to P6 (Figure 2.6). LPA is an inverted cone-shaped molecule and its presence makes membrane fission energetically unfavourable (Figure 2.1). In *pex16Δ* mutant cells, which lack Pex16p, PA and DAG accumulated and LPA disappeared even

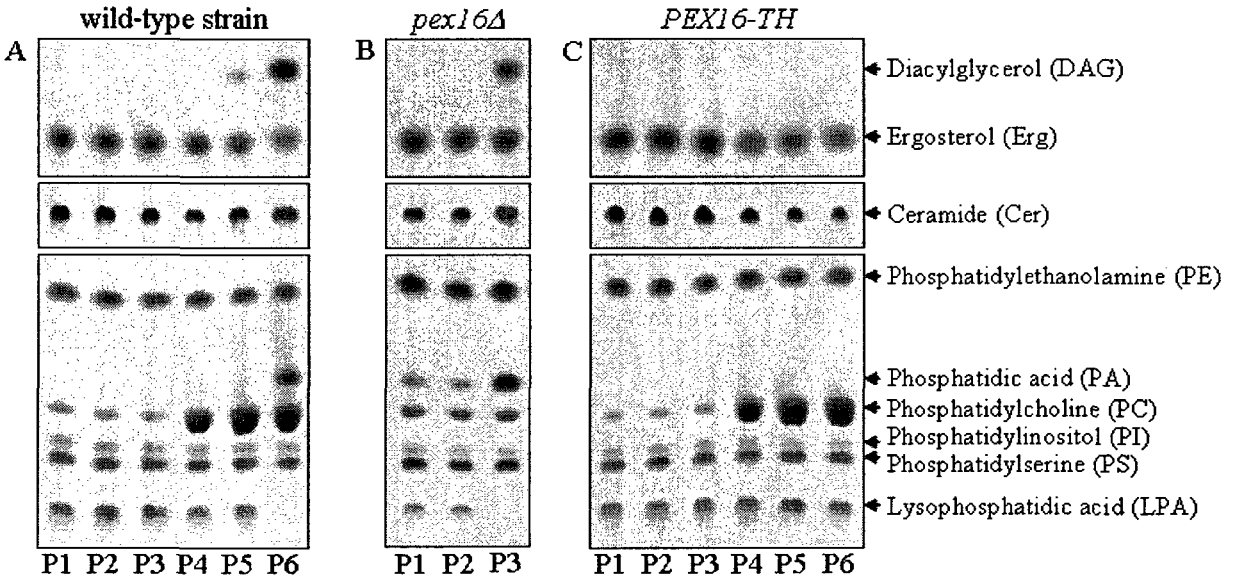


**Figure 2.6.** As peroxisomes mature to become division-competent, LPA is converted into PA and DAG. A) In wild-type cells, P6 contains negligible amounts of LPA and increased amounts of PA and DAG as compared to immature peroxisomal subforms. B) In cells lacking Pex16p, the conversion of LPA to PA and DAG occurs even in immature peroxisomes P3. These mutant cells cannot assemble P4, P5 or P6 peroxisomes. C) In cells that overproduce Pex16p, peroxisomes can mature but LPA is not converted to PA or DAG and therefore never becomes division-competent.

in the membrane of immature peroxisomal vesicles P3 (Figure 2.6). This pattern coincided with the excessive proliferation of immature peroxisomal vesicles P3 and their inability to be converted to P4 in *pex16Δ* mutant cells [126]. Conversely, *PEX-TH* mutant cells, which overproduce Pex16p [1261], did not accumulate PA or DAG and maintained high levels of LPA even in the membrane of P6 (Figure 2.6). Importantly, I found that in peroxisomal liposomes reconstituted from P1 liposomes and radiolabeled [$^{14}$C]LPA, the amount of [$^{14}$C]PA increased as the amount of [$^{14}$C]LPA decreased provided the liposomes were depleted of Pex16p (Figure 2.7). Over time, these P1 liposomes would

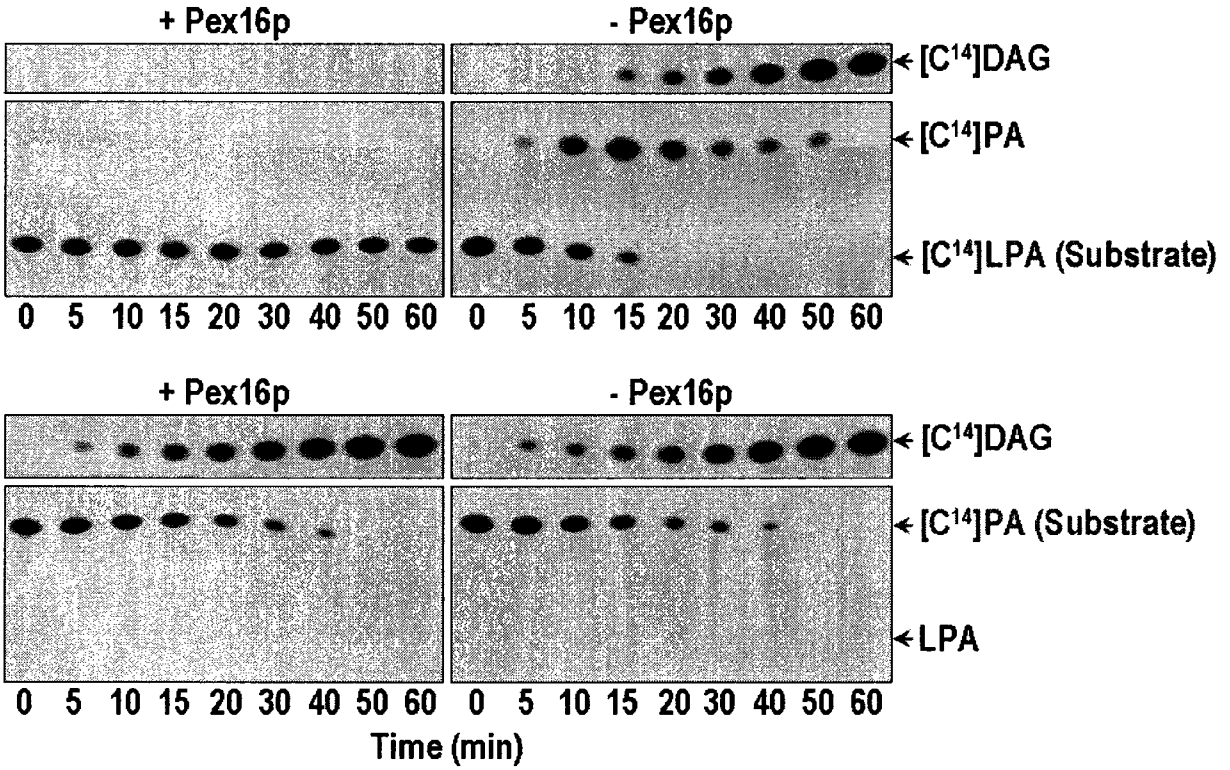


**Figure 2.7.** Dynamics of radiolabeled lipids in P1 liposomes that contain Pex16p (+ Pex16p) or lack it (- Pex16p). In the absence of Pex16p, LPA acid is converted into PA and then DAG in about 1 hour. By contrast, LPA is not metabolized in the presence of Pex16p. Conversely, the conversion of PA to DAG is independent of the presence of Pex16p.

contain decreasing amounts of [$^{14}$C]PA and increasing amounts of [$^{14}$C]DAG (Figure 2.7). However, if P1 liposomes were reconstituted with [$^{14}$C]PA instead of [$^{14}$C]LPA, I found that [$^{14}$C]DAG accumulated in the presence or absence of Pex16p (Figure 2.7).

Taken together, my aforementioned findings provide evidence that: 1) the conversion of P5 to P6 is marked by the biosynthesis of PA and DAG in the peroxisomal membrane; 2) PA and DAG are formed in a two-step biosynthetic pathway, which includes two consecutive enzymatic reactions catalyzed by an LPA acyltransferase (LPAAT) and a PA phosphatase (PAP); and 3) Pex16p, a negative regulator of the division of immature peroxisomal vesicles, inhibits LPAAT (Figure 2.8).

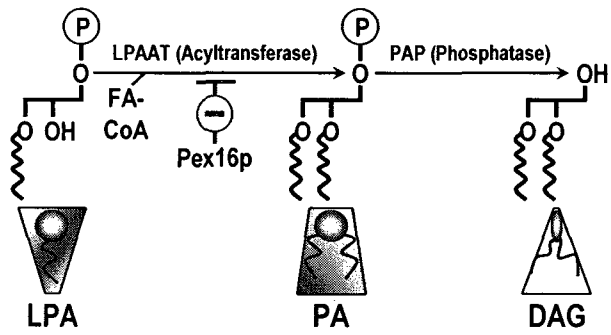


**Figure 2.8.** Pex16p inhibits LPAAT, the first enzyme in a two-step biosynthetic pathway leading to the formation of DAG in the peroxisomal membrane during conversion of P5 to P6.

### 2.4.2 The conversion of LPA to PA and then to DAG is a two-step biosynthetic pathway carried out by Slc1p (an LPAAT) and Dpp1p (a PAP)

Dr. Guo provided evidence that the LPAAT and PAP reactions are the only reactions leading to the formation of PA and DAG, respectively, in the peroxisomal membrane. She found that this membrane lacked the activities of all other enzymes that can promote

the biosynthesis of PA or DAG [141, 175, 176], including phospholipase D, inositol phosphosphingolipid phospholipase C (PLC), phosphoinositide-specific PLC, DAG kinase, inositol phosphorylceramide synthase, and inositolphosphotransferase 1). Furthermore, Dr. Guo purified LPAAT and PAP from the membrane of P6. Using mass spectrometry, Dr. Guo identified purified LPAAT and PAP as Slc1p, an acylglycerol-3-phosphate acyltransferase [177], and Dpp1p, a diacylglycerol pyrophosphate phosphatase [178], respectively. Using highly purified peroxisomes of wild-type cells, she found that all six peroxisomal subforms have similar amounts of both Slc1p (LPAAT) and Dpp1p (PAP). Dr. Guo also demonstrated that, akin to the peroxisomal integral membrane protein Pex2p [126] and in contrast to the peroxisomal peripheral membrane protein Pex16p [126], neither Slc1p (LPAAT) nor Dpp1p (PAP) was solubilized by either 1 M NaCl or 0.1 M $Na_2CO_3$ (pH 11.0) [51]. She therefore concluded that both Slc1p (LPAAT) and Dpp1p (PAP) are integral membrane proteins. Furthermore, Dr. Guo found that, like Pex16p attached to the lumenal face [126] and unlike the peripheral membrane protein Pex19p on the cytosolic face of peroxisomes [126], both Slc1p (LPAAT) and Dpp1p (PAP) were resistant to digestion by external protease added to intact peroxisomes [51]. Altogether, these data of Dr. Guo imply that, in all six peroxisomal subforms, both Slc1p (LPAAT) and Dpp1p (PAP) are integral membrane proteins that do not face the cytosol, being integrated into the lumenal leaflet of the membrane.

I therefore decided to investigate the effect of mutations eliminating Slc1p or Dpp1p on lipid composition of the peroxisomal membrane and on the ability of mature peroxisomes P6 to divide. I found that the lack of LPAAT in *slc1Δ* mutant cells: 1)

abolished the formation of PA and DAG and prevented the disappearance of LPA in the membrane of P6 (Figure 2.9); and 2) resulted in a reduced number of greatly enlarged mature peroxisomes (Figure 2.10). Moreover, I found that the lack of PAP in *dpp1Δ* mutant cells: 1) did not impair the Slc1p (LPAAT)-dependent biosynthesis of PA from LPA in the membrane of P6 (Figure 2.9); 2) prevented the conversion of PA to DAG in the membrane of P6 (Figure 2.9); and 3) resulted in fewer, but greatly enlarged, mature peroxisomes (Figure 2.10).

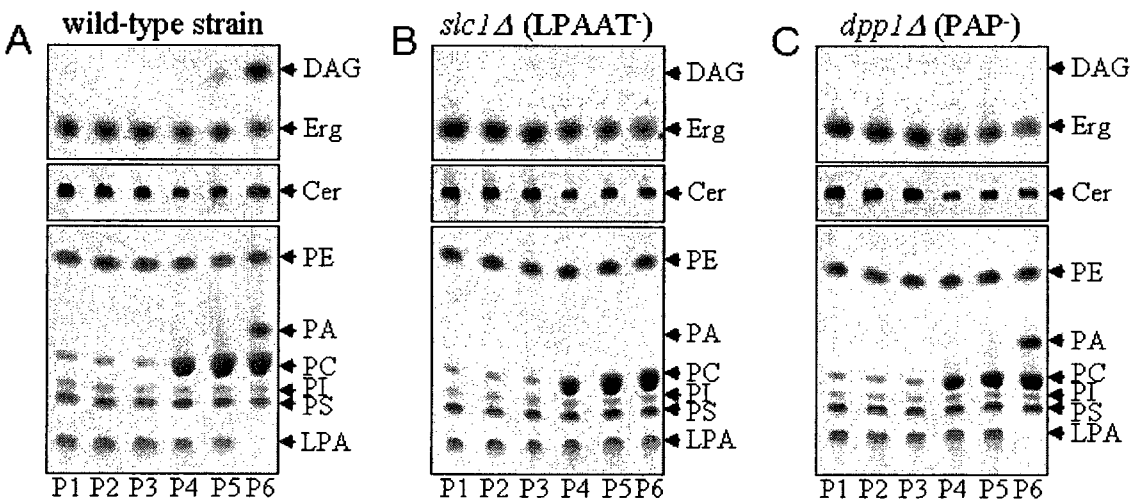


**Figure 2.9.** Slc1p promotes the conversion of LPA to PA, whereas Dpp1p catalyzes the subsequent biosynthesis of DAG from PA. A) In wild-type cells, mature peroxisomes P6 are able to convert LPA to PA and DAG. B) Mature P6 peroxisomes in cells lacking Slc1p are unable to convert LPA to PA. C) Mature P6 peroxisomes in cells lacking Dpp1p gene cannot convert PA to DAG.

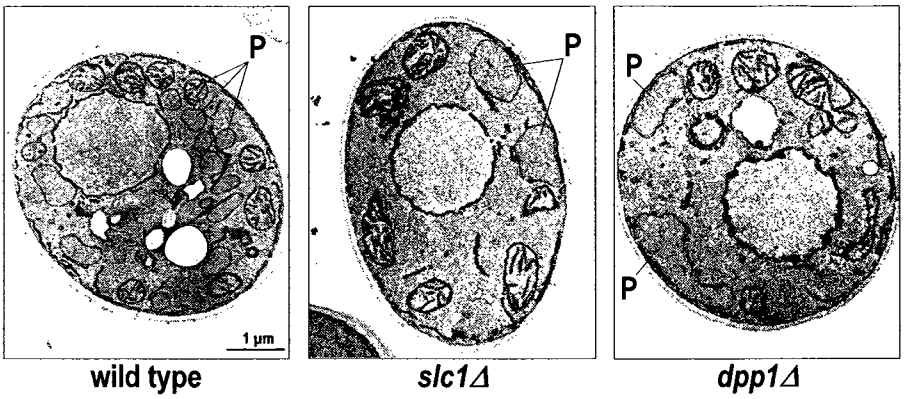


**Figure 2.10.** Lack of Slc1p (LPAAT) or Dpp1p (PAP) greatly increases the size of peroxisomes and dramatically reduces their number. Transmission electron micrographs of the wild-type, *slc1Δ* and *dpp1Δ* strains grown for 9 h in oleic acid-containing medium. P, peroxisome.

Altogether, my aforementioned findings provide evidence that: 1) both the Slc1p (LPAAT)-dependent formation of PA from LPA and the subsequent Dpp1p (PAP)-dependent biosynthesis of DAG from PA, which occur in the lumenal leaflet of the peroxisomal membrane only during conversion of P5 to P6, are essential for the division of P6; and 2) although the biosynthesis of PA is necessary for the division of P6, the presence of PA alone is not sufficient for promoting this process, which also requires the biosynthesis of DAG. It remains to be established whether DAG alone stimulates peroxisome division or, alternatively, the simultaneous presence of PA and DAG in the membrane of P6 is mandatory for its fission.

### 2.4.3 The binding of Pex16p to LPA prevents the formation of PA and DAG in the membranes of immature peroxisomal vesicles

Because Pex16p inhibits LPAAT in the membranes of P1 to P5, thereby preventing the formation of both PA and DAG, I sought to define the mechanism for the negative

regulation of LPAAT by Pex16p in immature peroxisomal vesicles. I found that Pex16p solubilized with the detergent n-octyl-ß-D-glucopyranoside (n-OG) from the membranes of P1 to P5 purified from wild-type cells was able to bind only to LPA, a substrate of LPAAT, but not to any other lipid tested (Figure 2.11). In contrast, n-OG-soluble Pex16p of mature peroxisomes P6 did not bind to LPA if these peroxisomes were recovered from

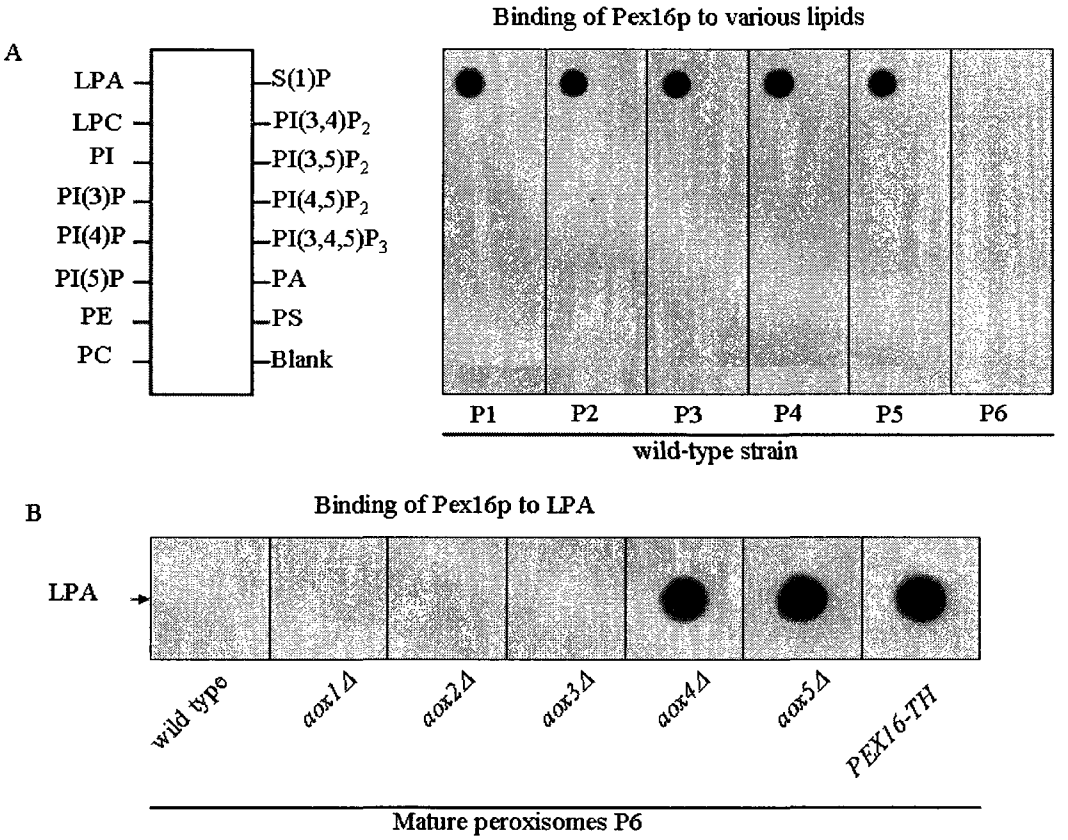


**Figure 2.11.** Pex16p binds to LPA only in the membranes of division-incompetent peroxisomal subforms. (A and B) Different peroxisomal subforms purified from wild-type cells (A) and highly purified mature peroxisomes P6 of wild-type and mutant strains (B) were osmotically lysed and subjected to centrifugation. The pellet of membranes after such centrifugation was solubilized with a detergent, n-OG. Equal quantities of detergent-soluble membrane proteins were analyzed by protein-lipid overlay assay using commercial PIP-Strips. Pex16p was detected by immunoblotting with anti-Pex16p antibodies.

wild-type or *aox1Δ*, *aox2Δ* and *aox3Δ* mutant strains (Figure 2.11). I found that all these strains lack LPA and carry both PA and DAG in the membranes of their division-competent mature peroxisomes (Figure 2.12). Of note, Pex16p has been shown to be attached to the membranes of immature peroxisomal vesicles only in its free form, whereas all the Pex16p on the inner face of mature peroxisomes of wild-type or *aox1Δ*, *aox2Δ* and *aox3Δ* mutant cells is titrated by its interaction with Aox [51]. Importantly, the interaction between Pex16p and Aox is not affected by n-OG (Dr. Guo's data). Altogether, my aforementioned findings suggest that the binding of Aox to Pex16p in mature peroxisomes of wild-type cells greatly decreases the affinity between Pex16p and LPA, thereby allowing LPA to enter the two-step biosynthetic pathway leading to the formation of PA and DAG. My hypothesis is supported by the observation that n-OG-soluble Pex16p of mature peroxisomes was capable of binding to LPA if these mature peroxisomes were purified from *aox4Δ*, *aox5Δ* or *PEX16-TH* strains (Figure 2.11). All these mutant strains: 1) carry Pex16p in a free form that is not titrated by its interaction with Aox; 2) are deficient in the division of mature peroxisomes; and 3) accumulate a reduced number of greatly enlarged mature peroxisomes [45] that contain LPA but lack both PA and DAG (Figure 2.12).

### 2.4.4 The relocation of Aox from the matrix to the membrane of P6 peroxisomes is due only to an increase in the total mass of matrix proteins above a critical level

I hypothesized that there might be three molecular mechanisms underlying the observed relocation of Aox from the matrix to the membrane within mature peroxisomes P6. First,

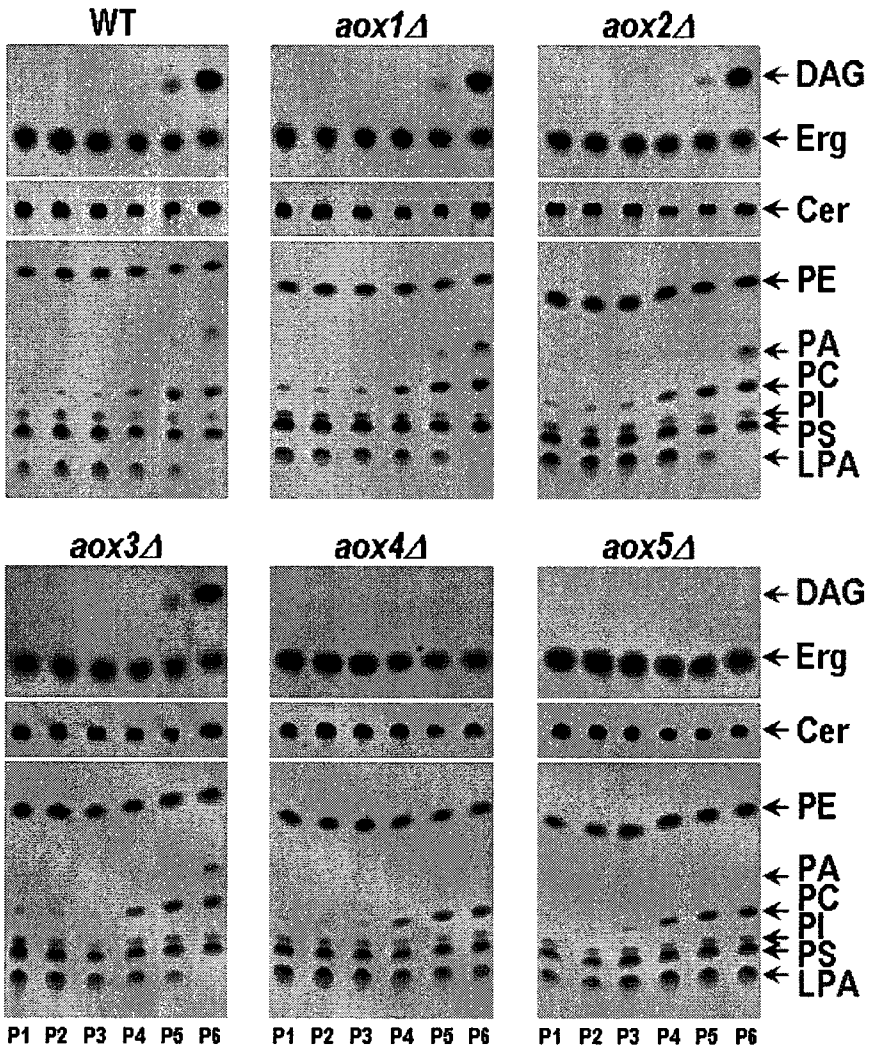


**Figure 2.12.** Mutations that abolish the binding of Aox to Pex16p, thereby impairing peroxisome division, prevent the biosynthesis of PA and DAG in the peroxisomal membrane. Highly purified peroxisomal subforms were osmotically lysed and subjected to centrifugation. Equal quantities of the pelleted membrane proteins recovered from different peroxisomal subforms were subjected to lipid extraction, which was followed by TLC and visualization of lipids.

it is plausible that the relocation of Aox is due only to an increase in the total mass of matrix proteins above a critical level. In this mechanism, this movement of Aox is not

caused by its interaction with any specific protein in the matrix (Figure 2.3). Second, it is possible that: 1) a specific matrix protein rather than protein mass in the peroxisomal matrix initiates the relocation of Aox from the matrix to the membrane; and 2) this specific matrix protein is present already in the early peroxisomal precursors P1 and P2 and is activated only when the total mass of matrix proteins exceeds a critical level (Figure 2.4). Third, it is conceivable that: 1) a specific matrix protein rather than protein mass in the peroxisomal matrix initiates the relocation of Aox; and 2) this specific matrix protein is imported to the peroxisome only during the last step of peroxisome maturation,

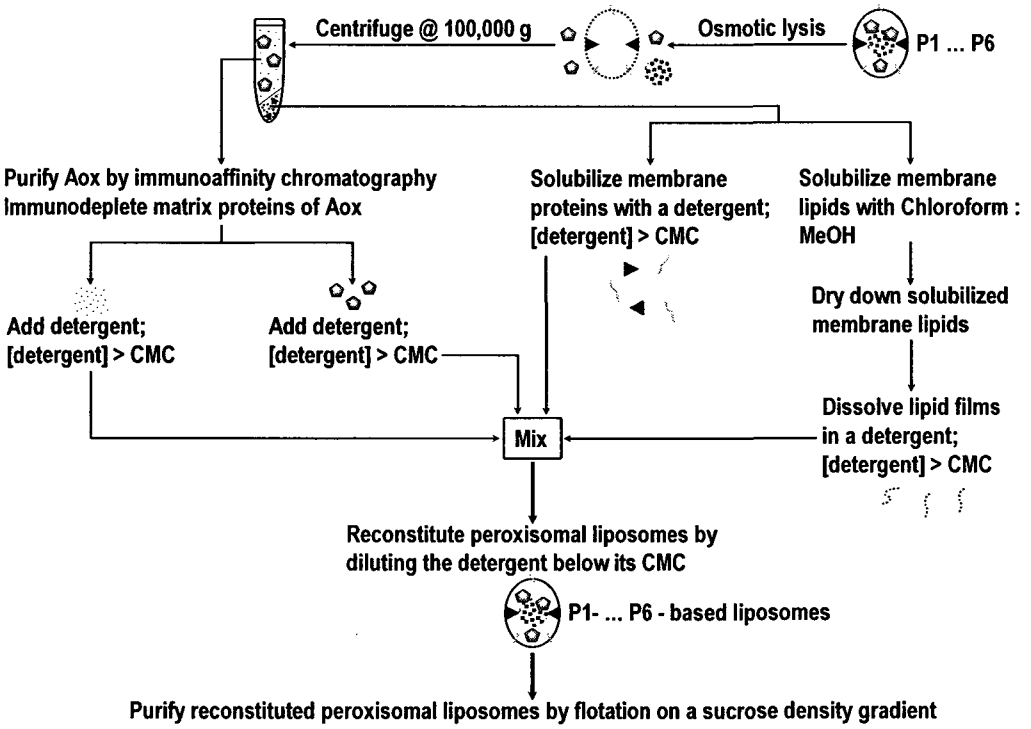


**Figure 2.13.** Reconstructing *in vitro* (*i.e.*, in peroxisomal liposomes) the relocation of Aox from the matrix to the membrane and its interaction with membrane-bound Pex16p using peroxisomal matrix and membrane proteins recovered from each of the six peroxisomal subforms purified from wild-type strain of the yeast *Y. lipolytica*. See Materials and methods for details.

during the conversion of P5 to P6 (Figure 2.5). To test if the third of the aforementioned mechanisms is responsible for the relocation of Aox from the matrix to the membrane in mature peroxisomes P6, I reconstituted such relocation of Aox *in vitro* (*i.e.*, in peroxisomal liposomes) using peroxisomal matrix and membrane proteins recovered from each of the six peroxisomal subforms purified from wild-type strain of the yeast *Y. lipolytica* (Figure 2.13). Importantly, I found that, regardless of which of the six peroxisomal subforms has been taken for the reconstruction of peroxisomal liposomes, Aox associated with their membranes if the concentration of matrix proteins used for the reconstruction exceeded a certain level (Figures 2.14 and 2.15). In fact, the percentage of

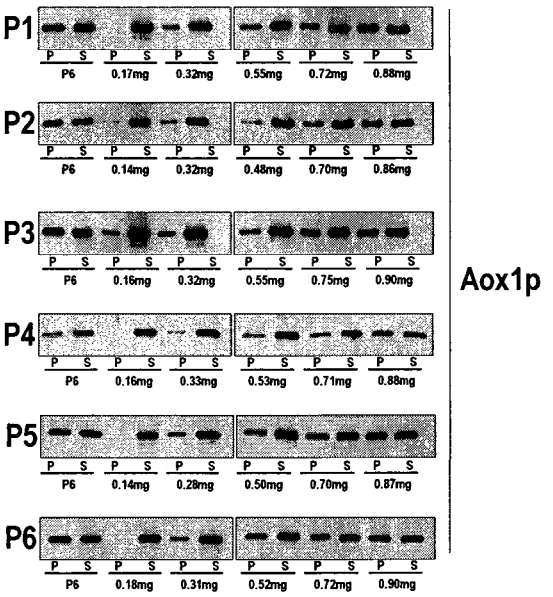


**Figure 2.14.** Regardless of which of the six peroxisomal subforms has been taken for the reconstruction of peroxisomal liposomes, the percentage of membrane-bound Aox1p subunit of the Aox complex in these peroxisomal liposomes was proportional to the level of matrix proteins that have been taken for their reconstitution and recovered in their matrix.

membrane-bound Aox1p and Aox5p subunits in these peroxisomal liposomes was proportional to the level of matrix proteins that have been taken for their reconstitution and recovered in their matrix (Figures 2.14 and 2.15). It should be stressed that the observed relocation from the matrix of peroxisomal liposomes to their membranes was observed only for Aox but not for malate synthase or thiolase, the two abundant proteins in the matrices of various peroxisomal subform (note that thiolase is not present in P1 [45] (Figures 2.16 and 2.17). Altogether, my aforementioned findings invalidate the third possible molecular mechanism for the relocation of Aox from the matrix to the membrane of P6, in which a specific matrix protein imported to the peroxisome only during the last step of peroxisome maturation (*i.e.*, during the conversion of P5 to P6) initiates such relocation (Figure 2.5).

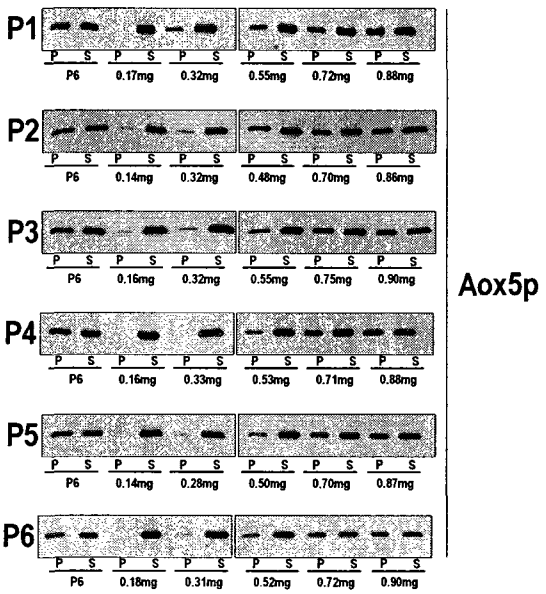


**Figure 2.15.** Regardless of which of the six peroxisomal subforms has been taken for the reconstruction of peroxisomal liposomes, the percentage of membrane-bound Aox5p subunit of the Aox complex in these peroxisomal liposomes was proportional to the level of matrix proteins that have been taken for their reconstitution and recovered in their matrix.

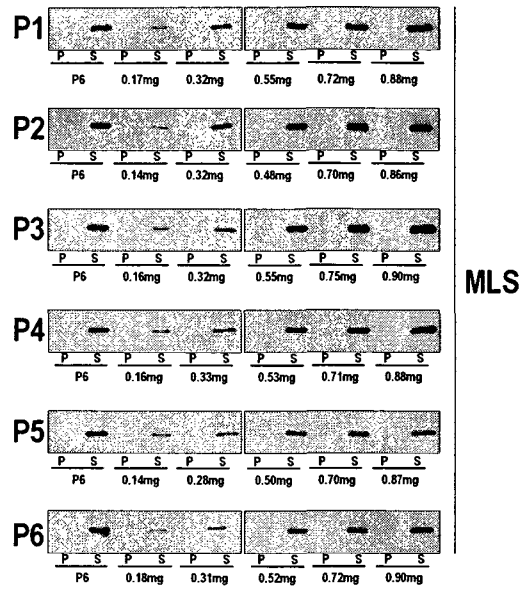


**Figure 2.16.** In contrast to Aox, malate synthase (MLS) does not relocate from the matrix to the membrane of peroxisomal liposomes reconstituted from various amounts of matrix proteins that have been recovered from the six different peroxisomal subforms.

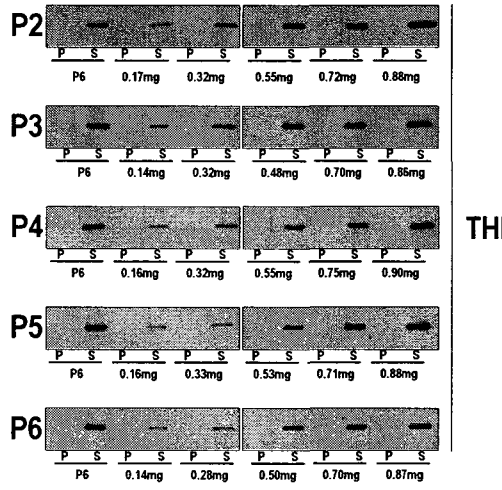


**Figure 2.17.** In contrast to Aox, thiolase (THI) does not relocate from the matrix to the membrane of peroxisomal liposomes reconstituted from various amounts of matrix proteins that have been recovered from the five different peroxisomal subforms. Note that thiolase is not imported into the immature peroxisomal vesicle P1 [45].

To test if the second of the aforementioned mechanisms is responsible for the relocation of Aox from the matrix to the membrane in mature peroxisomes P6, I reconstituted such relocation of Aox *in vitro* (*i.e.*, in peroxisomal liposomes) using several non-peroxisomal proteins (Figure 2.18). Importantly, I found that, regardless of which of the six peroxisomal subforms has been taken for the reconstruction of peroxisomal liposomes, Aox associated with their membranes if the concentration of the non-peroxisomal proteins cytochrome c, bovine serum albumin or apoferritin used for the reconstruction exceeded a certain level (Figures 2.19, 2.20, 2.21, 2.22, 2.23 and 2.24). In fact, the percentage of membrane-bound Aox1p and Aox5p subunits in these peroxisomal liposomes was proportional to the level of the non-peroxisomal proteins cytochrome c,

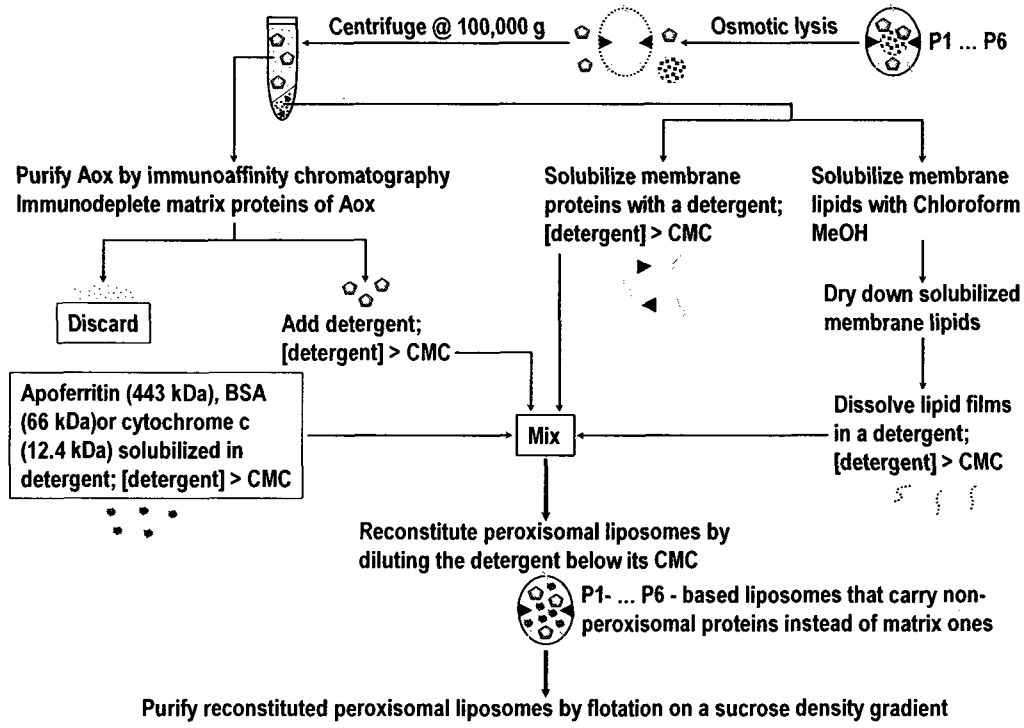


**Figure 2.18.** Reconstructing *in vitro* (*i.e.*, in peroxisomal liposomes) the relocation of Aox from the matrix to the membrane and its interaction with membrane-bound Pex16p using non-peroxisomal. See Materials and methods for details.

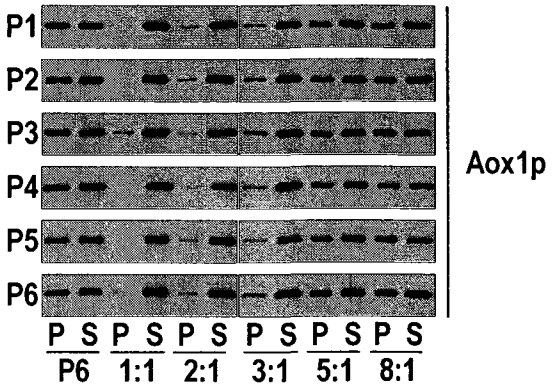


**Figure 2.19.** Regardless of which of the six peroxisomal subforms has been taken for the reconstruction of peroxisomal liposomes, the percentage of membrane-bound Aox1p subunit of the Aox complex in these peroxisomal liposomes was proportional to the level of the non-peroxisomal protein cytochrome c that has been taken for their reconstitution and recovered in their matrix.

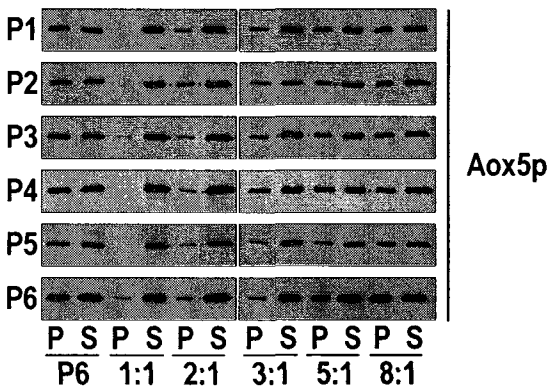


**Figure 2.20.** Regardless of which of the six peroxisomal subforms has been taken for the reconstruction of peroxisomal liposomes, the percentage of membrane-bound Aox5p subunit of the Aox complex in these peroxisomal liposomes was proportional to the level of the non-peroxisomal protein cytochrome c that has been taken for their reconstitution and recovered in their matrix.

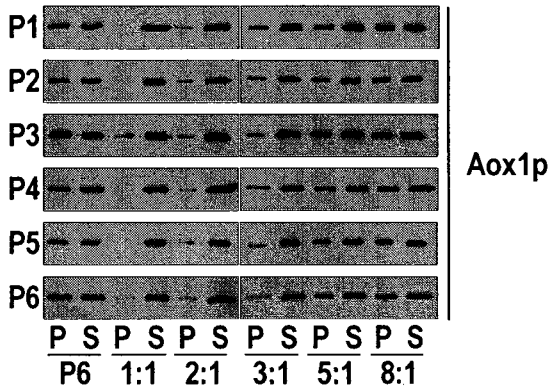


**Figure 2.21.** Regardless of which of the six peroxisomal subforms has been taken for the reconstruction of peroxisomal liposomes, the percentage of membrane-bound Aox1p subunit of the Aox complex in these peroxisomal liposomes was proportional to the level of the non-peroxisomal protein bovine serum albumin that has been taken for their reconstitution and recovered in their matrix.

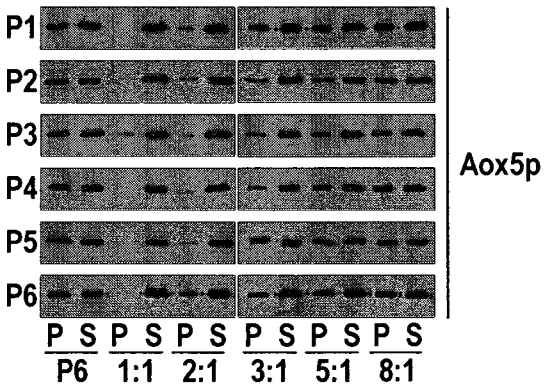


**Figure 2.22.** Regardless of which of the six peroxisomal subforms has been taken for the reconstruction of peroxisomal liposomes, the percentage of membrane-bound Aox5p subunit of the Aox complex in these peroxisomal liposomes was proportional to the level of the non-peroxisomal protein bovine serum albumin that has been taken for their reconstitution and recovered in their matrix.

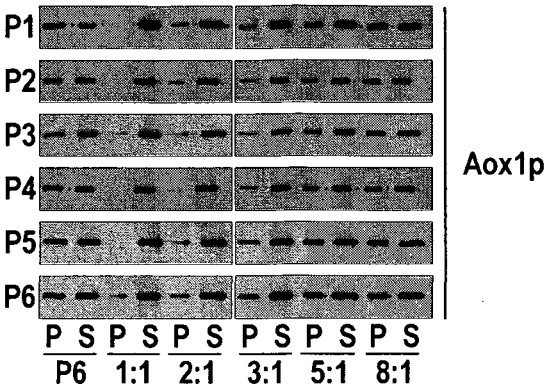


**Figure 2.23.** Regardless of which of the six peroxisomal subforms has been taken for the reconstruction of peroxisomal liposomes, the percentage of membrane-bound Aox1p subunit of the Aox complex in these peroxisomal liposomes was proportional to the level of the non-peroxisomal protein apoferritin that has been taken for their reconstitution and recovered in their matrix.

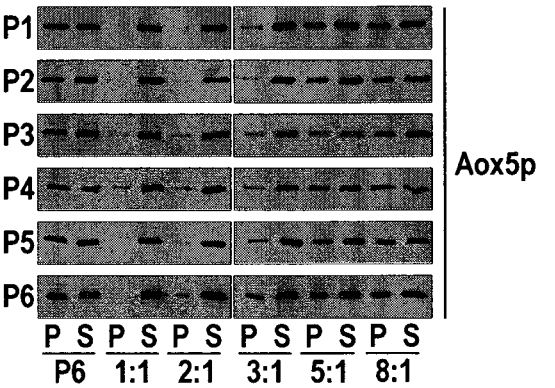


**Figure 2.24.** Regardless of which of the six peroxisomal subforms has been taken for the reconstruction of peroxisomal liposomes, the percentage of membrane-bound Aox5p subunit of the Aox complex in these peroxisomal liposomes was proportional to the level of the non-peroxisomal protein apoferritin that has been taken for their reconstitution and recovered in their matrix.

bovine serum albumin or apoferritin that have been taken for their reconstitution and recovered in their matrix (Figures 2.19, 2.20, 2.21, 2.22, 2.23 and 2.24). It should be

emphasized that my data strongly suggest that the observed ability of the non-peroxisomal proteins, if present in a concentration exceeding a critical level, to cause the relocation of Aox from the matrix to the membrane of reconstituted peroxisomal liposomes is specific. Indeed, as I found, such relocation requires both the Aox4p subunit of the Aox complex (which is known to be required for the attachment of the entire complex to the peroxisomal membrane [51] and Pex16p (Figures 2.25, 2.26, 2.27 and 2.28). Taken together, my aforementioned findings invalidate the second possible molecular mechanism for the relocation of Aox from the matrix to the membrane of P6, in which a specific matrix protein present already in the earliest peroxisomal precursors P1 and P2 promotes such relocation only when the total mass of other matrix proteins

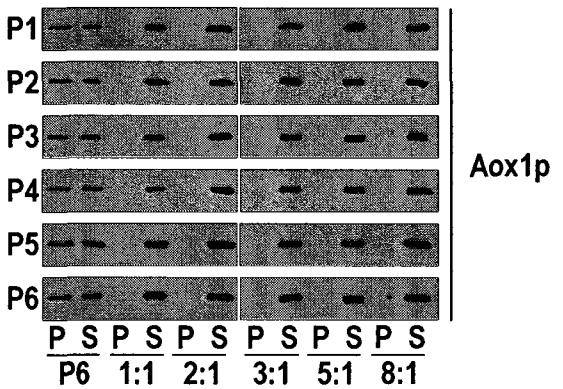


**Figure 2.25.** The observed relocation of the Aox complex from the matrix to the membrane of peroxisomal liposomes "packed" with cytochrome c requires Aox4p, a subunit of this heteropentameric protein complex that is essential for the anchoring of the entire complex to the peroxisomal membrane. Peroxisomal liposomes were reconstituted using various amounts of cytochrome c, membrane proteins immunodepleted of Aox, and Aox complex purified from *aox4Δ* mutant cells.

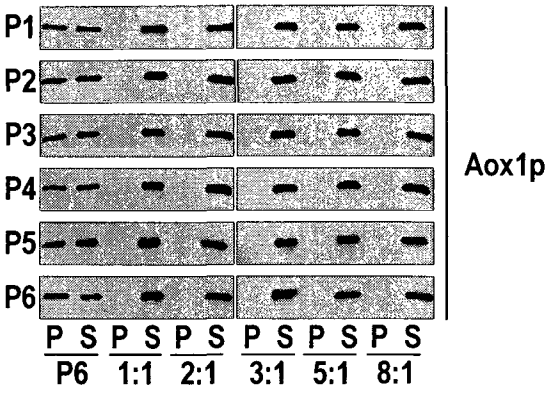


**Figure 2.26.** The observed relocation of the Aox complex from the matrix to the membrane of peroxisomal liposomes "packed" with bovine serum albumin requires Aox4p, a subunit of this heteropentameric protein complex that is essential for the anchoring of the entire complex to the peroxisomal membrane. Peroxisomal liposomes were reconstituted using various amounts of bovine serum albumin, membrane proteins immunodepleted of Aox, and Aox complex purified from *aox4Δ* mutant cells.

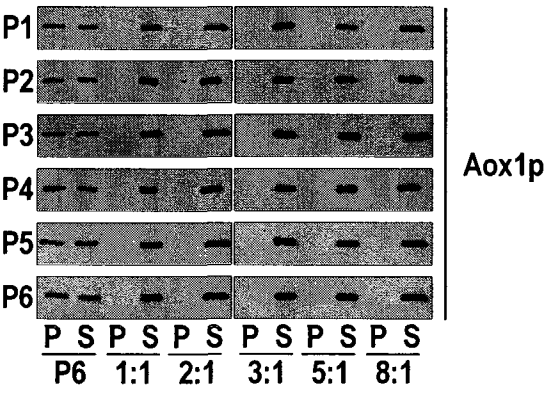


**Figure 2.27.** The observed relocation of the Aox complex from the matrix to the membrane of peroxisomal liposomes "packed" with cytochrome c requires Pex16p, a membrane-bound docking factor for the entire Aox complex. Peroxisomal liposomes were reconstituted using various amounts of cytochrome c, membrane proteins immunodepleted of Pex16p and Aox, and Aox complex purified from wild-type cells.

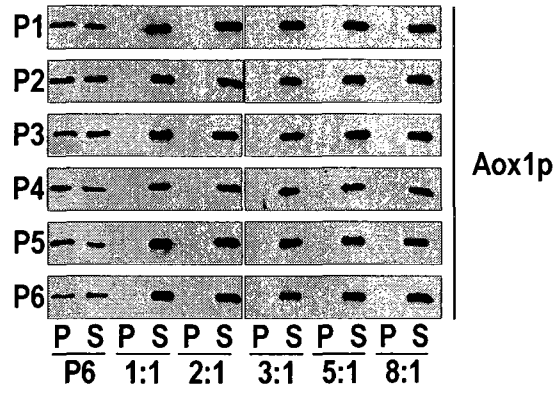


**Figure 2.28.** The observed relocation of the Aox complex from the matrix to the membrane of peroxisomal liposomes "packed" with bovine serum albumin requires Pex16p, a membrane-bound docking factor for the entire Aox complex. Peroxisomal liposomes were reconstituted using various amounts of bovine serum albumin, membrane proteins immunodepleted of Pex16p and Aox, and Aox complex purified from wild-type cells.

exceeds a critical level (*i.e.*, in mature peroxisomes P6).

Thus, my data provide comprehensive evidence for the validity of the first proposed mechanism underlying the relocation of Aox from the matrix to the membrane of P6. That is, such relocation of Aox: 1) is due only to an increase in the total mass of matrix proteins other than Aox above a critical level; and 2) is not promoted by the interaction of Aox with any specific matrix protein.

### 2.4.5 Dynamics of changes in the transbilayer distribution of DAG and phosphatidylserine (PS) in the peroxisomal membrane during peroxisome maturation

My aforementioned data strongly suggest that LPA enters the two-step pathway for the

biosynthesis of PA and DAG only when the efficiency of its binding to Pex16p declines. Pex16p is a peripheral membrane protein that is attached only to the lumenal leaflet of the peroxisomal membrane [179]. Furthermore, it seems unlikely that LPA can translocate from the lumenal to the cytosolic leaflet of the peroxisomal membrane, as its spontaneous transbilayer movement is very slow [45]. Moreover, as Dr. Guo demonstrated, neither LPAAT nor PAP faces the cytosol, being integrated into the lumenal leaflet of the peroxisomal membrane [45]. Altogether, these findings imply that the biosynthesis of PA and DAG is spatially restricted to the lumenal leaflet of the peroxisomal membrane.

To evaluate the arrangement of DAG between the two leaflets of the membrane bilayers in different peroxisomal subforms, I decided to reconstitute two types of resealed peroxisomes, termed RPA and RPB, from osmotically lysed intact peroxisomes. RPA were reconstituted in a MES-based buffer at pH 5.5, whereas RPB were made in a HEPES-based buffer at pH 7.5. I found that, similar to intact peroxisomes [51], both RPA and RPB could float out of the most dense sucrose during centrifugation to equilibrium in sucrose density gradients (Figure 2.29 A) and were bound by a single membrane (Figure 2.29 C). In intact peroxisomes, Pex19p is a peripheral membrane protein that resides on the cytosolic face of the peroxisome, whereas the peripheral membrane protein Pex16p is attached to its lumenal face (Figure 2.29, B and D). In RPA, most of Pex19p, but only a minor portion of Pex16p, was accessible to trypsin and to the corresponding antigen-specific IgG molecules exogenously added to this type of resealed peroxisomes (Figure 2.29, B and D). Therefore, I concluded that the membrane delimiting most of the RPA

species formed during peroxisome resealing was present in the outside-out orientation, whereas only a minor fraction of RPA species had their membrane resealed in the inside-out orientation. In contrast, in RPB, only a minor portion of Pex19p, but most of Pex16p, was accessible to trypsin and to the corresponding antigen-specific IgG molecules exogenously added to this type of resealed peroxisomes (Figure 2.29, B and D). Hence, I concluded that only a minor fraction of RPB had their membrane resealed in the outside-out orientation, while the membrane delimiting most of the RPB species formed during peroxisome resealing was present in the inside-out orientation. Using a Pex19p-specific fluorescent probe, I then calculated the percentage of outside out- and inside out-oriented species of RPA and RPB that were formed by resealing of osmotically lysed peroxisomal subforms P1 to P6 (Figure 2.29, E and F).

The ability to calculate the percentage of outside out- and inside out-oriented species of RPA and RPB allowed me to calculate the percentage of DAG residing in the cytosolic and lumenal leaflets of the membrane bilayers in intact peroxisomes. The DAG-binding C1b domain of protein kinase C [51] labeled with the fluorophore Alexa Fluor 488 was used as a DAG-specific fluorescent probe. In intact P5, only 13 ± 4% of the total pool of DAG was detected in the cytosolic leaflet of the membrane bilayer (Figure 2.29 H). Thus, DAG resides predominantly in the lumenal membrane leaflet of P5. In contrast, DAG is distributed symmetrically between the two leaflets of the membrane bilayer in mature peroxisomes P6. In fact, 57 ± 3% of this lipid resided in the cytosolic membrane leaflet of P6 (Figure 2.29 H).

I then used monoclonal antibodies to PS, a lipid that has a cylindrical shape [135],

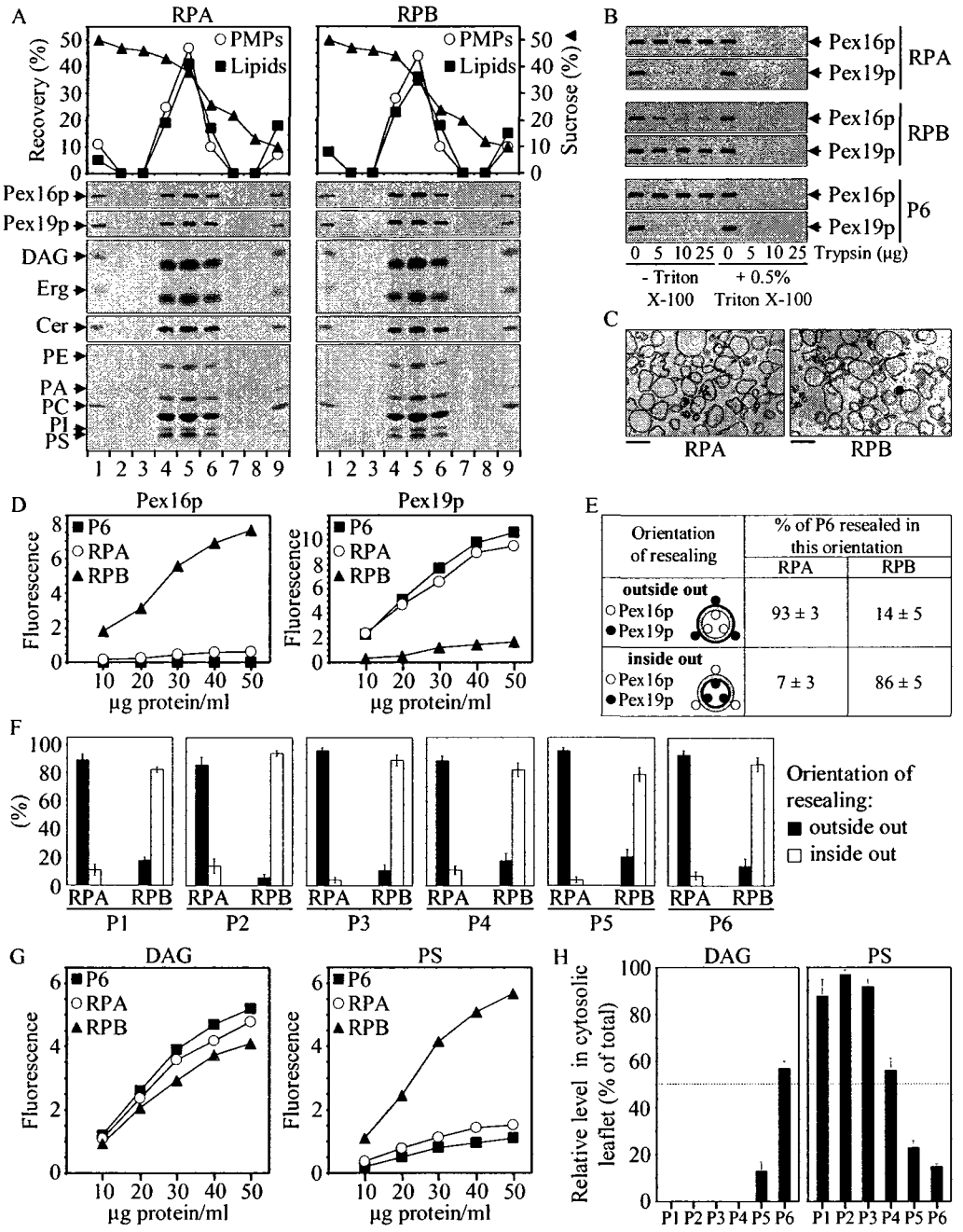


**Figure 2.29.** As peroxisomes mature, DAG and PS change their transbilayer distribution in the peroxisomal membrane. A) Resealed peroxisomes RPA and RPB were created from osmotically lysed mature peroxisomes P6 as described in Materials and methods. RPA and RPB were subjected to flotation on a multistep sucrose gradient. Resealed peroxisomes floated to low density during centrifugation in the sucrose density gradient. Proteins from equal volumes of gradient fractions were analyzed by immunoblotting with antibodies to the PMPs Pex16p and Pex19p. Equal volumes of gradient fractions were

also subjected to lipid extraction, which was followed by TLC and visualization of lipids. Sucrose density (%, w/w) of fractions, as well as the percentage of PMPs and lipids recovered in fractions, are presented. (B) Resealed peroxisomes RPA and RPB, which were recovered in the peak fractions of the flotation gradients, and a highly purified subform of the intact peroxisomes P6 from which these two types of resealed peroxisomes were formed, were subjected to protease protection analysis. Equal aliquots (10 μg of total protein) of RPA, RPB and intact peroxisomes P6 were treated with the indicated amounts of trypsin in the absence (-) or presence (+) of 0.5% (vol/vol) Triton X-100 for 30 min on ice. Samples were subjected to SDS-PAGE and immunoblotting with antibodies to Pex16 and Pex19. (C) Electron micrographs of the P6-based RPA and RPB recovered in the peak fraction 5 of the flotation sucrose density gradient presented in A. Bars, 500 nm. (D) Resealed peroxisomes RPA and RPB, which were recovered in the peak fractions of the flotation gradients, and a highly purified subform of the intact peroxisomes P6 from which these two types of resealed peroxisomes were formed, were exposed to the Pex16p- and Pex19p-specific fluorescent reporter molecules as described in Materials and methods. The Alexa Fluor 488 fluorescence at 510 nm was monitored in individual samples. (E) The percentage of the P6-based RPA and RPB present in the outside-out or inside-out orientation. The percentage of the RPA or RPB species that were resealed in the outside-out or inside-out orientation was calculated as described in Materials and methods. (F) The percentage of RPA and RPB resealed in the outside-out or inside-out orientation following osmotic lysis of different peroxisomal subforms. (G) Resealed peroxisomes RPA and RPB, which were recovered in the peak fractions of the flotation gradients, and a highly purified subform of the intact peroxisomes P6 from which these two types of resealed peroxisomes were formed, were exposed to the DAG- and PS-specific fluorescent reporter molecules as described in Materials and methods. The Alexa Fluor 488 fluorescence at 510 nm was monitored in individual samples. (H) The percentage of a monitored lipid, either DAG or PS, residing in the cytosolic leaflet of the membrane bilayer was calculated for intact peroxisomes P1 to P6 as described in Materials and methods.

to monitor its transbilayer distribution in the membranes of different peroxisomal subforms. I found that PS in the membranes of immature peroxisomal vesicles P1 to P3 resides predominantly in their cytosolic leaflets (Figure 2.29 H). As peroxisomes mature, PS gradually moves from the cytosolic to the lumenal leaflets of their membranes. Indeed, only 15 ± 1% of this lipid resided in the cytosolic membrane leaflet of P6 (Figure 2.29 H). In summary, the aforementioned findings led me to the conclusion that the

assembly of mature peroxisomes promotes the specific redistribution of DAG and PS between the two leaflets of the peroxisomal membrane. Specifically, I found that the movement of DAG from the lumenal to the cytosolic leaflet of the membrane bilayer coincides with the translocation of PS in the opposite direction.

### 2.4.6 Endoplasmic reticulum-derived phosphatidylcholine in the peroxisomal membrane activates both LPAAT and PAP

As I found, the levels of phosphatidylcholine (PC), a major glycerophospholipid of the peroxisomal membrane [179], in P4, P5 and P6 peroxisomes of wild-type cells were significantly higher than in P1, P2 and P3 peroxisomes (Figure 2.6 A). I concluded that the observed increase in the levels of PC was not due to its *de novo* synthesis. In fact, the membranes of P3 and P4 did not contain PA and DAG (Figure 2.6 A), two substrates for PC biosynthesis via the PE methylation and CDP-choline pathways, respectively [141]. Thus, I assumed that PC is transported to the membranes of P3 and P4 during their conversion to P4 and P5, respectively. Three established mechanisms of intracellular lipid transport to organellar membranes include: 1) transport catalyzed by cytosolic lipid transfer proteins [180, 181]; 2) vesicle-mediated transport [182, 183]; and 3) transport at regions of close apposition between specialized microdomains of the endoplasmic reticulum (ER) membrane and the membranes of the trans Golgi or mitochondria [181, 184]. My data imply that: 1) PC is transferred from the donor membrane of a distinct subcompartment of the ER to the acceptor membranes of P3 and P4 associated with this subcompartment; and 2) this transfer of PC requires the peroxisome-associated peroxin

Pex2p, provides membranes of P3 and P4 with the bulk quantities of PC, and is essential for the conversion of P4 to P5. My hypothesis is based on the following findings. First, a distinct form of the ER co-purifies with P3 and P4 peroxisomes and can be separated from them by treatment with EDTA [50, 64]. Second, the P3- and P4-associated ER subcompartment can be distinguished from the free form of the ER by buoyant density and the total level of membrane glycerophospholipids [64], as well as by protein spectrum (Figure 2.30 B). Third, the *pex2Δ* mutation increases the levels of membrane glycerophospholipids in the P3- and P4-associated subcompartment of the ER [64],

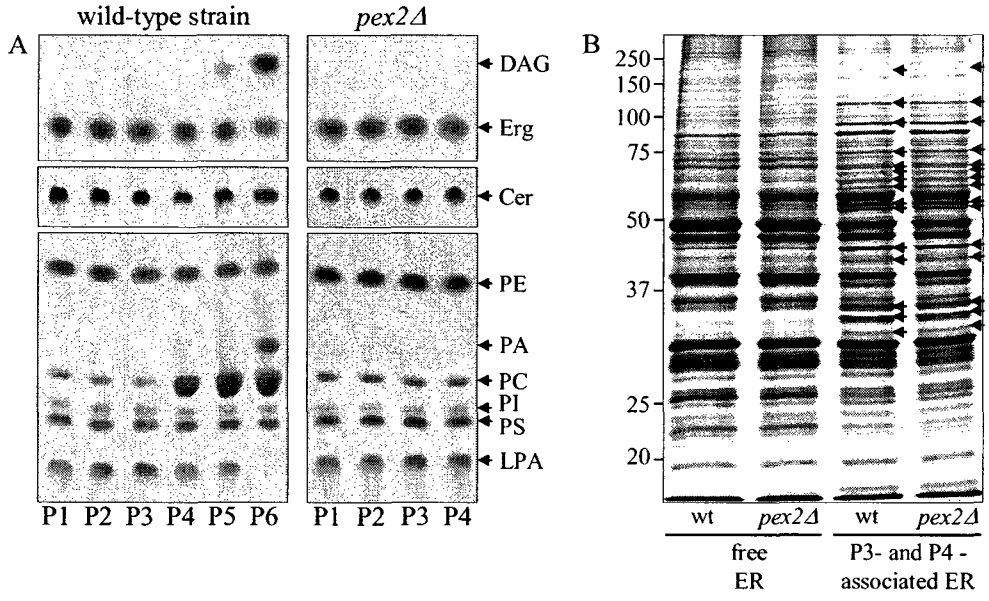


**Figure 2.30.** The Pex2p-dependent transfer of PC from a P3- and P4-associated subcompartment of the ER provides the peroxisomal membrane with the bulk quantities of this lipid. (A) The spectra of lipids found in the membranes of different peroxisomal subforms that were purified from wild-type and *pex2Δ* mutant cells. (B) The spectra of proteins recovered in the free form of the ER and in the P3- and P4-associated subcompartment of the ER. Organelles were purified from wild-type and *pex2Δ* mutant cells as described in Materials and Methods. Arrowheads mark proteins found only in the ER subcompartment associated with P3 and P4 or significantly enriched in this subcompartment of the ER as compared with its free form.

substantially decreases the level of PC in P4 (Figure 2.30 A), and impairs its conversion to P5 (Guo et al., unpublished data).

Moreover, some of my findings strongly suggest that PC in the peroxisomal membrane is a positive regulator of both LPAAT and PAP. In fact, the specific activities of these two membrane-bound enzymes in liposomes reconstituted from the Pex16p-immunodepleted PMPs and membrane lipids of P1, P2 and P3 were significantly lower than in liposomes reconstituted from membrane components of P4, P5 and P6 (Figure 2.31, A and B). Importantly, I found that LPAAT and PAP activities detected in the membranes of these peroxisomal liposomes were proportional to the steady-state levels of PC recovered in these membranes (Figure 2.31, A and B). Moreover, I was able to reconstruct the positive effect of PC on both LPAAT and PAP in four different types of the Pex16p-immunodepleted liposomes that were reconstituted from membrane components of P1, P2 or P3 and varied only in the quantities of PC present in their membranes (Figure 2.31, C, D, E, and F). Noteworthy, I found that, by rising the quantities of PC in the membranes of P1-, P2- and P3-based liposomes to the levels comparable to those present in the membranes of P4-, P5- and P6-based liposomes, both LPAAT and PAP could be significantly stimulated, matching their enzymatic activities in liposomes reconstituted from membrane components of P4, P5 and P6 (Figure 2.31, E and F). Considering that all six peroxisomal subforms have similar amounts of both LPAAT and PAP [51], my aforementioned findings support the notion that PC in the peroxisomal membrane activates these two enzymes.

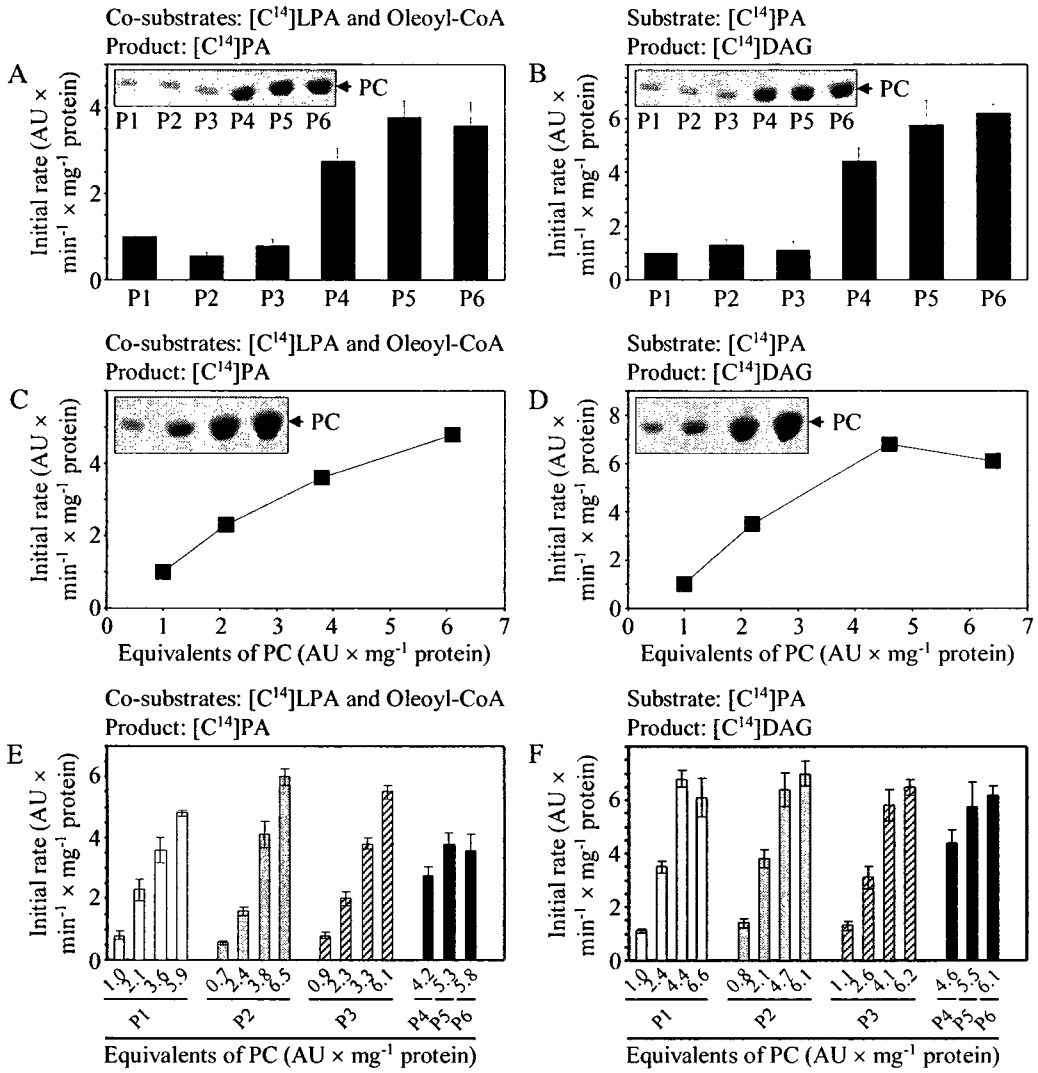


**Figure 2.31.** PC in the peroxisomal membrane is a positive regulator of both LPAAT and PAP. (A and B) The initial rates of the LPAAT (A) and PAP (B) reactions and the levels of PC recovered in the membranes of liposomes reconstituted from the Pex16p-immunodepleted PMPs and membrane lipids of different peroxisomal subforms. Peroxisomal liposomes that lack Pex16p were reconstituted as described in Materials and Methods. [$^{14}$C]-labeled lipid substrates were incorporated into liposomes during their reconstitution. (C - F) The initial rates of the LPAAT (C and E) and PAP (D and F) reactions and the levels of PC recovered in the membranes of four different types of liposomes reconstituted from the Pex16p-immunodepleted PMPs and membrane lipids of P1 (C, D, E and F), P2 (E and F) or P3 (E and F) peroxisomes. These four different types of P1-, P2- or P3-based liposomes varied only in the quantities of PC used for their reconstitution and recovered in their membranes after the reconstitution. For comparison,

the initial rates of the LPAAT (E) and PAP (F) reactions and the levels of PC recovered in the membranes of liposomes reconstituted from the Pex16p-immunodepleted PMPs and membrane lipids of P4, P5 and P6 peroxisomes are shown. To calculate the initial rates of the LPAAT and PAP reactions, the [$^{14}$C]-labeled LPA, PA and DAG were separated by TLC and quantified by autoradiography. To visualize non-radiolabeled PC, lipids were separated by TLC and detected using phosphomolybdic acid.

### 2.4.7 The biosynthesis of PA and DAG in the peroxisomal membrane promotes the recruitment of Vps1p from the cytosol to the surface of the mature peroxisome

The *S. cerevisiae* protein Vps1p is essential for peroxisome division [185]. Vps1p is a member of the dynamin protein superfamily of large GTPases that carry out a broad range of functions including organelle division and fusion, budding of transport vesicles, and cytokinesis [187]. In an attempt to test an assumption that, akin to its *S. cerevisiae* counterpart, *Y. lipolytica* Vps1p is required for peroxisome division, I found that lack of this protein in *Y. lipolytica* resulted in a reduced number of greatly enlarged peroxisomes (Figure 2.32). Morphometric analysis of random electron sections further confirmed that lack of Vps1p impairs the ability of completely assembled peroxisomes to divide, resulting in fewer, but greatly enlarged, mature peroxisomes. Importantly, these morphological patterns of the *vps1Δ* mutant were very similar to those observed in the *aox4Δ* and *PEX16-TH* mutant strains deficient in the division of mature peroxisomes P6 (Figure 2.32).

*S. cerevisiae* Vps1p is mainly a cytosolic protein [186]. It can also be found in a variety of cellular locations, including the Golgi, peroxisomes and vacuoles [185]. Likewise, as Dr. Guo found, most of *Y. lipolytica* Vps1p localized to the cytosol, whereas the minor portion of it was associated with both low-speed (20,000 × g) and high-speed

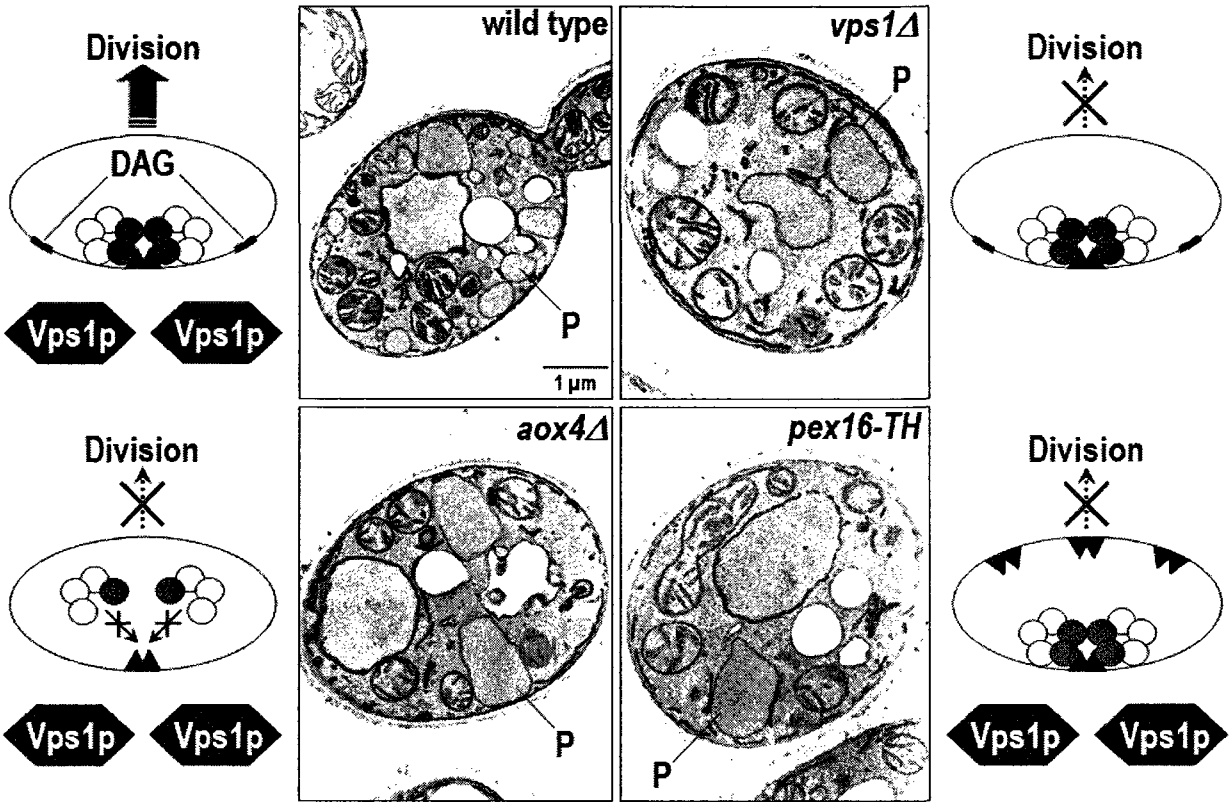


**Figure 2.32.** The dynamin-related large GTPase Vps1p is essential for the division of mature peroxisomes. Transmission electron micrographs of the wild-type, *vps1Δ*, *aox4Δ* and *PEX16-TH* strains grown for 9 h in oleic acid-containing medium. P, peroxisome.

(200,000 × g) pelletable organelles [51]. Using highly purified peroxisomal subforms of wild-type cells, Dr. Guo revealed that Vps1p was only present in division-competent mature peroxisomes P6 but not in the division-incompetent immature peroxisomal vesicles P1 to P5 [45]. Dr. Guo also provided evidence that Vps1p is a peripheral membrane protein associated with the outer (cytosolic) face of mature peroxisomes P6 [45].

Taken together, my aforementioned findings and Dr. Guo's data suggested that the conversion of P5 to P6 in wild-type cells is marked by the recruitment of Vps1p from

the cytosol to the surface of mature peroxisomes P6, where Vps1p drives their division. But how does such recruitment relate to the Pex16p/Aox intraperoxisomal signaling cascade that regulates the fission of the membrane delimiting mature peroxisomes P6? The answer to this question came from my observation that Vps1p was bound to division-competent mature peroxisomes of wild-type or *aox1Δ*, *aox2Δ* and *aox3Δ* mutant strains (Figure 2.33). In the membranes of mature peroxisomes of all these strains, LPA was converted to PA and DAG (Figure 2.6). In contrast, Vps1p was not attached to mature peroxisomes of *aox4Δ*, *aox5Δ* or *PEX16-TH* mutant strains (Figure 2.33). All these strains are deficient in the division of mature peroxisomes [45], being unable to convert LPA to PA and DAG in the peroxisomal membrane (Figures 2.6 and 2.12). I therefore concluded that the recruitment of Vps1p from the cytosol to the surface of mature peroxisomes relies on the Pex16p/Aox-dependent biosynthesis of PA and DAG in their membranes.

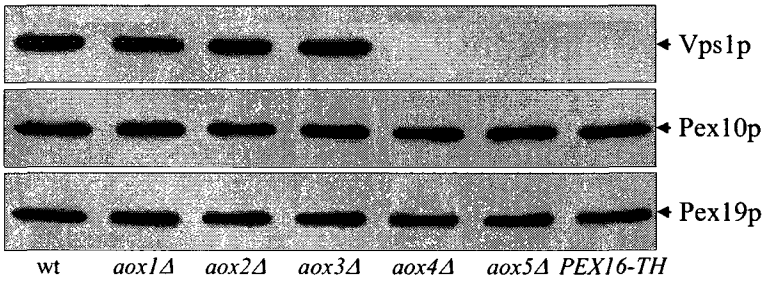


**Figure 2.33.** Only division-competent mature peroxisomes recruit Vps1p from the cytosol to the outer face of their membrane. Mature peroxisomes P6 were purified from wild-type and mutant cells. Equal quantities (20 μg) of protein from these peroxisomes were analyzed by immunoblotting with the indicated antibodies.

### 2.4.8 The recruitment of Vps1p to the peroxisomal membrane results in the formation of a multiprotein complex

To test whether Vps1p interacts with other components of the peroxisomal membrane, Dr. Guo used a combination of cross-linking, immunoprecipitation with anti-Vps1p antibodies and mass spectrometry of co-immunoprecipitated proteins. Using this approach, she revealed a Vps1p-containing complex on the outer face of the peroxisomal membrane. The following 6 components of this complex were identified by mass spectrometry: 1) Vps1p, a dynamin-like GTPase that is required for the division of mature peroxisomes (see above); 2) Sla1p, a protein that regulates actin cytoskeleton organization and dynamics [188]; 3) Abp1p, a protein that promotes F-actin assembly [189]; 4) Act1p, a structural constituent of actin cytoskeleton in yeast [190]; 5) the peroxin Pex19p, a protein required for the import and/or membrane assembly of numerous PMPs [15, 165]; and 6) the peroxin Pex10p, an integral PMP required for peroxisomal matrix protein import [15]. Dr. Guo also provided evidence that: 1) the Pex10p- and Pex19p-dependent recruitment of Vps1p from the cytosol to the surface of the mature peroxisome is mandatory for the attachment of Sla1p, Abp1p and Act1p to this division-competent peroxisomal subform [51]; 2) Vps1p, Sla1p and Abp1p initially form a complex in the cytosol; 3) this complex is then targeted from the cytosol to the surface of mature peroxisomes; and 4) only after its binding to mature peroxisomes, the Vps1p-Sla1p-Abp1p complex is able to promote the attachment of Act1p to the peroxisomal membrane.

But what is the role of Vps1p-associated proteins in the division of mature

peroxisomes P6? My electron microscopic analysis revealed that, akin to Vps1p (see above), each of the two other components of the Vps1p-Sla1p-Abp1p complex is required for the division of mature peroxisomes P6. In fact, lack of either Sla1p or Abp1p resulted in a reduced number of greatly enlarged peroxisomes (Figure 2.34).

In summary, my findings and Dr. Guo's data strongly suggest that the assembly of the Vps1p-Sla1p-Abp1p complex in the cytosol precedes its attachment to the surface of division-competent mature peroxisomes P6. The Vps1p-Sla1p-Abp1p complex binds to P6 by interacting with Pex19p, a component of the Pex10p-Pex19p complex that is formed in the peroxisomal membrane during the earliest steps of peroxisome assembly and maturation. Only after it has been attached to the membrane of P6, the Vps1p-Sla1p-Abp1p complex is able to interact with Act1p, thereby promoting the recruitment of actin to the surface of these division-competent peroxisomes.

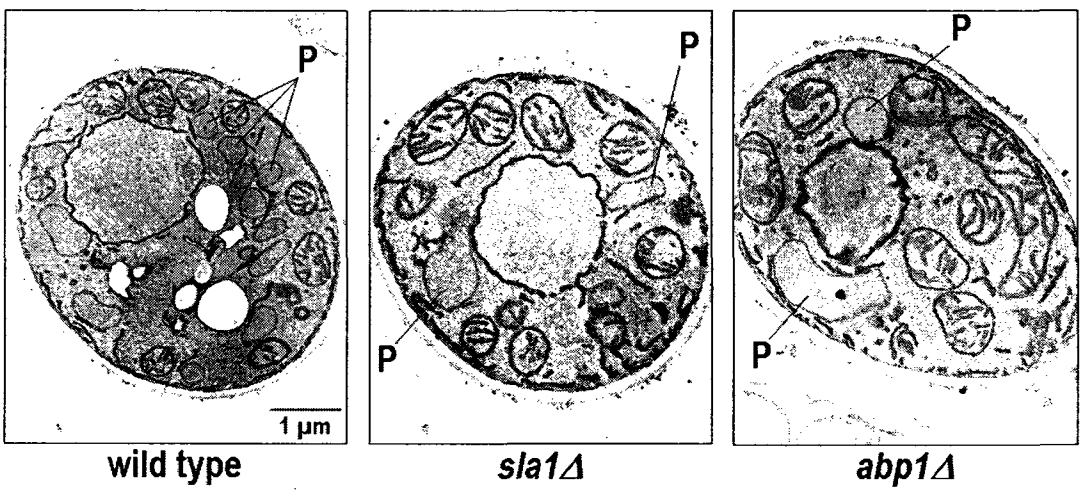


**Figure 2.34.** The Sla1p and Abp1p components of the Vps1p-Sla1p-Abp1p complex are required for the division of mature peroxisomes P6. Transmission electron micrographs of wild-type, *sla1Δ* and *abp1Δ* strains grown for 9 h in oleic acid-containing medium. P, peroxisome.

## 2.5 Discussion

Altogether the above findings suggest the following model for peroxisome division in *Y. lipolytica* (Figure 2.35). In immature peroxisomal vesicles P1 to P5, Pex16p binds LPA in the lumenal leaflet of the peroxisomal membrane. The binding of Pex16p to LPA prevents the biosynthesis of PA and DAG in a two-step pathway, which includes two consecutive enzymatic reactions catalyzed by Slc1p (LPAAT) and Dpp1p (PAP). The stepwise import of distinct subsets of matrix proteins into immature peroxisomal vesicles P1 to P5 provides them with an increasing fraction of the matrix proteins present in mature peroxisomes. The increase in the total mass of matrix proteins above a critical level, which occurs only inside mature peroxisomes, causes the redistribution of Aox from the matrix to the membrane and its subsequent binding to Pex16p. This, in turn, greatly decreases the affinity between Pex16p and LPA, thereby allowing LPA to enter the two-step biosynthetic pathway leading to the formation of PA and DAG. The glycerophospholipid PC, which is transferred to the peroxisomal membrane from the P3- and P4-associated subcompartment of the ER, activates both LPAAT and PAP. The resulting accumulation of PA and DAG in the lumenal leaflet of the membrane of mature peroxisomes triggers a cascade of events ultimately leading to peroxisome division. This cascade of events is initiated by the spontaneous flipping of DAG, which is known for its very fast transbilayer translocation, between the two membrane leaflets. The movement of DAG, a particularly potent cone-shaped inducer of membrane bending, from the lumenal to the cytosolic leaflet of the membrane bilayer coincides with the translocation of the glycerophospholipid PS in the opposite direction. This bi-directional movement of

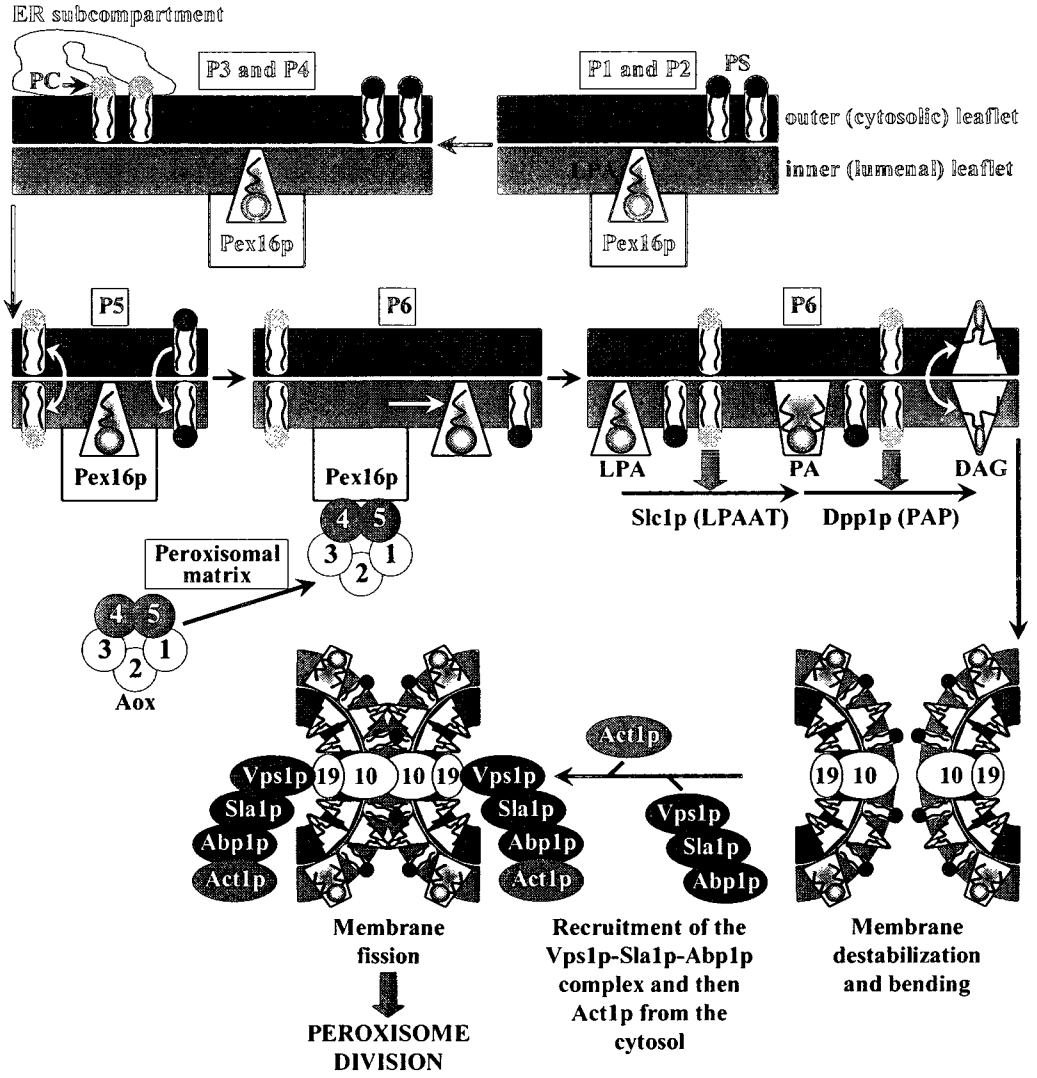


**Figure 2.35.** The Pex16p- and Aox-dependent intraperoxisomal signaling cascade drives the division of mature peroxisomes P6 by promoting the stepwise remodeling of lipid and protein composition of the peroxisomal membrane. See Discussion for details.

DAG and PS generates a lipid imbalance across the bilayer, which may promote the destabilization and bending of the membrane. The biosynthesis of PA and DAG in the membrane of mature peroxisomes and, perhaps, the bending of the membrane due to the bi-directional transbilayer movement of DAG and PS promote the docking of the Vps1p-

Sla1p-Abp1p complex to the surface of mature peroxisomes. This pre-assembled in the cytosol protein complex binds to mature peroxisomes by interacting with the peroxin Pex19p. Pex19p is a component of the Pex10p-Pex19p complex that is formed in the peroxisomal membrane during the earliest steps of peroxisome assembly. After its attachment to the peroxisomal membrane, the Vps1p-Sla1p-Abp1p complex interacts with Act1p, thereby recruiting this structural constituent of actin cytoskeleton to the surface of mature peroxisomes. The subsequent fission of the peroxisomal membrane leads to peroxisome division.

It remains to be established how exactly Vps1p promotes peroxisome division. Initially, this dynamin-like GTPase interacts in the cytosol with Sla1p and Abp1p. Vps1p then functions in the attachment of the Vps1p-Sla1p-Abp1p protein complex to its docking factor Pex19p on the surface of mature peroxisomes, thereby promoting the subsequent recruitment of actin to the membrane of division-competent peroxisomes. Therefore, it seems unlikely that Vps1p acts only as a mechanochemical enzyme [187] whose GTPase activity provides the mechanical force required for membrane fission in the constricted neck. Our data suggest that this dynamin-like protein may rather function as a regulatory GTPase [100] whose GTP-bound form promotes the multistep assembly of the membrane fission machinery, initially in the cytosol and then on the surface of division-competent mature peroxisomes. This machinery includes the Sla1p, Abp1p and Act1p components of actin cytoskeleton. The mechanism by which actin cytoskeleton regulates the terminal step of peroxisome division is currently being investigated.

Similar to mitotic Golgi fragmentation [160, 191] and mitochondrial division

during apoptosis [192], peroxisome division is served by a protein team that is assembled on the peroxisomal surface in a stepwise fashion. The multicomponent protein machineries serving Golgi fragmentation and mitochondrial division are assembled in response to extraorganellar stimuli [160, 192]. In contrast, the protein team that executes peroxisome division undergoes multistep assembly in response to an intraperoxisomal signaling cascade (Figure 2.35). While this Pex16p- and Aox-dependent signaling cascade is turned off inside immature peroxisomal vesicles, it is activated inside mature peroxisomes. Thus, it seems likely that the intraperoxisomal cascade for fine-tuning the fission of peroxisomal membrane is an intrinsic feature of the multistep peroxisome biogenesis program. Perhaps, this program has been evolved in order to separate the dramatic changes in the composition and architectural design of the membrane bilayer, all of which occur during peroxisome division, from the process of protein translocation across this bilayer, which takes place during peroxisome assembly. One of the benefits of employing such a strategy for the temporal separation of the processes of peroxisome assembly and division is that some of the membrane components can efficiently function in both processes. In fact, the peroxins Pex10p and Pex19p known for their essential role in peroxisomal import of numerous matrix proteins and PMPs [15] are also required for the assembly of the peroxisome division machinery on the surface of mature peroxisomes.

## 2.6 Conclusions

My findings support the notion that a distinct set of lipid metabolic pathways operating in

organellar membranes and specific changes in the distribution of some lipids across the membrane bilayers provide a driving force for organelle division [141, 157 - 160, 163, 193]. It is tempting to speculate that, after its spontaneous flipping between the two leaflets of the peroxisomal membrane (Figure 2.35), DAG undergoes the selective enrichment in distinct lipid domains that: 1) facilitate membrane fission through coordinated changes in local membrane curvature; 2) initiate the assembly of the Vps1p-containing protein complexes on the surface of peroxisomes; and/or 3) promote the clustering of these protein complexes at the membrane fission site. A challenge for the future will be to define the spatial distribution of DAG and Vps1p-containing protein complexes in the membrane of division-competent mature peroxisomes.

# 3 The role of Acyl-CoA oxidase and other peroxisomal enzymes of fatty acid oxidation in controlling the rate of chronological aging

## 3.1 Abstract

Calorie restriction (CR) is found to extend lifespan in a wide variety of Eukaryotes including the single-celled budding yeast *Saccharomyces cerevisiae*. The commonly accepted "free radical theory" of aging proclaims that: (1) A variety of metabolic reactions within the cell and exogenous agents generate free radicals, including ROS; (2) ROS damage various cellular constituents such as nucleic acids, proteins and lipids; (3) some of this damage cannot be reversed, and thus accumulates over time; and (4) the accumulation of damaged cellular constituents causes aging and associated degenerative disorders. My findings provide the first comprehensive evidence that ROS that are produced in the peroxisome in the first, Aox-catalyzed reaction of fatty acid β-oxidation do not regulate longevity in yeast under CR conditions. Moreover, I found that mitochondria, not peroxisomes generate the bulk of ROS in chronologically aging yeast placed on a CR diet. Unexpectedly, my studies aimed at elucidating the role for peroxisomal fatty acid oxidation in yeast longevity revealed that the formation of acetyl-CoA, not of ROS, via peroxisomal β-oxidation of neutral lipids-derived fatty acids is mandatory for extending lifespan of CR yeast. My findings also led to the conclusion that the rate of peroxisomal β-oxidation of fatty acids that originate from stored neutral lipids controls the pace of chronological aging by modulating essential processes taken place in mitochondria.

## 3.2 Introduction

Most of the known genetic manipulations that extend lifespan have been shown to cause major side effects, including irreversible developmental or reproductive defects [194]. An alternative way in which lifespan has been shown to be lengthened in various organisms is to impose a calorie restriction (CR) diet, which refers to a dietary regimen low in calories without undernutrition. It is well established that CR significantly extends lifespan of a remarkable range of organisms, including yeast, rotifers, spiders, worms, fish, mice, rats, and nonhuman primates [79, 81, 82, 194, 195]. This longevity results from the limitation of total calories derived from carbohydrates, fats or proteins to a level 25% - 60% below that of control animals fed *ad libitum* [79, 194].

In yeast, CR can be imposed by reducing the glucose concentration in the complete YEPD medium from the usual 2% to 0.5% [89] or to 0.2% (this study). Because cells continue to feed on yeast extract plus peptone, which are rich in amino acids, nucleotides, and vitamins, the growth rate remains rapid as glucose levels are lowered. Thus, the reduction in glucose from 2% to 0.5% or to 0.2% could impose a state of partial energy (ATP) limitation.

Even though CR is known for many years as the most effective way of extending lifespan of various organisms without genetically altering them, the mechanism(s) of its anti-aging action remain(s) unclear. Its complexity lies in multiple effects including metabolic, neuroendocrine, and apoptotic changes, which vary in intensity and exhibit striking differences among specific organ systems [73, 77]. A leading theory is that aging is caused by cumulative oxidative damage generated by ROS produced during respiration

[94, 95]. Oxidative damage to DNA, RNA, protein, and lipids has indeed been demonstrated to occur with aging [93 - 96]. This damage may limit life span. In fact, overexpression of the enzyme superoxide dismutase (SOD), which reduces ROS, extends lifespan in *Drosophila* [97] and in stationary phase yeast cells [98].

ROS are generated in multiple compartments and by multiple enzymes within the cell (Figure 3.1). Although the vast majority (estimated at approximately 90%) of these harmful compounds is produced in mitochondria (Figure 3.1) [99 - 102], ROS are also generated by NADP/H oxidases and phagocytic oxidases in the plasma membrane [99 - 102], in several oxidative reactions that are catalyzed by amino acid oxidases, cyclooxygenases, lipid oxigenase and xanthine oxidase in the cytosol [99 - 102], and during lipid metabolism in peroxisomes [7, 30] (Figure 3.1). The steady-state level of ROS within the cell is the result of a delicate balance that exists between the rates of ROS formation and of their detoxification in antioxidant scavenger reactions taking place in various cellular locations (Figure 3.2). The CuZnSOD (SOD1) subform of superoxide dismutase in the cytosol and the MnSOD (SOD2) subform of this enzyme in the mitochondrion convert superoxide radicals to a less toxic and more stable compound, namely hydrogen peroxide (Figure 3.2) [99 - 102]. The subsequent detoxification of hydrogen peroxide depends on the following enzymes (Figure 3.2) [99 - 102]: 1) glutathione peroxidases in the cytosol, mitochondria and peroxisomes; 2) catalases in the cytosol, mitochondria and peroxisomes; and 3) peroxiredoxins in the cytosol, mitochondria and peroxisomes.

Lipid metabolism in peroxisomes generates ROS [7, 30]. The only chemical

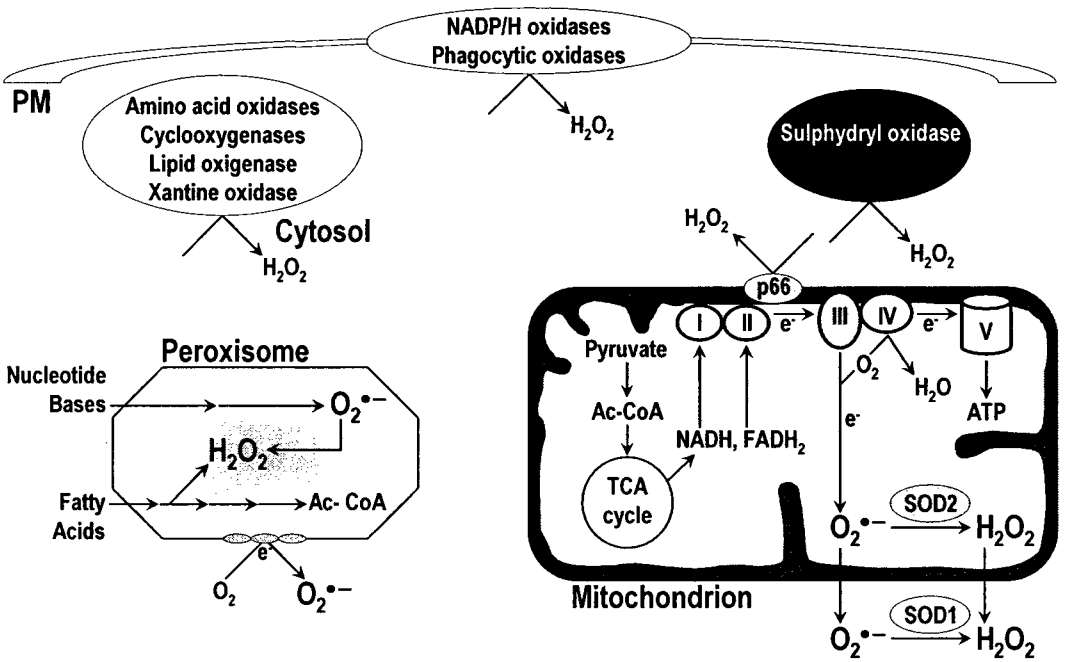


**Figure 3.1.** ROS are generated by numerous enzymes in multiple compartments within the cell, mostly (~ 90%) within mitochondria.

reaction leading to the formation of hydrogen peroxide, the most abundant ROS molecule in the cell, is catalyzed by Aox. This peroxisomal enzyme promotes the first step in the metabolic pathway for β-oxidation of fatty acids, thereby controlling the level of ROS produced in the peroxisome. On the other hand, a peroxisomal catalase, encoded by the *CTA1* gene, can detoxify hydrogen peroxide inside the organelle, and is known to aid in the resistance to exogenously added hydrogen peroxide.

My research began investigating a possible link between steady state levels of peroxisomal ROS and CR-dependant chronological lifespan extension. By reducing the steady state level of ROS in peroxisomes of CR yeast using genetic manipulations, I was hoping to extend lifespan by further limiting the amount of ROS produced in the cell.

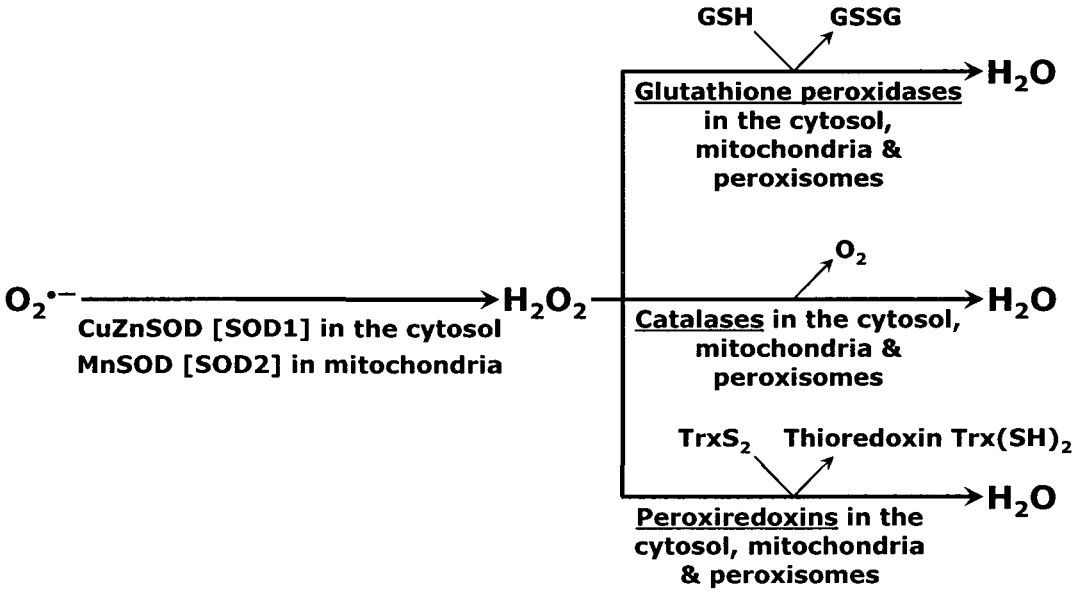


**Figure 3.2.** Detoxification of ROS occurs in antioxidant scavenger reactions that take place in the cytosol, mitochondria and peroxisomes.

Unexpectedly, I discovered that lack of the ROS-producing peroxisomal Aox shortened, not extended, the chronological lifespan of CR yeast. Thus, contrary to my initial hypothesis, the rate of ROS production in peroxisomes does not control the rate of chronological aging. On the other hand, my observation that lack of Aox causes premature aging suggested that some processes taking place in the peroxisome, perhaps β-oxidation of fatty acids, play essential role in the aging process. I therefore decided to elucidate: 1) how exactly, in molecular terms, lipid metabolism in peroxisomes control yeast aging; and 2) what are the logistics of integrating peroxisomal lipid metabolism into a network of cellular processes that govern yeast aging.

## 3.3 Materials and Methods

### Strains and media

The wild-type strain *Saccharomyces cerevisiae* BY4742 (*MATα his3Δ1 leu2Δ0 lys2Δ0 ura3Δ0*) and mutant strains *pex1Δ* (*MATα his3Δ1 leu2Δ0 lys2Δ0 ura3Δ0 pex1Δ::kanMX4*), *pex5Δ* (*MATα his3Δ1 leu2Δ0 lys2Δ0 ura3Δ0 pex5Δ::kanMX4*), *pex6Δ* (*MATα his3Δ1 leu2Δ0 lys2Δ0 ura3Δ0 pex6Δ::kanMX4*), *pex7Δ* (*MATα his3Δ1 leu2Δ0 lys2Δ0 ura3Δ0 pex7Δ::kanMX4*), *fox1Δ* (*MATα his3Δ1 leu2Δ0 lys2Δ0 ura3Δ0 fox1Δ::kanMX4*), *cta1Δ* (*MATα his3Δ1 leu2Δ0 lys2Δ0 ura3Δ0 cta1Δ::kanMX4*), *fox2Δ* (*MATα his3Δ1 leu2Δ0 lys2Δ0 ura3Δ0 fox2Δ::kanMX4*), *mdh3Δ* (*MATα his3Δ1 leu2Δ0 lys2Δ0 ura3Δ0 mdh3Δ::kanMX4*), and *fox3Δ* (*MATα his3Δ1 leu2Δ0 lys2Δ0 ura3Δ0 fox3Δ::kanMX4*) were used in this study. Media components were as follows: 1) YEPD (0.2% Glucose), 1% yeast extract, 2% peptone, 0.2% glucose; and 2) YEPD (2% Glucose), 1% yeast extract, 2% peptone, 2% glucose.

### A plating assay for the analysis of chronological life span

Cells were grown in YEPD (0.2% Glucose) medium at 30°C with rotational shaking at 200 rpm in Erlenmeyer flasks at a flask volume/medium volume ratio of 5:1. A sample of cells was removed from each culture at various time points. A fraction of the cell sample was diluted in order to determine the total number of cells per ml of culture using a hemacytometer. 10 µl of serial dilutions (1:10 to $1:10^3$) of cells were applied to the hemacytometer, where each large square is calibrated to hold 0.1 µl. The number of cells in 4 large squares was then counted and an average was taken in order to ensure greater

accuracy. The concentration of cells was calculated as follows: number of cells per large square x dilution factor x 10 x 1,000 = total number of cells per ml of culture. A second fraction of the cell sample was diluted and serial dilutions ($1:10^2$ to $1:10^5$) of cells were plated onto YEPD (2% Glucose) plates in triplicate in order to count the number of viable cells per ml of each culture. 100 µl of diluted culture was plated onto each plate. After a 48-h incubation at 30°C, the number of colonies per plate was counted. The number of colony forming units (CFU) equals to the number of viable cells in a sample. Therefore, the number of viable cells was calculated as follows: number of colonies x dilution factor x 10 = number of viable cells per ml. For each culture assayed, % viability of the cells was calculated as follows: number of viable cells per ml / total number of cells per ml x 100%. The % viability of cells in mid-logarithmic phase was set at 100% viability for that particular culture.

**Plating assays for the analysis of resistance to various stresses**

For the analysis of hydrogen peroxide resistance, serial dilutions ($1:10^0$ to $1:10^5$) of wild-type and mutant cells removed from mid-logarithmic phase (day 1) and from diauxic phase (days 2 and 3) in YEPD (0.2% Glucose) were spotted onto two sets of plates. One set of plates contained YEPD (2% Glucose) medium alone, whereas the other set contained YEPD (2% Glucose) medium supplemented with 5 mM hydrogen peroxide. Pictures were taken after a 3-day incubation at 30°C.

For the analysis of oxidative stress resistance, serial dilutions ($1:10^0$ to $1:10^5$) of wild-type and mutant cells removed from mid-logarithmic phase (day 1) and from

diauxic phase (days 2 and 3) in YEPD (0.2% Glucose) were spotted onto two sets of plates. One set of plates contained YEPD (2% Glucose) medium alone, whereas the other set contained YEPD (2% Glucose) medium supplemented with 2.5 mM of the superoxide/hydrogen peroxide-generating agent paraquat. Pictures were taken after a 3-day incubation at 30°C.

For the analysis of heat-shock resistance, serial dilutions ($1:10^0$ to $1:10^5$) of wild-type and mutant cells removed from mid-logarithmic phase (day 1) and from diauxic phase (days 2 and 3) in YEPD (0.2% Glucose) were spotted onto two sets of YEPD (2% Glucose) plates. One set of plates was incubated at 30°C. The other set of plates was initially incubated at 55°C for 30 min, and was then transferred to 30°C. Pictures were taken after a 3-day incubation at 30°C.

For the analysis of salt stress resistance, serial dilutions ($1:10^0$ to $1:10^5$) of wild-type and mutant cells removed from mid-logarithmic phase (day 1) and from diauxic phase (days 2 and 3) in YEPD (0.2% Glucose) were spotted onto two sets of plates. One set of plates contained YEPD (2% Glucose) medium alone, whereas the other set contained YEPD (2% Glucose) medium supplemented with 0.5 M NaCl. Pictures were taken after a 3-day incubation at 30°C.

For the analysis of osmotic stress resistance, serial dilutions ($1:10^0$ to $1:10^5$) of wild-type and mutant cells removed from mid-logarithmic phase (day 1) and from diauxic phase (days 2 and 3) in YEPD (0.2% Glucose) were spotted onto two sets of plates. One set of plates contained YEPD (2% Glucose) medium alone, whereas the other set contained YEPD (2% Glucose) medium supplemented with 1 M sorbitol. Pictures

were taken after a 3-day incubation at 30°C.

**Monitoring the formation of ROS**

Wild-type and mutant cells grown in YEPD (0.2% Glucose) were tested microscopically for the production of ROS by incubation with dihydrorhodamine 123 (DHR). In the cell, this nonfluorescent compound can be oxidized to the fluorescent chromophore rhodamine 123 by ROS. Cells were also probed with a fluorescent counterstain Calcofluor White M2R (CW), which stains the yeast cell walls fluorescent blue. CW was added to each sample in order to label all cells for their proper visualization. DHR was stored in the dark at –20°C as 50 µl aliquots of a 1 mg/ml solution in ethanol. CW was stored in the dark at –20°C as the 5 mM stock solution in anhydrous DMSO (dimethylsulfoxide).

The concurrent staining of cells with DHR and CW was carried out as follows. The required amounts of the 50 µl DHR aliquots (1 mg/ml) and of the 5 mM stock solution of CW were taken out of the freezer and warmed to room temperature. The solutions of DHR and CW were then centrifuged at 21,000 x g for 5 min in order to clear them of any aggregates of fluorophores. For cell cultures with a titre of ~ $10^7$ cells/ml, 100 µl was taken out of the culture to be treated. If the cell titre was lower, proportionally larger volumes were used. 6 µl of the 1 mg/ml DHR and 1 µl of the 5 mM CW solutions were added to each 100 µl aliquot of culture. After a 2-h incubation in the dark at room temperature, the samples were centrifuged at 21,000 x g for 5 min. Pellets were resuspended in 10 µl of PBS buffer (20 mM $KH_2PO_4$/KOH, pH 7.5, and 150 mM NaCl). Each sample was then supplemented with 5 µl of mounting medium, added to a

microscope slide, covered with a coverslip, and sealed using nail polish. Once the slides were prepared, they were visualized under the Zeiss Axioplan fluorescence microscope mounted with a SPOT Insight 2 megapixel color mosaic digital camera. Several pictures of the cells on each slide were taken, with two pictures taken of each frame. One of the two pictures was of the cells seen through a rhodamine filter in order to detect cells dyed with DHR. The second picture was of the cells seen through a DAPI filter in order to visualize CW, and therefore all the cells present in the frame.

For evaluating the percentage of DHR-positive cells, the UTHSCSA Image Tool (Version 3.0) software was used to calculate both the total number of cells and the number of stained cells. Fluorescence of individual DHR-positive cells in arbitrary units was determined by using the UTHSCSA Image Tool software (Version 3.0). In each of 3-5 independent experiments, the value of median fluorescence was calculated by analyzing at least 800-1000 cells that were collected at each time point. The median fluorescence values were plotted as a function of the number of days cells were cultured.

**Visualization of intracellular lipid bodies**

Wild-type and mutant cells grown in YEPD (0.2% Glucose) were tested microscopically for the presence of intracellular lipid bodies (LB) by incubation with BODIPY 493/503. Cells were also probed with a fluorescent counterstain CW in order to visualize all cells in the population. BODIPY 493/503 was stored in the dark at –20°C as 100 µl aliquots of a 1 mM solution in ethanol. CW was stored in the dark at –20°C as the 5 mM stock solution in anhydrous DMSO.

The concurrent staining of cells with BODIPY 493/503 and CW was carried out as follows. The required amounts of the 100 µl BODIPY 493/503 aliquots (1 mM) and of the 5 mM stock solution of CW were taken out of the freezer and warmed to room temperature. The solutions of DHR and CW were then centrifuged at 21,000 x g for 5 min in order to clear them of any aggregates of fluorophores. For cell cultures with a titre of ~ $10^7$ cells/ml, 100 µl was taken out of the culture to be treated. If the cell titre was lower, proportionally larger volumes were used. The samples were then centrifuged at 21,000 x g for 1 min, and pelleted cells were resuspended in 100 µl of TNT buffer (25 mM Tris/HCl (pH 7.5), 150 mM NaCl and 0.2 % Triton X-100). After a 10-min incubation at room temperature, the samples were centrifuged at 21,000 x g for 1 min. Pellets were then resuspended in 100 µl of TN buffer (25 mM Tris/HCl (pH 7.5), 150 mM NaCl), and the samples were subjected to centrifugation at 21,000 x g for 1 min. Pelleted cells were finally resuspended in 100 µl of TN buffer. Each 100 µl aliquot of cells was then supplemented with 1 µl of the 1 mM BODIPY 493/503 and 1 µl of the 5 mM CW solutions. After a 15-min incubation in the dark at room temperature, the samples were centrifuged at 21,000 x g for 5 min. Pellets were resuspended in 100 µl of TN buffer. The samples were centrifuged again at 21,000 x g for 5 min, and pellets were resuspended in 100 µl of TN buffer. 10 µl of the BODIPY 493/503- and CW-treated cell suspension was then added to a microscope slide and covered with a coverslip. The slides were then sealed using nail polish. Once the slides were prepared, they were visualized under the Zeiss Axioplan fluorescence microscope mounted with a SPOT Insight 2 megapixel color mosaic digital camera. Several pictures of the cells on each slide were

taken, with two pictures taken of each frame. One of the two pictures was of the cells seen through a fluorescein filter in order to detect cells dyed with BODIPY 493/503. The second picture was of the cells seen through a DAPI filter in order to visualize CW, and therefore all the cells present in the frame. For evaluating the percentage of BODIPY 493/503-positive cells, the UTHSCSA Image Tool (Version 3.0) software was used to calculate both the total number of cells and the number of stained cells.

**Immunofluorescence microscopy**

Cell cultures were fixed in 3.7% formaldehyde for 45 min at room temperature. The cells were washed in solution B (100 mM $KH_2PO_4$/KOH pH 7.5, 1.2 M sorbitol), treated with Zymolyase 100T (MP Biomedicals, 1 μg Zymolyase 100T/1 mg cells) for 30 min at 30°C and then processed as previously described [66]. Monoclonal antibody raised against porin (Invitrogen, 0.25 μg/μl in TBSB buffer [20 mM Tris/HCl pH 7.5, 150 mM NaCl, 1mg/ml BSA]) was used as a primary antibody. Alexa Fluor 568 goat anti-mouse IgG (Invitrogen, 2 μg/μl in TBSB buffer) was used as a secondary antibody. The labeled samples were mounted in mounting solution (16.7 mM Tris/HCl pH 9.0, 1.7 mg/ml *p*-phenylenediamine, 83% glycerol). Images were collected with a Zeiss Axioplan fluorescence microscope (Zeiss) mounted with a SPOT Insight 2 megapixel color mosaic digital camera (Spot Diagnostic Instruments).

**Oxygen consumption assay**

The rate of oxygen consumption by yeast cells recovered at various time points was

measured continuously in a 2-ml stirred chamber using a custom-designed biological oxygen monitor (Science Technical Center of Concordia University) equipped with a Clark-type oxygen electrode. 1 ml of YEPD medium supplemented with 0.2% glucose was added to the electrode for approximately 5 minutes to obtain a baseline. Cultured cells of a known titre were spun down at 3,000 x g for 5 minutes. The resulting pellet was resuspended in YEPD medium supplemented with 0.2% glucose and then added to the electrode with the medium that was used to obtain a baseline. The resulting slope was used to calculate the rate of oxygen consumption in $O_2\%$ x $min^{-1}$ x $10^9$ cells.

**Electron microscopy and morphometric analysis**

Cells were fixed in 1.5% $KMnO_4$ for 20 min at room temperature, dehydrated by successive incubations in increasing concentrations of ethanol, and embedded in Poly/Bed 812 epoxy resin (Polysciences). Ultrathin sections were cut using an Ultra-Cut E Microtome (Reichert-Jung). Silver/gold thin sections from the embedded blocks were examined in a JEOL JEM-2000FX transmission electron microscope. For morphometric analysis of random electron microscopic sections of cells, digitized images were analyzed using the UTHSCSA Image Tool (Version 3.0) software. In each of 2 independent experiments, the percentage of cells that contain pexopodia and/or accumulate gnarled LB was calculated by analyzing at least 300 cells that were collected at each time point. The values of the percentage of cells containing pexopodia and/or accumulating gnarled LB were plotted as a function of the number of days cells were cultured.

## 3.4 Results

### 3.4.1 Kinetics of growth and aging of wild-type cells on various glucose concentrations

Cells were grown in an aqueous medium containing YEP (1% yeast extract and 2% bacto peptone) and one of four concentrations of glucose: 0.2%, 0.5%, 1%, and 2%. The full growth cycle of wild-type culture in each of these four media begins with logarithmic phase and progresses through diauxic and post-diauxic phases to stationary phase (Figure 3.3 A). In logarithmic phase, the cells use glucose to make energy via glycolysis (Figure 3.3 B). The diauxic and post-diauxic phases occur when nutrients become limited and energy metabolism shifts to respiration, at which point mitochondrial proteins are synthesized, growth rate slows, and cells utilize ethanol and other two and three carbon compounds for energy production. After a 7-day incubation, wild-type cells enter stationary phase. In this phase, the metabolic rate slows and cells are unable to divide.

Using a plate assay for monitoring chronological lifespan (Figure 3.4; see the "Materials and methods" section of this chapter for a detailed description of the assay), I examined the lifespans of yeast cultures grown on four different concentrations of glucose. It should be stressed that the plate assay that we are employing for monitoring chronological life span is a standard assay that is routinely used for this purpose by other laboratories (Figure 3.5) [196]. Furthermore, the terms "survival" and "alive cells" (Figure 3.5) are widely used for referring to survival by quiescent yeast cells of the aging-promoted accumulation of molecular and cellular damage [196].

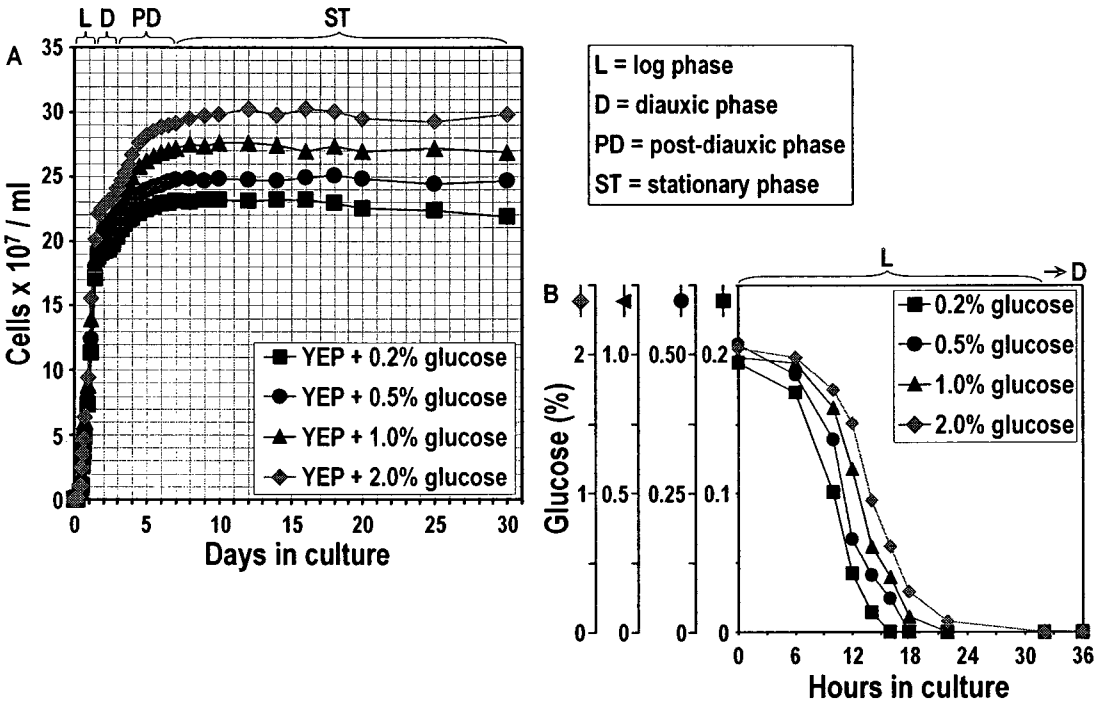


**Figure 3.3.** Kinetics of growth and glucose consumption by wild-type strain. (A) Cells undergo four phases of growth. In the logarithmic (L) phase, cells ferment glucose and grow exponentially. In the diauxic (D) phase, cells use ethanol as a carbon source and their growth rate is reduced. In the post-diauxic (PD) phase, the growth rate is reduced even more and finally in stationary (ST) phase the cells stop dividing. (B) Glucose in the medium is almost entirely consumed by the end of the first day of cell growth, regardless of how much was in the medium to begin with.

As shown in Figure 3.6, CR cells grown on 0.5% or 0.2% glucose lived significantly longer than non-CR-yeast grown on 1% or 2% glucose. Mean lifespan of the cells grown on 0.5% glucose nearly doubled that of those grown on 2% (Figures 3.6 B and C). Thus, 0.5% is an optimal concentration of glucose for achieving the benefit of CR-dependent age extension. Those cells grown at 1% outlived those grown at 2%, while those grown at 0.5% outlived those grown at 1%, representing a dose-response relationship between the rate of chronological aging and the degree of CR (Figure 3.6 B).

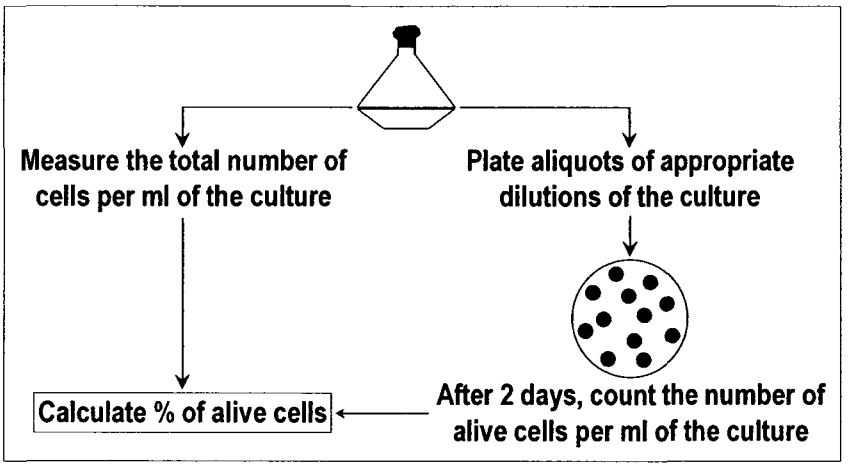


**Figure 3.4.** A plating assay for the analysis of chronological lifespan. Chronological lifespan in yeast, which mimics aging of nondividing or "post-mitotic" cells of higher eukaryotic organisms, is the length of time a population of yeast cells remains viable in a nondividing state.

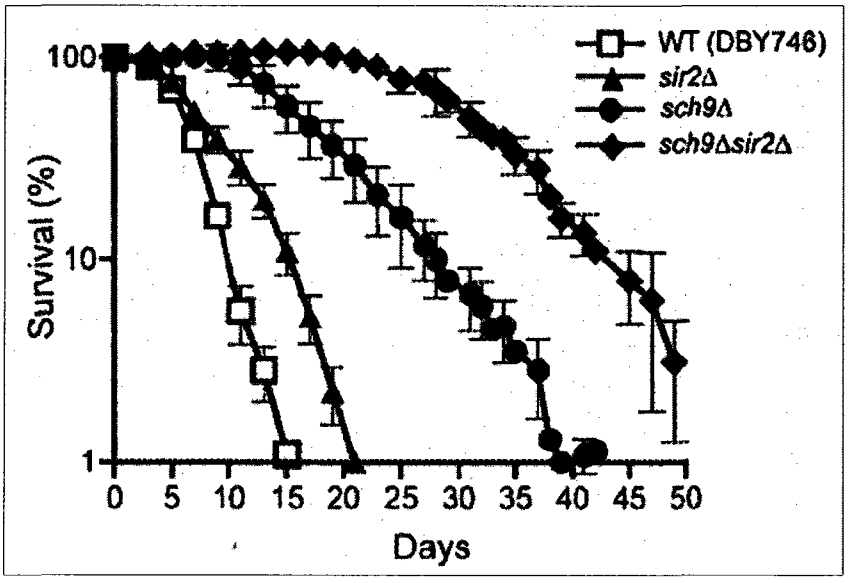


**Figure 3.5.** The plate assay that we are employing for monitoring chronological life span is a standard assay that is routinely used for this purpose by other laboratories. Data from Fabrizio *et al. Cell* (2005) 123:655-667.

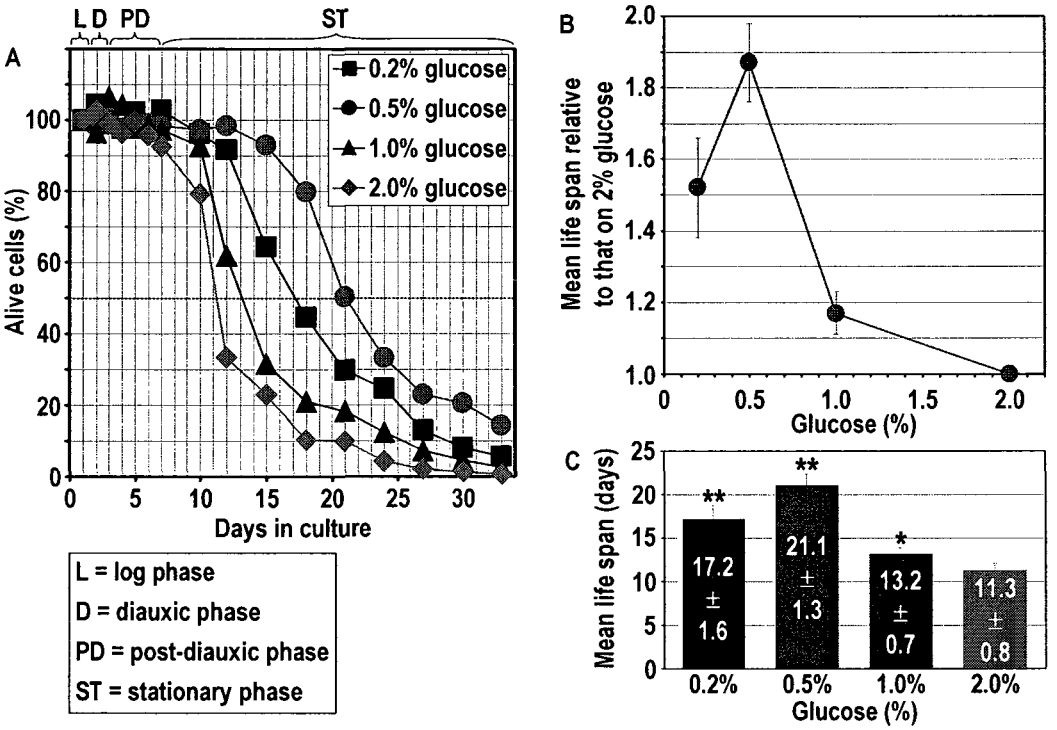


**Figure 3.6.** A dose-response relationship between the rate of aging and the degree of calorie restriction. (A) Cells begin to die by the end of the post-diauxic phase. The death of cells grown under CR conditions (*i.e.*, on 0.2% or 0.5% glucose) is delayed, as compared to cells grown under non-CR conditions (*i.e.*, on 1.0% or 2.0% glucose). (B) Cells grown on 0.5% glucose have the highest mean lifespan of cells grown on the four glucose concentrations tested. (C) Mean lifespans of cells grown on 0.2%, 0.5%, 1.0% or 2.0% glucose.

Importantly, the measurement of ATP in cells grown on four different concentrations of glucose revealed that the intracellular levels of ATP and the dynamics of their change during chronological aging were very similar in CR and non-CR yeasts (unpublished data from Dr. Titorenko's laboratory). Thus, yeast cells placed on the CR diet are not starving. Based on my aforementioned findings, I hypothesized that: (1) CR yeast remodel their metabolism in order to match the level of ATP produced by non-CR yeast; and (2) such specific remodeling of metabolism in CR yeast extends their lifespan.

### 3.4.2 ROS that are produced in peroxisomes are not essential for chronological aging

With a portion of the intracellular ROS being produced in the Aox-dependent reaction of peroxisomal fatty acid oxidation, I set out to see if the amount of peroxisome-produced ROS plays a role in chronological aging under CR conditions. Peroxisomal Aox, a product of the *S. cerevisiae FOX1* gene, catalyzes the reaction whereby activated free fatty acids are oxidized to form trans-2-enol-CoA. This reaction produces a quantity of hydrogen peroxide that can then be detoxified, using the peroxisomal catalase Cta1p, to form water and molecular oxygen (Figure 3.7). I tested a *fox1Δ* mutant strain for the rate of chronological aging on 0.2% glucose, hence knocking out its ROS-producing reaction, with the hypothesis that limiting the amount of ROS in the peroxisome may increase the lifespan of yeast cells. Contrary to my expectation, the mutant strain exhibited a shortened lifespan, aging prematurely once the cells reached the stationary phase of growth (Figure 3.7). In addition to the *fox1Δ* mutant strain, I also tested a *cta1Δ* mutant strain placed on the CR diet, under the same hypothesis as that was made for Fox1p. It appeared that lack of the ROS-decomposing peroxisomal catalase Cta1p has little effect on chronological aging under CR conditions (Figure 3.7). Not only does this finding suggest a very little or no role for peroxisomal ROS in chronological aging under CR, but it also provides evidence for an important regulatory role for peroxisomal β-oxidation of fatty acids in delaying chronological aging.

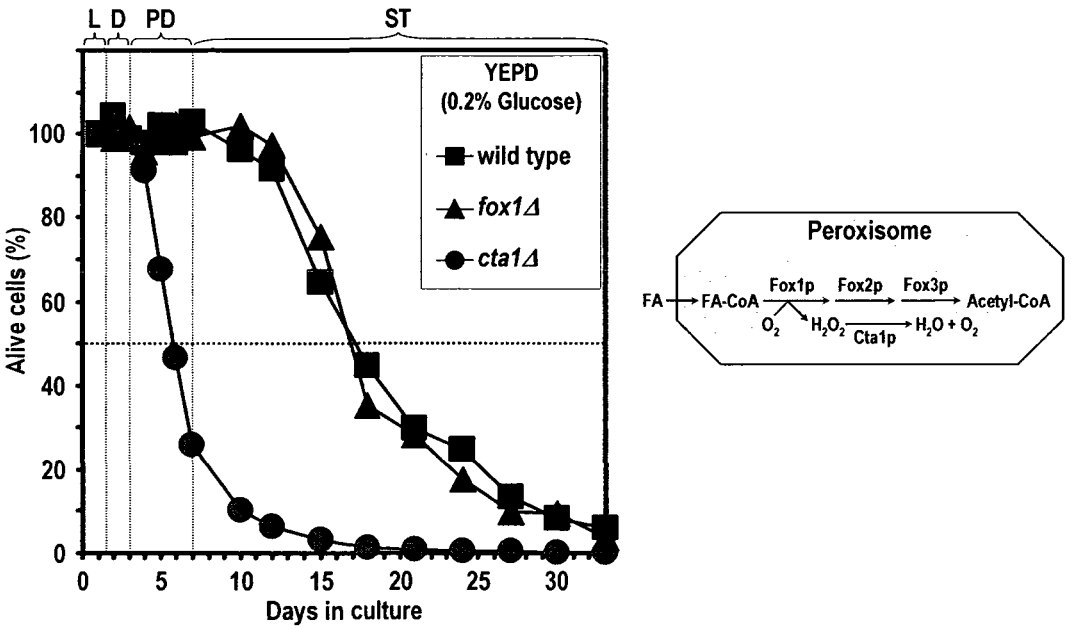


**Figure 3.7.** ROS that are produced in peroxisomes during fatty acid oxidation are not essential for chronological aging of CR yeast. Lack of the $H_2O_2$-producing peroxisomal Fox1p shortens, not extends, life span. Lack of the $H_2O_2$-decomposing peroxisomal Cta1p has little effect on chronological aging under CR.

### 3.4.3 Mitochondria, not peroxisomes, consume the vast majority of $O_2$ and produce the bulk of ROS

To test further my hypothesis that peroxisomal ROS produced in the oxygen-consuming reaction catalyzed by Fox1p (Aox) do not affect the rate of chronological aging in CR-dieting yeast, I measured the rate of oxygen consumption and the level of ROS production by CR cells that lack this protein. I found that the rate of oxygen consumption by CR cells of wild-type strain significantly increased when these cells entered the diauxic phase of growth on 0.2% glucose and then gradually declined through the post-diauxic and stationary phases (Figure 3.8). In contrast, after a dramatic increase in CR cells entering the diauxic phase of growth on 0.2% glucose to the levels that

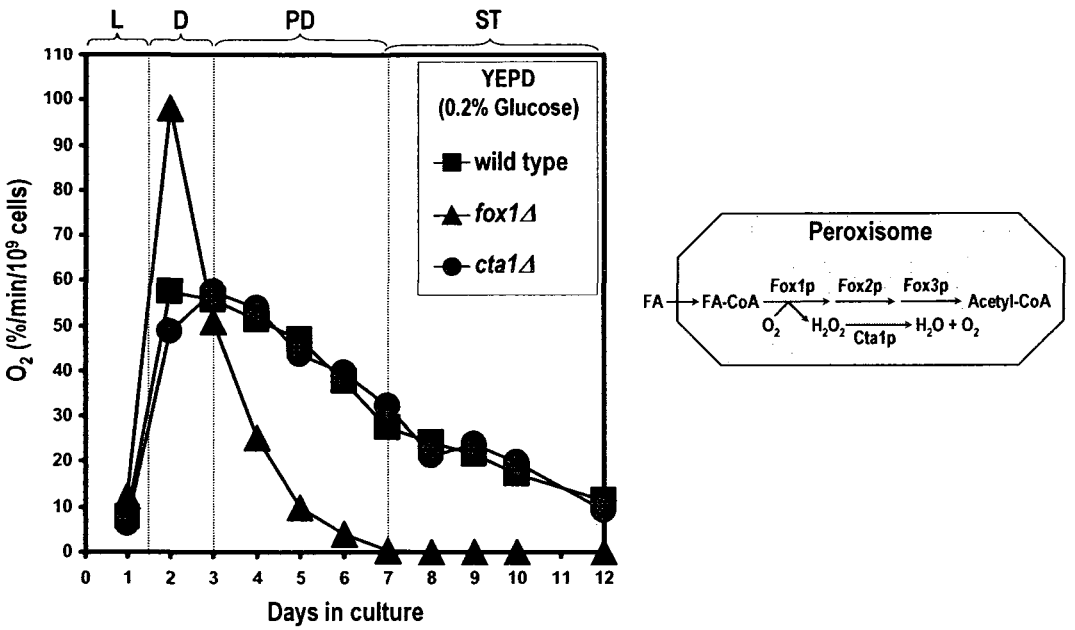


**Figure 3.8.** Peroxisomes do not consume significant amounts of oxygen in CR yeast cells. Dynamics of changes in the rate of oxygen consumption by CR cells during chronological aging of the wild-type, *fox1Δ* and *cta1Δ* strains grown on 0.2% glucose.

significantly exceeded those by respiring wild-type cells, the rate of oxygen consumption by *fox1Δ* mutant cells abruptly decreased so that upon entering stationary phase mutant cells consumed negligible amounts of oxygen (Figure 3.8). The observed during diauxic phase spike in the rate of oxygen consumption by *fox1Δ* mutant cells lacking Aox, which is the only known oxygen-consuming peroxisomal protein, strongly suggest that: (1) peroxisomes do not consume significant amounts of oxygen in CR yeast cells; and (2) the bulk of oxygen in CR yeast is consumed by mitochondria engaged into oxidative phosphorylation. My findings also suggested that the observed abrupt decline of oxygen consumption rate by CR *fox1Δ* mutant cells during post-diauxic phase, which followed the spike of respiration rate in diauxic phase, was due to the failure of oxidative

phosphorylation in mitochondria of *fox1Δ* mutant cells placed on the CR diet. This second assumption appeared to be correct (please see below).

I then used the fluorescent dye Dihydrorhodamine-123 (DHR) for monitoring the dynamics of changes in the intracellular levels of ROS during chronological aging of wild-type and mutant strains. In the cell, this nonfluorescent compound can be oxidized to the fluorescent chromophore rhodamine 123 by ROS (Figure 3.9). I found that the number of ROS-positive CR cells of wild-type strain significantly increased when these cells entered the diauxic phase of growth on 0.2% glucose and then gradually declined through the post-diauxic and stationary phases (Figures 3.10 and 3.11). In contrast, after a substantial increase of ROS-positive CR cells of *fox1Δ* mutant strain entering the diauxic phase of growth on 0.2% glucose to the numbers very similar to those for wild-type strain, the number of ROS-positive *fox1Δ* mutant cells abruptly decreased so that only a minor portion of these cells had detectable levels of ROS upon entering stationary phase (Figures 3.10 and 3.11). The quantitation of the intensity of fluorescence signal detected by fluorescence microscopy in ROS-positive cells revealed that the intracellular level of ROS in CR wild-type strain significantly increased when these cells entered the diauxic phase of growth on 0.2% glucose and then gradually declined through the post-diauxic and stationary phases (Figure 3.11). In contrast, after a dramatic increase in CR cells entering the diauxic phase of growth on 0.2% glucose to the level that significantly exceeded that detected in wild-type cells, the intracellular level of ROS in *fox1Δ* mutant strain rapidly decreased so that upon entering stationary phase mutant cells possessed negligible amounts of ROS (Figure 3.11). The observed during diauxic phase spike in the

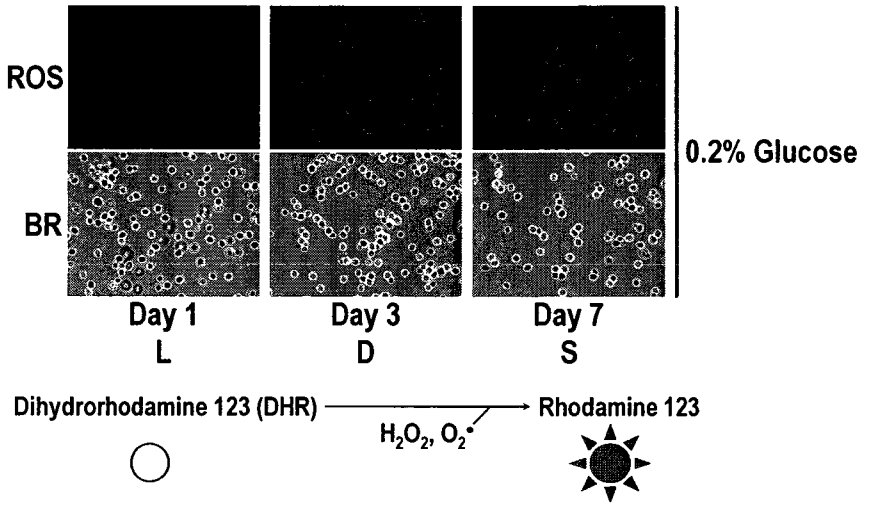


**Figure 3.9.** Using the fluorescent dye Dihydrorhodamine-123 (DHR) for monitoring the dynamics of changes in the intracellular levels of ROS during chronological aging of CR wild-type strain grown on 0.2% glucose. In the cell, DHR can be oxidized to the fluorescent chromophore rhodamine 123 by ROS. *BR*, bright-field image.

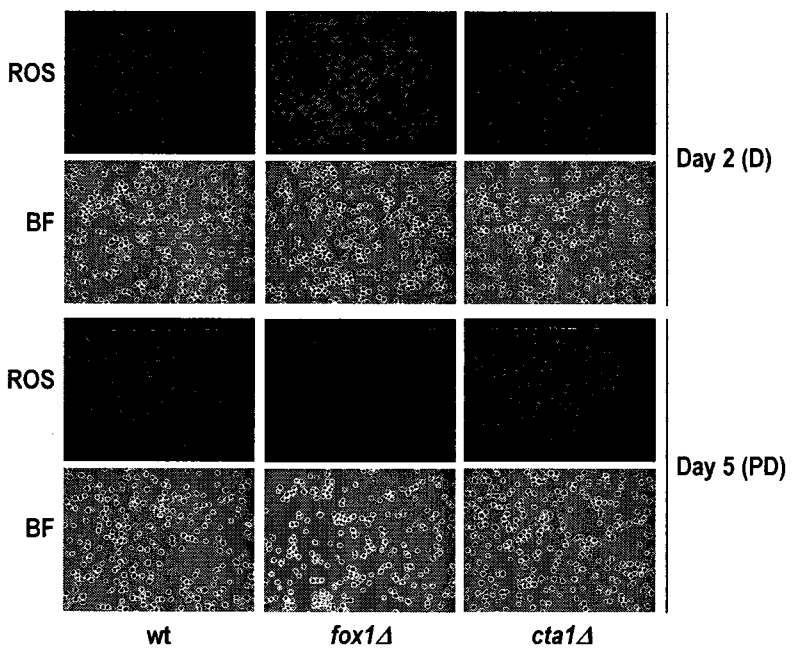


**Figure 3.10.** Peroxisomes do not produce significant amounts of ROS in CR yeast. ROS were visualized using fluorescence microscopy with DHR.

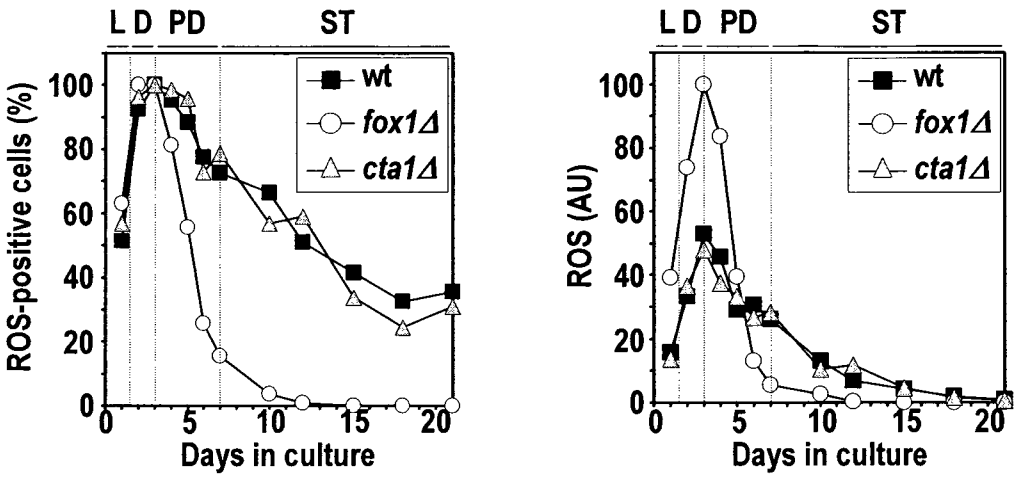


**Figure 3.11.** Peroxisomes do not produce the major portion of ROS in CR yeast. Dynamics of changes in the number of ROS-positive cells and intracellular level of ROS during chronological aging of the wild-type, *fox1Δ* and *cta1Δ* strains grown on 0.2% glucose.

intracellular level of ROS in *fox1Δ* mutant strain lacking Aox, which is the only known ROS-generating peroxisomal protein, strongly suggest that: (1) peroxisomes do not produce significant amounts of ROS in CR yeast; and (2) the bulk of ROS in CR yeast is produced by mitochondria due to the transfer of electrons from components of the electron transport chain to oxygen consumed by these organelles. My conclusion that peroxisomes do not produce significant amounts of ROS in CR yeast cells was further supported by my observation that both the number of ROS-positive cells and the intracellular levels of ROS during aging of the *cta1Δ* mutant strain lacking catalase, which is the only known ROS-degrading peroxisomal protein, were very similar to those found in aging wild-type strain (Figure 3.11).

### 3.4.4 The formation of acetyl-CoA via peroxisomal β-oxidation of neutral lipids-derived fatty acids is required for extending lifespan of CR yeast

Altogether, my aforementioned findings provided evidence that: (1) the Aox-dependent reaction in peroxisomes does not consume significant amounts of oxygen in CR yeast cells; and (2) the Aox-dependent reaction in peroxisomes does not produce significant amounts of ROS in CR yeast cells. On the other hand, lack of Aox in the *fox1Δ* mutant strain led to premature chronological aging of CR cells. Not only do these findings suggest a very little or no role for the Aox-dependent generation of peroxisomal ROS in modulating the pace of chronological aging under CR conditions, but they also strongly suggest that peroxisomal β-oxidation of fatty acids plays an important regulatory role in the beneficial effect of CR on yeast longevity. Because Aox catalyzes the first step in a three-step pathway of fatty acid oxidation in the peroxisome, I hypothesized that the formation of acetyl-CoA via peroxisomal β-oxidation of fatty acids is required for extending lifespan of CR yeast cells. I therefore tested the rates of chronological aging of the mutant strains *fox2Δ* and *fox3Δ*. These two mutants lack the enzymes that catalyze, respectively, the second and third steps of peroxisome-associated β-oxidation of free fatty acids leading to the formation of acetyl-CoA (Figure 3.12). I found that lack of any of these two proteins shortened chronological life span in a fashion similar to that for the strain lacking Fox1p, with a sharp decline in the percentage of alive cells occurring after entering the post-diauxic phase of growth on 0.2% glucose (Figure 3.12). In addition, each mutant lacking either one of the three peroxisomal β-oxidation enzymes suffered from the same sharp decrease in the rate of oxygen consumption after the diauxic phase

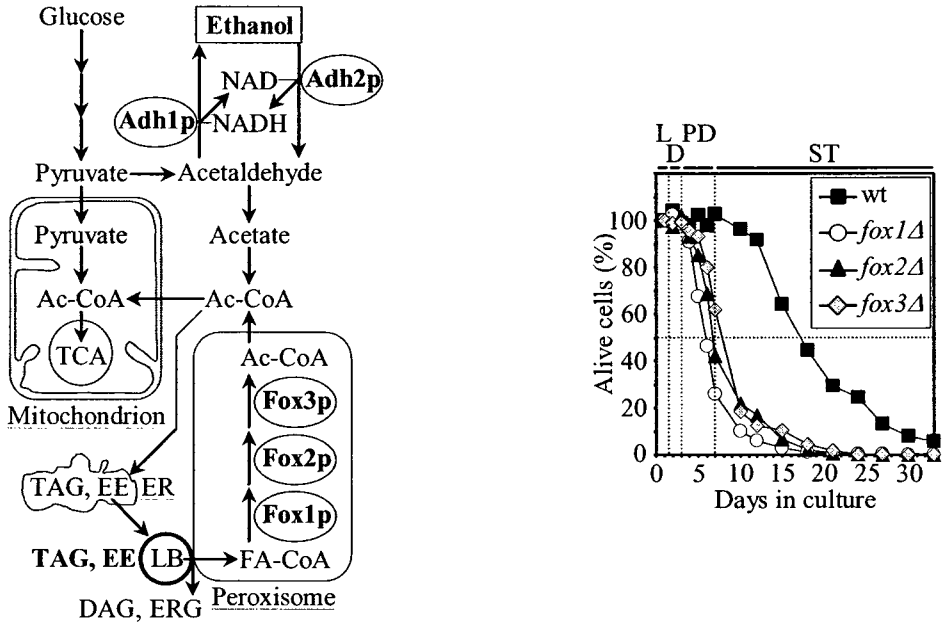


**Figure 3.12.** Any yeast mutant that lacks an enzyme required for the formation of acetyl-CoA in peroxisomes ages and dies as soon as it enters the post-diauxic phase of growth on 0.2% glucose.

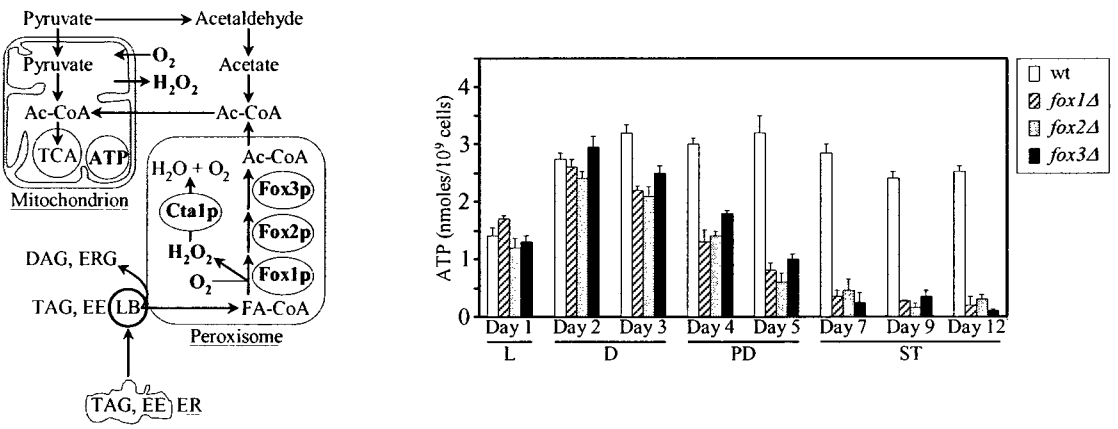


**Figure 3.13.** The inability of CR yeast entering post-diauxic phase to produce acetyl-CoA in peroxisomes results in the sharp decrease of mitochondrially synthesized ATP.

of growth (Figure 3.8). Taken together, my findings strongly suggested that the formation of acetyl-CoA via peroxisomal β-oxidation of fatty acids is required for extending lifespan of CR yeast cells only when they enter post-diauxic phase. The inability of CR yeast entering post-diauxic phase to produce acetyl-CoA in peroxisomes resulted in the sharp decrease of mitochondrially synthesized ATP (Figure 3.13), and thereby accelerated the aging process.

It should be stressed that the CoA-activated pool of fatty acids entering the β-oxidation pathway in peroxisomes is formed due to the lipolysis of neutral lipids that are deposited in lipid bodies (LB) [197]. LB of the yeast *S. cerevisiae* consist of a highly hydrophobic core of neutral lipids, mainly triacylglycerols and ergosteryl esters, surrounded by a phospholipid monolayer [198, 199]. Yeast LB also contain 16 major proteins, all of which are involved in lipid synthesis and degradation [197, 198]. The well known function of LB is storage of neutral lipids and fatty acids as an energy source and as a source of components needed for membrane biogenesis [197 - 199]. A reduction in the intracellular level of neutral lipids, the most abundant lipid of LB, was proposed to be a primary way by which calorie restriction extends lifespan [200, 201]. Therefore, I used fluorescent microscopy to monitor the kinetics of changes in the abundance of LB during chronological aging of wild-type and *fox* mutant cells. The neutral lipids stored in LB were visualized in living cells using the fluorescence lipophilic dye BODIPY 493/503 (Figure 3.14). I found that the entering of wild-type cells into the post-diauxic growth phase on 0.2% glucose initiates rapid consumption of LB (Figures 3.14 and 3.15). In CR wild-type cells LB were almost entirely consumed by the beginning of stationary phase

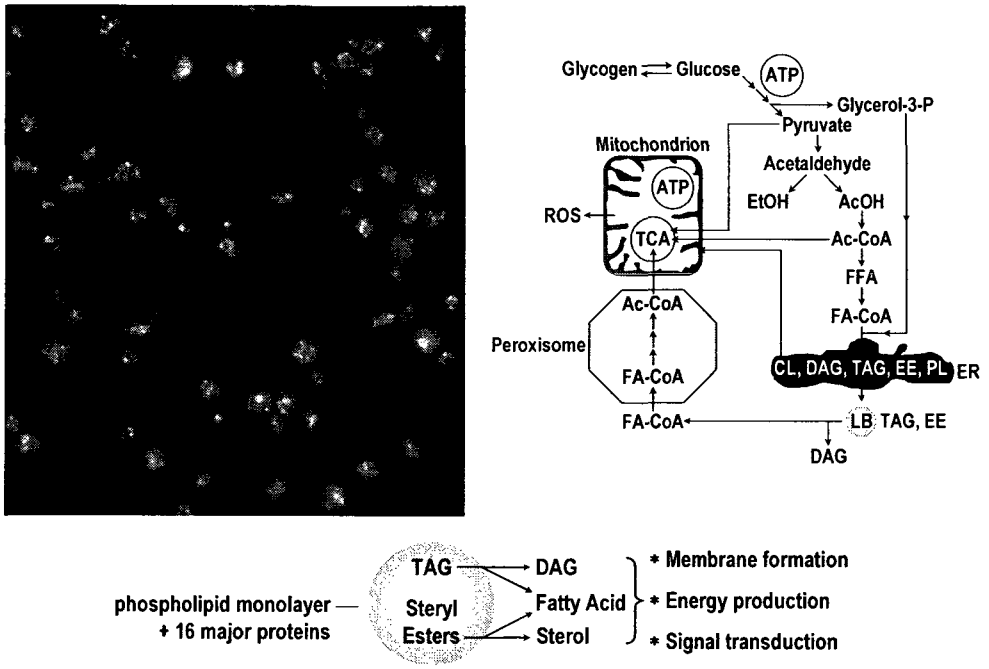


**Figure 3.14.** Using BODIPY 493/503 for visualizing neutral lipids that are stored in lipid bodies.

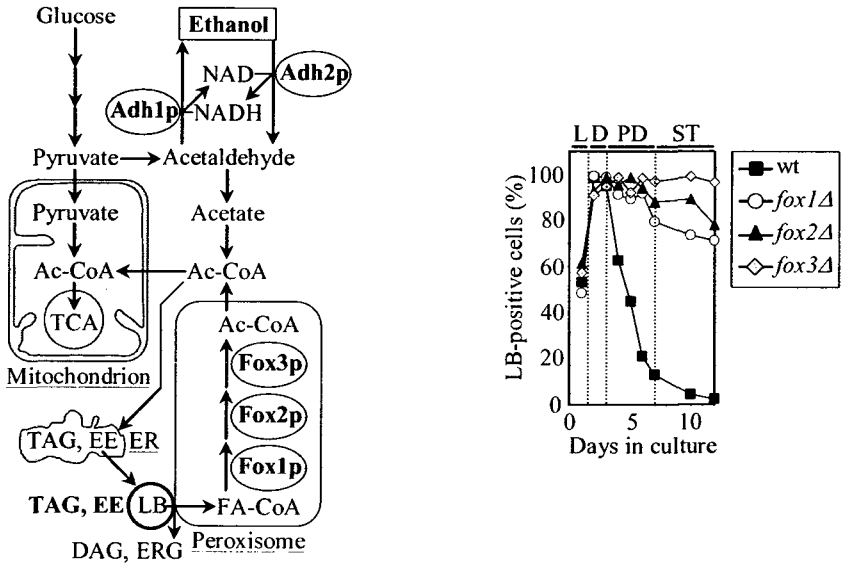


**Figure 3.15.** Lack of any of the three enzymes involved in peroxisomal β-oxidation of fatty acids impairs the mobilization of neutral lipids from lipid bodies. In CR wild-type cells lipid bodies were almost entirely consumed by the beginning of stationary phase. In contrast, no dramatic decrease in the abundance of lipid bodies was seen in chronologically aging CR cells of the short-lived *fox1Δ*, *fox2Δ* and *fox3Δ* mutant strains grown on 0.2% glucose.

(Figures 3.14 and 3.15). In contrast, no dramatic decrease in the abundance of LB was seen in chronologically aging CR cells of the short-lived *fox1Δ*, *fox2Δ* and *fox3Δ* mutant strains grown on 0.2% glucose (Figure 3.15). Thus, lack of any of the three enzymes involved in peroxisomal β-oxidation of fatty acids impaired the mobilization of neutral lipids from LB, perhaps by preventing or slowing down the lipolysis of LB-stored neutral lipids.

This hypothesis has been confirmed by using thin-layer chromatography (TLC) of neutral lipids extracted from whole cells of the wild-type and *fox* mutant strains. I revealed that, in aging wild-type cells, CR promoted: (1) lipolysis of the two neutral lipids, triacylglycerols (TAG) and ergosteryl esters (EE), whose hydrolysis by lipases represents the first step in the generation of free fatty acids (FFA) in LB; (2) the consumption of diacylglycerol (DAG), a product of the lipolysis of TAG by LB-bound lipases and a substrate of the second lipolytic reaction leading to the formation of FFA in LB; and (3) the consumption of FFA (Figures 3.16 and 3.17). Importantly, any of the three mutants (*i.e.*, *fox1Δ*, *fox2Δ* and *fox3Δ*) that lacks an enzyme of the peroxisomal β-oxidation of neutral lipids-derived FFA, when grown on 0.2% glucose, was unable to hydrolyze TAG, EE and DAG (Figures 3.18 and 3.19). Furthermore, as soon as any of the three *fox* mutants enters stationary phase on 0.2% glucose, it begins accumulating FFA (Figures 3.18 and 3.19). Interestingly, the closer to the beginning of the peroxisomal β-oxidation pathway the missing in a *fox* mutant reaction is, the more of FFA is accumulated within cells (Figures 3.18 and 3.19).

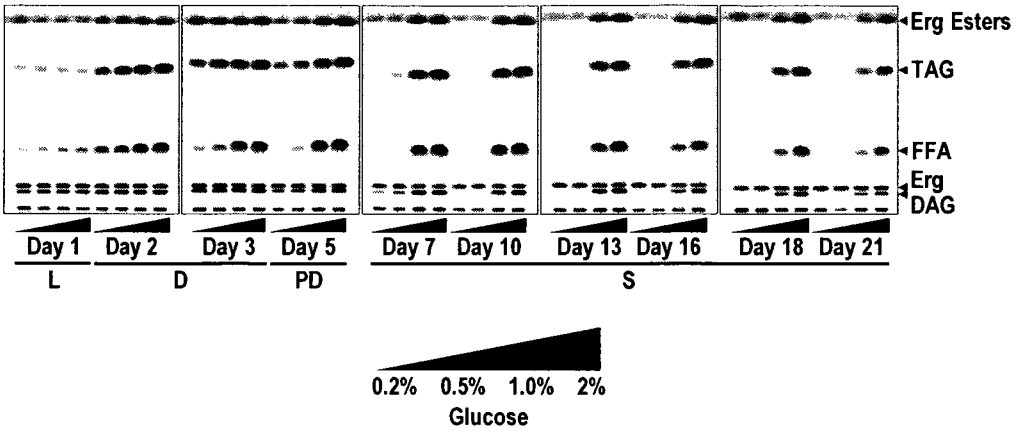


**Figure 3.16.** In aging wild-type cells, CR promotes: 1) lipolysis of the two neutral lipids, triacylglycerols (TAG) and ergosteryl esters (EE), whose hydrolysis by lipases represents the first step in the generation of free fatty acids (FFA) in lipid bodies (LB); 2) the consumption of diacylglycerol (DAG), a product of the lipolysis of TAG by LB-bound lipases and a substrate of the second lipolytic reaction leading to the formation of FFA in LB; and 3) the consumption of FFA.

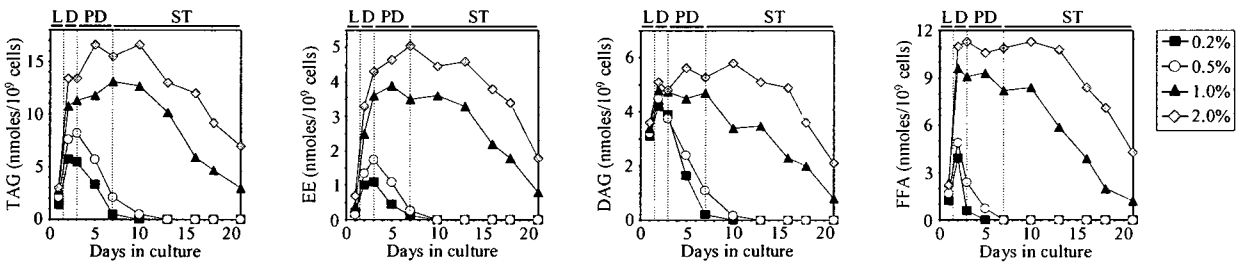


**Figure 3.17.** In aging wild-type cells, CR promotes the lipolysis of triacylglycerols (TAG) and ergosteryl esters (EE), degradation of diacylglycerol (DAG) and the consumption of free fatty acids (FFA).

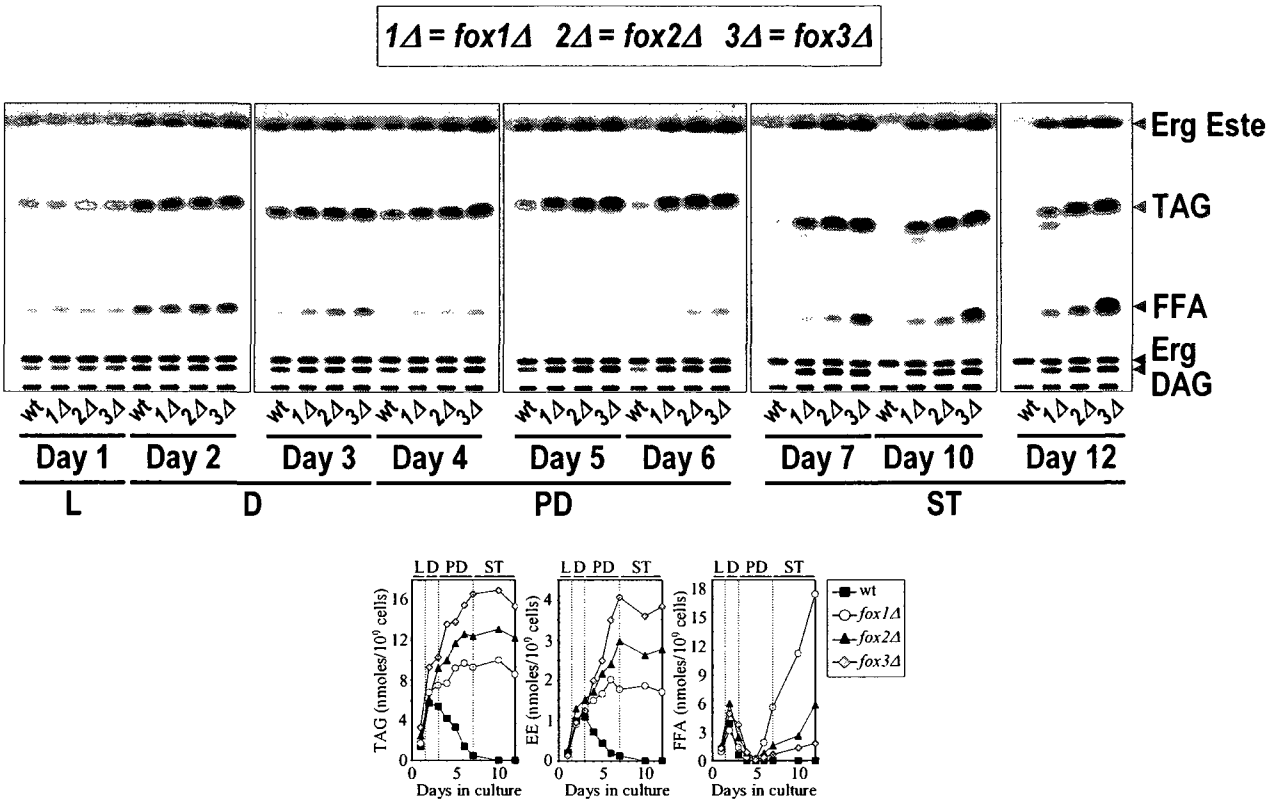


**Figure 3.18.** Any mutant that lacks an enzyme of the peroxisomal β-oxidation of neutral lipids-derived FFA, when grown on 0.2% glucose, is unable to hydrolyze TAG, EE and DAG deposited in lipid bodies. As soon as any of the three *fox* mutants enters stationary phase on 0.2% glucose, it begins accumulating FFA. The closer to the beginning of the peroxisomal β-oxidation pathway the missing in a *fox* mutant reaction is, the more of FFA is accumulated within cells.

But where in the cells of *fox* mutants entering stationary phase on 0.2% glucose these various lipid species (i.e., TAG, EE, DAG and FFA) accumulated? Using the TLC analysis of lipids extracted from purified ER (which serves as a template for the formation of LB) and LB, I demonstrated that the prematurely aging *fox* mutants grown on 0.2% glucose accumulate FFA, as well as TAG, EE and DAG, in their ER-derived LB

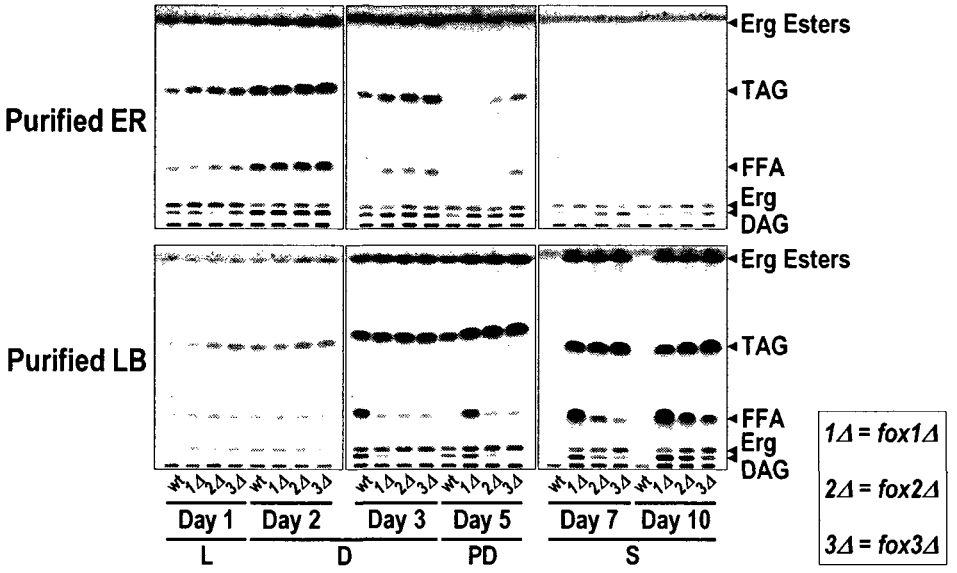


**Figure 3.19.** The prematurely aging *fox* mutants grown on 0.2% glucose accumulate FFA, as well as TAG, EE and DAG, in their ER-derived lipid bodies (LB). The closer to the beginning of the peroxisomal β-oxidation pathway the missing in a *fox* mutant reaction is, the more of FFA and DAG is accumulated in LB.

(Figure 3.19). Interestingly, the closer to the beginning of the peroxisomal β-oxidation pathway the missing in a *fox* mutant reaction is, the more of FFA and DAG is accumulated in LB (Figure 3.19).

But where in the cells of *fox* mutants entering stationary phase on 0.2% glucose these various lipid species (i.e., TAG, EE, DAG and FFA) accumulated? Using the TLC analysis of lipids extracted from purified ER (which serves as a template for the formation of LB) and LB, I demonstrated that the prematurely aging *fox* mutants grown on 0.2% glucose accumulate FFA, as well as TAG, EE and DAG, in their ER-derived LB (Figure 3.19). Interestingly, the closer to the beginning of the peroxisomal β-oxidation pathway the missing in a *fox* mutant reaction is, the more of FFA and DAG is accumulated in LB (Figure 3.19).

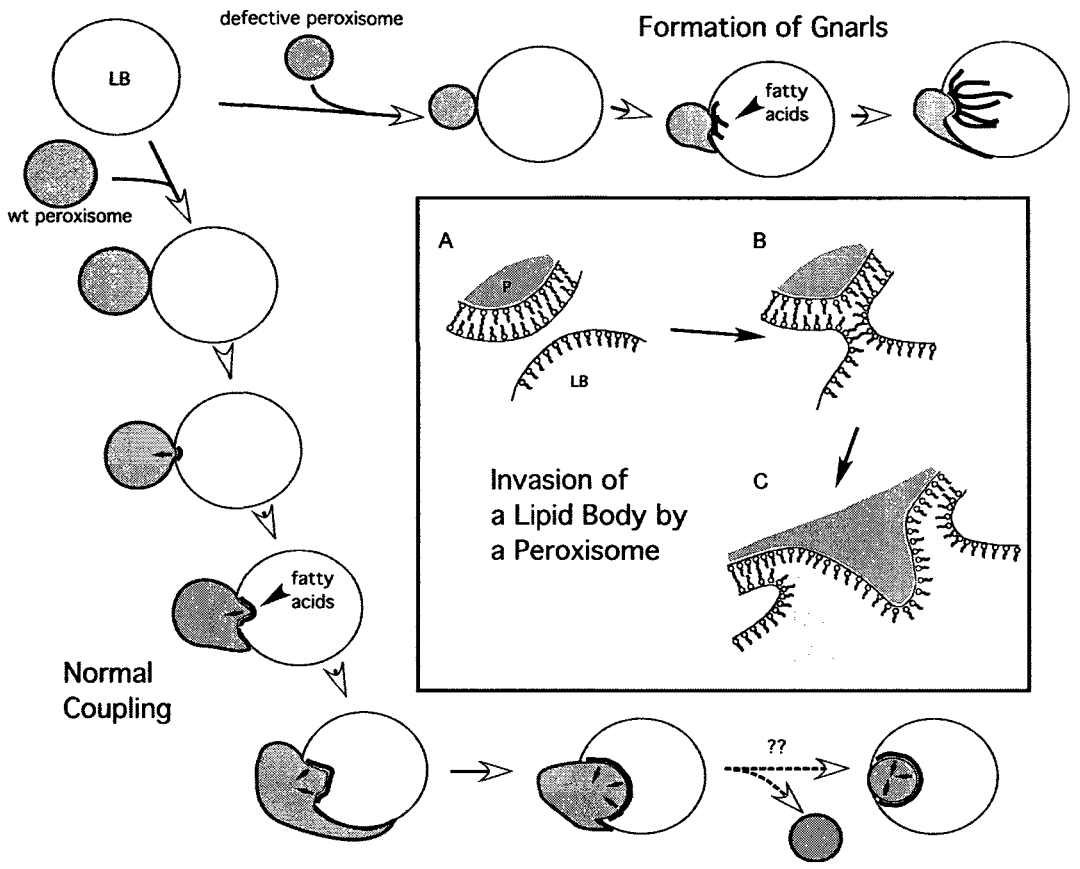


**Figure 3.20.** In yeast cells grown on oleic acid, the extensive physical contact between peroxisomes and lipid bodies (LB) promotes the coupling of lipolysis of neutral lipids within LB with oxidation of FFA in peroxisomes (Binns *et al. J. Cell Biol.* (2006) 173:719-731).

It should be noted that, in yeast cells grown on oleic acid, the extensive physical contact between peroxisomes and LB promotes the coupling of lipolysis of neutral lipids within LB with oxidation of FFA in peroxisomes (Figure 3.20) [202]. Using transmission electron microscopy followed by morphometric analysis, I showed that, as soon as *fox* mutants enter stationary phase on 0.2% glucose, their LB begin to build up so called "pexopodia" and "gnarls". "Pexopodia" represent extensions and intrusions of peroxisomes into LB, whereas "gnarls" epitomize organized arrays of FFA accumulated

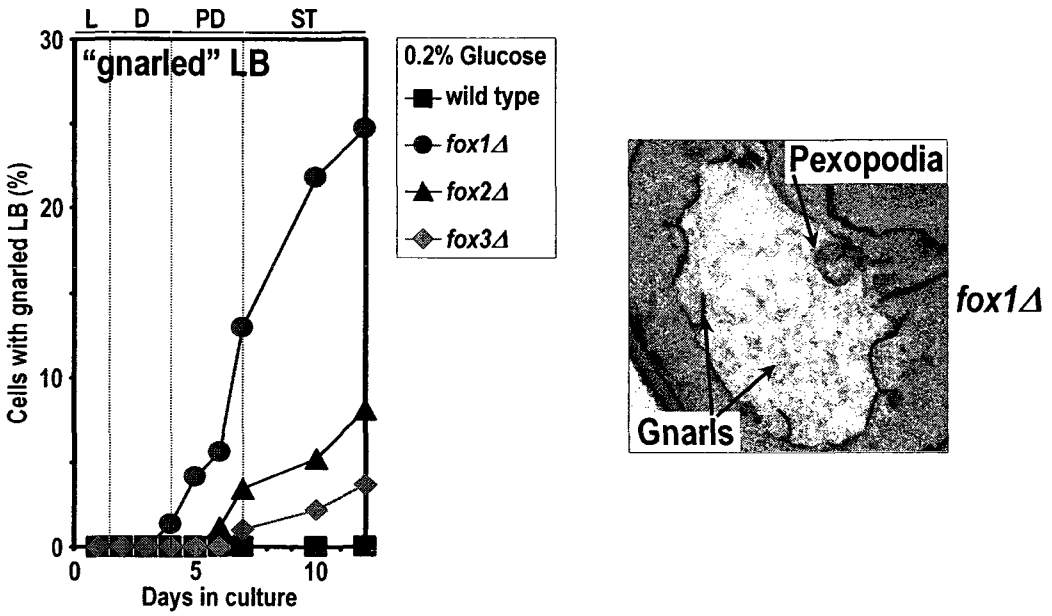


**Figure 3.21.** As soon as *fox* mutants enter stationary phase on 0.2% glucose, their lipid bodies (LB) begin build up so called "pexopodia" and "gnarls". "Pexopodia" represent extensions and intrusions of peroxisomes into LB, whereas "gnarls" epitomize organized arrays of FFA accumulated within LB. The closer to the beginning of the peroxisomal β-oxidation pathway the missing in a *fox* mutant reaction is, the more of both "pexopodia" and "gnarls" are accumulated within LB.

within LB (Figure 3.21) [202]. It should be stressed that the closer to the beginning of the peroxisomal β-oxidation pathway the missing in a *fox* mutant reaction is, the more of both "pexopodia" and "gnarls" are accumulated within LB (Figure 3.21).

Altogether, my aforementioned findings provide the comprehensive evidence that: (1) the formation of acetyl-CoA via peroxisomal β-oxidation of neutral lipids-derived fatty acids is required for extending lifespan of CR yeast cells; (2) in CR yeast, the extensive physical contact between peroxisomes and LB promotes the coupling of lipolysis of neutral lipids within LB with oxidation of FFA in peroxisomes; and (3) the

rate of peroxisomal β-oxidation of neutral lipids-derived fatty acids is a key factor controlling the rate of lipolysis of neutral lipids within LB and, ultimately, the rate of chronological aging in yeast placed on the CR diet.

### 3.4.5 The rate of peroxisomal β-oxidation of neutral lipids-derived fatty acids controls the rate of chronological aging by modulating essential processes in mitochondria

As described above, lack of any of the three Fox proteins: (1) shortened chronological life span of CR yeast; (2) in "young" CR cells entering diauxic growth phase, dramatically increased the amplitude of the observed spike in the rates of oxygen consumption and ROS generation by mitochondria; (3) in aging CR cells entering post-diauxic growth phase, resulted in the sharp decrease of the rates of oxygen consumption and ROS generation by mitochondria; and (4) in aging CR cells entering post-diauxic growth phase, considerably decreased the intracellular level of mitochondrially synthesized ATP.

All these findings strongly suggest that the formation of acetyl-CoA via peroxisomal β-oxidation of neutral lipids-derived fatty acids modulate essential processes in mitochondria, including the electron transport chain and oxidative phosphorylation. It seems that that the observed spike in the rate of ROS generation by mitochondria of the *fox* mutants irreversibly damages key mitochondrial proteins. In fact, lack of any of the three Fox proteins resulted in rapid inactivation of cytochrome c oxidase and aconitase in

mitochondria of the prematurely aging *fox* mutants entering post-diauxic growth phase (Figure 3.22). Both these mitochondrial proteins represent the key targets for the oxidative damage by ROS [99 - 102].

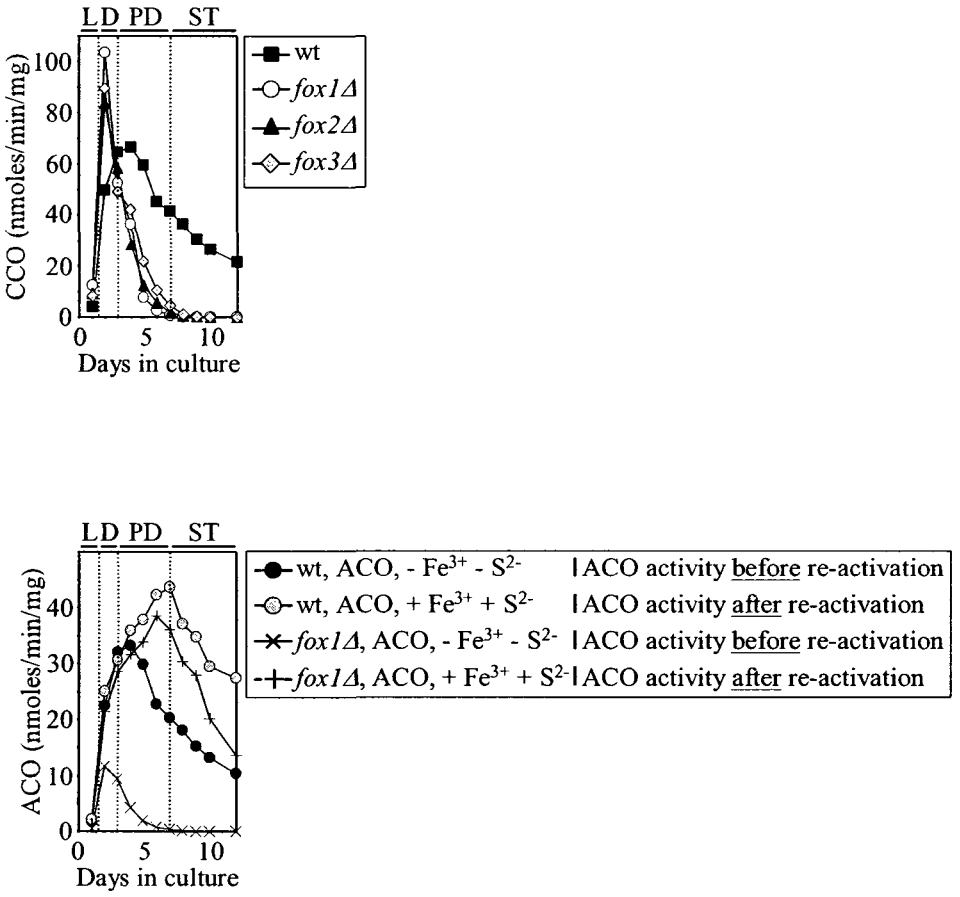


**Figure 3.22.** Lack of any of the three Fox proteins results in rapid inactivation of cytochrome c oxidase and aconitase in mitochondria of the prematurely aging *fox* mutants entering post-diauxic growth phase. Both these mitochondrial proteins represent the key targets for the oxidative damage by ROS. *Abbreviations*: CCO, cytochrome c oxidase; ACO, aconitase.

Furthermore, using the fluorescence dye Rhodamine 123 for monitoring the mitochondrial membrane potential ($\Delta\Psi$) (Figure 3.23), I demonstrated that lack of any of the three Fox proteins: (1) in "young" CR cells entering diauxic growth phase,

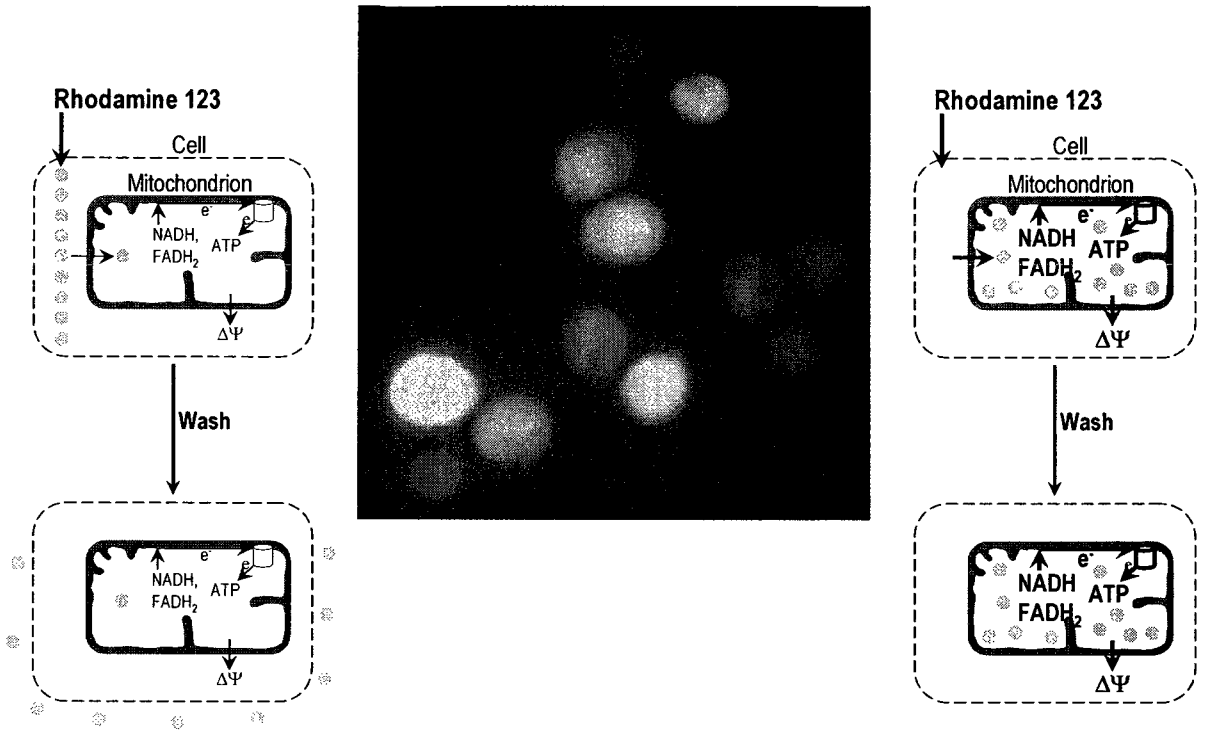


**Figure 3.23.** Using Rhodamine 123 for monitoring the mitochondrial membrane potential (ΨΔ) in living cells.

dramatically increased the value of ΔΨ, thereby leading to the hyper-polarization of the inner mitochondrial membrane (Figures 3.24 and 3.25); and (2) in aging CR cells entering post-diauxic growth phase, resulted in the sharp decrease of the value of ΔΨ (Figures 3.24 and 3.25), thereby rapidly abrogating the ΔΨ-dependent processes in mitochondria, including the transport of solutes and the synthesis of ATP.

Although lack of any of the three Fox proteins caused age-related changes in essential mitochondrial processes, it did not affect the abundance of mitochondria in chronologically aging CR yeast. In fact, the level of porin – one of the most abundant mitochondrial proteins – in CR cells of prematurely aging *fox* mutants entering post-

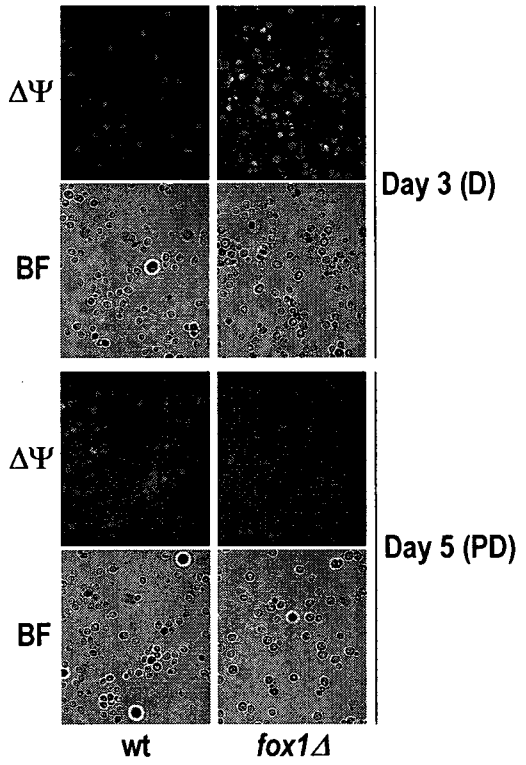


**Figure 3.24.** The *fox1Δ* mutation greatly increases the mitochondrial membrane potential (ΔΨ) in cells entering diauxic (D) phase and causes its sharp decline in cells entering post-diauxic (PD) phase.

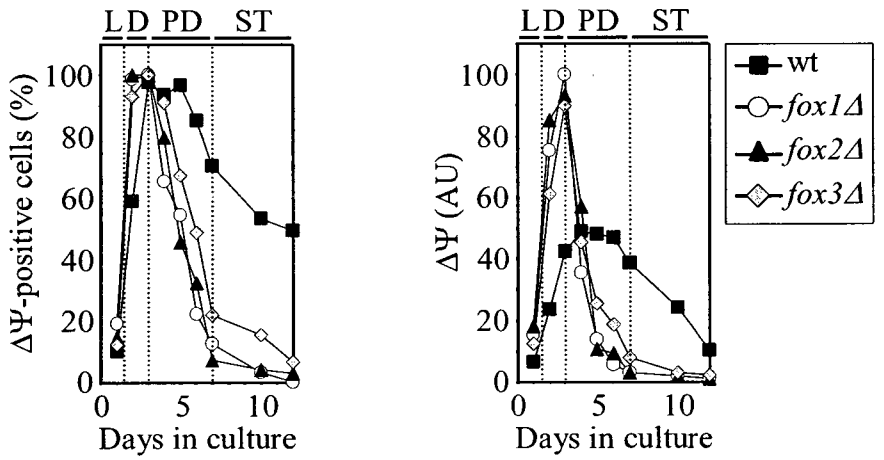


**Figure 3.25.** Lack of any of the three Fox proteins: (1) in "young" CR cells entering diauxic growth phase, dramatically increases the value of ΨΔ, thereby leading to the hyper-polarization of the inner mitochondrial membrane; and (2) in aging CR cells entering post-diauxic growth phase, results in the sharp decrease of the value of ΨΔ.

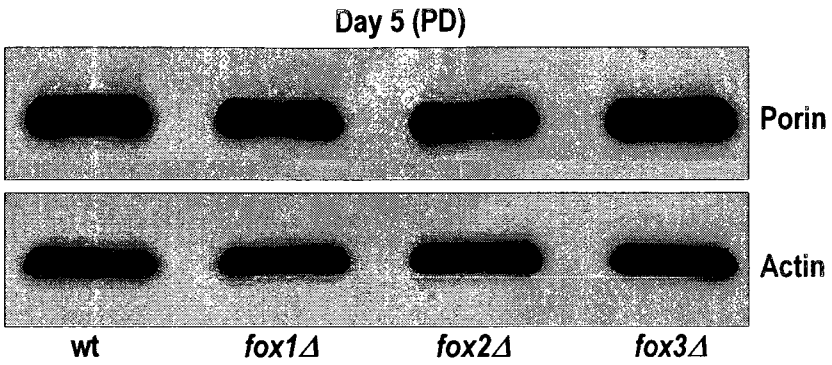


**Figure 3.26.** Although lack of any of the three Fox proteins causes age-related changes in essential mitochondrial processes, it does not affect the abundance of mitochondria in CR yeast.

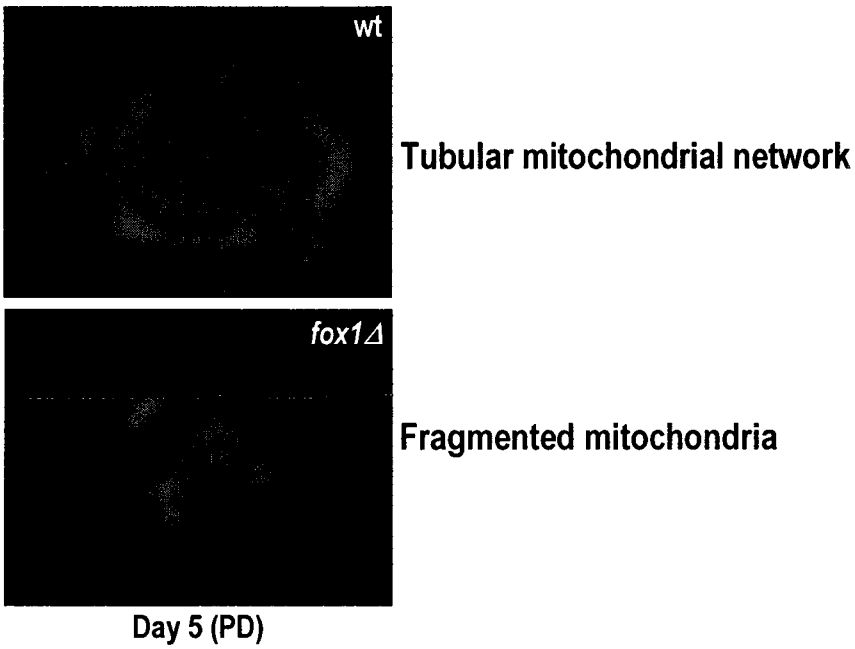


**Figure 3.27.** Lack of any of the three Fox proteins greatly affects the morphology of mitochondria in CR yeast. The morphology of mitochondria was visualized using immunofluorescence microscopy with anti-porin antibodies.

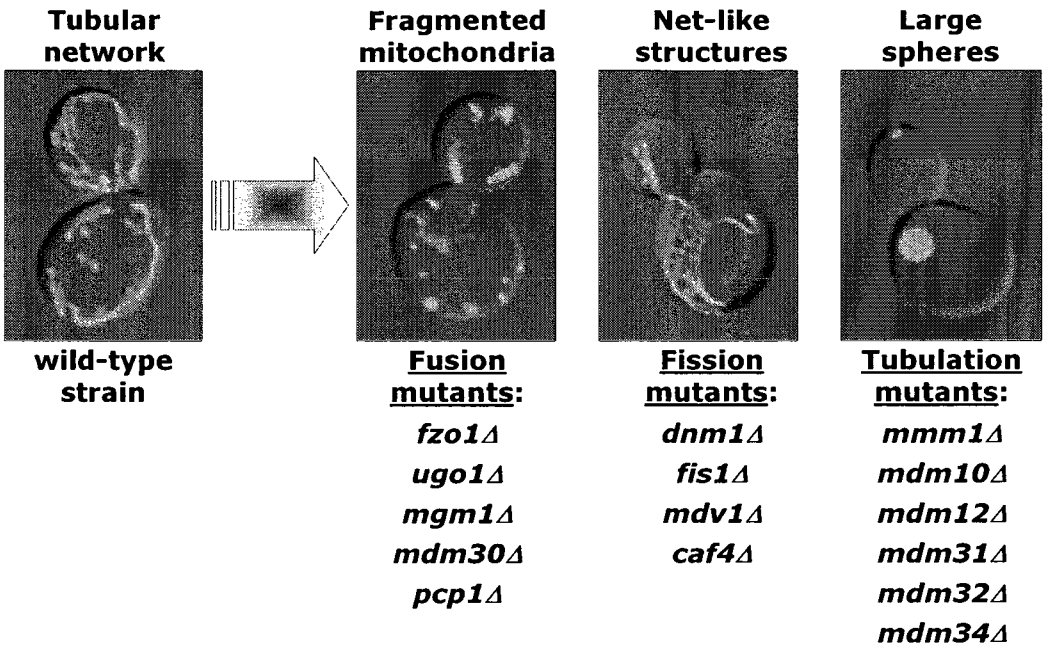


**Figure 3.28.** Morphology of mitochondria depends on a balance between the processes of mitochondrial fission, fusion & tubulation.

diauxic growth phase was very similar to that seen in wild-type cells (Figure 3.26). However, I found that lack of any of the three Fox proteins greatly affected the morphology of mitochondria in CR yeast. In fact, mitochondria in chronologically aging WT cells formed a tubular network (Figure 3.27). In contrast, in the *fox1Δ* mutant strain, this network was fragmented into individual mitochondria (Figure 3.27). Thus, the efficiency with which peroxisomes supply acetyl-CoA for its oxidation via the TCA cycle in mitochondria modulates, by a yet-to-be established mechanism, a delicate balance between the processes of mitochondrial fission, fusion and tubulation. Such balance plays a pivotal role in establishing and maintaining the morphological appearance of mitochondria (Figure 3.28) [203, 204].

## 3.5 Discussion

To study the effect of CR on the chronological lifespan of the yeast *S. cerevisiae*, I incubated wild-type strain BY4742 in rich YP medium initially containing 0.2%, 0.5%, 1% or 2% glucose. I chose YP medium for chronological aging studies because, in contrast to a synthetic medium, it is rich in amino acids, nucleotides, vitamins and other nutrients. I therefore thought that the reduction of glucose concentration in YP medium would lower the number of available calories without compromising the supply of essential nutrients, thereby modeling a traditional CR dietary regimen established in experiments with laboratory rodents [205]. An equally important reason for choosing rich YP medium for chronological aging studies is that the recent isolation of quiescent and nonquiescent cells from yeast stationary-phase cultures grown in this medium provided a novel, valuable system for elucidating the mechanisms linking chronological aging to quiescence, the mitotic cell cycle and apoptosis [206, 207]. My choice of the strain BY4742 was based on its relatively short chronological lifespan [208], thereby offering considerable time savings for chronological aging studies of yeast cultivated in rich YP medium. Importantly, this yeast strain serves as one of the two haploid genetic backgrounds of the widely used Yeast Knock-Out Collection available from Open Biosystems. Using the developed assay for studying the chronological aging of yeast, I found that CR cells grown on 0.2% or 0.5% glucose lived significantly longer than cells grown under non-CR conditions on 1% or 2% glucose.

The mean chronological lifespan of cells grown on 0.2% glucose was extended by more than 60% and that of cells grown on 0.5% glucose was extended by almost 2-fold,

as compared to the mean chronological lifespan of cells grown on 2% glucose. Thus, the chronological lifespan of yeast can be extended by CR in a dose-dependent manner. Of note, CR yeast grown on 0.5% glucose lived longer than CR yeast grown on 0.2% glucose. Hence, 0.5% is an optimal concentration of glucose for achieving the benefit of CR-dependent longevity extension. Moreover, my findings imply that CR yeast cells remodel their metabolism in order to match the level of ATP produced by non-CR yeast cells. It is conceivable that such specific remodeling of metabolism in CR yeast cells extends their life span. The validity of this hypothesis has been recently confirmed in Dr. Titorenko's laboratory by using a systems biological approach for analyzing the age-dependent dynamics of changes in proteomes and metabolomes of chronologically aging yeast.

One of my objectives was to understand what role (if any) acyl-CoA oxidase and, perhaps, other peroxisomal enzymes of fatty acid oxidation may play in regulating yeast longevity. A priory, there are two different mechanisms by which fatty acid oxidation in peroxisomes could influence longevity of yeast under CR conditions. First, the formation of hydrogen peroxide in the Aox (Fox1p)-dependent reaction of fatty acid oxidation and its decomposition by peroxisomal catalase could modulate the level of this ROS molecule, which is known for its essential role in regulating longevity. However, my evaluation of the chronological lifespans of the *fox1Δ* mutant strain, which lacks the hydrogen peroxide-producing Aox, and the *cta1Δ* mutant strain, which lacks the hydrogen peroxide-decomposing peroxisomal catalase, provided convincing evidence that peroxisomally produced ROS do not influence yeast longevity under CR conditions.

Moreover, by monitoring the age-dependent dynamics of changes in the rates of oxygen consumption and ROS production by *fox1Δ* and *cta1Δ* cells, I established that in chronologically aging CR yeast: (1) peroxisomes do not consume significant amounts of oxygen and do not produce significant amounts of ROS; and (2) the bulk of oxygen is consumed and the major portion of ROS is generated by mitochondria due to the transfer of electrons from components of the electron transport chain to oxygen consumed by these organelles. Another mechanism by which fatty acid oxidation in peroxisomes could influence longevity of yeast under CR conditions consists in the ability of peroxisomes to generate considerable levels of acetyl-CoA, the final product of peroxisomal fatty acid oxidation. I hypothesized that, following its delivery to mitochondria for the oxidation via the tricarboxylic acid cycle, this peroxisomally produced acetyl-CoA could be responsible for the synthesis of the major portion of ATP in mitochondria. In support of this hypothesis, my analysis of the lifespans of mutants lacking Fox1p, Fox2p or Fox3p, along with the monitoring of oxygen consumption and ATP synthesis by their cells, provided evidence that the formation of acetyl-CoA via peroxisomal β-oxidation of fatty acids is mandatory for the beneficial effect of CR on yeast longevity. Moreover, by monitoring the age-dependent dynamics of changes in the abundance of various lipid species during chronological aging of wild-type and *fox* mutant cells, I established that the rate of peroxisomal β-oxidation of neutral lipids-derived fatty acids is a key factor controlling the rate of lipolysis of neutral lipids within LB and, ultimately, the rate of chronological aging in yeast placed on the CR diet. Finally, my evaluation of the effect of mutations eliminating individual enzymes of peroxisomal β-oxidation of neutral lipids-

derived fatty acids on mitochondria-confined processes provided evidence that the formation of acetyl-CoA - the end product of such fatty acid oxidation - modulates essential processes in mitochondria, including enzymatic activities of cytochrome c oxidase, succinate dehydrogenase and aconitase, the mitochondrial membrane potential ($\Delta\Psi$), and a balance between the processes of mitochondrial fission, fusion and tubulation.

## 3.6 Conclusions

Altogether, my aforementioned findings led to the following conclusions. First, peroxisomes do not produce significant quantities of ROS in chronologically aging CR yeast. Second, ROS that are produced in peroxisomes during fatty acid oxidation are not essential for chronological aging of yeast placed on a CR diet. Third, both the formation of free fatty acids due to lipolysis of LB-deposited neutral lipids and their subsequent Fox1p (Aox)-, Fox2p- and Fox3p-dependent peroxisomal oxidation are mandatory for the observed extension of lifespan by CR. Fourth, by the beginning of PD phase, CR yeast synthesize the bulk of their ATP in mitochondria by oxidizing the pool of acetyl-CoA that has been generated in peroxisomes via Fox1p (Aox)-, Fox2p- and Fox3p-dependent fatty acid oxidation. I therefore concluded that fatty acid oxidation in peroxisomes controls longevity by modulating the rate of ATP synthesis in mitochondria, but not by generating the ROS hydrogen peroxide. Finally, my findings led to the conclusion that the efficiency of acetyl-CoA formation via peroxisomal fatty acid oxidation modulates: (1) the efficiencies of electron flow through the mitochondrial electron transport chain;

(2) activities of several well-known target enzymes for the oxidative damage by ROS (*i.e.*, cytochrome c oxidase, succinate dehydrogenase and aconitase); (3) the mitochondrial membrane potential ($\Delta\Psi$); and (4) a balance between the processes of mitochondrial fission, fusion and tubulation, which plays a pivotal role in establishing and maintaining the morphological appearance of mitochondria.

# 4 By modulating ROS production in mitochondria, a distinct set of peroxisomal proteins mediates the ability of a novel anti-aging small molecule to extend yeast longevity

## 4.1 Abstract

Recent studies in Dr. Titorenko's laboratory identified 22 novel small molecules that greatly increase the chronological lifespan of yeast. My experiments with one of these novel anti-aging drugs, a commercially available compound further referred to as "LA", revealed that it extends yeast longevity under CR conditions. My studies aimed at elucidating the molecular mechanisms by which LA increases yeast lifespan revealed that lack of Aox or any other enzyme of peroxisomal fatty acid oxidation does not impair the anti-aging effect of LA. Thus, although fatty acid oxidation in peroxisomes is essential for delaying aging, it is not required for the ability of LA to extend yeast longevity. Moreover, my findings imply that the presence of peroxisomes in yeast cells is not a requirement for life-span extending ability of LA. However, two proteins needed for the import of soluble proteins into the peroxisomal matrix, which are called Pex1p and Pex6p, appeared to be critical for the ability of LA to extend yeast longevity. The essential role of at least one of these proteins - the AAA ATPase Pex6p - in mediating life-span extending ability of LA is due to its involvement in promoting the ability of another organelle, the mitochondrion, to maintain ROS homeostasis within a cell. My findings demonstrated that LA extends yeast longevity by: (1) reducing the damaging effect of ROS on cellular macromolecules; and (2) amplifying the so-called "hormetic" effect of ROS through the activation of stress-protecting and other anti-aging proteins.

## 4.2 Introduction

Using a custom-designed microplate assay for monitoring yeast chronological lifespan, Dr. Titorenko's laboratory recently conducted a high-throughput screening of several combinatorial chemical libraries in search for small molecules that can increase yeast longevity. This screening procedure resulted in the identification of 22 novel compounds that cause a 6- to 10-fold extension of the chronological lifespan of a short-lived mutant strain and belong to 5 chemically distinct groups. My experiments with a commercially available compound that belongs to one of these groups and is called LA revealed that, similar to its effect on the short-lived mutant used for the high-throughput screen, LA extends the chronological lifespan of wild-type strain under CR conditions (Figure 4.1). Importantly, all of the novel anti-aging compounds that have identified by Dr. Titorenko's laboratory – including LA - are structurally distinct from resveratrol, a constituent of red wine that extends the replicative lifespan of yeast [209] and the chronological lifespans of worms, flies and fishes [210 – 215] by activating so-called sirtuins of the Sir2p protein family. Furthermore, all these novel anti-aging compounds – including LA - are structurally unrelated to several other small molecules that, similar to resveratrol, activate the sirtuin SIRT1, improve health and survival, and delay the onset of age-related diseases in rodent models [216 – 218]. Thus, it is conceivable that LA and the other novel anti-aging compounds that have been identified by Dr. Titorenko's laboratory target longevity-related cellular processes that are not modulated by resveratrol and other known activators of sirtuins.

My studies described in Chapter 3 led to the conclusion that the formation of

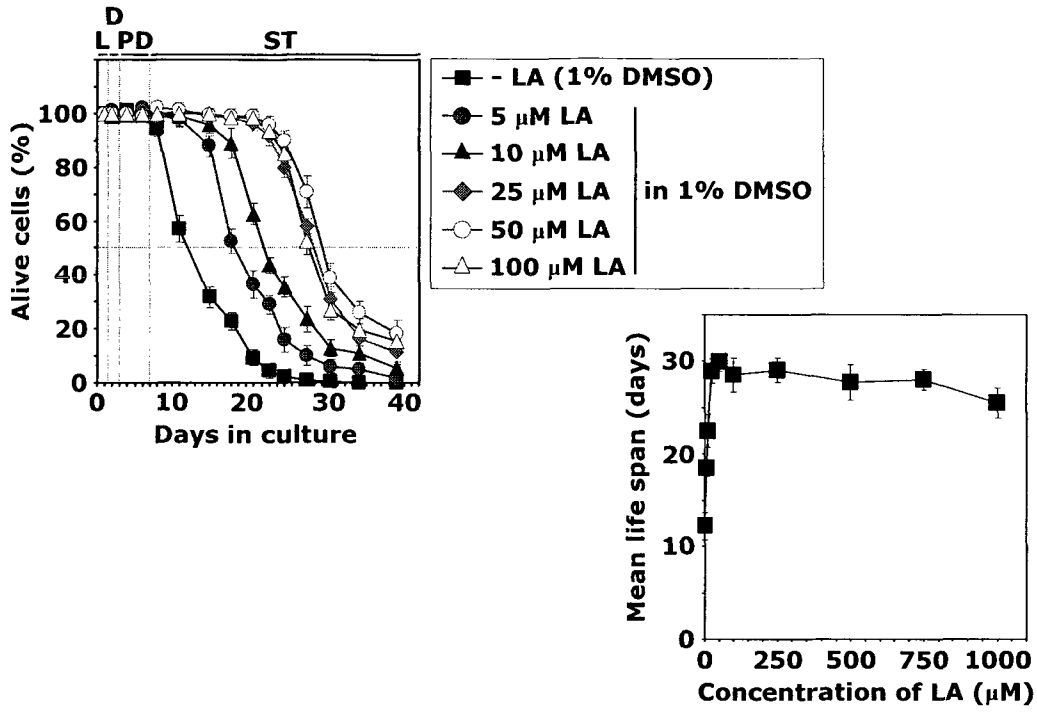


**Figure 4.1.** The anti-aging small molecule LA extends the chronological life span of wild-type strain.

acetyl-CoA via peroxisomal β-oxidation of neutral lipids-derived fatty acids is mandatory for increasing the chronological lifespan of CR yeast. I was intrigued therefore by a role (if any) for the Fox1p (Aox)-, Fox2p- and Fox3p-dependent peroxisomal fatty oxidation in the ability of LA to extend longevity of CR yeast. Moreover, the proper localization of Fox1p (Aox), Fox2p and Fox3p to the peroxisomal matrix depends on a distinct subset of at least 32 proteins that are collectively termed peroxins and encoded by the *PEX* genes [6 -8, 18, 22, 219 – 223]. The peroxins Pex1p, Pex5p and Pex6p are required for peroxisomal import of numerous matrix proteins targeted to the peroxisome by their carboxyl-terminal peroxisomal targeting signal type 1 (PTS1), including Fox1p (Aox) and Fox2p (Figure 4.2) [2, 30]. Therefore, the *pex1Δ*, *pex5Δ* and *pex6Δ* mutants are

deficient in peroxisomal import of Fox1p (Aox) and Fox2p and accumulate them in the cytosol (Figure 4.2) [6, 8]. In contrast, thiolase (Fox3p), the third enzyme of peroxisomal β-oxidation of fatty acids, does not contain the PTS1, is targeted to the peroxisome by its amino-terminal PTS2 and, thus, accumulates only in the matrix of peroxisomes in *pex1Δ*, *pex5Δ* and *pex6Δ* mutant cells (Figure 4.2) [7, 8]. Furthermore, the peroxin Pex7p functions as a cytosolic shuttling receptor for peroxisomal import of Fox3p (thiolase), the third enzyme of peroxisomal β-oxidation of fatty acids that carries the PTS2 (Figure 4.2) [6, 8]. Therefore, Fox3p accumulates exclusively in the cytosol of *pex7Δ* mutant cells (Figure 4.2) [30]. In contrast, the *pex7Δ* mutation does not affect peroxisomal import of the first two enzymes of β-oxidation of fatty acids, namely Fox1p (Aox) and Fox2p (Figure 4.2) [2, 30]. Consequently, both these enzymes can be found exclusively in the peroxisomal matrix of *pex7Δ* mutant cells (Figure 4.2) [6, 8]. Moreover, the peroxin Pex3p is required for the formation of peroxisomes from the ER template (Figure 4.2) [125, 224]. Hence, all three enzymes of peroxisomal fatty acid oxidation accumulate exclusively in the cytosol of *pex3Δ* mutant cells (Figure 4.2). The ability of mutant strains carrying various *pex* mutations to have the entire peroxisomal fatty acid β-oxidation pathway, or only some of its individual reactions, to take place in the cytosol opened an opportunity to evaluate the requirement of peroxisomal localization of this pathway for the ability of LA to extend longevity of CR yeast.

It should be stressed that some peroxins and peroxisomal proteins possess a dual subcellular localization and function. Although proteins belonging to this distinct group have initially been recognized for their essential roles in peroxisome biogenesis and

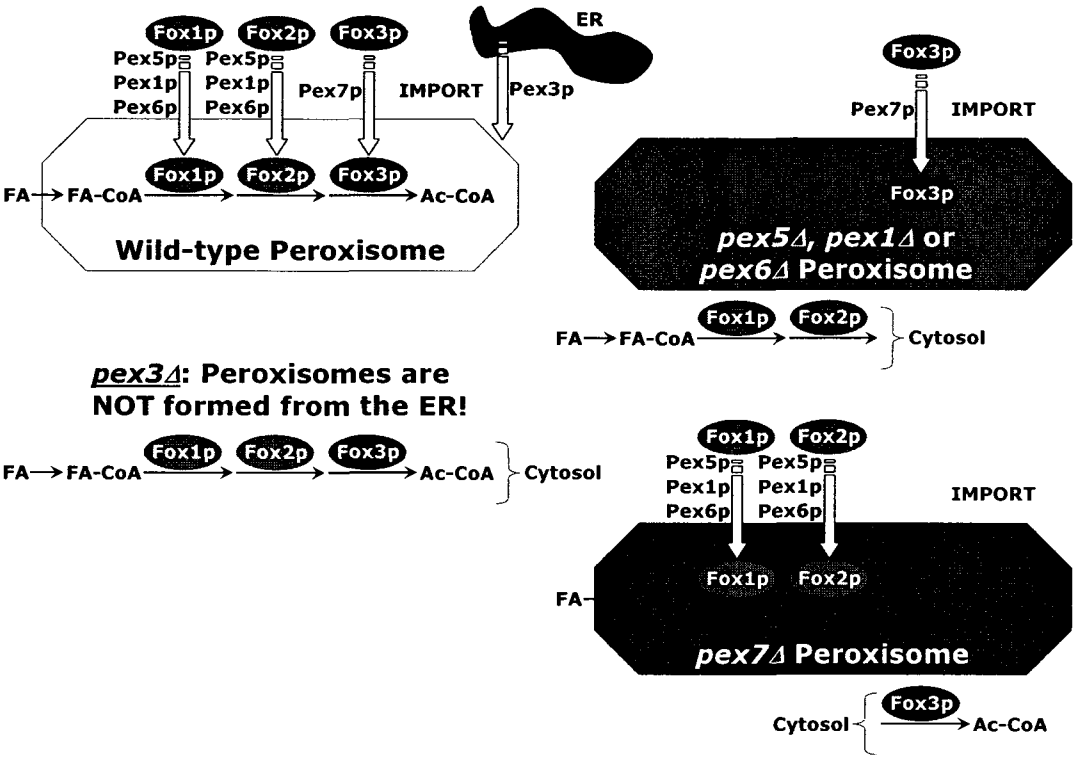


**Figure 4.2.** Roles for Pex and Fox proteins in peroxisome biogenesis and function.

function, they have turned out to be also required for a distinct set of cellular processes that do not directly relate to peroxisome biogenesis and function, including certain developmental, differentiation and morphogenetic programs [38]. Recent studies have provided strong evidence that the developmental role of these bifunctional peroxisomal proteins with dual subcellular localization is independent of metabolic pathways operating in peroxisomes. In particular, while the peroxisome-associated pools of these proteins operate in peroxisome biogenesis and function, their pools in other subcellular organelles promote certain developmental decisions regardless of the metabolic state of peroxisomes [38]. For example, the human peroxin Pex14p is an integral peroxisomal membrane protein that functions as the initial docking site for cargo-laden cytosolic

shuttling receptors of peroxisomal matrix proteins [7]. Human Pex14p is also a nuclear protein [33]. Targeted to the nucleus by its nuclear localization signal, human Pex14p interacts specifically with the p45 subunit of a DNA binding transcription factor, NF-E2. NF-E2 is a transcriptional regulator of erythroid and megakaryotic genes in pluripotential hematopoietic stem cells of the blood and lymphoid systems [33]. In the nucleus, a complex formed between Pex14p and a histone deacetylase is proposed to act as a corepressor of the NF-E2-mediated transcription of these genes [33]. Furthermore, the essential roles of three peroxisome-bound peroxins of the yeast *Yarrowia lipolytica*, Pex2p, Pex6p and Pex16p, in peroxisome biogenesis are well established [38]. *Y. lipolytica* Pex2p and Pex16p are initially sorted to the ER and are then delivered in a Pex6p-dependent manner from the ER to peroxisomes via ER-derived vesicles [23, 42]. Whereas the major portion of Pex2p, Pex6p and Pex16p resides in peroxisomes, a minor fraction is ER-associated [42]. While the peroxisome-bound pools of Pex2p, Pex6p and Pex16p operate in peroxisome assembly and division, their ER-bound pools orchestrate a specific cell polarization and differentiation program, the dimorphic transition from a round yeast form to a filamentous (mycelial) form, by promoting the delivery of mycelium-specific proteins from the ER to the cell envelope 23, 42]. The role for at least one peroxisome- and ER-localized bifunctional protein, Pex16p, in development and differentiation is evolutionarily conserved among yeasts and plants. The *Arabidopsis* ortholog of *Y. lipolytica* Pex16p, the SSE1 protein, is required not only for peroxisome assembly but also for the biogenesis of protein and lipid bodies, a cellular differentiation program for energy storage in maturing seeds [24]. The biogenesis of protein and lipid

bodies depends on the ER and involves the sorting of oleosins, the most abundant protein components of oil bodies, via the ER [225]. Importantly, Pex16p complements developmental defects in a cross-species fashion, as the *Arabidopsis* SSE1 protein re-establishes the dimorphic transition in the *Y. lipolytica pex16* mutant deficient in the delivery of mycelium-specific proteins from the ER to the tip of the growing filament [24]. Moreover, another bifunctional peroxisomal membrane protein of plants, CTS, is not only involved in the transport of acyl-CoA esters of fatty acids (FA-CoAs) into the peroxisome but is also essential for the transition from dormancy to germination, an important step in the embryonic development of *Arabidopsis* [32]. Seeds carrying *cts* mutations do not germinate and exhibit a "forever dormant" phenotype. Importantly, the inability of *cts* mutants to metabolize lipid body-derived FA-CoAs cannot account for the "forever dormant" phenotype, suggesting that the functions of CTS in the peroxisomal transport of FA-CoAs and in embryo development are different [32]. CTS is an ortholog of the human peroxisomal protein ALDP, a member of the ABC transporter family. Because the binding of other known ABC transporters to certain passive ion channels modulates their development-related activities [226], it has been proposed that the activity of CTS in embryo dormancy may involve its interaction with such channels [32]. It remains to be established what subcellular compartment serves as an organizing platform for the involvement of CTS in development. It is noteworthy that a human peroxisomal ABC transporter is present in a specialized subdomain of the ER from which peroxisomes form [227]. It has been therefore proposed that the ER-associated form of CTS promotes embryo development, while its peroxisomal form functions in the

transport of FA-CoAs into this organelle [38]. Finally, the peroxin Pex6p in the yeast *S. cerevisiae* functions not only in peroxisome biogenesis (Figure 4.2) but also in the import of the Atp2p, a β-subunit of $F_1F_0$-ATPase, into mitochondria [228].

Altogether, the aforementioned findings greatly stimulated my interest in defining a role (if any) for peroxisome-associated enzymes (including Aox) and peroxins in the anti-aging effect of LA. The objective of studies described in this chapter was therefore to investigate if the ability of the peroxisome to oxidize fatty acids (*i.e.*, a Fox-dependent function) or assemble properly (*i.e.*, a Pex-dependent function) is essential for the ability of LA to increase the chronological lifespan of CR yeast. I was also intrigued by a possibility that some of the peroxins could mediate the anti-aging effect of LA by being involved in the cellular processes that do not directly relate to peroxisome biogenesis and function.

## 4.3 Materials and Methods

### Strains and media

The wild-type strain *Saccharomyces cerevisiae* BY4742 (*MATα his3Δ1 leu2Δ0 lys2Δ0 ura3Δ0*) and mutant strains *pex1Δ* (*MATα his3Δ1 leu2Δ0 lys2Δ0 ura3Δ0 pex1Δ::kanMX4*), *pex5Δ* (*MATα his3Δ1 leu2Δ0 lys2Δ0 ura3Δ0 pex5Δ::kanMX4*), *pex6Δ* (*MATα his3Δ1 leu2Δ0 lys2Δ0 ura3Δ0 pex6Δ::kanMX4*), *pex7Δ* (*MATα his3Δ1 leu2Δ0 lys2Δ0 ura3Δ0 pex7Δ::kanMX4*), *fox1Δ* (*MATα his3Δ1 leu2Δ0 lys2Δ0 ura3Δ0 fox1Δ::kanMX4*), *cta1Δ* (*MATα his3Δ1 leu2Δ0 lys2Δ0 ura3Δ0 cta1Δ::kanMX4*), *fox2Δ* (*MATα his3Δ1 leu2Δ0 lys2Δ0 ura3Δ0 fox2Δ::kanMX4*), *mdh3Δ* (*MATα his3Δ1 leu2Δ0*

*lys2Δ0 ura3Δ0 mdh3Δ::kanMX4*), and *fox3Δ* (*MATα his3Δ1 leu2Δ0 lys2Δ0 ura3Δ0 fox3Δ::kanMX4*) were used in this study. Media components were as follows: 1) YEPD (0.2% Glucose), 1% yeast extract, 2% peptone, 0.2% glucose; and 2) YEPD (2% Glucose), 1% yeast extract, 2% peptone, 2% glucose.

**A plating assay for the analysis of chronological life span**

Cells were grown in YEPD (0.2% Glucose) medium at 30°C with rotational shaking at 200 rpm in Erlenmeyer flasks at a flask volume/medium volume ratio of 5:1. A sample of cells was removed from each culture at various time points. A fraction of the cell sample was diluted in order to determine the total number of cells per ml of culture using a hemacytometer. 10 μl of serial dilutions (1:10 to $1:10^3$) of cells were applied to the hemacytometer, where each large square is calibrated to hold 0.1 μl. The number of cells in 4 large squares was then counted and an average was taken in order to ensure greater accuracy. The concentration of cells was calculated as follows: number of cells per large square x dilution factor x 10 x 1,000 = total number of cells per ml of culture. A second fraction of the cell sample was diluted and serial dilutions ($1:10^2$ to $1:10^5$) of cells were plated onto YEPD (2% Glucose) plates in triplicate in order to count the number of viable cells per ml of each culture. 100 μl of diluted culture was plated onto each plate. After a 48-h incubation at 30°C, the number of colonies per plate was counted. The number of colony forming units (CFU) equals to the number of viable cells in a sample. Therefore, the number of viable cells was calculated as follows: number of colonies x dilution factor x 10 = number of viable cells per ml. For each culture assayed, % viability

of the cells was calculated as follows: number of viable cells per ml / total number of cells per ml x 100%. The % viability of cells in mid-logarithmic phase was set at 100% viability for that particular culture.

**Plating assays for the analysis of resistance to various stresses**

For the analysis of hydrogen peroxide resistance, serial dilutions ($1:10^0$ to $1:10^5$) of wild-type and mutant cells removed from mid-logarithmic phase (day 1) and from diauxic phase (days 2 and 3) in YEPD (0.2% Glucose) were spotted onto two sets of plates. One set of plates contained YEPD (2% Glucose) medium alone, whereas the other set contained YEPD (2% Glucose) medium supplemented with 5 mM hydrogen peroxide. Pictures were taken after a 3-day incubation at 30°C.

For the analysis of oxidative stress resistance, serial dilutions ($1:10^0$ to $1:10^5$) of wild-type and mutant cells removed from mid-logarithmic phase (day 1) and from diauxic phase (days 2 and 3) in YEPD (0.2% Glucose) were spotted onto two sets of plates. One set of plates contained YEPD (2% Glucose) medium alone, whereas the other set contained YEPD (2% Glucose) medium supplemented with 2.5 mM of the superoxide/hydrogen peroxide-generating agent paraquat. Pictures were taken after a 3-day incubation at 30°C.

For the analysis of heat-shock resistance, serial dilutions ($1:10^0$ to $1:10^5$) of wild-type and mutant cells removed from mid-logarithmic phase (day 1) and from diauxic phase (days 2 and 3) in YEPD (0.2% Glucose) were spotted onto two sets of YEPD (2% Glucose) plates. One set of plates was incubated at 30°C. The other set of plates was

initially incubated at 55°C for 30 min, and was then transferred to 30°C. Pictures were taken after a 3-day incubation at 30°C.

For the analysis of salt stress resistance, serial dilutions ($1:10^0$ to $1:10^5$) of wild-type and mutant cells removed from mid-logarithmic phase (day 1) and from diauxic phase (days 2 and 3) in YEPD (0.2% Glucose) were spotted onto two sets of plates. One set of plates contained YEPD (2% Glucose) medium alone, whereas the other set contained YEPD (2% Glucose) medium supplemented with 0.5 M NaCl. Pictures were taken after a 3-day incubation at 30°C. For the analysis of osmotic stress resistance, serial dilutions ($1:10^0$ to $1:10^5$) of wild-type and mutant cells removed from mid-logarithmic phase (day 1) and from diauxic phase (days 2 and 3) in YEPD (0.2% Glucose) were spotted onto two sets of plates. One set of plates contained YEPD (2% Glucose) medium alone, whereas the other set contained YEPD (2% Glucose) medium supplemented with 1 M sorbitol. Pictures were taken after a 3-day incubation at 30°C.

**Monitoring the formation of ROS**

Wild-type and mutant cells grown in YEPD (0.2% Glucose) were tested microscopically for the production of ROS by incubation with dihydrorhodamine 123 (DHR). In the cell, this nonfluorescent compound can be oxidized to the fluorescent chromophore rhodamine 123 by ROS. Cells were also probed with a fluorescent counterstain Calcofluor White M2R (CW), which stains the yeast cell walls fluorescent blue. CW was added to each sample in order to label all cells for their proper

visualization. DHR was stored in the dark at –20°C as 50 µl aliquots of a 1 mg/ml solution in ethanol. CW was stored in the dark at –20°C as the 5 mM stock solution in anhydrous DMSO (dimethylsulfoxide).

The concurrent staining of cells with DHR and CW was carried out as follows. The required amounts of the 50 µl DHR aliquots (1 mg/ml) and of the 5 mM stock solution of CW were taken out of the freezer and warmed to room temperature. The solutions of DHR and CW were then centrifuged at 21,000 x g for 5 min in order to clear them of any aggregates of fluorophores. For cell cultures with a titre of ~ $10^7$ cells/ml, 100 µl was taken out of the culture to be treated. If the cell titre was lower, proportionally larger volumes were used. 6 µl of the 1 mg/ml DHR and 1 µl of the 5 mM CW solutions were added to each 100 µl aliquot of culture. After a 2-h incubation in the dark at room temperature, the samples were centrifuged at 21,000 x g for 5 min. Pellets were resuspended in 10 µl of PBS buffer (20 mM $KH_2PO_4$/KOH, pH 7.5, and 150 mM NaCl). Each sample was then supplemented with 5 µl of mounting medium, added to a microscope slide, covered with a coverslip, and sealed using nail polish. Once the slides were prepared, they were visualized under the Zeiss Axioplan fluorescence microscope mounted with a SPOT Insight 2 megapixel color mosaic digital camera. Several pictures of the cells on each slide were taken, with two pictures taken of each frame. One of the two pictures was of the cells seen through a rhodamine filter in order to detect cells dyed with DHR. The second picture was of the cells seen through a DAPI filter in order to visualize CW, and therefore all the cells present in the frame.

For evaluating the percentage of DHR-positive cells, the UTHSCSA Image Tool

(Version 3.0) software was used to calculate both the total number of cells and the number of stained cells. Fluorescence of individual DHR-positive cells in arbitrary units was determined by using the UTHSCSA Image Tool software (Version 3.0). In each of 3-5 independent experiments, the value of median fluorescence was calculated by analyzing at least 800-1000 cells that were collected at each time point. The median fluorescence values were plotted as a function of the number of days cells were cultured.

**Visualization of intracellular lipid bodies**

Wild-type and mutant cells grown in YEPD (0.2% Glucose) were tested microscopically for the presence of intracellular lipid bodies (LB) by incubation with BODIPY 493/503. Cells were also probed with a fluorescent counterstain CW in order to visualize all cells in the population. BODIPY 493/503 was stored in the dark at –20°C as 100 µl aliquots of a 1 mM solution in ethanol. CW was stored in the dark at –20°C as the 5 mM stock solution in anhydrous DMSO.

The concurrent staining of cells with BODIPY 493/503 and CW was carried out as follows. The required amounts of the 100 µl BODIPY 493/503 aliquots (1 mM) and of the 5 mM stock solution of CW were taken out of the freezer and warmed to room temperature. The solutions of DHR and CW were then centrifuged at 21,000 x g for 5 min in order to clear them of any aggregates of fluorophores. For cell cultures with a titre of ~ $10^7$ cells/ml, 100 µl was taken out of the culture to be treated. If the cell titre was lower, proportionally larger volumes were used. The samples were then centrifuged at 21,000 x g for 1 min, and pelleted cells were resuspended in 100 µl of TNT buffer (25

mM Tris/HCl (pH 7.5), 150 mM NaCl and 0.2 % Triton X-100). After a 10-min incubation at room temperature, the samples were centrifuged at 21,000 x g for 1 min. Pellets were then resuspended in 100 µl of TN buffer (25 mM Tris/HCl (pH 7.5), 150 mM NaCl), and the samples were subjected to centrifugation at 21,000 x g for 1 min. Pelleted cells were finally resuspended in 100 µl of TN buffer. Each 100 µl aliquot of cells was then supplemented with 1 µl of the 1 mM BODIPY 493/503 and 1 µl of the 5 mM CW solutions. After a 15-min incubation in the dark at room temperature, the samples were centrifuged at 21,000 x g for 5 min. Pellets were resuspended in 100 µl of TN buffer. The samples were centrifuged again at 21,000 x g for 5 min, and pellets were resuspended in 100 µl of TN buffer. 10 µl of the BODIPY 493/503- and CW-treated cell suspension was then added to a microscope slide and covered with a coverslip. The slides were then sealed using nail polish. Once the slides were prepared, they were visualized under the Zeiss Axioplan fluorescence microscope mounted with a SPOT Insight 2 megapixel color mosaic digital camera. Several pictures of the cells on each slide were taken, with two pictures taken of each frame. One of the two pictures was of the cells seen through a fluorescein filter in order to detect cells dyed with BODIPY 493/503. The second picture was of the cells seen through a DAPI filter in order to visualize CW, and therefore all the cells present in the frame. For evaluating the percentage of BODIPY 493/503-positive cells, the UTHSCSA Image Tool (Version 3.0) software was used to calculate both the total number of cells and the number of stained cells.

**Immunofluorescence microscopy**

Cell cultures were fixed in 3.7% formaldehyde for 45 min at room temperature. The cells were washed in solution B (100 mM $KH_2PO_4$/KOH pH 7.5, 1.2 M sorbitol), treated with Zymolyase 100T (MP Biomedicals, 1 μg Zymolyase 100T/1 mg cells) for 30 min at 30°C and then processed as previously described [47]. Monoclonal antibody raised against porin (Invitrogen, 0.25 μg/μl in TBSB buffer [20 mM Tris/HCl pH 7.5, 150 mM NaCl, 1mg/ml BSA]) was used as a primary antibody. Alexa Fluor 568 goat anti-mouse IgG (Invitrogen, 2 μg/μl in TBSB buffer) was used as a secondary antibody. The labeled samples were mounted in mounting solution (16.7 mM Tris/HCl pH 9.0, 1.7 mg/ml *p*-phenylenediamine, 83% glycerol). Images were collected with a Zeiss Axioplan fluorescence microscope (Zeiss) mounted with a SPOT Insight 2 megapixel color mosaic digital camera (Spot Diagnostic Instruments).

**Oxygen consumption assay**

The rate of oxygen consumption by yeast cells recovered at various time points was measured continuously in a 2-ml stirred chamber using a custom-designed biological oxygen monitor (Science Technical Center of Concordia University) equipped with a Clark-type oxygen electrode. 1 ml of YEPD medium supplemented with 0.2% glucose was added to the electrode for approximately 5 minutes to obtain a baseline. Cultured cells of a known titre were spun down at 3,000 x g for 5 minutes. The resulting pellet was resuspended in YEPD medium supplemented with 0.2% glucose and then added to the electrode with the medium that was used to obtain a baseline. The resulting slope was

used to calculate the rate of oxygen consumption in $O_2\%$ x $min^{-1}$ x $10^9$ cells.

**Electron microscopy and morphometric analysis**

Cells were fixed in 1.5% $KMnO_4$ for 20 min at room temperature, dehydrated by successive incubations in increasing concentrations of ethanol, and embedded in Poly/Bed 812 epoxy resin (Polysciences). Ultrathin sections were cut using an Ultra-Cut E Microtome (Reichert-Jung). Silver/gold thin sections from the embedded blocks were examined in a JEOL JEM-2000FX transmission electron microscope. For morphometric analysis of random electron microscopic sections of cells, digitized images were analyzed using the UTHSCSA Image Tool (Version 3.0) software. In each of 2 independent experiments, the percentage of cells that contain pexopodia and/or accumulate gnarled LB was calculated by analyzing at least 300 cells that were collected at each time point. The values of the percentage of cells containing pexopodia and/or accumulating gnarled LB were plotted as a function of the number of days cells were cultured.

## 4.4 Results

### 4.4.1 Fatty acid oxidation in peroxisomes is not essential for the ability of LA to increase the chronological lifespan of CR yeast

To investigate if the ability of the peroxisome to oxidize fatty acids (*i.e.*, a Fox-dependent function) or assemble properly (*i.e.*, a Pex-dependent function) is a requirement for the anti-aging action of LA in chronologically aging yeast under CR conditions, I developed a definition of a protein or process that is critical for such action

of LA (Figure 4.3). I assumed that if lack of a protein or a mutational impairment of a process does not cause a statistically significant reduction or rise of the fold increase of mean chronological lifespan by LA, such protein or process is not essential for the anti-aging action of LA (Figure 4.3). Conversely, if lack of a protein or a mutational impairment of a process causes a statistically significant reduction of the fold increase of mean chronological lifespan by LA, such protein or process is essential for the ability of LA to extend longevity (Figure 4.3). Furthermore, if lack of a protein or a mutational impairment of a process causes a statistically significant rise of the fold increase of mean

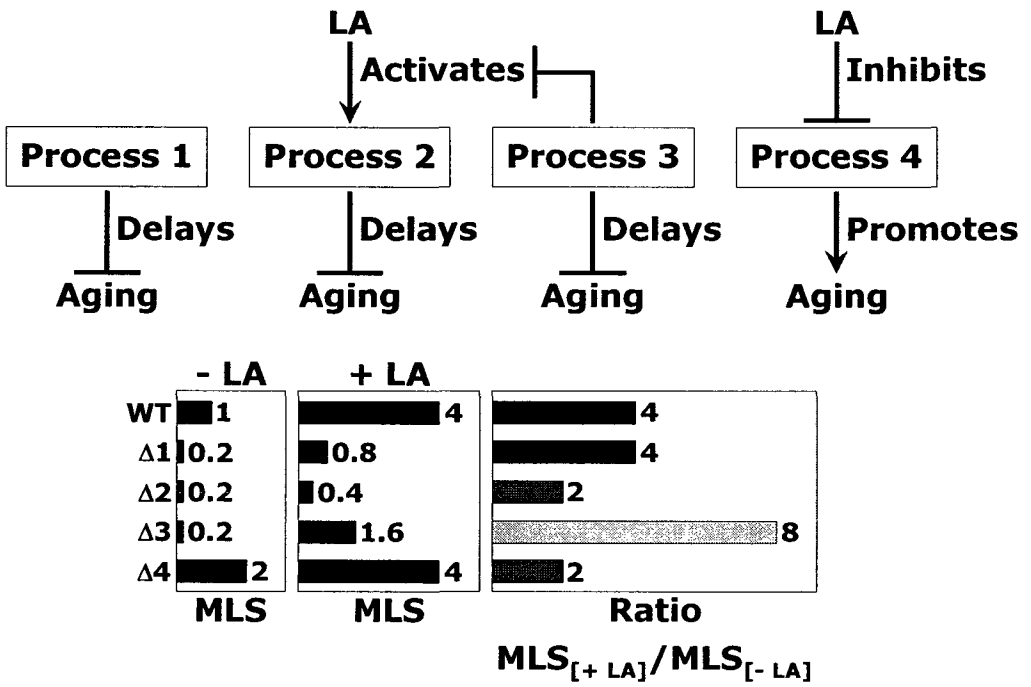


**Figure 4.3.** A definition of a protein or process that is critical for the ability of LA to extend longevity of chronologically aging yeast under CR conditions. Process 1 is not essential for the anti-aging action of LA. Processes 2 and 4 are essential for the ability of LA to extend longevity. Process 3 weakens the anti-aging effect of LA. *MLS*, mean chronological life span.

chronological lifespan by LA, such protein or process weakens the ability of LA to extend longevity (Figure 4.3). It should be stressed that my definition of a protein or process that is critical for the anti-aging action of LA ignores an age-related or age-unrelated role that this protein or process might play in the absence of LA. Such role could consist in the ability of a protein or process to delay or promote aging in the absence of exogenous LA or simply to maintain fitness of yeast that are not exposed to this anti-aging compound.

According to the definition of a protein or process that is critical for the ability of LA to extend longevity of chronologically aging yeast under CR conditions, none of the

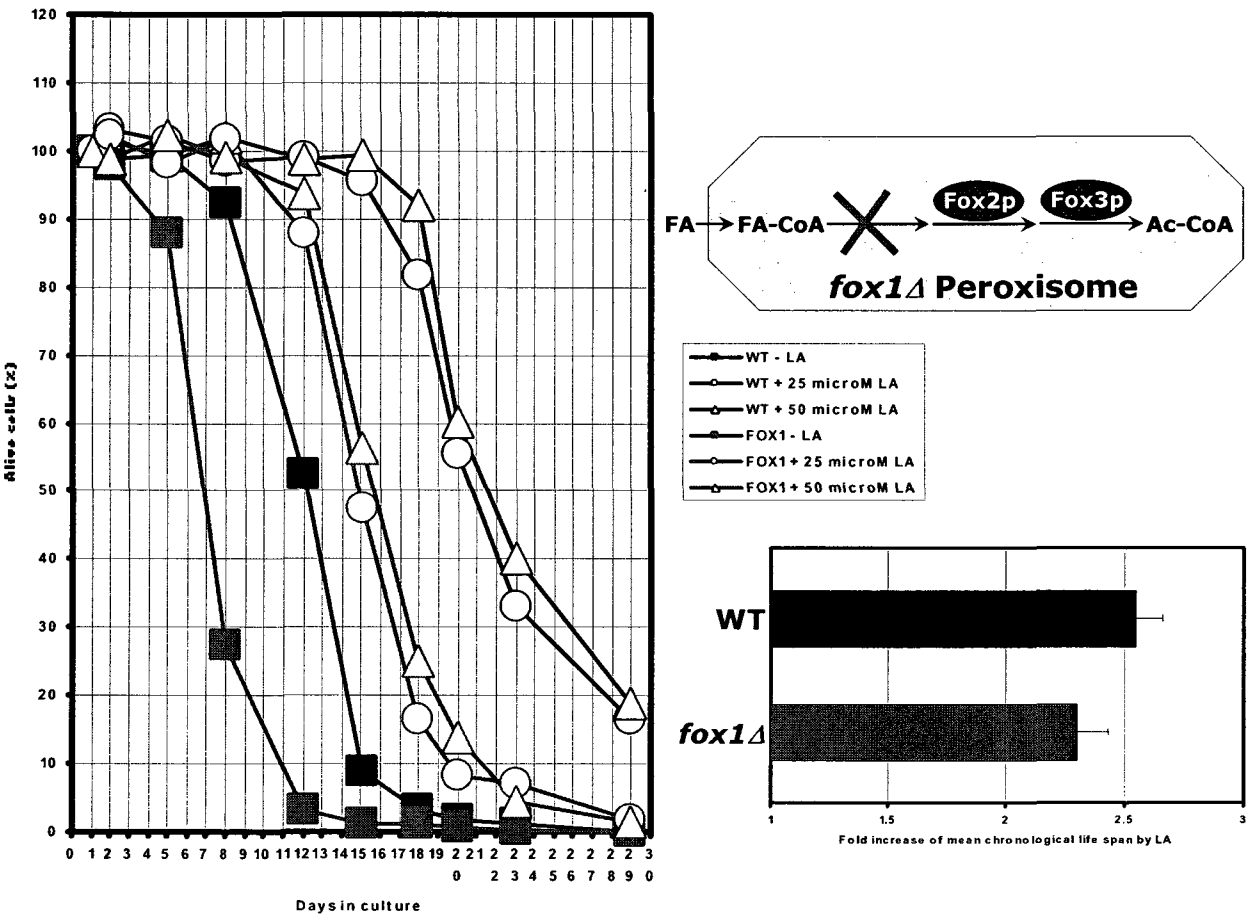


**Figure 4.4.** Fox1p (Aox) is not essential for the ability of LA to extend yeast longevity under CR conditions.

three enzymes of peroxisomal fatty acid oxidation (*i.e.*, Fox1p (Aox), Fox2p and Fox3p) is essential for the anti-aging action of LA. In fact, although the *fox1Δ*, *fox2Δ* and *fox3Δ* mutations decreased the chronological lifespan of CR yeast that have not been exposed to LA, none of these mutations caused a statistically significant reduction or rise of the fold increase of mean chronological lifespan by LA (Figures 4.4, 4.5 and 4.6). Therefore, I concluded that, although fatty acid oxidation in peroxisomes is essential for delaying aging or increasing fitness of yeast under CR conditions, it is not required for the ability of LA to extend their longevity.

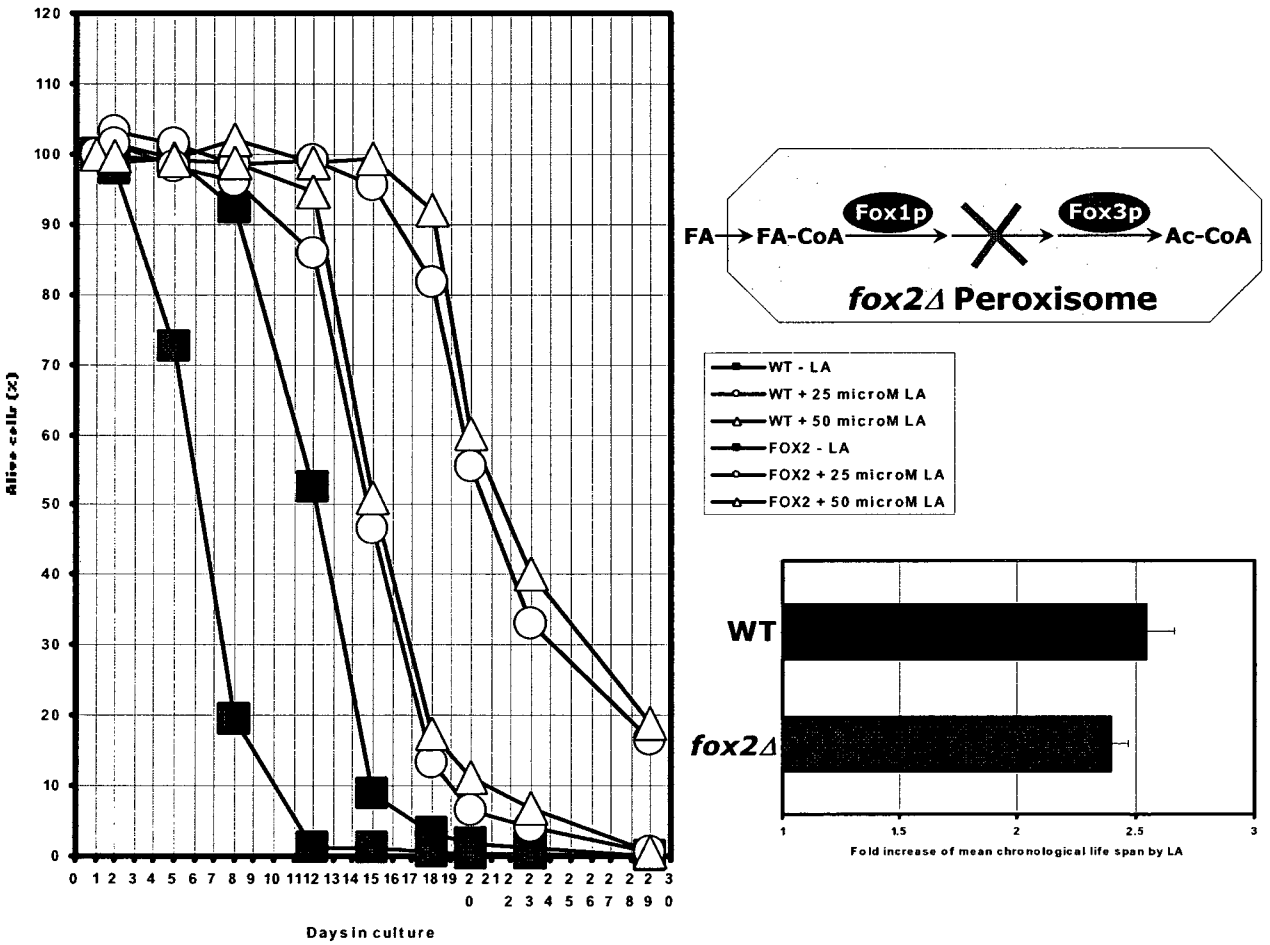


**Figure 4.5.** Fox2p is not essential for the ability of LA to extend yeast longevity under CR conditions.

### 4.4.2 Import of soluble proteins into the peroxisomal matrix is not essential for the ability of LA to increase the chronological lifespan of CR yeast

The peroxin Pex5p is a cytosolic shuttling receptor for peroxisomal import of numerous matrix proteins targeted to the peroxisome by their carboxyl-terminal PTS1, including Fox1p (Aox) and Fox2p (Figure 4.2) [2, 30].

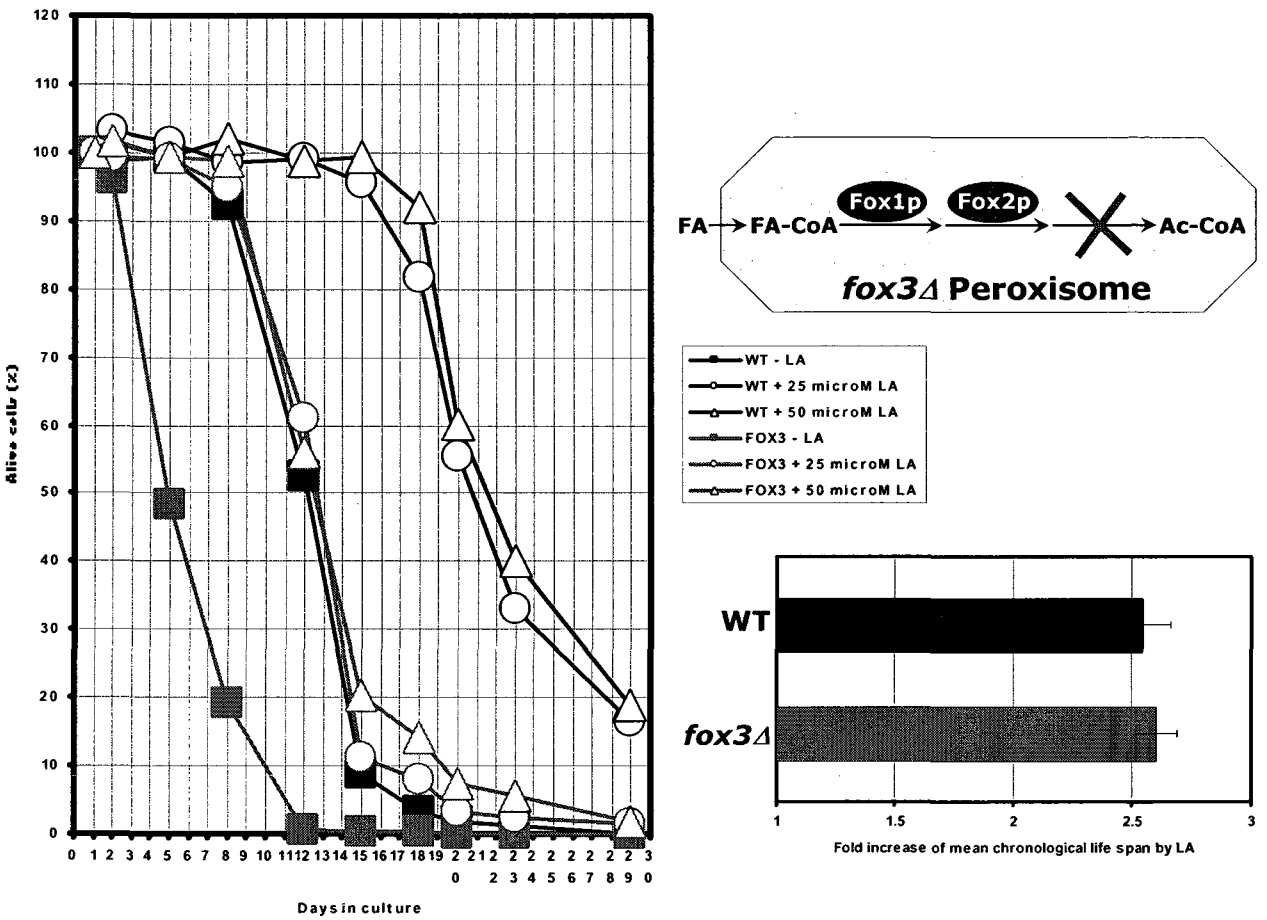


**Figure 4.6.** Fox3p is not essential for the ability of LA to extend yeast longevity under CR conditions.

Furthermore, the peroxin Pex7p functions as a cytosolic shuttling receptor for peroxisomal import of Fox3p (thiolase), the third enzyme of peroxisomal β-oxidation of fatty acids that carries the PTS2 (Figure 4.2) [6, 8].

According to the definition of a protein or process that is critical for the ability of LA to extend longevity of chronologically aging yeast under CR conditions, neither

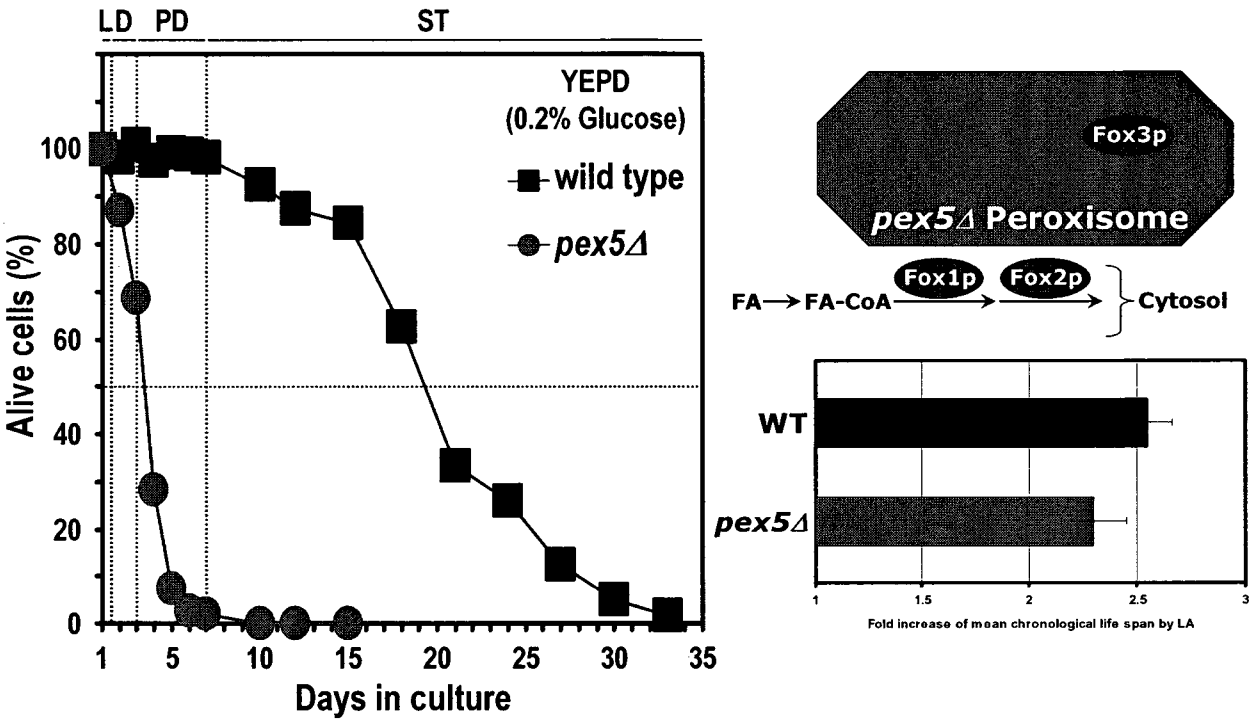


**Figure 4.7.** Pex5p is not essential for the ability of LA to extend longevity of CR yeast.

Pex5p nor Pex7p is essential for such anti-aging ability of LA. Indeed, although the *pex5Δ* and *pex7Δ* mutations decreased the chronological lifespan of CR yeast that have not been exposed to LA, none of these mutations caused a statistically significant reduction or rise of the fold increase of mean chronological lifespan by LA (Figures 4.7 and 4.8). I therefore concluded that, although both the Pex5p-dependent peroxisomal import of PTS1-containing proteins and Pex7p-dependent peroxisomal import of PTS2-containing proteins are essential for delaying aging or increasing fitness of yeast under CR conditions, none of these processes is required for the ability of LA to extend their

longevity.

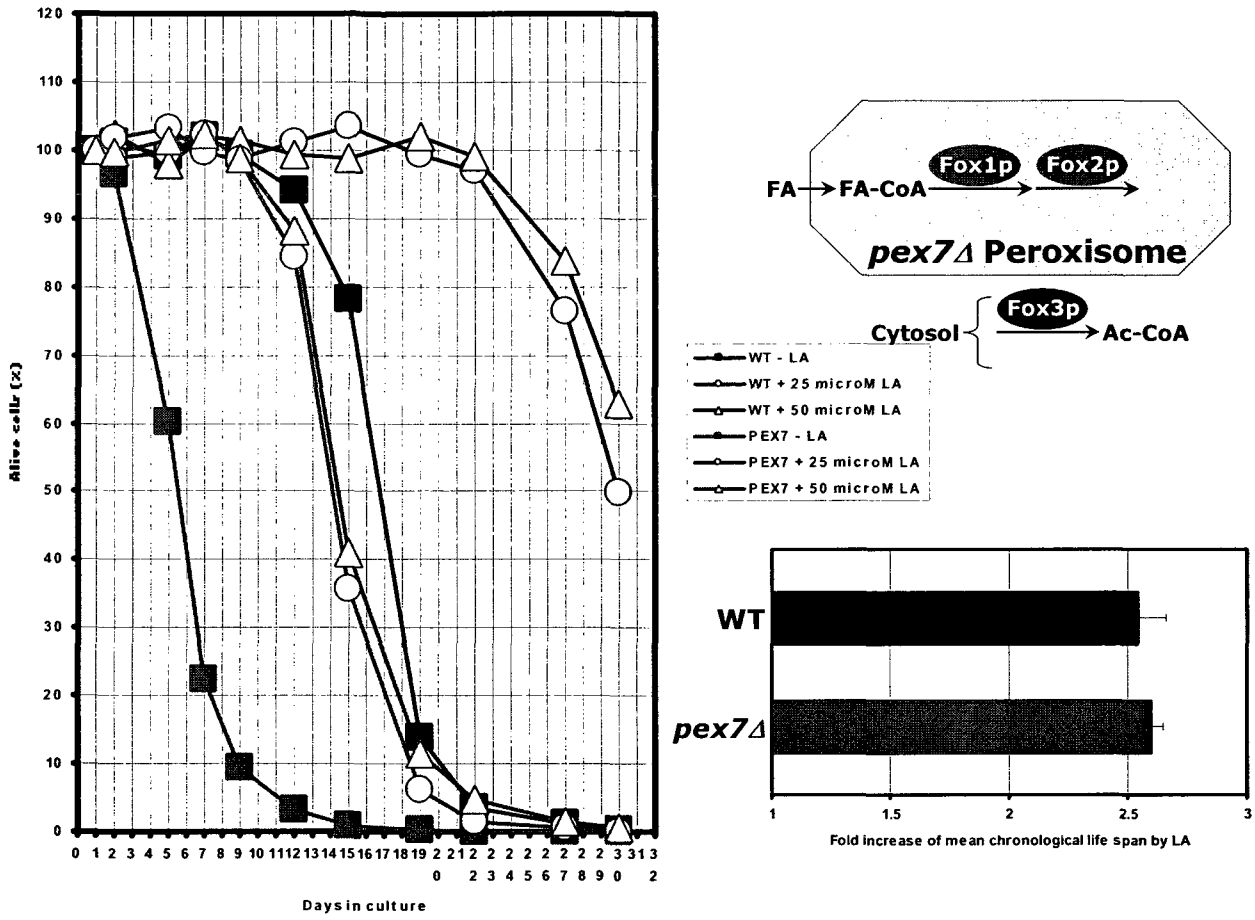


**Figure 4.8.** Pex7p is not essential for the ability of LA to extend longevity of CR yeast.

### 4.4.3 Presence of peroxisomes in yeast cells is not a requirement for life-span extending ability of LA

The peroxin Pex3p is required for the formation of peroxisomes from the ER template (Figure 4.2) [125, 224]. According to the definition of a protein or process that is critical for the ability of LA to extend longevity of chronologically aging yeast under CR conditions, Pex3p not is essential for such anti-aging ability of LA. Indeed, although the *pex3Δ* mutation decreased the chronological lifespan of CR yeast that have not been

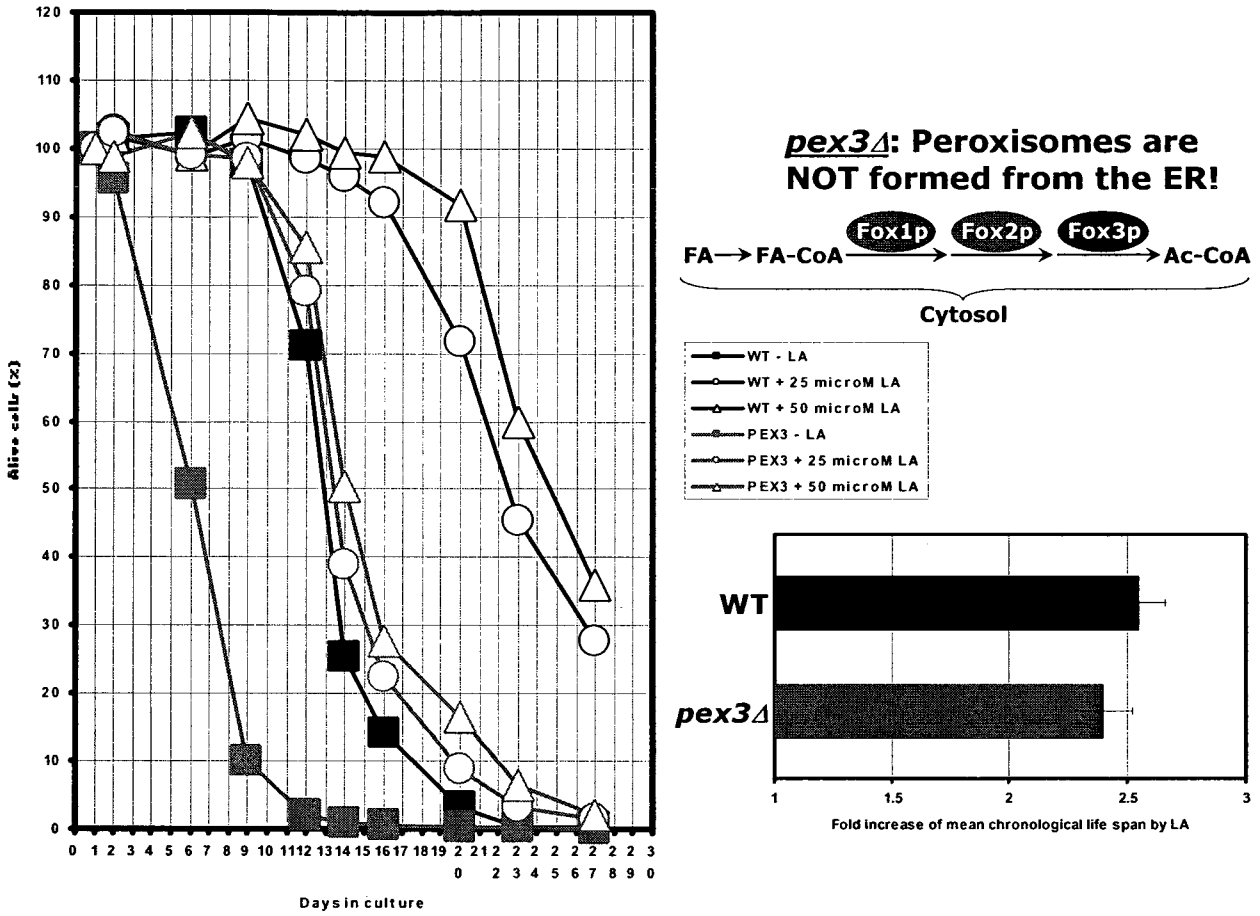


**Figure 4.9.** Pex3p is not essential for the ability of LA to extend longevity of CR yeast.

exposed to LA, it did not cause a statistically significant reduction or rise of the fold increase of mean chronological lifespan by LA (Figure 4.9). I therefore concluded that, although the ability to form peroxisomes from the ER template is essential for delaying aging or increasing fitness of yeast under CR conditions, it is not required for the ability of LA to extend yeast longevity. Thus, presence of peroxisomes in yeast cells is not a requirement for life-span extending ability of LA.

### 4.4.4 Pex1p weakens the ability of LA to extend the chronological lifespan of CR yeast

Together with Pex5p and Pex6p, the peroxin Pex1p is required for peroxisomal import of numerous matrix proteins targeted to the peroxisome by their carboxyl-terminal peroxisomal targeting signal type 1 (PTS1), including Fox1p (Aox) and Fox2p (Figure 4.2) in evolutionarily distant organisms [2, 30].

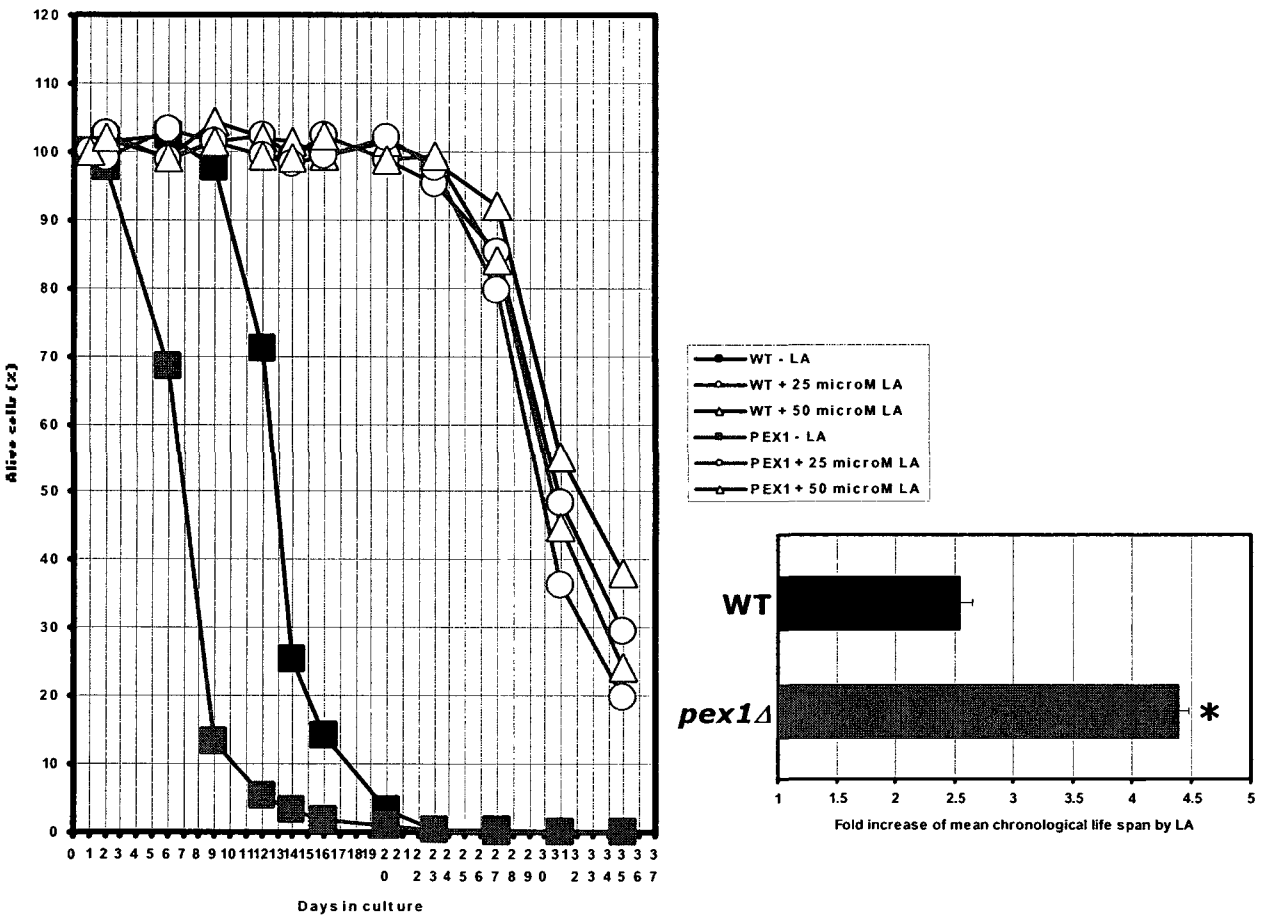


**Figure 4.10.** Pex1p weakens the ability of LA to extend longevity of CR yeast.

Additionally, in the yeast *Yarrowia lipolytica* and *Pichia pastoris*, Pex1p - in cooperation

with Pex6p - drives the fusion of immature peroxisomal vesicles during an early stage of the multistep peroxisome assembly pathway (see Chapter 2) [7, 30, 45, 46, 50, 125, 171]. According to the definition of a protein or process that is critical for the ability of LA to extend longevity of chronologically aging yeast under CR conditions, Pex1p weakens such anti-aging ability of LA. Indeed, although the *pex1Δ* mutation decreased the chronological lifespan of CR yeast that have not been exposed to LA, it caused a statistically significant rise of the fold increase of mean chronological lifespan by LA (Figure 4.10). Thus, lack (or low level) of Pex1p is a requirement for the ability of LA to extend yeast longevity.

### 4.4.5 Pex6p is essential for the ability of LA to extend the chronological lifespan of CR yeast

Jointly with Pex1p and Pex5p, the peroxin Pex6p is required for peroxisomal import of numerous matrix proteins targeted to the peroxisome by their carboxyl-terminal peroxisomal targeting signal type 1 (PTS1), including Fox1p (Aox) and Fox2p (Figure 4.2) across phyla [2, 30]. Moreover, in the yeast *Yarrowia lipolytica* and *Pichia pastoris*, Pex1p - in concert with Pex6p - promotes the fusion of immature peroxisomal vesicles during an early stage of the multistep peroxisome assembly pathway (see Chapter 2) [7, 30, 45, 46, 50, 125, 171]. Furthermore, in the yeast *S. cerevisiae* Pex6p functions not only in peroxisome biogenesis but also in the import of the Atp2p, a β-subunit of $F_1F_0$-ATPase, into mitochondria [228]. According to the definition of a protein or process that is critical for the ability of LA to extend longevity of chronologically aging yeast under

CR conditions, Pex6p is essential for the ability of LA to extend the chronological lifespan of CR yeast. In fact, not only the *pex6Δ* mutation decreased the chronological lifespan of CR yeast that have not been exposed to LA, but it also almost completely abolished the anti-aging effect of LA under CR conditions (Figure 4.11).

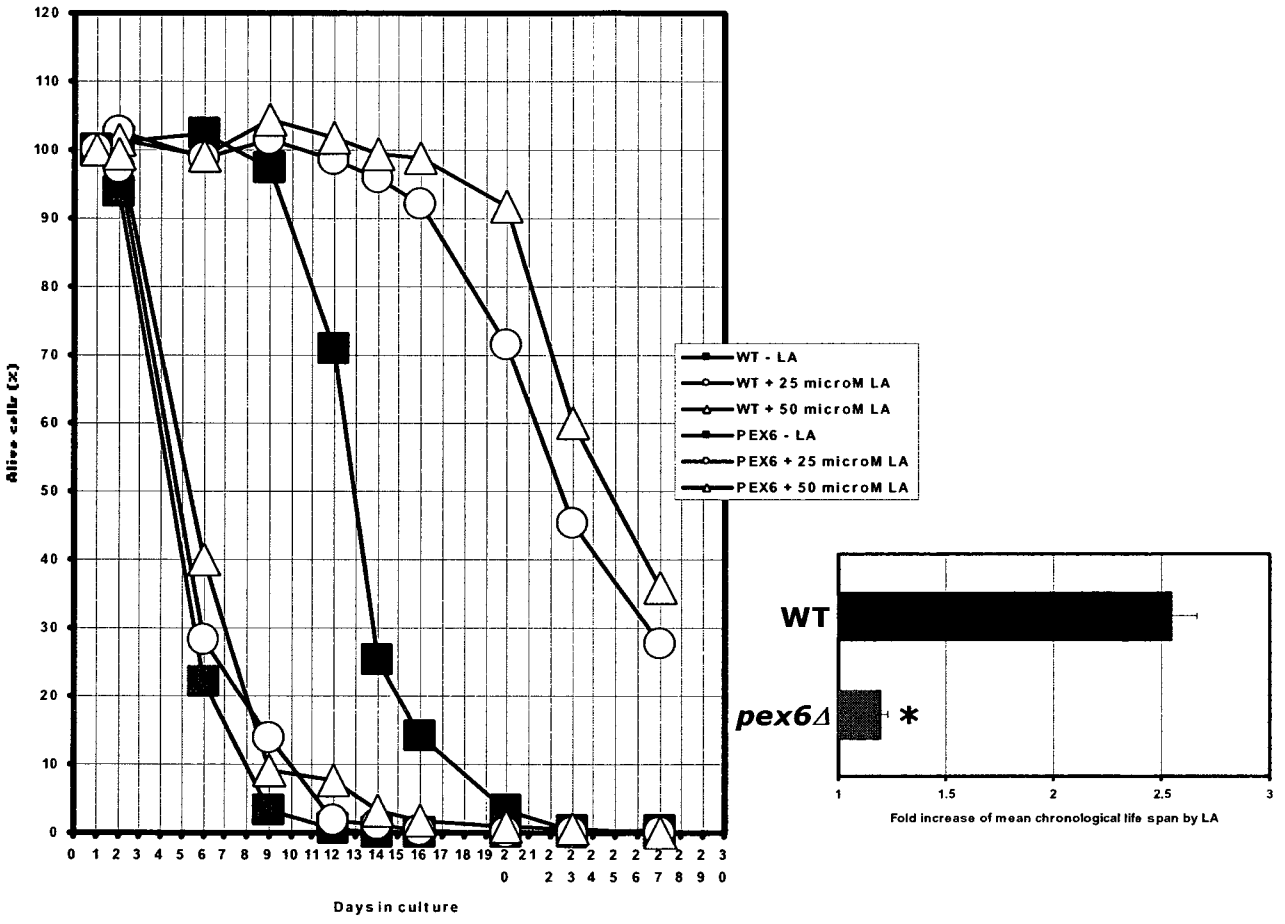


**Figure 4.11.** Pex6p is essential for the ability of LA to extend longevity of CR yeast.

### 4.4.6 LA alters the age-dependent dynamics of several mitochondrial activities in CR yeast: A hypothesis for a dual role of ROS in regulating longevity

My aforementioned findings provided evidence that the presence of peroxisomes in yeast cells is not a requirement for life-span extending ability of LA. However, the peroxin Pex1p weakens the ability of LA to extend the chronological lifespan of CR yeast (Chapter 4.4.4), whereas Pex6p - another AAA ATPase - is indispensable for such ability, being essential for the anti-aging action of LA (Chapter 4.4.5). Taken together, these findings strongly suggest that the critical role of both Pex1p and Pex6p in mediating the anti-aging effect of LA on CR yeast does not relate to their involvement in peroxisome biogenesis. It should be stressed that at least one of these two AAA ATPases, namely Pex6p, functions not only in peroxisome biogenesis but also in the import of the Atp2p, a β-subunit of $F_1F_0$-ATPase, into mitochondria [228]. Thus, Pex6p not only controls the biogenesis of the peroxisome but also modulates the functional state of another cellular organelle, the mitochondrion. I therefore suggested that the functionality of mitochondria is a requirement for the anti-aging effect of LA on CR yeast. This suggestion is indirectly supported by my observation that LA alters the age-dependent dynamics of several mitochondrial activities in CR yeast, including oxygen consumption, mitochondrial membrane potential ($\Delta\Psi$) and ROS generation. In particular, in CR yeast entering D phase, LA decreases the amplitude of the spike in all these mitochondrial activities (Figures 4.12, 4.13 and 4.14). Furthermore, during PD and ST phases, LA prevents a sharp decline of all these activities, maintaining them at the levels they reached by the end of PD phase (Figures 4.12, 4.13 and 4.14). Based on these findings, I

hypothesized that one of the mechanisms by which mitochondria regulate yeast longevity is based on the LA-dependent ability of mitochondria in aging yeast to maintain ROS homeostasis. I proposed that ROS, which are mostly generated as by-products of mitochondrial respiration [229, 230], play a dual role in regulating longevity. First, if

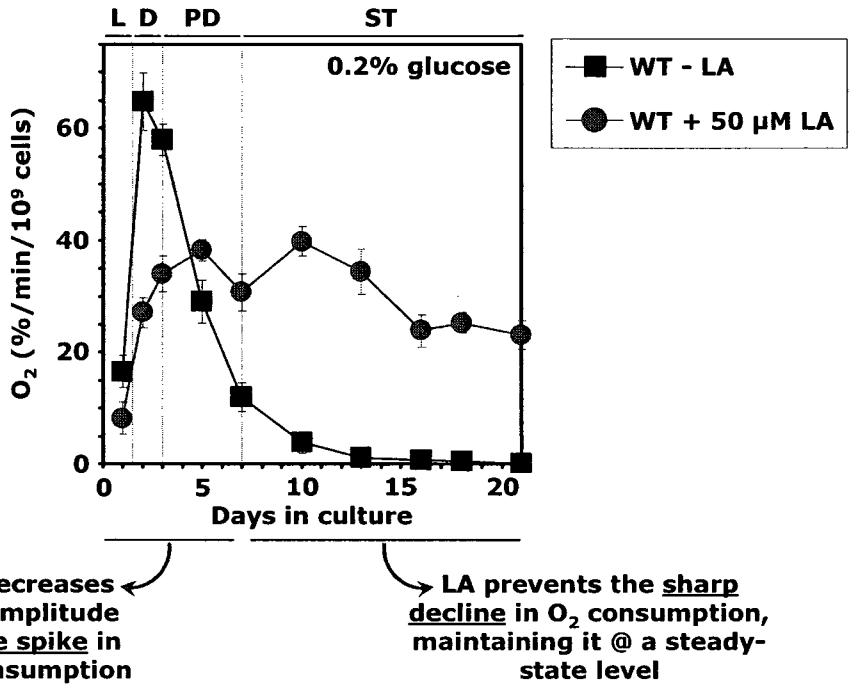


**Figure 4.12.** LA alters the age-dependent dynamics of cellular respiration by modulating mitochondrial oxygen consumption.

yeast mitochondria are unable - due to a dietary regimen (see Chapter 3) or unavailability of LA - to maintain ROS concentration below a critically high level, ROS promote aging by oxidatively damaging certain mitochondrial proteins (such as cytochrome c oxidase [CCO], succinate dehydrogenase [SDH] and aconitase [ACO]; see Chapter 3). Second, if yeast mitochondria can - due to a dietary regimen (see Chapter 3) or availability of LA –

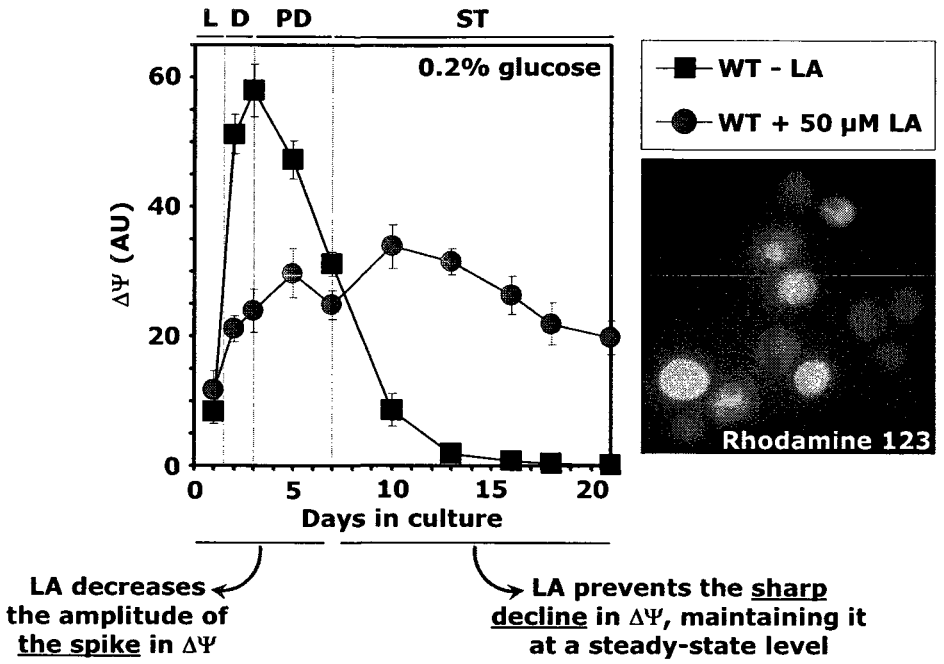


**Figure 4.13.** LA alters the age-dependent dynamics of mitochondrial membrane potential (ΨΔ).

maintain ROS concentration at an "optimal" level, ROS delay aging. This "optimal" level of ROS is insufficient to damage cellular macromolecules but can activate certain signaling networks [101, 229, 231 – 235] that extend life span by increasing the abundance or activity of stress-protecting and other anti-aging proteins. The term "mitohormesis" has been coined for such anti-aging role of mitochondrially produced ROS [236]; the term "hormesis" refers to a beneficial defence response of an organism to a low-intensity biological stress [237, 238]. In my hypothesis for a dual role of ROS in regulating longevity, LA extends the chronological lifespan of CR yeast by: (1) reducing the damaging effect of ROS on cellular macromolecules during L, D and PD growth phases; and (2) amplifying the "hormetic" effect of ROS during ST growth phase (*i.e.*, in senescent yeast cells) through the activation of stress-protecting and other anti-aging

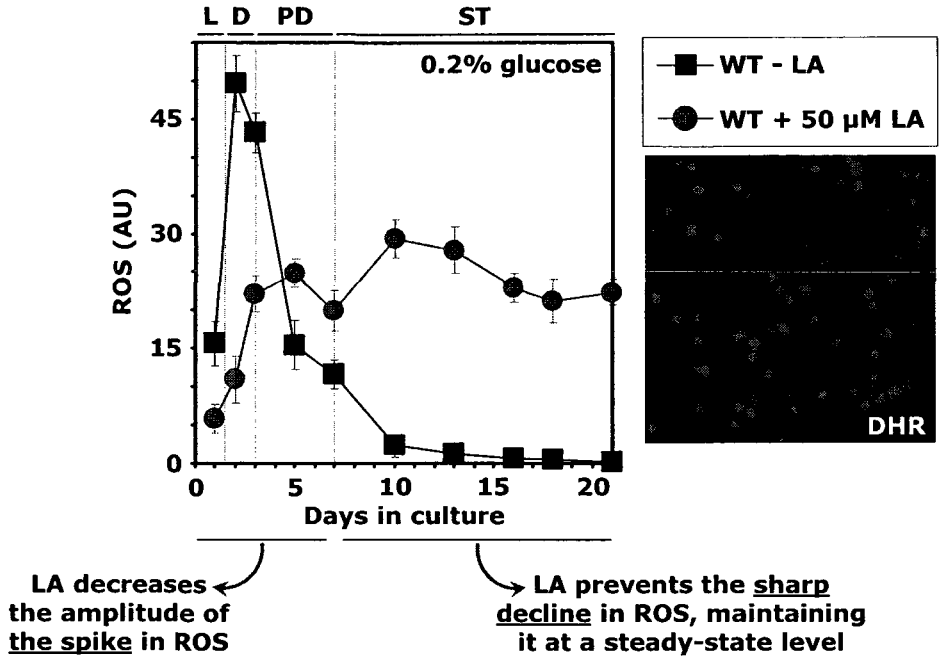


**Figure 4.14.** LA alters the age-dependent dynamics of ROS generation in mitochondria.

proteins (Figure 4.15). Recent data from Dr. Titorenko's laboratory provided a conformation for the ability of LA to amplify the "hormetic" effect of ROS in senescent yeast cells through the activation of stress-protecting and other anti-aging proteins by showing that: (1) LA greatly enhances the resistance of non-proliferating yeast cells that have reached ST phase to acute oxidative stress and heat shock; and (2) LA considerably increases the intracellular levels of molecular chaperones protecting yeast from oxidative stress-induced protein aggregation.

### 4.4.7 The age-dependent dynamics of changes in the levels of ROS in cells of *Δfox* and *Δpex* mutants exposed to LA confirms the validity of the hypothesis for a dual role of ROS in regulating longevity

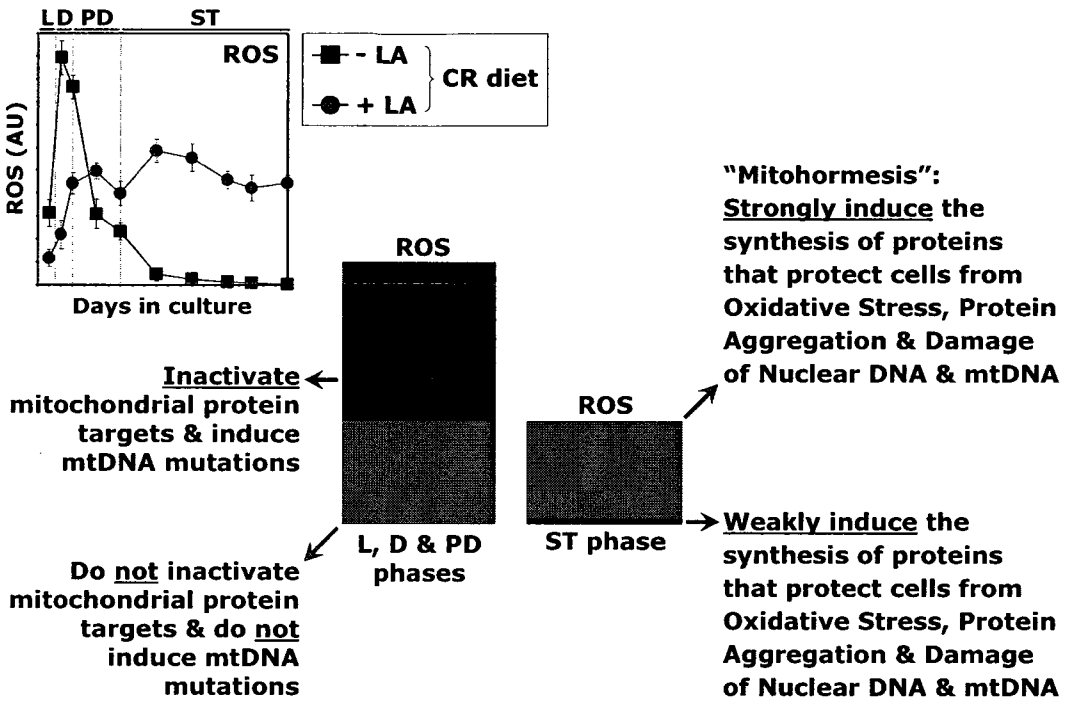


**Figure 4.15.** In my hypothesis for a dual role of ROS in regulating longevity, LA extends the chronological lifespan of CR yeast by: (1) reducing the damaging effect of ROS on cellular macromolecules during L, D and PD growth phases; and (2) amplifying the "hormetic" effect of ROS during ST growth phase (*i.e.*, in senescent yeast cells) through the activation of stress-protecting and other anti-aging proteins.

In my hypothesis for a dual role of ROS in regulating longevity, LA extends the chronological lifespan of CR yeast by: (1) reducing the damaging effect of ROS on cellular macromolecules during L, D and PD growth phases; and (2) amplifying the "hormetic" effect of ROS during ST growth phase (*i.e.*, in senescent yeast cells) through the activation of stress-protecting and other anti-aging proteins. If my hypothesis is valid, then any *Δfox* or *Δpex* mutation that in the presence of LA significantly decreases (as compared to LA-untreated wild-type cells) the "early" spike in ROS during L and D phases and, simultaneously, significantly increases (as compared to LA-untreated wild-type cells) the "late" spike in ROS during ST phase could enhance the anti-aging effect of

LA. In fact, such a mutation is expected - according to my hypothesis - to reduce the damaging effect of ROS on cellular macromolecules during L and D phases and, simultaneously, to enhance the "hormetic" effect of ROS during ST phase. The validity of my hypothesis is supported by the observation that the *pex1Δ* mutation - which in the presence of LA resulted in a considerable reduction of ROS level during L and D phases and, simultaneously, in a significant rise of ROS level during ST phase (Figure 4.16) - caused a statistically significant rise of the fold increase of mean chronological lifespan by LA (Figure 4.10). Furthermore, if my hypothesis is valid, then any *Δfox* or *Δpex* mutation that in the presence of LA significantly increases (as compared to LA-untreated wild-type cells) the "early" spike in ROS during L and D phases and, simultaneously,

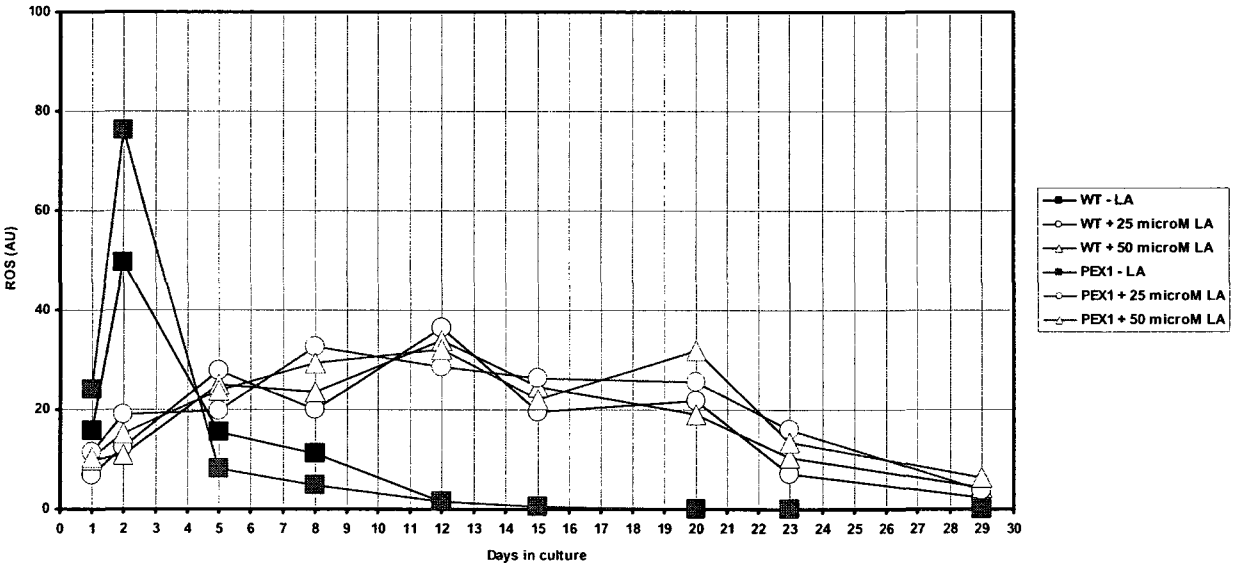


**Figure 4.16.** In the presence of LA, the *pex1Δ* mutation - which causes a statistically significant rise of the fold increase of mean chronological lifespan by LA (Figure 4.10) - results in a considerable reduction (as compared to LA-untreated wild-type cells) of ROS level during L and D phases and, simultaneously, in a significant rise (as compared to LA-untreated wild-type cells) of ROS level during ST phase.

significantly decreases (as compared to LA-untreated wild-type cells) the "late" spike in ROS during ST phase could eliminate the anti-aging effect of LA. Indeed, such a mutation is expected - according to my hypothesis - to enhance the damaging effect of ROS on cellular macromolecules during L and D phases and, simultaneously, to weaken the "hormetic" effect of ROS during ST phase. The validity of my hypothesis is supported by the observation that the *pex6Δ* mutation - which in the presence of LA resulted in a considerable rise of ROS level during L and D phases and, simultaneously, in a significant decrease of ROS level during ST phase (Figure 4.17) - caused a statistically significant reduction of the fold increase of mean chronological lifespan by LA (Figure 4.11). Finally, if my hypothesis is valid, then any *Δfox* or *Δpex* mutation that

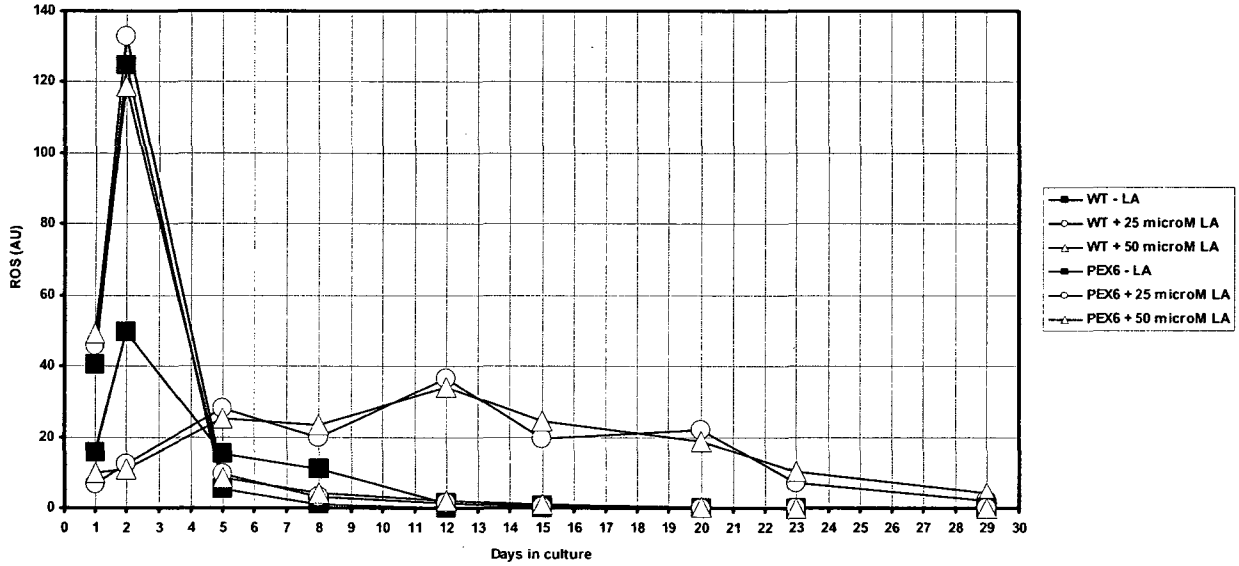


**Figure 4.17.** In the presence of LA, the *pex6Δ* mutation - which causes a statistically significant reduction of the fold increase of mean chronological lifespan by LA (Figure 4.11) - results in a considerable rise (as compared to LA-untreated wild-type cells) of ROS level during L and D phases and, simultaneously, in a significant decrease (as compared to LA-untreated wild-type cells) of ROS level during ST phase.

in the presence of LA significantly increases (as compared to LA-untreated wild-type

cells) the "early" spike in ROS during L and D phases and, simultaneously, significantly increases (as compared to LA-untreated wild-type cells) the "late" spike in ROS during ST phase could have no influence on the anti-aging effect of LA. Indeed, although such a mutation is expected - according to my hypothesis - to enhance the damaging effect of ROS on cellular macromolecules during L and D phases, it would at the same time enhance the "hormetic" effect of ROS during ST phase. The validity of my hypothesis is supported by the observation that none of the *fox1Δ*, *fox2Δ*, *fox3Δ*, *pex3Δ* and *pex7Δ* mutations - all of which in the presence of LA resulted in a considerable rise of ROS level during L and D phases and, simultaneously, in an increase of ROS level during ST phase (Figures 4.18, 4.19, 4.20, 4.21 and 4.22) - caused a statistically significant

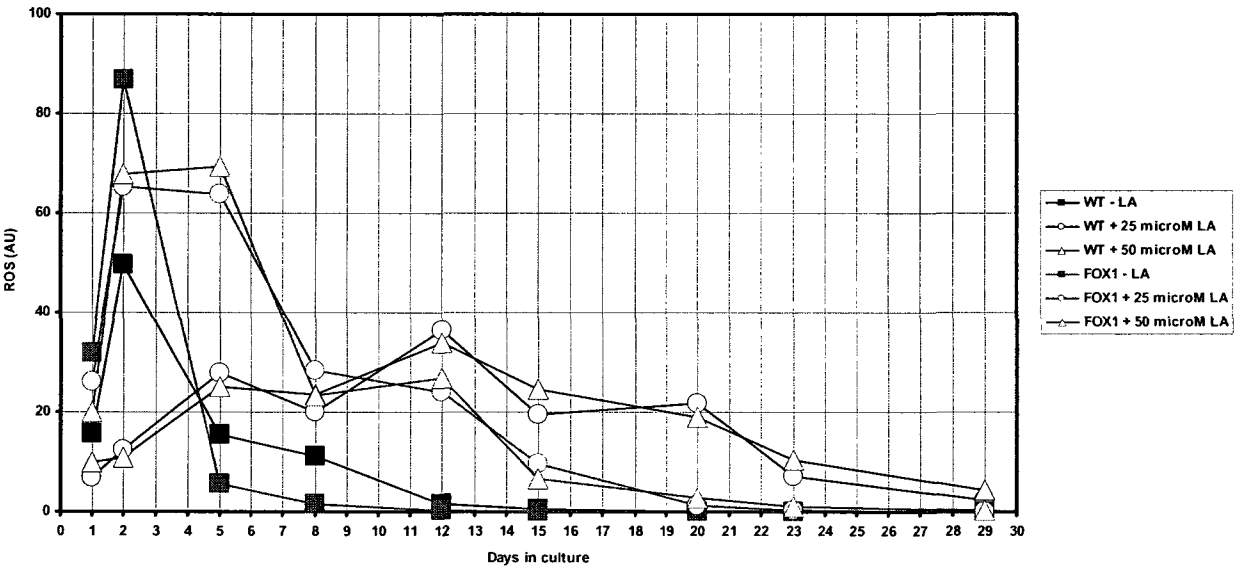


**Figure 4.18.** In the presence of LA, the *fox1Δ* mutation – which does not cause a statistically significant reduction or rise of the fold increase of mean chronological lifespan by LA (Figure 4.4) - results in an increase (as compared to LA-untreated wild-type cells) of ROS level during L and D phases and, simultaneously, in an increase (as compared to LA-untreated wild-type cells) of ROS level during ST phase.

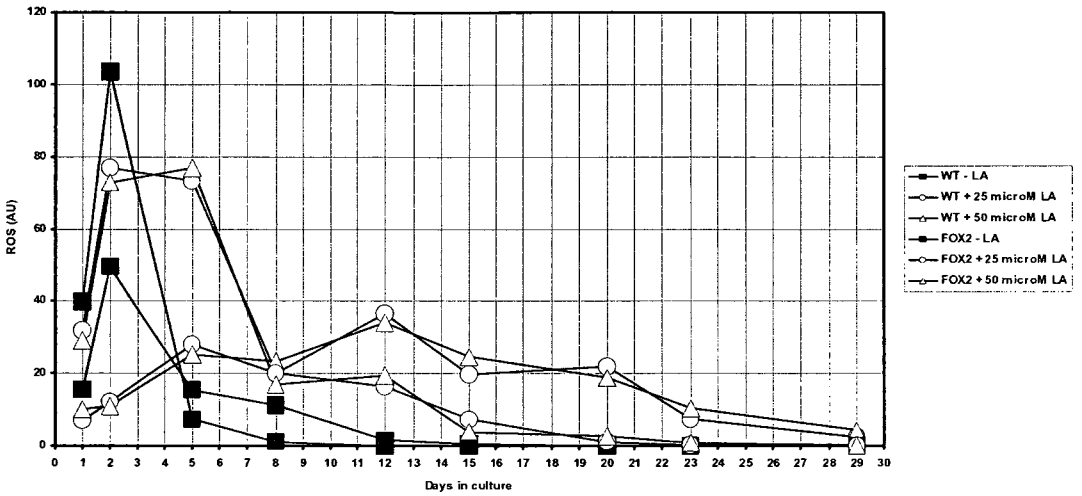


**Figure 4.19.** In the presence of LA, the *fox2Δ* mutation – which does not cause a statistically significant reduction or rise of the fold increase of mean chronological lifespan by LA (Figure 4.5) - results in an increase (as compared to LA-untreated wild-type cells) of ROS level during L and D phases and, simultaneously, in an increase (as compared to LA-untreated wild-type cells) of ROS level during ST phase.

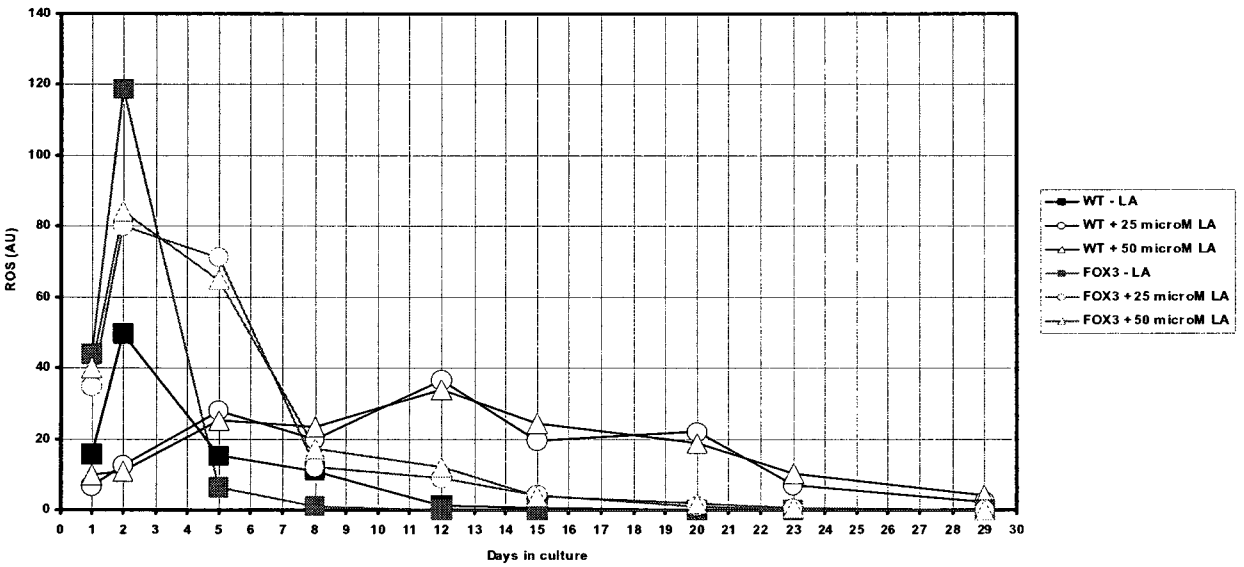


**Figure 4.20.** In the presence of LA, the *fox3Δ* mutation – which does not cause a statistically significant reduction or rise of the fold increase of mean chronological lifespan by LA (Figure 4.6) - results in an increase (as compared to LA-untreated wild-type cells) of ROS level during L and D phases and, simultaneously, in an increase (as compared to LA-untreated wild-type cells) of ROS level during ST phase.

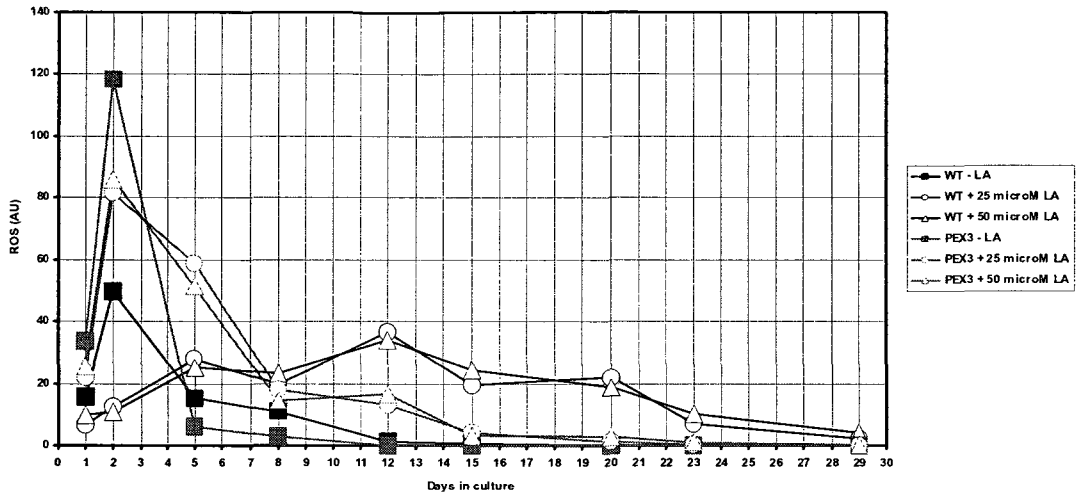


**Figure 4.21.** In the presence of LA, the *pex3Δ* mutation – which does not cause a statistically significant reduction or rise of the fold increase of mean chronological lifespan by LA (Figure 4.9) - results in an increase (as compared to LA-untreated wild-type cells) of ROS level during L and D phases and, simultaneously, in an increase (as compared to LA-untreated wild-type cells) of ROS level during ST phase.

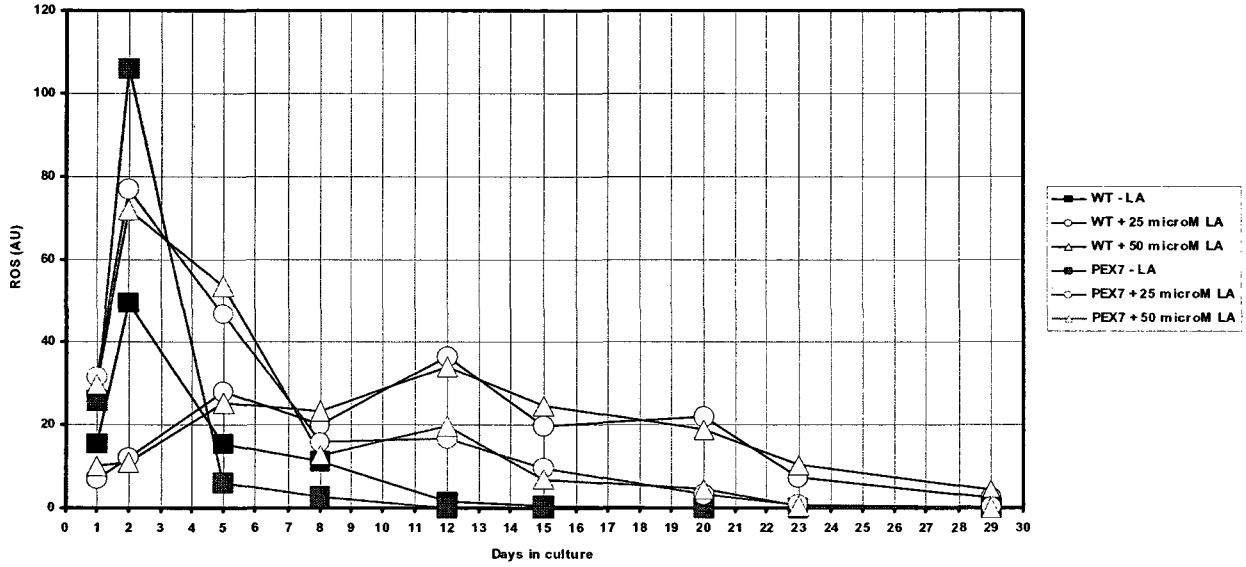


**Figure 4.22.** In the presence of LA, the *pex7Δ* mutation – which does not cause a statistically significant reduction or rise of the fold increase of mean chronological lifespan by LA (Figure 4.8) - results in an increase (as compared to LA-untreated wild-type cells) of ROS level during L and D phases and, simultaneously, in an increase (as compared to LA-untreated wild-type cells) of ROS level during ST phase.

reduction or rise of the fold increase of mean chronological lifespan by LA (Figures 4.4, 4.5, 4.6, 4.7, 4.8 and 4.9).

### 4.4.8 Chronology of aging biomarkers in the *idh1Δ* and *idh2Δ* mutants confirms the validity of the hypothesis for a dual role of ROS in regulating longevity

In my hypothesis for a dual role of ROS in regulating longevity, if yeast mitochondria are unable - due to a dietary regimen (see Chapter 3) or unavailability of LA (see sections 4.4.6 and 4.4.7 of this chapter) - to maintain ROS concentration below a critically high level, ROS promote aging by oxidatively damaging certain mitochondrial proteins (such as CCO, SDH and ACO; see Chapter 3). Conversely, if yeast mitochondria can - due to a dietary regimen (see Chapter 3) or availability of LA (see sections 4.4.6 and 4.4.7 of this chapter) - maintain ROS concentration at an "optimal" level, ROS delay aging. This "optimal" level of ROS is insufficient to damage cellular macromolecules but can activate certain signaling networks [101, 229, 231 – 235] that extend life span by increasing the abundance or activity of stress- protecting and other anti-aging proteins. My analysis of the age-dependent dynamics of changes in the levels of ROS in cells of *Δfox* and *Δpex* mutants exposed to LA validated this hypothesis (see section 4.4.7 of this chapter). To further evaluate the validity of my hypothesis, I developed and tested a complementary experimental approach that uses a different longevity-extending intervention. This approach is based on the fact that certain components of the mitochondrial tricarboxylic acid (TCA) cycle and electron transport chain (ETC) are redundant. The redundant components of the mitochondrial TCA cycle

include the Pdx1p and Lpd1p subunits of pyruvate dehydrogenase, the Cit1p, Cit2p and Cit3p isoforms of citrate synthase, the Idh1p and Idh2p subunits of isocitrate dehydrogenase, the Lsc1p and Lsc2p subunits of succinyl-CoA ligase, and the Sdh1p, Sdh2p, Sdh3p and Sdh4p subunits of SDH (Figure 4.23A). I reason that mitochondria lacking a single redundant component would still be able to produce NADH and $FADH_2$, the two donors of electrons for the ETC, but in reduced amounts. This, in turn, would reduce mitochondrial ROS generated as by-products of electron flow through the ETC. The same logic applies to the NADH:ubiquinone oxidoreductase Ndi1p, the Cyc1p and Cyc2p isoforms of cytochrome c, and the cytochrome c peroxidase Ccp1p. While lack of any of these redundant ETC components does not affect growth in glucose-containing medium [239], it would reduce mitochondrial ROS by weakening electron flow through the ETC. I expected therefore that, if my hypothesis that mitochondrial ROS play a dual role in regulating longevity is accurate, lack of a single redundant component of the ETC or TCA cycle would extend the life span of CR yeast grown on 0.2% glucose. This glucose concentration provides a modest life-span extension, as compared to that for 0.5% glucose (see Chapter 3). I reason that, by decreasing the level of mitochondrial ROS, a mutation that eliminates only one of these redundant components would enable mitochondria of yeast grown on 0.2% glucose to maintain ROS at a level that is insufficient to damage cellular macromolecules but can increase the abundance and/or activity of stress-protecting proteins that delay aging. Remarkably, my analysis of yeast strains carrying mutations that eliminate either the Idh1p or the Idh2p subunit of isocitrate dehydrogenase revealed that both mutations extend the chronological lifespan

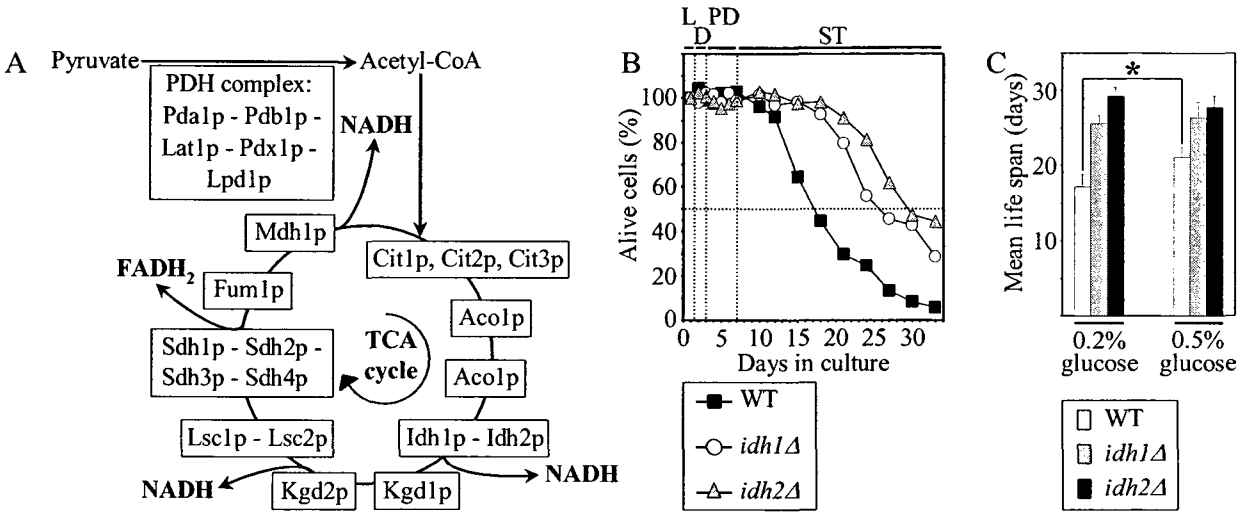


**Figure 4.23.** The *idh1Δ* and *idh2Δ* mutations extend the chronological life span of CR yeast. (A) Outline of metabolic flux through the mitochondrial TCA cycle. (B) Survival of chronologically aging WT, *idh1Δ* and *idh2Δ*. (C) The mean life spans of WT, *idh1Δ* and *idh2Δ*. Data are presented as ± SEM (n = 3-5). Cells were cultured in YEP medium containing 0.2% glucose.

of CR yeast grown on 0.2% glucose (Figure 4.23B), making it very similar to that of CR yeast grown on 0.5% glucose (Figure 4.23C). Furthermore, as my hypothesis for a dual role of ROS in regulating longevity predicts, the *idh1Δ* and *idh2Δ* mutations altered the age-dependent dynamics of mitochondrial oxygen consumption, ROS production, $\Delta\Psi$ maintenance, and activities of CCO, SDH and ACO. Specifically, in CR yeast entering the D phase of growth on 0.2% glucose, both mutations decreased the amplitude of the spike in all of these mitochondrial activities (Figure 4.24). Moreover, during PD and ST phases, both mutations prevented a sharp decline of all of these activities, maintaining them at the steady-state levels they reached by the end of PD phase (Figure 4.24).

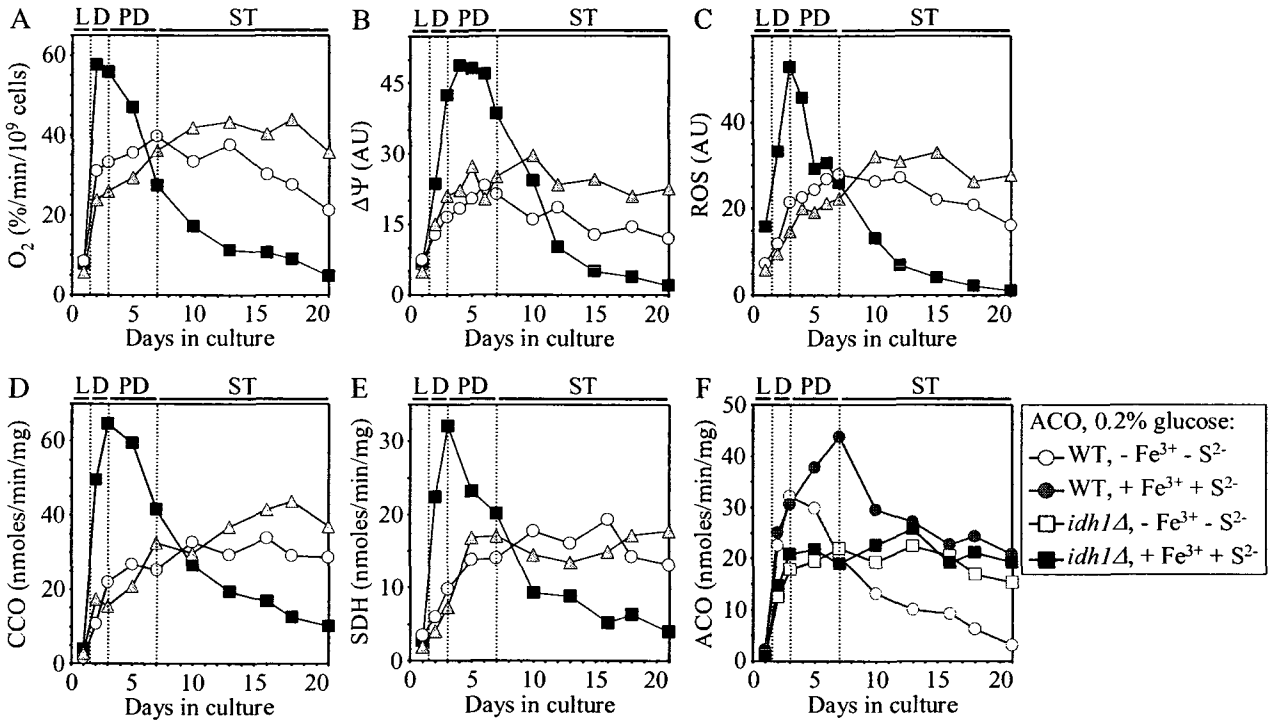


**Figure 4.24.** The *idh1Δ* and *idh2Δ* mutations alter the age-dependent dynamics of essential mitochondrial processes. The age-dependent dynamics of oxygen consumption (A), mitochondrial membrane potential ΨΔ (B), intracellular levels of reactive oxygen species (ROS) (C), and enzymatic activities of cytochrome c oxidase (CCO) (D), succinate dehydrogenase (SDH) (E) and aconitase (ACO) (F) for WT, *idh1Δ* and *idh2Δ*. The ACO activity was measured with or without the reactivation agents $Fe^{3+}$ and $Na_2S$. Cells were cultured in YEP medium containing 0.2% glucose.

Noteworthy, the *idh1Δ* and *idh2Δ* averted the loss of CCO and SDH activities, which represent the major mitochondrial targets of oxidative damage by ROS [101, 106] (Figures 4.24D and 4.24E). Moreover, both mutations protected mitochondrial ACO from inactivation (Figure 4.24F) caused by the oxidation-dependent loss of one iron from its Fe/S cluster [240]. It should be stressed that recent studies in Dr. Titorenko's laboratory revealed that both mutations increased the abundance of cytosolic and

mitochondrial anti-stress chaperones, ROS-decomposing proteins, and proteins that bind to mitochondrial DNA and protect it from oxidative damage. Consistent with the elevated levels of these proteins, I found that both mutations enhanced heat-shock and oxidative stress resistance of chronologically aging CR yeast (Figure 4.25).

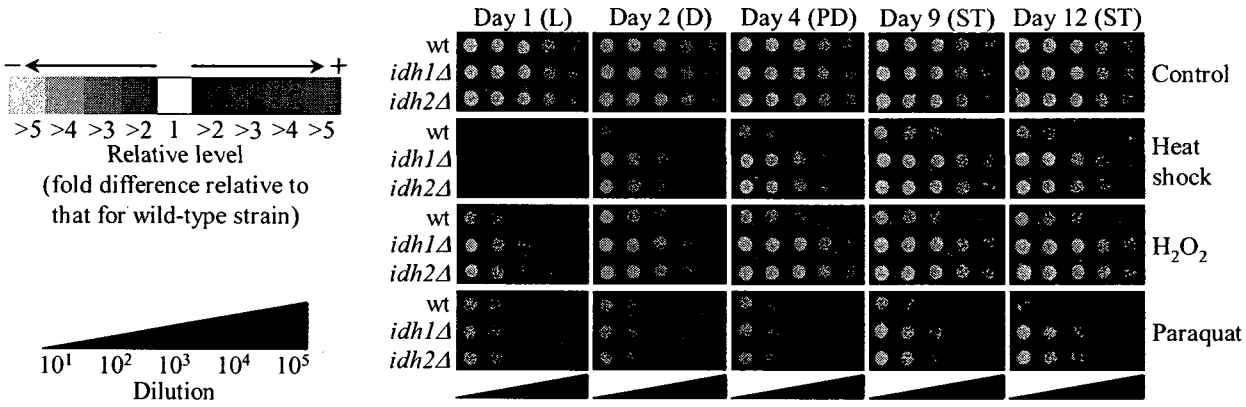


**Figure 4.25.** The *idh1Δ* and *idh2Δ* mutations enhance stress resistance of CR yeast. Heat-shock and oxidative stress resistance of WT, *idh1Δ* and *idh2Δ*. Cells grown in YEP medium containing 0.2% glucose were taken for analyses at the indicated time-points.

## 4.5 Discussion

In a high-throughput screening of several combinatorial chemical libraries that Dr. Titorenko's laboratory used to identify novel anti-aging small molecules, the short-lived *pex5Δ* mutant was used as a tester strain. This mutant strain lacks Pex5p, a cytosolic shuttling receptor for peroxisomal import of numerous matrix proteins targeted to the peroxisome by their carboxyl-terminal PTS1, including Fox1p (Aox) and Fox2p [2, 30]. My experiments with one of the novel anti-aging drugs identified by Dr. Titorenko's laboratory, a commercially available compound LA, revealed that it extends longevity not only of the *pex5Δ* mutant but also of wild-type strain cultured under CR conditions.

Based on these findings, it was conceivable that LA extends the lifespan of the *pex5Δ* mutant by somehow by-passing the function of Pex5p in peroxisome biogenesis. Furthermore, my findings described in Chapter 3 led to the conclusion that the rate of peroxisomal β-oxidation of fatty acids that originate from stored neutral lipids controls the pace of chronological aging under CR conditions. Altogether, these data suggested that LA could extend yeast longevity in part by targeting certain processes related to the biogenesis and/or function of peroxisomes. To investigate if the ability of the peroxisome to oxidize fatty acids (*i.e.*, a Fox-dependent function) or assemble properly (*i.e.*, a Pex-dependent function) is a requirement for the anti-aging action of LA in chronologically aging yeast under CR conditions, I developed a definition of a protein or process that is critical for such action of LA (see section 4.4.1 of this chapter). Using my approach for defining processes that are critical for the ability of LA to extend longevity of chronologically aging yeast, I found - somewhat unexpectedly - that, although fatty acid oxidation in peroxisomes is essential for delaying aging or increasing fitness of yeast under CR conditions, it is not required for the ability of LA to extend their longevity (see section 4.4.1 of this chapter). Furthermore, my analysis of the ability of LA to influence the chronological lifespans of the *pex5Δ* and *pex7Δ* mutant strains provided evidence that, although both the Pex5p-dependent peroxisomal import of PTS1-containing proteins and Pex7p-dependent peroxisomal import of PTS2-containing proteins are essential for delaying aging or increasing fitness of yeast under CR conditions, none of these processes is required for the ability of LA to extend their longevity (see section 4.4.2 of this chapter). Moreover, my finding that the *pex3Δ* mutation - which eliminates a peroxin

essential for the formation of peroxisomes from the ER template [125, 224] - does not cause a statistically significant reduction or rise of the fold increase of mean chronological lifespan by LA implies that the ability to form peroxisomes from the ER template is not required for the ability of LA to extend yeast longevity (see section 4.4.3 of this chapter). Taken together, my findings provide conclusive evidence that the presence of peroxisomes in yeast cells is not a requirement for life-span extending ability of LA. However, it appeared that at least two peroxins that play an essential role in peroxisome biogenesis, namely the AAA ATPases Pex1p and Pex6p, are critical for the ability of LA to extend longevity of chronologically aging yeast under CR conditions. One of these peroxins, Pex1p, weakens the anti-aging ability of LA so that the absence of this protein causes a statistically significant rise of the fold increase of mean chronological lifespan by LA (see section 4.4.4 of this chapter). It remains to be established how exactly, in molecular terms, Pex1p modulates the ability of LA to extend yeast longevity. One could suggest that, in addition to its essential role in peroxisome biogenesis, this peroxin controls an age-related process that does not relate to its function in the assembly of the peroxisome and is one of the targets of LA. This suggestion seems reasonable considering my finding that another AAA ATPase, Pex6p, functions not only in peroxisome biogenesis but also in the import of the Atp2p, a β-subunit of $F_1F_0$-ATPase, into mitochondria [228] and - as I revealed - is indispensable for the anti-aging ability of LA (see section 4.4.5 of this chapter). Thus, Pex6p not only controls the biogenesis of the peroxisome but also modulates - in an LA-dependent fashion - the functional state of another cellular organelle, the mitochondrion. It should be stressed that

my conclusion that the critical roles of the peroxins Pex1p and Pex6p in the anti-aging ability of LA do not relate to their function in peroxisome biogenesis further support a concept [38] that some peroxins are bifunctional proteins controlling not only peroxisomal functions but also vital cellular processes unrelated to peroxisome assembly and maintenance.

Based on the essential role of Pex1p in modulating - in an LA-dependent fashion - the aging-related functional state of the mitochondrion and taking into consideration my observation that LA alters the age-dependent dynamics of several mitochondrial activities in CR yeast, including oxygen consumption, mitochondrial membrane potential ($\Delta\Psi$) and ROS generation (see section 4.4.6 of this chapter), I hypothesize that one of the mechanisms by which mitochondria regulate yeast longevity is based on the LA-dependent ability of mitochondria in aging yeast to maintain ROS homeostasis. In particular, I propose that ROS, which are mostly generated as by-products of mitochondrial respiration [229, 230], play a dual role in regulating longevity. First, if yeast mitochondria are unable - due to a dietary regimen (see Chapter 3) or unavailability of LA - to maintain ROS concentration below a critically high level, ROS promote aging by oxidatively damaging certain mitochondrial proteins (such as CCO, SDH and ACO; see Chapter 3). Second, if yeast mitochondria can - due to a dietary regimen (see Chapter 3) or availability of LA - maintain ROS concentration at an "optimal" level, ROS delay aging. While this "optimal" level of ROS is insufficient to damage cellular macromolecules, it can activate certain signaling networks [101, 229, 231 – 235] that extend life span by increasing the abundance or activity of stress-protecting and other

anti-aging proteins. Two lines of evidence described in this chapter support my hypothesis for a dual role of ROS in regulating longevity. First, my analysis of the age-dependent dynamics of changes in the levels of ROS in cells of *Δfox* and *Δpex* mutants exposed to LA provides evidence that LA extends the chronological lifespan of CR yeast by: (1) reducing the damaging effect of ROS on cellular macromolecules during L, D and PD growth phases; and (2) amplifying the "hormetic" effect of ROS during ST growth phase (*i.e.*, in senescent yeast cells) through the activation of stress-protecting and other anti-aging proteins (see section 4.4.7 of this chapter). Second, my analysis of yeast strains carrying mutations eliminating either the Idh1p or the Idh2p subunit of isocitrate dehydrogenase - the two redundant components of the mitochondrial TCA cycle - revealed that, in agreement with hypothesis, both mutations: (1) extend the chronological lifespan of CR yeast; (2) alter the age-dependent dynamics of mitochondrial oxygen consumption, ROS production, $\Delta\Psi$ maintenance, and activities of CCO, SDH and ACO; (3) avert the loss of CCO and SDH activities, which represent the major mitochondrial targets of oxidative damage by ROS [101, 106]; (4) protect mitochondrial ACO from inactivation, which is known to be caused by the oxidation-dependent loss of one iron from its Fe/S cluster [240]; and (5) enhance heat-shock and oxidative stress resistance of chronologically aging CR yeast (see section 4.4.8 of this chapter).

## 4.6 Conclusions

Altogether, my findings described in this chapter led to the following conclusions. First, although the ability of the peroxisome to oxidize fatty acids (*i.e.*, a Fox-dependent

function) or assemble properly (*i.e.*, a Pex-dependent function) is essential for delaying aging or increasing fitness of yeast under CR conditions, it is not a requirement for the anti-aging action of LA. My data provide the comprehensive evidence that the presence of peroxisomes in yeast cells is not required for life-span extending ability of LA. Second, at least two peroxins that play an essential role in peroxisome biogenesis, namely the AAA ATPases Pex1p and Pex6p, are critical for the ability of LA to extend yeast longevity under CR conditions. The ability of one of these peroxins, the AAA ATPase Pex1p, to weaken the anti-aging effect of LA does not relate to its essential role in the assembly of a functional peroxisome. Another AAA ATPase, Pex6p, which functions not only in peroxisome biogenesis but also in mitochondrial import of the β-subunit of $F_1F_0$-ATPase, is indispensable for the anti-aging ability of LA. It seems that the essential role of Pex6p in mediating the longevity-extending effect of LA relates to its involvement in the biogenesis of mitochondria, not peroxisomes. Thus, some peroxins are bifunctional proteins controlling not only peroxisomal functions but also vital cellular processes that do not relate to peroxisome assembly and maintenance and are targeted by the anti-aging drug LA. Third, mitochondrially produced ROS play a dual role in regulating longevity. If yeast mitochondria are unable - due to a dietary regimen, unavailability of LA or genotype - to maintain ROS concentration below a critically high level, ROS promote aging by oxidatively damaging its mitochondrial target proteins (such as CCO, SDH and ACO). Conversely, if yeast mitochondria can - due to a dietary regimen, availability of LA or genotype - maintain ROS concentration at an "optimal" level, ROS delay aging.

While this "optimal" level of ROS is insufficient to damage cellular macromolecules, it can activate certain signaling networks that extend lifespan by increasing the abundance or activity of stress-protecting and other anti-aging proteins.

# 5 Conclusions and suggestions for future work

## 5.1 General conclusions

### 5.1.1 Aox controls a multistep process of peroxisome division

Altogether, my findings reported in Chapter 2 suggest the following model for peroxisome division in *Y. lipolytica* (Figure 5.1). In immature peroxisomal vesicles P1 to P5, Pex16p binds LPA in the lumenal leaflet of the peroxisomal membrane. The binding of Pex16p to LPA prevents the biosynthesis of PA and DAG in a two-step pathway, which includes two consecutive enzymatic reactions catalyzed by Slc1p (LPAAT) and Dpp1p (PAP). The stepwise import of distinct subsets of matrix proteins into immature peroxisomal vesicles P1 to P5 provides them with an increasing fraction of the matrix proteins present in mature peroxisomes. The increase in the total mass of matrix proteins above a critical level, which occurs only inside mature peroxisomes, causes the redistribution of Aox from the matrix to the membrane and its subsequent binding to Pex16p. This, in turn, greatly decreases the affinity between Pex16p and LPA, thereby allowing LPA to enter the two-step biosynthetic pathway leading to the formation of PA and DAG. The glycerophospholipid PC, which is transferred to the peroxisomal membrane from the P3- and P4-associated subcompartment of the ER, activates both LPAAT and PAP. The resulting accumulation of PA and DAG in the lumenal leaflet of the membrane of mature peroxisomes triggers a cascade of events ultimately leading to peroxisome division. This cascade of events is initiated by the spontaneous flipping of DAG, which is known for its very fast transbilayer translocation, between the two

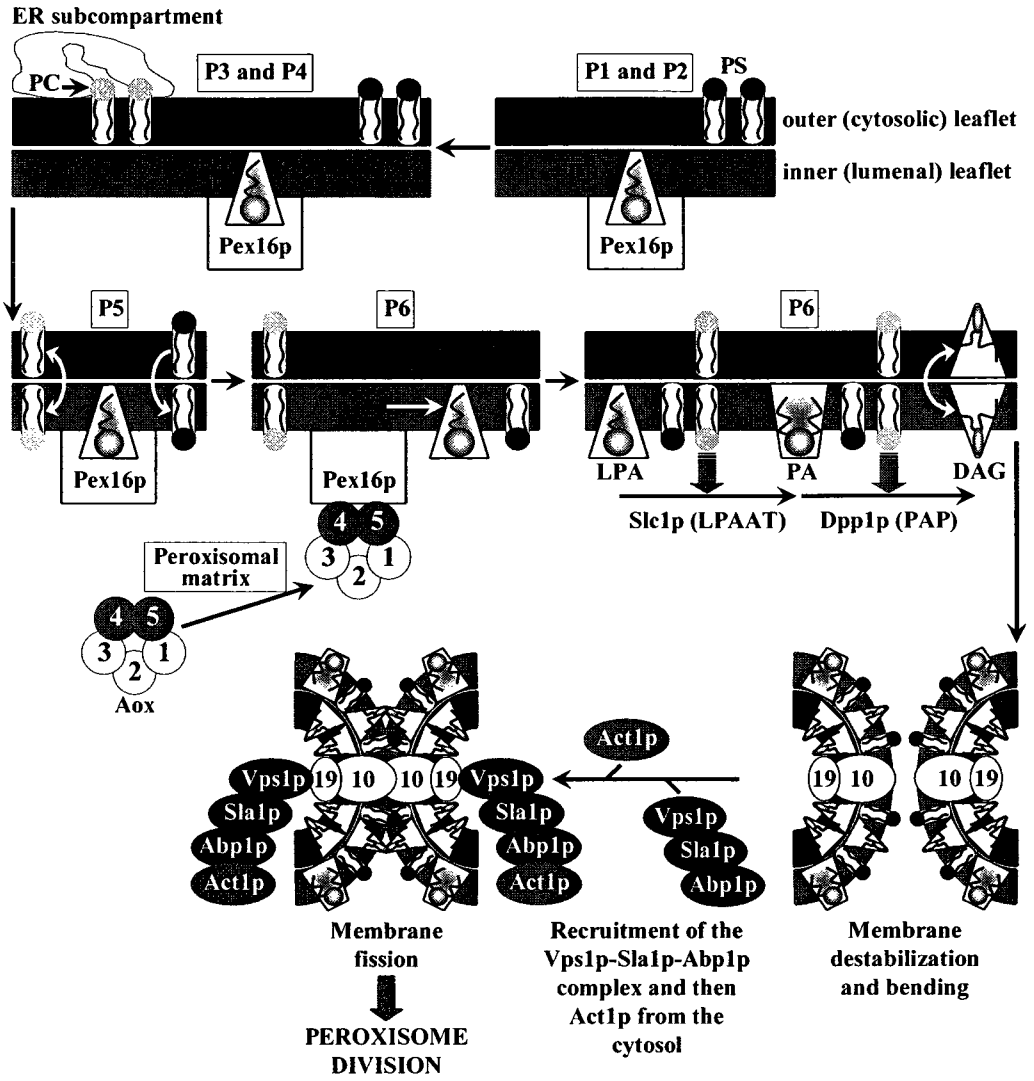


**Figure 5.1.** The Pex16p- and Aox-dependent intraperoxisomal signaling cascade drives the division of mature peroxisomes P6 by promoting the stepwise remodeling of lipid and protein composition of the peroxisomal membrane. See Discussion for details.

membrane leaflets. The movement of DAG, a particularly potent cone-shaped inducer of membrane bending, from the lumenal to the cytosolic leaflet of the membrane bilayer coincides with the translocation of the glycerophospholipid PS in the opposite direction. This bi-directional movement of DAG and PS generates a lipid imbalance across the

bilayer, which may promote the destabilization and bending of the membrane. The biosynthesis of PA and DAG in the membrane of mature peroxisomes and, perhaps, the bending of the membrane due to the bi-directional transbilayer movement of DAG and PS promote the docking of the Vps1p-Sla1p-Abp1p complex to the surface of mature peroxisomes. This pre-assembled in the cytosol protein complex binds to mature peroxisomes by interacting with the peroxin Pex19p. Pex19p is a component of the Pex10p-Pex19p complex that is formed in the peroxisomal membrane during the earliest steps of peroxisome assembly. After its attachment to the peroxisomal membrane, the Vps1p-Sla1p-Abp1p complex interacts with Act1p, thereby recruiting this structural constituent of actin cytoskeleton to the surface of mature peroxisomes. The subsequent fission of the peroxisomal membrane leads to peroxisome division.

### 5.1.2 CR extends yeast lifespan by modulating the Aox-dependent fatty acid oxidation in peroxisomes

Taken together, my findings described in Chapter 3 led to the following conclusions. First, peroxisomes do not produce significant quantities of ROS in chronologically aging CR yeast. Second, ROS that are produced in peroxisomes during fatty acid oxidation are not essential for chronological aging of yeast placed on a CR diet. Third, both the formation of free fatty acids due to lipolysis of LB-deposited neutral lipids and their subsequent Fox1p (Aox)-, Fox2p- and Fox3p-dependent peroxisomal oxidation are mandatory for the observed extension of lifespan by CR. Fourth, by the beginning of PD phase, CR yeast synthesize the bulk of their ATP in mitochondria by

oxidizing the pool of acetyl-CoA that has been generated in peroxisomes via Fox1p (Aox)-, Fox2p- and Fox3p-dependent fatty acid oxidation. I therefore concluded that fatty acid oxidation in peroxisomes controls longevity by modulating the rate of ATP synthesis in mitochondria, but not by generating the ROS hydrogen peroxide. Finally, my findings led to the conclusion that the efficiency of acetyl-CoA formation via peroxisomal fatty acid oxidation modulates: (1) the efficiencies of electron flow through the mitochondrial electron transport chain; (2) activities of several well-known target enzymes for the oxidative damage by ROS (*i.e.*, cytochrome c oxidase, succinate dehydrogenase and aconitase); (3) the mitochondrial membrane potential ($\Delta\Psi$); and (4) a balance between the processes of mitochondrial fission, fusion and tubulation, which plays a pivotal role in establishing and maintaining the morphological appearance of mitochondria.

### 5.1.3 A novel anti-aging small molecule LA extends yeast longevity by modulating mitochondrial ROS production in a Pex1p- and Pex6p-dependent fashion

Altogether, my findings reported in Chapter 4 led to the following conclusions. First, although the ability of the peroxisome to oxidize fatty acids (*i.e.*, a Fox-dependent function) or assemble properly (*i.e.*, a Pex-dependent function) is essential for delaying aging or increasing fitness of yeast under CR conditions, it is not a requirement for the anti-aging action of LA. My data provide the comprehensive evidence that the presence of peroxisomes in yeast cells is not required for life-span extending ability of LA. Second, at least two peroxins that play an essential role in peroxisome biogenesis, namely the AAA ATPases Pex1p and Pex6p, are critical for the ability of LA to extend yeast

longevity under CR conditions. The ability of one of these peroxins, the AAA ATPase Pex1p, to weaken the anti-aging effect of LA does not relate to its essential role in the assembly of a functional peroxisome. Another AAA ATPase, Pex6p, which functions not only in peroxisome biogenesis but also in mitochondrial import of the β-subunit of $F_1F_0$-ATPase, is indispensable for the anti-aging ability of LA. It seems that the essential role of Pex6p in mediating the longevity-extending effect of LA relates to its involvement in the biogenesis of mitochondria, not peroxisomes. Thus, some peroxins are bifunctional proteins controlling not only peroxisomal functions but also vital cellular processes that do not relate to peroxisome assembly and maintenance and are targeted by the anti-aging drug LA. Third, mitochondrially produced ROS play a dual role in regulating longevity. If yeast mitochondria are unable - due to a dietary regimen, unavailability of LA or genotype - to maintain ROS concentration below a critically high level, ROS promote aging by oxidatively damaging its mitochondrial target proteins (such as CCO, SDH and ACO). Conversely, if yeast mitochondria can - due to a dietary regimen, availability of LA or genotype - maintain ROS concentration at an "optimal" level, ROS delay aging. While this "optimal" level of ROS is insufficient to damage cellular macromolecules, it can activate certain signaling networks that extend lifespan by increasing the abundance or activity of stress-protecting and other anti-aging proteins.

## 5.2 Suggestions for future work

In my model for peroxisome division (Figure 5.1), the movement of DAG, which is synthesized in the inner leaflet of the membrane, into the outer leaflet of the membrane

in mature peroxisomes promotes their division. It is tempting to speculate that, after its spontaneous flipping between the two membrane leaflets, DAG undergoes the selective enrichment in distinct lipid domains that facilitate membrane scission through coordinated changes in local membrane curvature. To test this hypothesis, one would use fluorescence microscopy (FM) and immunoelectron microscopy (IEM) to monitor DAG in the outer leaflet of the membranes of different peroxisomal forms. I have used the DAG-binding C1b domain of protein kinase C for monitoring the dynamics of changes in the transbilayer distribution of DAG in the peroxisomal membrane during peroxisome maturation [51]. C1b would be produced, purified and labeled with the fluorophore Alexa Fluor 488 as described in the "Materials and methods" chapter. In addition, one would raise antibodies specific for C1b and use them for monitoring DAG in the membrane by IEM. Furthermore, one would use FM and IEM to visualize membrane lipids other than DAG. The following lipid-specific probes would be used for microscopy: 1) a tandem FYVE domain that specifically binds PI(3)P [167, 241]; 2) MED [242] and ENTH [243] domains specific for $PI(4,5)P_2$ [244]; 3) the intrinsically fluorescent ergosterol ligand filipin and a biotinylated derivative of the sterol-binding ligand perfringolysin O [245, 246]; 4) the PS-specific antibodies [45] and fluorescent sensor PSS-380 [247]; and 5) antibodies to ceramide [45]. The presence and spatial distribution of DAG and other lipid species in the outer leaflet of the peroxisomal membrane would be microscopically monitored in intact immature peroxisomal vesicles and mature peroxisomes. These organelles would be purified from wild-type cells and from *aox1Δ* to *aox5Δ* and *PEX16-TH* mutant cells. Furthermore, using lipid-specific fluorescent probes, one would use the

established procedure for evaluating the arrangement of DAG and other lipid species between the two leaflets of the membrane bilayers in different peroxisomal subforms of the mutant strains *aox4Δ*, *aox5Δ*, *PEX16-TH*, *slc1Δ*, *dpp1Δ*, *vps1Δ*, *sla1Δ* and *abp1Δ*, all of which are deficient in peroxisome division (please see a detailed description of the procedure in the "Materials and methods" chapter).

My data imply that the Pex2p-dependent transfer of PC from the P3- and P4-associated ER subcompartment to the acceptor membranes of P3 and P4 provides these peroxisomal membranes with the bulk quantities of PC and is essential for the conversion of P4 to P5 (see Chapter 2). A distinct set of proteins associated only with the P3- and P4-bound ER subcompartment but not with the free form of the ER (see Chapter 2) may operate in the transfer of PC from the ER subcompartment to the membranes of P3 and P4 peroxisomes via membrane contact sites. These proteins would be analyzed by mass spectrometry and identified by database searching as described in the "Materials and methods" chapter. My data on mass spectrometric identification of proteins associated only with the P3- and P4-bound ER subcompartment would be then used to disrupt the encoding genes. The effects of knocking out these genes on the efficiency of delivery of PC to the membranes of different peroxisomal subforms *in vivo* would be determined.

My findings provided evidence that the targeting of the dynamin-like protein Vps1p, which is essential for peroxisome division in this yeast, to the cytosolic face of mature peroxisomes from *Y. lipolytica* relies on the Pex16p/Aox-dependent biosynthesis of PA and/or DAG in their membranes (see Chapter 2). In order to elucidate the role of various species of membrane lipids in the recruitment of Vps1p to the cytosolic face of

mature peroxisomes, one would monitor the efficiency of the binding of Vps1p to the outer face of liposomes reconstituted (as described in the "Materials and methods" chapter) with different quantities of DAG and other lipid species, including PA and PC, that, similar to DAG, regulate peroxisome division. To test whether Vps1p co-localizes with DAG and/or any other "regulatory lipid" in the outer leaflet of the membrane of mature peroxisomes, the wild-type strain and mutant strains deficient in peroxisome division, as well as P6 peroxisomes purified from these strains, would be analyzed by FM, IFM and IEM. Samples will be processed for double labelling with anti-Vps1p antibodies and with lipid-specific probes for monitoring the distribution of DAG, PI(3)P, PI(4,5)P2, ergosterol, PS and ceramide as described above.

My findings provided evidence that ROS, which are mostly generated as by-products of mitochondrial respiration, play a dual role in regulating longevity (see Chapters 3 and 4). First, if yeast mitochondria are unable - due to a dietary regimen, unavailability of LA or genotype - to maintain ROS concentration below a critically high level, ROS promote aging by oxidatively damaging certain mitochondrial proteins (such as CCO, SDH and ACO). Second, if yeast mitochondria can - due to a dietary regimen, availability of LA or genotype - maintain ROS concentration at an "optimal" level, ROS delay aging. This "optimal" level of ROS is insufficient to damage cellular macromolecules but can activate certain signaling networks that extend life span by increasing the abundance or activity of stress-protecting and other anti-aging proteins (see Chapters 3 and 4). To further evaluate the validity of my hypothesis for a dual role of ROS in regulating longevity, one would first change the levels of ROS accumulated in

CR yeast at different stages of the aging process by using genetic manipulations that alter the abundance of various antioxidant enzymes involved in the major ROS scavenging pathways. The abundance of the following ROS scavenging enzymes would be altered (Figure 5.2): 1) cytosolic (Sod1p) and mitochondrial (Sod2p) superoxide dismutases; 2) cytosolic (Ctt1p) and peroxisomal (Cta1p) catalases; 3) mitochondrial cytochrome-c peroxidase (Ccp1p); 4) mitochondrial thioredoxin (Trx3p) and thioredoxin reductase (Trr2p); 5) cytosolic thioredoxins 1 (Trx1p) and 2 (Trx2p), thioredoxin peroxidases 1 (Tsa1p) and 2 (Tsa2p), and thioredoxin reductase (Trr1p); and 6) glutathione peroxidases 1 (Gpx1p) and 2 (Gpx2p). Two sets of mutant strains would be used in these experiments. One set would include mutants that lack each of the aforementioned enzymes, whereas the other set would include mutants that overproduce each of them under the control of a strong promoter. Mutant strains would be grown in medium containing 0.2% glucose plus LA. Concurrently with the assessment of the effect of LA on the life span of each of these mutants, one would measure ROS (visualized by fluorescence microscopy as described in "Materials and methods") accumulated in their cells at different stages of the aging process. Will genetic manipulations that increase ROS concentration in late ST phase above a certain "optimal" level or decrease it below such level annul the anti-aging effect of LA? Will genetic manipulations that further decrease the amplitude of the spike in ROS concentration during D phase enhance the beneficial effect of LA on longevity?

As a further test of the validity of my hypothesis, one would use mass spectrometry-based quantitative proteomics to examine the effect of LA on the age-

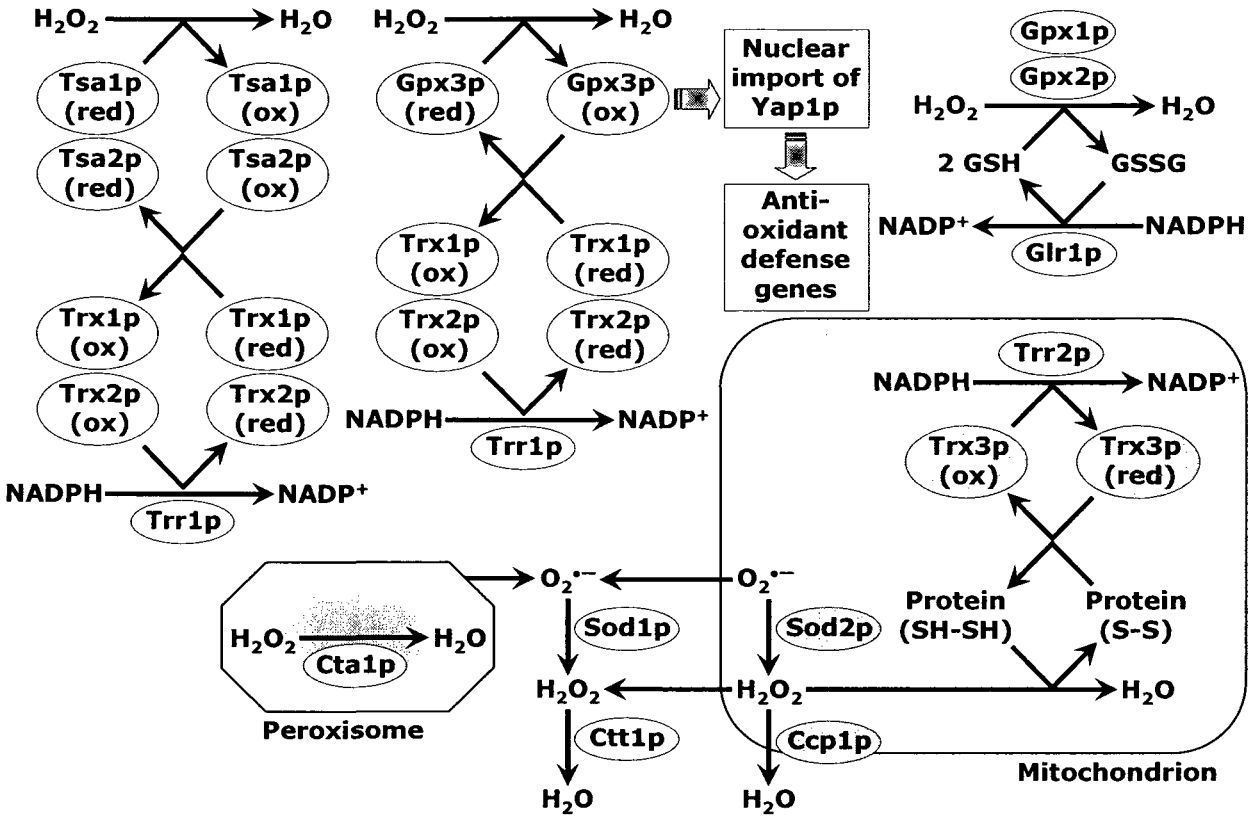


**Figure 5.2.** ROS scavenging enzymes of the yeast S. cerevisiae.

related dynamics of changes in cellular and mitochondrial proteomes taking place in aging CR yeast. Will LA - perhaps, due to its ability to modulate the level of mitochondrially produced ROS - increase the abundance of cytosolic and mitochondrial anti-stress chaperones, ROS-decomposing proteins, and proteins that protect mtDNA from oxidative damage? Will the observed effect of LA on cellular and mitochondrial proteomes be reminiscent of that seen in the long-lived *idh1Δ* and *idh2Δ* mutants (unpublished data from Dr. Titorenko's laboratory)? Of note, both these mutants exhibit

the age-dependent dynamics of ROS that is similar to that observed in WT cells chronically exposed to LA (see Chapter 4). It is conceivable that the altered abundance of many stress-protecting proteins seen in the long-lived *idh1Δ* and *idh2Δ* mutants (and, based on the protective effect of LA on CR yeast exposed to chronic oxidative stress, is likely to be also observed in LA-treated WT cells) could be due to the global change in transcription of genes encoding these proteins. Therefore, as a step towards defining signaling pathways and downstream transcriptional networks through which the LA-dependent modulation of ROS levels could extend longevity, one would compare age-related transcriptional profiles between LA-treated and untreated yeast. Using DNA microarrays, one would examine age-related changes in gene expression during aging of WT cells grown in medium containing 0.2% glucose alone or 0.2% glucose plus LA. Cells would be taken at different stages of the aging process. It should be stressed that the genome-wide transcriptional profiles of yeast mutants that lack transcription factors regulating gene expression in response to various stresses (including oxidative stress) have been established and annotated [248 – 250]. Thus, the global analysis of gene expression changes caused by LA could help to identify transcription factors that orchestrate a distinct genomic expression program in response to LA-dependent modulation of ROS levels.

## 6 References


1. Lazarow, P.B., and Fujiki, Y. (1985). Biogenesis of peroxisomes. *Annu. Rev. Cell Biol.* 1:489-530.
2. Subramani, S. (1993). Protein import into peroxisomes and biogenesis of the organelle. *Annu. Rev. Cell Biol.* 9:445-478.
3. Purdue, P.E., and Lazarow, P.E. (2001). Peroxisome biogenesis. *Annu. Rev. Cell Dev. Biol.* 17:701-52.
4. Bodnar, A.G., and Rachubinski, R.A. (1991). Characterization of the integral membrane polypeptides of rat liver peroxisomes isolated from untreated and clofibrate-treated rats. *Biochem. Cell Biol.* 69:499-508.
5. Kim, P.K., Mullen, R.T., Schumann, W., and Lippincott-Schwartz, J. (2006). The origin and maintenance of mammalian peroxisomes involves a *de novo* Pex16-dependent pathway from the ER. *J. Cell Biol.* 173:521-532.
6. Sacksteder, K.A., and Gould, S.J. (2000). The genetics of peroxisome biogenesis. *Annu. Rev. Genet.* 34:623-652.
7. Titorenko, V.I. and Rachubinski, R.A. (2001b). The life cycle of the peroxisome. *Nature Rev. Mol. Cell Biol.* 2:357-368.
8. Eckert, J.H., and Erdmann, R. (2003). Peroxisome biogenesis. *Rev. Physiol. Biochem. Pharmacol.* 147:75-121.
9. Subramani, S. (1993). Protein import into peroxisomes and biogenesis of the organelle. *Annu. Rev. Cell Biol.* 9: 445-478.

10. Wanders, R.J., Vreken, P., Ferdinandusse, S., Jansen, G.A., Waterham, H.R., van Roermund, C.W., and Van Grunsven, E.G. (2001). Peroxisomal fatty acid alpha- and beta-oxidation in humans: enzymology, peroxisomal metabolite transporters and peroxisomal diseases. *Biochem. Soc. Trans.* 29:250-267.

11. Wanders, R.J., and Tager, J.M. (1998). Lipid metabolism in peroxisomes in relation to human disease. *Mol. Aspects Med.* 19;69-154.

12. Fujiki, Y. (2000). Peroxisome biogenesis and peroxisome biogenesis disorders. *FEBS Lett.* 476:42-46.

13. Gould, S.J., and Valle, D. (2000). Peroxisome biogenesis disorders: genetics and cell biology. *Trends Genet.* 16:340-345.

14. Subramani, S. (1997). *PEX* genes on the rise. *Nature Genet.* 15:331-333.

15. Subramani, S., Koller, A., and Snyder, W.B. (2000). Import of peroxisomal matrix and membrane proteins. *Annu. Rev. Biochem.* 69:399-418.

16. Wanders, R.J. (1999). Peroxisomal disorders: clinical, biochemical, and molecular aspects. *Neurochem. Res.* 24:565-580.

17. Gould, S.G., Valle, D., and Raymond, G.V. (2001). The peroxisome biogenesis disorders. *In* The Metabolic and Molecular Bases of Inherited Disease. C.R. Scriver, A.L. Beaudet, W.S. Sly, and Valle, editors. McGraw-Hill, New York, pp. 3181-3217.

18. Matsumoto, N., Tamura, S., and Fujiki, Y. (2003). The pathogenic peroxin Pex26p recruits the Pex1p-Pex6p AAA ATPase complexes to peroxisomes. *Nature Cell Biol.* 5:454-460.

19. Powers, J.M., and Moser, H.W. (1998). Peroxisomal disorders: genotype, phenotype, major neuropathologic lesions, and pathogenesis. *Brain Pathol.* 8:101-120.

20. Moser, H.W. (1999) Genotype-phenotype correlations in disorders of peroxisome biogenesis. *Mol. Genet. Metab.* 68:316-327.

21. Purdue, P.E., Skoneczny, M., Yang, X., Zhang, J.W., and Lazarow, P.B. (1999). Rhizomelic chondrodysplasia puncatata, a peroxisomal biogenesis disorder caused by defects in Pex7p, a peroxisomal protein import receptor: a minireview. *Neurochem. Res.* 24:581-586

22. Eckert, J.H., and Erdmann, R. (2003). Peroxisome biogenesis. *Rev. Physiol. Biochem. Pharmacol.* 147:75-121.

23. Titorenko, V.I., Ogrydziak, D.M., and Rachubinski, R.A. (1997). Four distinct secretory pathways serve protein secretion, cell surface growth, and peroxisome biogenesis in the yeast *Yarrowia lipolytica. Mol. Cell. Biol.* 17:5210-5226.

24. Lin, Y., Sun, L., Nguyen, L.V., Rachubinski, R.A., and Goodman, H.M. (1999). The Pex16p homolog SSE1 and storage organelle formation in Arabidopsis seeds. *Science* 284:328-330.

25. Cohen, G.B., Rangan, V.S., Chen, B.K., Smith, S., and Baltimore, D. (2000). The human thioesterase II protein binds to a site on HIV-1 Nef critical for CD4 down-regulation. *J. Biol.Chem.* 275:23097-23105.

26. Jedd, G., and Chua, N.-H. (2000). A new self-assembled peroxisomal vesicle required for efficient resealing of the plasma membrane. *Nature Cell Biol.* 2: 226-231.

27. Kersten, S., Desvergne, B., and Wahli, W. (2000). Roles of PPARs in health and disease. *Nature* 405:421-424.

28. Motley, A.M., Hettema, E.H., Ketting, R., Plasterk, R., and Tabak, H.F. (2000). *Caenorhabditis elegans* has a single pathway to target matrix proteins to peroxisomes. *EMBO Rep.* 1:40-46.

29. Kimura, A., Takano, Y., Furusawa, I., and Okuno, T. (2001). Peroxisomal metabolic function is required for appressorium-mediated plant infection by *Colletotrichum lagenarium*. *Plant Cell* 13:1945-1957.

30. Titorenko, V.I. and Rachubinski, R.A. (2001a). Dynamics of peroxisome assembly and function. *Trends Cell Biol.* 11:22-29.

31. Di-Poi, N., Tan, N.S., Michalik, L., Wahli, W., and Desvergne, B. (2002). Antiapoptotic role of PPARβ in keratinocytes via transcriptional control of the Akt1 signalling pathway. *Mol. Cell* 10:721-733.

32. Footitt, S., Slocombe, S.P., Larner, V., Kurup, S., Wu, Y., Larson, T., Graham, I., Baker, A., and Holdsworth, M. 2002. Control of germination and lipid mobilization by COMATOSE, the *Arabidopsis* homologue of human ALDP. *EMBO J.* 21:2912-2922.

33. Gavva, N.R., Wen, S.C., Daftari, P., Moniwa, M., Yang, W.M., Yang-Feng, L.P., Seto, E., Davie, J.R., and Shen, C.K. (2002). NAPP2, a peroxisomal membrane protein, is also a transcriptional corepressor. *Genomics* 79:423-431.

34. Hu, J., Aguirre, M., Peto, C., Alonso, J., Ecker, J., and Chory, J. 2002. A role for peroxisomes in photomorphogenesis and development of *Arabidopsis*. *Science* 297: 405-409.

35. Ma, L., Gao, Y., Qu, L., Chen, Z., Li, J., Zhao, H., and Deng, X.W. (2002). Genomic evidence for COP1 as a repressor of light-regulated gene expression and development in *Arabidopsis*. *Plant Cell* 14: 2383-2398.

36. Michalik, L., Desvergne, B., Dreyer, C., Gavillet, M., Laurini, R.N., and Wahli, W. (2002). PPAR expression and function during vertebrate development. *Int. J. Dev. Biol.* 46:105-114.

37. Mohan, K.V., Som, I., and Atreya, C.D. (2002). Identification of a type 1 peroxisomal targeting signal in a viral protein and demonstration of its targeting to the organelle. *J. Virol.* 76:2543-2547. *Molecular Cell Biology*, 4th edition. W.H. Freeman and Co., New York.

37. Petriv, O.I., Pilgrim, D.B., Rachubinski, R.A., and Titorenko, V.I. (2002). RNA interference of peroxisome-related genes in *C. elegans*: a new model for human peroxisomal disorders. *Physiol. Genomics* 10:79-91.

38. Titorenko, V.I. and Rachubinski, R.A. (2004). The peroxisome: orchestrating important developmental decisions from inside the cell. *J. Cell Biol.* 164:641-645.

39. Alberts, B., Bray, B., Johnson, A., Lewis, J., Raff, M., Roberts, K., Walter, P. *Essential Cell Biology: An introduction to the Molecular Biology of the Cell.* Garland Publishing, Inc. New York, USA. (1998). p. 584-586.

40. Cooper, G. (2000). *The Cell: A Molecular Approach*, 2nd edition. ASM Press., Washington, D.C. Sinauer Associates, Inc., Sunderland, MA.

41. Lodish, H., Berk, A., Zipursky, S.L., Matsudaira, P., Baltimore, D., and Darnell, J. (2000). *Molecular Cell Biology*, 4th edition. W.H. Freeman and Co., New York, NY.

42. Titorenko, V.I., and R.A. Rachubinski. (1998). Mutants of the yeast *Yarrowia lipolytica* defective in protein exit from the endoplasmic reticulum are also defective in peroxisome biogenesis. *Mol. Cell. Biol.* 18:2789-2803.

43. Titorenko, V.I., and Rachubinski, R.A. (1998b). The endoplasmic reticulum plays an essential role in peroxisome biogenesis. *Trends Biochem.* Sci. 23:231-233.

44. Titorenko, V.I., and Rachubinski, R.A. (1998a). Mutants of the yeast *Yarrowia lipolytica* defective in protein exit from the endoplasmic reticulum are also defective in peroxisome biogenesis. *Mol. Cell. Biol.* 18: 2789-2803.

45. Guo, T., Kit, Y.Y., Nicaud, J.-M., Le Dall, M.-T., Sears, S.K., Vali, H., Chan, H., Rachubinski, R.A., and Titorenko, V.I. (2003). Peroxisome division in the yeast *Yarrowia lipolytica* is regulated by a signal from inside the peroxisome. *J. Cell Biol.* 162:1255-1266.

46. Titorenko, V.I., and R.A. Rachubinski. (2000). Peroxisomal membrane fusion requires two AAA family ATPases, Pex1p and Pex6p. *J. Cell Biol.* 150:881-886.

47. Titorenko, V.I., Nicaud, J.-M., Wang, H., Chan, H., and Rachubinski. R.A. (2002). Acyl-CoA oxidase is imported as a heteropentameric, cofactor-containing complex into peroxisomes of *Yarrowia lipolytica*. *J. Cell Biol.* 156:481-494.

48.. Titorenko VI, Smith JJ, Szilard RK, Rachubinski RA (1998) Pex20p of the yeast *Yarrowia lipolytica* is required for the oligomerization of thiolase in the cytosol and for its targeting to the peroxisome. *J. Cell Biol.* 142:403-420.

49. Titorenko, V.I., Smith, J.J., Szilard, R.K., and Rachubinski, R.A. (2000b). Peroxisome biogenesis in the yeast *Yarrowia lipolytica*. *Cell Biochem. Biophys.* 32:21-26.

50. Titorenko, V.I., H. Chan, and R.A. Rachubinski. (2000). Fusion of small peroxisomal vesicles in vitro reconstructs an early step in the in vivo multistep peroxisome assembly pathway of *Yarrowia lipolytica*. *J. Cell Biol.* 148:29-43.

51. Guo, T., Gregg, C., Boukh-Viner, T., Kyryakov, P., Goldberg, A., Bourque, S., Banu, F., Haile, S., Milijevic, S., San, K.H., Solomon, J., Wong, .V, and Titorenko, V.I. (2007). A signal from inside the peroxisome initiates its division by promoting the remodeling of the peroxisomal membrane. *J. Cell Biol.* 177:289-303.

52. Passreiter, M., M. Anton, D. Lay, R. Frank, C. Harter, F.T. Wieland, K. Gorgas, and W.W. Just. (1998). Peroxisome biogenesis: involvement of ARF and coatomer. *J. Cell Biol.* 141:373-383.

53. Lay, D., B.L. Grosshans, H. Heid, K. Gorgas, and W.W. Just. (2005). Binding and functions of ADP-ribosylation factor on mammalian and yeast peroxisomes. *J. Biol. Chem.* 280:34489-34499.

54. Lee, M.C., E.A. Miller, J. Goldberg, L. Orci, and R. Schekman. (2004). Bi-directional protein transport between the ER and Golgi. *Annu. Rev. Cell Dev. Biol.* 20:87-123.

55. McCartney, A.W., J.S. Greenwood, M.R. Fabian, K.A. White, and R.T. Mullen. (2005). Localization of the tomato bushy stunt virus replication protein p33 reveals a peroxisome-to-endoplasmic reticulum sorting pathway. *Plant Cell.* 17:3513-3531.

56. Mullen, R.T., A.W. McCartney, C.R. Flynn, and G.S.T. Smith. 2009. Peroxisome biogenesis and the formation of multivesicular peroxisomes during tombusvirus infection: A role for ESCRT? *Can. J. Bot.* In press.

57. Anton, M., M. Passreiter, D. Lay, T.P. Thai, K. Gorgas, and W.W. Just. (2000). ARF- and coatomer-mediated peroxisomal vesiculation. *Cell Biochem. Biophys.* 32:27-36.

58. Thoms, S., and R. Erdmann. (2005). Dynamin-related proteins and Pex11 proteins in peroxisome division and proliferation. *FEBS J.* 272:5169-5181.

59. Yan, M., Rayapuram, N., and Subramani, S. (2005). The control of peroxisome number and size during division and proliferation. *Curr. Opin. Cell Biol.* 17:376-383.

60. Veenhuis, M., and J.M. Goodman. (1990). Peroxisomal assembly: membrane proliferation precedes the induction of the abundant matrix proteins in the methylotrophic yeast *Candida boidinii. J. Cell Sci.* 96:583-590.

61. Purdue, P.E., and Lazarow, P.B. (2001). Peroxisome biogenesis. *Annu. Rev. Cell Dev. Biol.* 17:701-752.

62. Chapman, K.D., and R.N. Trelease. (1991). Acquisition of membrane lipids by differentiating glyoxysomes: role of lipid bodies. *J. Cell Biol.* 115:995-1007.

63. Bascom RA, Chan H, Rachubinski RA (2003) Peroxisome biogenesis occurs in an unsynchronized manner in close association with the endoplasmic reticulum in temperature-sensitive *Yarrowia lipolytica* Pex3p mutants. *Mol. Biol. Cell* 14:939-957.

64. Titorenko, V.I., Eitzen, G.A., and Rachubinski, R.A. (1996). Mutations in the *PAY5* gene of the yeast *Yarrowia lipolytica* cause the accumulation of multiple subpopulations of peroxisomes. J. *Biol. Chem.* 271:20307-20314.

65. Levine, T. (2004). Short-range intracellular trafficking of small molecules across endoplasmic reticulum junctions. *Trends Cell Biol.* 14: 483-490.

66. Kirkwood, T.B.L. (2005). Understanding the odd science of aging. *Cell* 120:437-447.

67. Campisi, J. (2005). Senescent cells, tumor suppression, and organismal aging: good citizens, bad neighbors. *Cell* 120:513-522.

68. Chien, K.R. and Karsenty, G. (2005). Longevity and lineages: toward the integrative biology of degenerative diseases in heart, muscle, and bone. *Cell* 120:533-544.

69. Tanzi, R.E. and Bertram, L. (2005). Twenty years of the Alzheimer's disease amyloid hypothesis: a genetic perspective. *Cell* 120:545-555.

70. Jazwinski, S.M. (2005). Yeast longevity and aging - the mitochondrial connection. *Mech. Ageing Dev.* 126:243-248.

71. Bitterman, K.J., Medvedik, O., and Sinclair, D.A. (2003). Longevity regulation in *Saccharomyces cerevisiae*: linking metabolism, genome stability, and heterchromatin. *Microbiol. Mol. Biol. Rev.* 67: 376-399.

72. Sinclair DA (2002). Paradigms and pitfalls of yeast longevity research. *Mech. Ageing Dev.* 123:857-867.

73. Sinclair, DA (2005). Toward a unified theory of caloric restriction and longevity regulation. *Mech. Ageing Dev.* 126:987-1002.

74. Lamming DW, Wood JG, Sinclair DA (2004). Small molecules that regulate lifespan: evidence for xenohormesis. *Mol. Microbiol.* 53:1003-1009.

75. Bordone L, Guarente L (2005). Calorie restriction, SIRT1 and metabolism: understanding longevity. *Nat. Rev. Mol. Cell Biol.* 6:298-305.

76. Guarente, L (2005). Calorie restriction - the SIR2 genes - towards a mechanism. *Mech. Ageing Dev.* 126:923-928.

77. Guarente, L. and Picard, F. (2005). Calorie restriction - the SIR2 connection. *Cell* 120:473-482.

78. Hekimi S, Guarente, L. (2003).Genetics and the specificity of the aging process. *Science* 299:1351-1354.

79. Richardson, A. 1985. The effect of age and nutrition on protein synthesis by cells and tissues from mammals. In *Handbook of nutrition in the aged* (ed. W.R. Watson), pp. 31-48. CRC Press, Boca Raton, FL.

80. Weindruch, R. and Walford, R.L. 1988. *The retardation of aging and disease by dietary restriction.* CC Thomas, Springfield, IL.

81. Sohal, R.S. and Weindruch, R. (1996). Oxidative stress, caloric restriction, and aging. *Science* 273:59-63.

82. Lane, M.A., Black, A., Handy, A., Tilmont, E.M., Ingram, D.K., and Roth, G.S. (2001). Caloric restriction in primates. *Ann. NY Acad. Sci.* 928:287-295.

83. Jazwinski, S.M. (2002). Biological aging research today: potential, peeves, and problems. *Exp. Gerontol.* 37:1141-1146.

84. Duan, W. and Mattson, M.P. (1999). Dietary restriction and 2-deoxyglucose administration improve behavioral outcome and reduce degeneration of dopaminergic neurons in models of Parkinson's disease. *J. Neurosci. Res.* 57:195-206.

85. Zhu, H., Guo, Q., and Mattson, M.P. (1999). Dietary restriction protects hippocampal neurons against the death-promoting action of presenilin-1 mutation. *Brain Res.* 842:224-229.

86. Ingram, D.K., Weindruch, R., Spangler, E.L., Freeman, J.R., and Walford, R.L. (1987). Dietary restriction benefits learning and motor performance of aged mice. *J. Gerontol.* 42:78-81.

87. Moroi-Fetters, S.E., Mervis, R.F., London, E.D., and Ingram, D.K. (1989). Dietary restriction suppresses age-related changes in dendritic spines. *Neurobiol. Aging* 10:317-322.

88. Mattson, M.P. (2000). Neuroprotective signaling and the aging brain: Take away my food and let me run. *Brain Res.* 886:47-53.

89. Lin, S.J., Defossez, P.A., and Guarente, L. (2000). Requirement of NAD and SIR2 for life-span extension by calorie restriction in *Saccharomyces cerevisiae. Science* 289:2126-2128.

90. Jiang, J., Wawryn, J., Shantha Kumara, H., and Jazwinski, S. (2002). Distinct roles of processes modulated by histone deacetylases Rpd3p, Hda1p, and Sir2p in life extension by caloric restriction in yeast. *Exp. Gerontol.* 37:1023-1030.

91. Jiang, J.C., Jaruga, E., Repnevskaya, M.V., and Jazwinski, S.M. (2000). An intervention resembling caloric restriction prolongs life span and retards aging in yeast. *FASEB J.* 14:2135-2137.

92. Harman, D. (1988). Free radicals in aging. *Mol. Cell. Biochem.* 84:155-161.

93. Fraga, C.G., Shigenaga, M.K., Park, J.W., Degan, P., and Ames, B.N. 1990. Oxidative damage to DNA during aging: 8-Hydroxy-2`-deoxyguanosine in rat organ DNA and urine. *Proc. Natl. Acad. Sci.* 87:4533-4537.

94. Stadtman, E.R. (1992). Protein oxidation and aging. *Science* 257:1220-1224.

95. Head, E., Liu, J., Hagen, T.M., Muggenburg, B.A., Milgram, N.W., Ames, B.N., and Cotman, C.W. 2002. Oxidative damage increases with age in a canine model of human brain aging. *J. Neurochem.* 82:375-381.

96. Liu, J., Head, E., Gharib, A.M., Yuan, W., Ingersoll, R.T., Hagen, T.M., Cotman, C.W., and Ames, B.N. (2002). Memory loss in old rats is associated with brain mitochondrial decay and RNA/DNA oxidation: Partial reversal by feeding acetyl-L-carnitine and/or R-α-lipoic acid. *Proc. Natl. Acad. Sci.* 99: 2356-2361.

97. Parkes, T.L., Elia, A.J., Dickinson, D., Hilliker, A.J., Phillips, J.P., and Boulianne, G.L. (1998). Extension of *Drosophila* lifespan by overexpression of human SOD1 in motorneurons. *Nat. Genet.* 19:171-174.

98. Longo, V.D., Liou, L.L., Valentine, J.S., and Gralla, E.B. (1999). Mitochondrial superoxide decreases yeast survival in stationary phase. *Arch. Biochem. Biophys.* 365:131-142.

99. Nicholls DG (2002) Mitochondrial function and dysfunction in the cell: its relevance to aging and aging related disease. *Int J Biochem Cell Biol.* 34:1372-1381.

100. Newmeyer DD, Ferguson-Miller S. (2003) Mitochondria: releasing power for life and unleashing the machineries of death. *Cell* 112:481-490.

101. Balaban, R.S., Nemoto, S., and Finkel, T. (2005). Mitochondria, oxidants, and aging. *Cell* 120:483-495.

102. Storz P. (2006) Reactive Oxygen species-mediated mitochondria-to-nucleus signaling: a key to aging and radical-caused diseases. *Sci STKE.* 332: Re3.

103. Adams JM. (2003) Ways of dying: multiple pathways to apoptosis. *Genes Dev.* 17:2481-2495.

104. Danial NN, Korsmeyer SJ. (2004) Cell death: critical control points. *Cell* 116:205-219.

105. Bredesen DE, Rao RV, Mehlen P. (2006) Cell death in the nervous system. *Nature* 443:796-802.

106. Lin MT, Beal MF (2006) Mitochondrial dysfunction and oxidative stress in neurodegenerative diseases. *Nature* 443:787-795.

107. Steller, H. 1995. Mechanisms and genes of cellular suicide. *Science* 267:1445-449.

108. Madeo, F., Herker, E., Wissing, S., Jungwirth, H., Eisenberg, T., and Frohlich, K.U. (2004). Apoptosis in yeast. *Current Option in Microbiology.* 7:655-660.

109. Madeo, F., Herker, E., Maldener, C., Wissing, S., Lachelt, S., Herlan, M., Fehr, M., Lauber, K., Sigrist, S.J., Wesselborg, S., and Frohlich, K.U. (2002). A caspase-related protease regulates apoptosis in yeast. *Molecular Cell* 9:911-917.

110. Madeo F, Fröhlich E, Ligr M, Grey M, Sigrist SJ, Wolf DH, Fröhlich KU (1999) Oxygen stress: a regulator of apoptosis in yeast. *J. Cell Biol.* 145:757-767.

111. Fahrenkrog, B., Sauder, U., and Aebi, U. (2004). The S. cerevisiae HtrA-like protein Nma111p is a nuclear serine protease that mediates yeast apoptosis. *J. Cell Science.* 117:115-126.

112. Wissing S, Ludovico P, Herker E, Büttner S, Engelhardt SM, Decker T, Link A, Proksch A, Rodrigues F, Corte-Real M, Fröhlich KU, Manns J, Candé C, Sigrist SJ, Kroemer G, Madeo F. (2004). An AIF orthologue regulates apoptosis in yeast. *J. Cell Sci.* 166:969-974.

113. Yamaki, M., Umehara, T., Chimura, T. and Horikoshi, M. (2001). Cell death with predominant apoptotic features in *Saccharomyces cerevisiae* mediated by deletion of the histone chaperone ASF1/CIA1. *Genes Cells* 6:1043–1054.

114. Fannjiang, Y., Cheng, W.C., Lee, S.J., Qi, B., Pevsner, J., McCaffery, J.M., Hill, R.B., Basañez, G. and Hardwick, J.M. (2004). Mitochondrial fission proteins regulate programmed cell death in yeast. *Genes Dev.* 18:2785–2797.

115. Herker, E., Jungwirth, H., Lehmann, K.A., Maldener, C., Frohlich, K.U., Wissing, S., Buttner, B., Markus, F., Sigrist, S., and Madeo, F. 2004. Chronological aging leads to apoptosis in yeast. *J. Cell. Biol.* 164:501-507.

116. Lazarow, P.B., and Y. Fujiki. (1985). Biogenesis of peroxisomes. *Annu. Rev. Cell Biol.* 1:489-530.

117. Lüers G, Hashimoto T, Fahimi HD, Völkl A. (1993) Biogenesis of peroxisomes: isolation and characterization of two distinct peroxisomal populations from normal and regenerating rat liver. *J. Cell Biol.* 121:1271-1280.

118. van Roermund CW, van den Berg M, Wanders RJ. (1995). Localization of peroxisomal 3-oxoacyl-CoA thiolase in particles of varied density in rat liver: implications for peroxisome biogenesis. *Biochim. Biophys. Acta* 1245:348-358.

119. Wilcke M, Hultenby K, Alexson SE. (1995). Novel peroxisomal populations in subcellular fractions from rat liver. Implications for peroxisome structure and biogenesis. *J Biol Chem.* 270:6949-6958.

120. Faber, K.N., J.A. Heyman, and S. Subramani (1998). Two AAA family peroxins, PpPex1p and PpPex6p, interact with each other in an ATP-dependent manner and are associated with different subcellular membranous structures distinct from peroxisomes. *Mol. Cell. Biol.* 18:936-943.

120. Titorenko, V.I., Chan, H., and Rachubinski, R.A. (2000). Fusion of small peroxisomal vesicles in vitro reconstructs an early step in the in vivo multistep peroxisome assembly pathway of *Yarrowia lipolytica*. *J. Cell Biol.* 148:29-43.

121. Heinemann P, Just WW. (1992) Peroxisomal protein import. *In vivo* evidence for a novel translocation competent compartment. *FEBS Lett.* 300:179-182.

122. South, S.T., and S.J. Gould (1999). Peroxisome synthesis in the absence of pre-existing peroxisomes. *J. Cell Biol.* 144:255-266.

123. Gould, S.J., and Valle, D. (2000). Peroxisome biogenesis disorders: genetics and cell biology. *Trends Genet.* 16:340-345.

124. Snyder, W.B., K.N. Faber, T.J. Wenzel, A. Koller, G.H. Luers, L. Rangell, G.A. Keller, and S. Subramani (1999). Pex19p interacts with Pex3p and Pex10p and is essential for peroxisome biogenesis in Pichia pastoris. *Mol. Biol. Cell* 10:1745-1761.

125. Titorenko, V.I. and Mullen, R.T. (2006) Peroxisome biogenesis: the peroxisomal endomembrane system and the role of the ER. *J. Cell Biol.* 174:11-17.

126. Eitzen, G.A., R.K. Szilard, and R.A. Rachubinski. (1997). Enlarged peroxisomes are present in oleic acid-grown *Yarrowia lipolytica* overexpressing the *PEX16* gene encoding an intraperoxisomal peripheral membrane peroxin. *J. Cell Biol.* 137:1265-1278.

127. Titorenko, V.I., J.J. Smith, R.K. Szilard, and R.A. Rachubinski. (1998). Pex20p of the yeast *Yarrowia lipolytica* is required for the oligomerization of thiolase in the cytosol and for its targeting to the peroxisome. *J. Cell Biol.* 142:403-420.

128. Burger, K.N.J. (2000). Greasing membrane fusion and fission machineries. *Traffic* 1:605-613.

129. Huttner, W.B., and Schmidt, A. (2000). Lipids, lipid modification and lipid-protein interaction in membrane budding and fission--insights from the roles of endophilin A1 and synaptophysin in synaptic vesicle endocytosis. *Curr. Opin. Neurobiol.* 10:543-551.

130. Huttner, W.B., and Schmidt, A.A. (2002). Membrane curvature: a case of endofeelin' ... *Trends Cell Biol.* 12:155-158.

131. Huttner, W.B., and Zimmerberg, J. (2001). Implications of lipid microdomains for membrane curvature, budding and fission. *Curr. Opin. Cell Biol.* 13:478-484.

132. Kozlov, M.M. (2001). Fission of biological membranes: interplay between dynamin and lipids. *Traffic* 2:51-65.

133. Chernomordik, L.V., and Kozlov, M.M. (2003). Protein-lipid interplay in fusion and fission of biological membranes. *Annu. Rev. Biochem.* 72:175-207.

134. Kooijman, E.E., V. Chupin, B. de Kruijff, and K.N.J. Burger. (2003). Modulation of membrane curvature by phosphatidic acid and lysophosphatidic acid. *Traffic* 4:162-174.

135. Sprong, H., van der Sluijs, P., and van Meer, G. (2001). How proteins move lipids and lipids move proteins. *Nature Rev. Mol. Cell Biol.* 2:504-513.

136. Rothman, J.H., Raymond, C.K., Gilbert, T., O'Hara, P.J., and Stevens, T.H. (1990). A putative GTP binding protein homologous to interferon-inducible Mx proteins performs an essential function in yeast protein sorting. *Cell* 61:1063–1074.

137. Schmidt, A., Wolde, M., Thiele, C., Fest, W., Kratzin, H., Podtelejnikov, A.V., Witke, W., Huttner, W.B., and Söling, H.-D. (1999). Endophilin I mediates synaptic vesicle formation by transfer of arachidonate to lysophosphatidic acid. *Nature* 401:133-141.

138. Takei, K., Slepnev, V.I., Haucke, V., and De Camilli, P. (1999). Functional partnership between amphiphysin and dynamin in clathrin-mediated endocytosis. *Nature Cell Biol.* 1:33-39.

139. Weigert, R., Silletta, M.G., Spano, S., Turacchio, G., Cericola, C., Colanzi, A., Senatore, S., Mancini, R., Polishchuk, E.V., Salmona, M., Facchiano, F., Burger, K.N., Mironov, A., Luini, A., and Corda, D. (1999). CtBP/BARS induces fission of Golgi membranes by acylating lysophosphatidic acid. *Nature* 402:429-433.

140. Farsad, K., Ringstad, N., Takei, K., Floyd, S.R., Rose, K., and De Camilli, P. (2001). Generation of high curvature membranes mediated by direct endophilin bilayer interactions. *J. Cell Biol.* 155:193-200.

141. Bankaitis, V.A. (2002). Slick recruitment to the Golgi. *Science* 295:290-291.

142. Baron, C.L., and Malhotra, V. (2002). Role of diacylglycerol in PKD recruitment to the TGN and protein transport to the plasma membrane. *Science* 295:325-328.

143. Corda, D., Hidalgo Carcedo, C., Bonazzi, M., Luini, A., and Spano, S. (2002). Molecular aspects of membrane fission in the secretory pathway. *Cell. Mol. Life Sci.* 59:1819-1832.

144. Ford, M.G.J., Mills, I.G., Peter, B.J., Vallis, Y., Praefcke, G.J., Evans, P.R., and McMahon, H.T. (2002). Curvature of clathrin-coated pits driven by epsin. *Nature* 419:361-366.

145. Bigay, J., Gounon, P., Robineau, S., and Antonny, B. (2003). Lipid packing sensed by ArfGAP1 couples COPI coat disassembly to membrane bilayer curvature. *Nature* 426:563-566.

146. Freyberg, Z., Siddhanta, A., and Shields, D. (2003). "Slip, sliding away": phospholipase D and the Golgi apparatus. *Trends Cell Biol.* 13:540-546.

147. Holthuis, J.C., and Burger, K.N. (2003). Sensing membrane curvature. *Dev. Cell* 5:821- 822.

148. Ktistakis, N.T., Delon, C., Manifava, M., Wood, E., Ganley, I., and Sugars, J.M. (2003). Phospholipase D1 and potential targets of its hydrolysis product, phosphatidic acid. *Biochem. Soc. Trans.* 31:94-97.

149. Diao, A., and Lowe, M. (2004). The Golgi goes fission. *Science* 305:48-49.

150. Hidalgo Carcedo, C., Bonazzi, M., Spanò, S., Turacchio, G., Colanzi, A., Luini, A., and Corda, D. (2004). Mitotic Golgi partitioning is driven by the membrane-fissioning protein CtBP3/BARS. *Science* 305:93-96.

151. Karbowski, M., Jeong, S.Y., and Youle, R.J. (2004). Endophilin B1 is required for the maintenance of mitochondrial morphology. *J. Cell Biol.* 166:1027-1039.

152. Lee, M.C., and Schekman, R. (2004). Cell biology. BAR domains go on a bender. *Science* 303:479-480.

153. Lee, Y.J., Jeong, S.Y., Karbowski, M., Smith, C.L., and Youle, R.J. (2004). Roles of the mammalian mitochondrial fission and fusion mediators Fis1, Drp1, and Opa1 in apoptosis. *Mol. Biol. Cell* 15:5001-5011.

154. Peter, B.J., Kent, H.M., Mills, I.G., Vallis, Y., Butler, P.J., Evans, P.R., and McMahon, H.T. (2004). BAR domains as sensors of membrane curvature: the amphiphysin BAR structure. *Science* 303:495-499.

155. Yoshida, Y., Kinuta, M., Abe, T., Liang, S., Araki, K., Cremona, O., Di Paolo, G., Moriyama, Y., Yasuda, T., De Camilli, P., and Takei, K. (2004). The stimulatory action of amphiphysin on dynamin function is dependent on lipid bilayer curvature. *EMBO J.* 23:3483-3491.

156. Cremona, O., and De Camilli, P. (2001). Phosphoinositides in membrane traffic at the synapse. *J. Cell Sci.* 114:1041-1052.

157. Farsad, K., and P. De Camilli. (2003). Mechanisms of membrane deformation. *Curr. Opin. Cell Biol.* 15:372-381.

158. Behnia, R., and S. Munro. (2005). Organelle identity and the signposts for membrane traffic. *Nature* 438:597-604.

159. McMahon, H.T., and J.L. Gallop. (2005). Membrane curvature and mechanisms of dynamic cell membrane remodelling. *Nature* 438:590-596.

160. Corda, D., A. Colanzi, and A. Luini. (2006). The multiple activities of CtBP/BARS proteins: the Golgi view. *Trends Cell Biol.* 16:167-173.

161. Goni, F.M., and Alonso, A. (1999). Structure and functional properties of diacylglycerols in membranes. *Prog. Lipid* Res. 38:1-48.

162. Szule, J.A., Fuller, N.L., and Rand, R.P. (2002). The effects of acyl chain length and saturation of diacylglycerols and phosphatidylcholines on membrane monolayer curvature. *Biophys. J.* 83:977-984.

163. Shemesh, T., A. Luini, V. Malhotra, K.N. Burger, and M.M. Kozlov. (2003). Prefission constriction of Golgi tubular carriers driven by local lipid metabolism: a theoretical model. *Biophys. J.* 85:3813-3827.

164. Wang, H.J., Le Dall, M.-T., Waché, Y., Laroche, C., Belin, J.-M., Gaillardin, C., and Nicaud, J.-M. (1999). Evaluation of acyl coenzyme A oxidase (Aox) isozyme function in the *n*-alkane-assimilating yeast *Yarrowia lipolytica*. *J. Bacteriol.* 181:5140-5148.

165. Lambkin, G.R., and R.A. Rachubinski. (2001). *Yarrowia lipolytica* cells mutant for the peroxisomal peroxin Pex19p contain structures resembling wild-type peroxisomes. *Mol. Biol. Cell.* 12:3353-3364.

166. Johnson, J.E., J. Giorgione, and A.C. Newton. (2000). The C1 and C2 domains of protein kinase C are independent membrane targeting modules, with specificity for phosphatidylserine conferred by the C1 domain. *Biochemistry.* 39:11360-11369.

167. Fratti, R.A., Jun, Y., Merz, A.J., Margolis, N., and Wickner, W. (2004). Interdependent assembly of specific regulatory lipids and membrane fusion proteins into the vertex ring domain of docked vacuoles. *J. Cell Biol.* 167:1087-1098.

168. Rieder SE, Emr SD (2000) Isolation of subcellular fractions from the yeast *Saccharomyces cerevisiae*. In: Bonifacino JS, Dasso M, Harford JB, Lippincott-Schwartz J, Yamada KM, editors. Current Protocols in Cell Biology. John Wiley & Sons, Inc. pp. 3.8.1-3.8.68.

169. Fried, B., and J. Sherma (1999). Thin-Layer Chromatography. Marcel Dekker, Inc., New York. 499 pp.

170. Szilard, R.K., V.I. Titorenko, M. Veenhuis, and R.A. Rachubinski. (1995). Pay32p of the yeast *Yarrowia lipolytica* is an intraperoxisomal component of the matrix protein translocation machinery. *J. Cell Biol.* 131:1453-1469.

171. Boukh-Viner, T., Guo, T., Alexandrian, A., Cerracchio, A., Gregg, C., Haile, S., Kyskan, R., Milijevic, S., Oren, D., Solomon, J., Wong, V., Nicaud, J.-M., Rachubinski, R.A., English, A.M., and Titorenko, V.I. (2005). Dynamic ergosterol- and ceramide-rich domains in the peroxisomal membrane serve as an organizing platform for peroxisome fusion. *J. Cell Biol.* 168:761-773.

172. Xu, Z., K. Sato, and W. Wickner. (1998). LMA1 binds to vacuoles at Sec18p (NSF), transfers upon ATP hydrolysis to a t-SNARE (Vam3p) complex, and is released during fusion. *Cell* 93:1125-1134.

173. Shevchenko A, Jensen ON, Podtelejnikov AV, Sagliocco F, Mortensen P, Shevchenko A, Boucherie H, Mann M (1996) Linking genome and proteome by mass spectrometry: large-scale identification of yeast proteins from two dimensional gels. *Proc. Natl. Acad. Sci. USA* 93:14440-14445.

174. Jiménez CR, Huang L, Qiu Y, Burlingame AL (1998) Searching sequence databases over the Internet: protein identification using MS-Fit. In: Coligan JE, Dunn BM, Ploegh HL, Speicher DW, Wigfield PT, editors. Current Protocols in Protein Science. John Wiley & Sons, Inc. pp.16.5.1-16.5.6.

175. Hannun, Y.A., Luberto, C., and Argraves, K.M. (2001). Enzymes of sphingolipid metabolism: from modular to integrative signaling. *Biochemistry* 40:4893-4903.

176. De Matteis, M., Godi, A., and Corda, D. (2002). Phosphoinositides and the Golgi complex. *Curr. Opin. Cell Biol.* 14:434-447.

177. Athenstaedt, K., and G. Daum. (1999). Phosphatidic acid, a key intermediate in lipid metabolism. *Eur. J. Biochem.* 266:1-16.

178. Carman, G.M., and G.S. Han. (2006). Roles of phosphatidate phosphatase enzymes in lipid metabolism. *Trends Biochem. Sci.* 31:694-699.

179. Schneiter, R., B. Brugger, R. Sandhoff, G. Zellnig, A. Leber, M. Lampl, K. Athenstaedt, C. Hrastnik, S. Eder, G. Daum, F. Paltauf, F.T. Wieland, and S.D. Kohlwein. (1999). Electrospray ionization tandem mass spectrometry (ESI-MS/MS) analysis of the lipid molecular species composition of yeast subcellular membranes reveals acyl chain-based sorting/remodeling of distinct molecular species en route to the plasma membrane. *J. Cell Biol.* 146:741-754.

180. Munro, S. (2003). Earthworms and lipid couriers. *Nature* 426:775-776.

181. Holthuis, J.C., and T.P. Levine. (2005). Lipid traffic: floppy drives and a superhighway. *Nature Rev. Mol. Cell Biol.* 6:209-220.

182. Sillence, D.J., and Platt, F.M. (2004). Glycosphingolipids in endocytic membrane transport. *Semin. Cell Dev. Biol.* 15:409-416.

183. van Meer, G., and H. Sprong. (2004.) Membrane lipids and vesicular traffic. *Curr. Opin. Cell Biol.* 16:373-378.

184. Voelker, D.R. (2005). Bridging gaps in phospholipid transport. *Trends Biochem. Sci.* 30:396-404.

185. Hoepfner, D., M. van den Berg, P. Philippsen, H.F. Tabak, and E.H. Hettema. (2001). A role for Vps1p, actin, and the Myo2p motor in peroxisome abundance and inheritance in *Saccharomyces cerevisiae*. *J. Cell Biol.* 155:979–990.

186. Peters, C., Baars, T.L., Bühler, S., and Mayer, A. (2004). Mutual control of membrane fission and fusion proteins. *Cell* 119:667-678.

187. Praefcke, G.J., and H.T. McMahon. (2004). The dynamin superfamily: universal membrane tubulation and fission molecules? *Nature Rev. Mol. Cell Biol.* 5:133-147.

188. Warren, D.T., Andrews, P.D., Gourlay, C.W., and Ayscough, K.R. (2002). Sla1p couples the yeast endocytic machinery to proteins regulating actin dynamics. *J. Cell Sci.* 115:1703-1715.

189. Olazabal, I.M., and Machesky, L.M. (2001). Abp1p and cortactin, new "hand-holds" for actin. *J. Cell Biol.* 154:679-682.

190. Pruyne, D., and A. Bretscher. (2000). Polarization of cell growth in yeast. I. Establishment and maintenance of polarity states. *J. Cell Sci.* 113:365-375.

191. Shorter J., and Warren, G. (2002). Golgi architecture and inheritance. Annu. *Rev. Cell Dev. Biol.* 18:379-420.

192. Youle, R.J., and Karbowski, M. (2005). Mitochondrial fission in apoptosis. *Nature Rev. Mol. Cell Biol.* 6:657-663.

193. Diaz Anel, A.M., and Malhotra, V. (2005). PKCη is required for β1γ2/β3γ2- and PKD-mediated transport to the cell surface and the organization of the Golgi apparatus. *J. Cell Biol.* 169:83-91.

194. Longo, V.D., Finch, C.E. (2003). Evolutionary medicine: from dwarf model systems to healthy centenarians? *Science* 299:1342-1346

194. Weindruch, R., Walford, R.L., Fligiel, S., and Guthrie, D. (1986). The retardation of aging in mice by dietary restriction: Longevity, cancer, immunity and lifetime energy intake. *J. Nutr.* 116:641-654.

195. Weindruch, R. and Walford, R.L. 1988. The retardation of aging and disease by dietary restriction. CC Thomas, Springfield, IL.

196. Fabrizio P, Gattazzo C, Battistella L, Wei M, Cheng C, McGrew K, Longo VD. (2005) Sir2 blocks extreme life-span extension. *Cell* 123:655-667.

197. Athenstaedt, K. and Daum, G. (2006). The life cycle of neutral lipids: synthesis, storage and degradation. *Cell. Mol. Life Sci.* 63:1355-1369.

198. Zweytick, D., Athenstaedt, K. and Daum, G. (2000). Intracellular lipid particles of eukaryotic cells. *Biochim. Biophys. Acta* 1469:101-120.

199. Brown, D.A. 2001. Lipid droplets: Proteins floating on a pool of fat. *Curr. Biol.* 11:R446-R449.

200. Blüher, M., Kahn, B. B. and Kahn, C. R. (2003). Extended longevity in mice lacking the insulin receptor in adipose tissue. *Science* 299:572-574.

201. Picard, F., Kurtev, M., Chung, N., Topark-Ngarm, A., Senawong, T., Machado De Oliveira, R., Leid, M., McBurney, M.W. and Guarente, L. (2004). Sirt1 promotes fat mobilization in white adipocytes by repressing PPAR-γ. *Nature* 429:771-776.

202. Binns D, Januszewski T, Chen Y, Hill J, Markin VS, Zhao Y, Gilpin C, Chapman KD, Anderson RG, Goodman JM. (2006). An intimate collaboration between peroxisomes and lipid bodies. *J Cell Biol.* 173:719-731.

203. Okamoto K, Shaw JM (2005) Mitochondrial morphology and dynamics in yeast and multicellular eukaryotes. *Annu. Rev. Genet.* 39:503-536;

204. Hoppins S, Lackner L, Nunnari J (2007) The machines that divide and fuse mitochondria. *Annu. Rev. Biochem.* 76:751-780.

205. Masoro, E.J. (2006). Caloric restriction and aging: controversial issues. *J. Gerontol. Biol. Sci.* 61A:14-19.

206. Allen, C., Büttner, S., Aragon, A.D., Thomas, J.A., Meirelles, O., Jaetao, J.E., Benn, D., Ruby, S.W., Veenhuis, M., Madeo, F., and Werner-Washburne, M. (2006). Isolation of quiescent and nonquiescent cells from yeast stationary-phase cultures. *J. Cell Biol.* 174:89-100.

207. Aragon, A.D., Rodriguez, A.L., Meirelles, O., Roy, S., Davidson, G.S., Tapia, P.H., Allen, C., Joe, R., Benn, D., and Werner-Washburne, M. (2008). Characterization of differentiated quiescent and nonquiescent cells in yeast stationary-phase cultures. *Mol. Biol. Cell* 19:1271-1280.

208. Bonawitz, N.D., Chatenay-Lapointe, M., Pan, Y., and Shadel, G.S. (2007). Reduced TOR signaling extends chronological life span via increased respiration and upregulation of mitochondrial gene expression. *Cell Metab.* 5:265-277.

209. Howitz, K.T., Bitterman, K.J., Cohen, H.Y., Lamming, D.W., Lavu, S., Wood, J.G., Zipkin, R.E., Chung, P., Kisielewski, A., Zhang, L.L., Scherer, B., and Sinclair, D.A. (2003). Small molecule activators of sirtuins extend *Saccharomyces cerevisiae* lifespan. *Nature* 425:191-196.

210. Bauer, J.H., Goupil, S., Garber, G.B., and Helfand, S.L. (2004). An accelerated assay for the identification of lifespan-extending interventions in Drosophila melanogaster. *Proc. Natl. Acad. Sci. USA* 101:12980-12985.

211. Wood, J.G., Rogina, B., Lavu, S., Howitz, K., Helfand, S.L., Tatar, M., and Sinclair, D. (2004). Sirtuin activators mimic caloric restriction and delay ageing in metazoans. *Nature* 430:686-689.

212. Viswanathan, M., Kim, S.K., Berdichevsky, A., and Guarente, L. (2005). A role for SIR-2.1 regulation of ER stress response genes in determining *C. elegans* life span. *Dev. Cell* 9:605-615.

213. Baur, J.A., Pearson, K.J., Price, N.L., Jamieson, H.A., Lerin, C., Kalra, A., Prabhu, V.V., Allard, J.S., Lopez-Lluch, G., Lewis, K., Pistell, P.J., Poosala, S., Becker, K.G., Boss, O., Gwinn, D., Wang, M., Ramaswamy, S., Fishbein, K.W., Spencer, R.G., Lakatta, E.G., Le Couteur, D., Shaw, R.J., Navas, P., Puigserver, P., Ingram, D.K., de Cabo, R., and Sinclair, D.A. (2006). Resveratrol improves health and survival of mice on a high-calorie diet. *Nature* 444:337-342.

214. Valenzano, D.R., Terzibasi, E., Genade, T., Cattaneo, A., Domenici, L., and Cellerino, A. (2006). Resveratrol prolongs lifespan and retards the onset of age-related markers in a short-lived vertebrate. *Curr. Biol.* 16:296-300.

215. Chen, D., and Guarente, L. (2007). SIR2: a potential target for calorie restriction mimetics. *Trends Mol. Med.* 13:64-71.

216. Curtis, R., Geesaman, B.J., and DiStefano, P.S. (2005). Ageing and metabolism: drug discovery opportunities. *Nat. Rev. Drug Discov.* 4:569-580.

217. Milne, J.C., Lambert, P.D., Schenk, S., Carney, D.P., Smith, J.J., Gagne, D.J., Jin, L., Boss, O., Perni, R.B., Vu, C.B., Bemis, J.E., Xie, R., Disch, J.S., Ng, P.Y., Nunes, J.J., Lynch, A.V., Yang, H., Galonek, H., Israelian, K., Choy, W., Iffland, A., Lavu, S., Medvedik, O., Sinclair, D.A., Olefsky, J.M., Jirousek, M.R., Elliott, P.J., and Westphal, C.H. (2007). Small molecule activators of SIRT1 as therapeutics for the treatment of type 2 diabetes. *Nature* 450:712-716;

218. Yang, H., Baur, J.A., Chen, A., Miller, C., Adams, J.K., Kisielewski, A., Howitz, K.T., Zipkin, R.E., and Sinclair, D.A. (2007). Design and synthesis of compounds that extend yeast replicative lifespan. *Aging Cell* 6:35-43.

219. Smith, J.J., Marelli, M., Christmas, R.H., Vizeacoumar, F.J., Dilworth, D.J., Ideker, T., Galitski, T., Dimitrov, K., Rachubinski, R.A., and Aitchison, J.D. (2002). Transcriptome profiling to identify genes involved in peroxisome assembly and function. *J. Cell Biol.* 158:259-271.

220. Tam, Y.Y., and Rachubinski, R.A. (2002). *Yarrowia lipolytica* cells mutant for the *PEX24* gene encoding a peroxisomal membrane peroxin mislocalize peroxisomal proteins and accumulate membrane structures containing both peroxisomal matrix and membrane proteins. *Mol. Biol. Cell* 13:2681-2691.

221. Tam, Y.Y.C., Torres-Guzman, J.C., Vizeacoumar, F.J., Smith, J.J., Marelli, M., Aitchison, J.D., and Rachubinski, R.A. (2003). Pex11-related proteins in peroxisome dynamics: a role for the novel peroxin Pex27p in controlling peroxisome size and number in *Saccharomyces cerevisiae*. *Mol. Biol. Cell.* 14:4089-4102.

222. Vizeacoumar, F.J., Torres-Guzman, J.C., Tam, Y.Y.C., Aitchison, J.D., and Rachubinski, R.A. (2003). YHR150w and YDR479c encode peroxisomal integral membrane proteins involved in the regulation of peroxisome number, size, and distribution in *Saccharomyces cerevisiae*. *J. Cell Biol.* 161:321-332.

223. Vizeacoumar, F.J., Torres-Guzman, J.C., Bouard, D., Aitchison, J.D., and Rachubinski, R.A. (2004). Pex30p, Pex31p, and Pex32p form a family of peroxisomal integral membrane proteins regulating peroxisome size and number in *Saccharomyces cerevisiae*. *Mol. Biol. Cell.* 15:665-677.

224. Titorenko, V.I. and Rachubinski, R.A. Spatiotemporal dynamics of the ER-derived peroxisomal endomembrane system. *Int. Rev. Cell Mol. Biol.* (2009) 272:in press.

225. Sarmiento, C., Ross, J.H.E., Herman, E., and Murphy, D.J. (1997). Expression and subcellular targeting of a soybean oleosin in transgenic rapeseed. Implications for the mechanism of oil-body formation in seeds. *Plant J.* 11:783-796.

226. Gaedeke, N., Klein, M., Kolukisaoglu, U., Forestier, C., Müller, A., Ansorge, M., Becker, D., Mamnun, Y., Kuchler, K., Schulz, B., Mueller-Roeber, B., and Martinoia, E. (2001). The *Arabidopsis thaliana* ABC transporter *At*MRP5 controls root development and stomata movement. *EMBO J.* 20:1875-1887.

227. Geuze, H.J., J.L. Murk, A.K. Stroobants, J.M. Griffith, M.J. Kleijmeer, M.J. Koster, A.J. Verkleij, B. Distel, and H.F. Tabak. (2003). Involvement of the endoplasmic reticulum in peroxisome formation. *Mol. Biol. Cell.* 14:2900-2907.

228. Seo, J.G., Lai, C.Y., Miceli, M.V., Jazwinski, S.M. (2007) A novel role of peroxin PEX6: suppression of aging defects in mitochondria. *Aging Cell.* 6:405-413.

229. D'Autréaux, B., and Toledano, M.B. (2007). ROS as signalling molecules: mechanisms that generate specificity in ROS homeostasis. *Nat. Rev. Mol. Cell Biol.* 8:813-824.

230. Giorgio, M., Trinei, M., Migliaccio, E., and Pelicci, P.G. (2007). Hydrogen peroxide: a metabolic by-product or a common mediator of ageing signals? *Nat. Rev. Mol. Cell Biol.* 8:722-728.

231. Ikner, A., and Shiozaki, K. (2005). Yeast signaling pathways in the oxidative stress response. *Mutat. Res.* 569:13-27.

232. Liu, H., Colavitti, R., Rovira, I.I., and Finkel, T. (2005). Redox-dependent transcriptional regulation. *Circ. Res.* 97:967-974.

233. Finkel, T. (2006). Intracellular redox regulation by the family of small GTPases. *Antioxid. Redox Signal.* 8:1857-1863.

234. Storz, P. (2007). Mitochondrial ROS - radical detoxification, mediated by protein kinase D. *Trends Cell Biol.* 17:13-18.

235. Veal, E.A., Day, A.M., and Morgan, B.A. (2007). Hydrogen peroxide sensing and signaling. *Mol. Cell* 26:1-14.

236. Schulz, T.J., Zarse, K., Voigt, A., Urban, N., Birringer, M., and Ristow, M. (2007). Glucose restriction extends *Caenorhabditis elegans* life span by inducing mitochondrial respiration and increasing oxidative stress. *Cell Metab.* 6:280-293.

237. Calabrese, E.J. (2004). Hormesis: from marginalization to mainstream: a case for hormesis as the default dose-response model in risk assessment. *Toxicol. Appl. Pharmacol.* 197:125-136.

238. Rattan, S.I. (2008). Hormesis in aging. *Ageing Res. Rev.* 7:63-78.

239. The *Saccharomyces* Genome Database. Department of Genetics at the School of Medicine, Stanford University. World Wide Web URL: http://www.yeastgenome.org/

240. Fabrizio, P., Pozza, F., Pletcher, S.D., Gendron, C.M. and Longo, V.D. (2001). Regulation of longevity and stress resistance by Sch9 in yeast. *Science* 292:288-290.

241. Gillooly, D.J., Morrow, I.C., Lindsay, M., Gould, R., Bryant, N.J., Gaullier, J.M., Parton, R.G., and Stenmark, H. (2000). *EMBO J.* 19:4577-4588.

242. Wang, J., Arbuzova, A., Hangyas-Mihalyne, G., and McLaughlin, S. (2001). The effector domain of myristoylated alanine-rich C kinase substrate binds strongly to phosphatidylinositol 4,5-bisphosphate. *J. Biol. Chem.* 276:5012-5019.

243. Rosenthal, J.A., Chen, H., Slepnev, V.I., Pellegrini, L., Salcini, A.E., Di Fiore, P.P., and DeCamilli, P. (1999). The epsins define a family of proteins that interact with components of the clathrin coat and contain a new protein module. *J. Biol. Chem.* 274, 33959-33965.

244. DiNitto, J.P., Cronin, T.C., and Lambright, D.G. (2003). Membrane recognition and targeting by lipid-binding domains. *Sci. STKE* 213:re16.

245. Möbius, W., Ohno-Iwashita, Y., van Donselaar, E.G., Oorschot, V.M., Shimada, Y., Fujimoto, T., Heijnen, H.F., Geuze, H.J., and Slot, J.W. (2002). Immunoelectron microscopic localization of cholesterol using biotinylated and non-cytolytic perfringolysin O. *J. Histochem. Cytochem.* 50:43-55.

246. Möbius, W., van Donselaar, E., Ohno-Iwashita, Y., Shimada, Y., Heijnen, H.F., Slot, J.W., and Geuze, H.J. (2003). Recycling compartments and the internal vesicles of multivesicular bodies harbor most of the cholesterol found in the endocytic pathway. *Traffic* 4:222-231.

247. Koulov, A.V., Stucker, K.A., Lakshmi, C., Robinson, J.P., and Smith, B.D. (2003). Detection of apoptotic cells using a synthetic fluorescent sensor for membrane surfaces that contain phosphatidylserine. *Cell Death Differ.* 10:1357-1359.

248. The ArrayExpress Database: http://www.ebi.ac.uk/microarray-as/ae/.

249. The Yeast Microarray Global Viewer Database: http://transcriptome.ens.fr/ymgv/index.php.

250. The Yeast Proteome Database: http://www.biobase- international.com.